Doctoral Dissertation

Reactivity Enhancement of a Nonheme Iron(IV)-Oxo Complex by Lewis Acids for Oxidation of Substrates

(非ヘム鉄(IV)オキソ錯体の酸化反応性のルイス酸による活性化)

Jiyun Park

January 2014

Graduate School of Engineering,

Osaka University

Contents

Department of Material and Life Science
Division of Advanced Science and Biotechnology
Graduate School of Engineering

General Introduction

The sunlight is the primary source of energy for all living things. By biological photosynthesis, solar energy is converted to chemical energy, such as coal, natural gas, firewood, and so on. Plants, algae and some bacteria utilize the solar energy from the sun in photosynthesis.[1-4] Photosynthesis is chemical process by which plants use solar energy to produce organic compounds required for life. During this process four electrons are removed from water to release oxygen into the air and carbon dioxide is reduced to a carbohydrate, when biological energy such as adenosine triphosphate (ATP) is produced.

The electron configuration of O_2 in which two unpaired electrons occupy two degenerate molecular orbitals indicates that the ground state is triplet, The triplet state prevents molecular oxygen from reacting directly with organic molecules, which are mostly singlet.[8] Thus, molecular oxygen is unreactive towards organic molecules at low temperatures because the reactions are spin-forbidden. Consequently, the oxygenation of organic molecules at physiological temperatures must involve the modification of the electronic structure of O_2 to activate O_2. Oxygenases such as cytochromes P450 or nonheme metalloenzymes perform this type of modifications by forming metal-oxo species by the reductive activation of O_2.

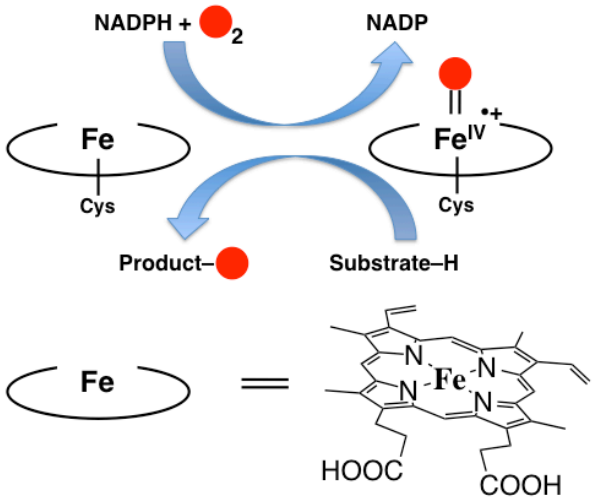

Figure 1. Structure and simplified redox chemistry of cytochrome P450 monooxygenases.

The cytochromes P450 constitute a large family of cysteinato-heme enzymes present in all forms of life, such as plants, bacteria and mammals. These enzymes are located in

the membrane of the endoplasmic reticulum and are able to perform various difficult oxidation reactions.[1-7] These monooxygenases are able to catalyze the many types of insertion of one oxygen atom of O_2 into many different substrates, the second oxygen atom of O_2 being reduced to H_2O.[4-7] Thetwo electrons required for this reductive activation of O_2 are provided by NADPH via a reductase (Figure 1). Cytochromes P450 catalyze the hydroxylation of saturated carbon-hydrogen bonds (eq 1), oxygen atom transfer, the epoxidation of double bonds, and dealkylation reactions, etc.[2,9]

$$RH + O_2 + 2e^- + 2H^+ \xrightarrow{\text{Cytochrome P450}} ROH + H_2O \quad (1)$$

The metal-oxo species involved in the enzymatic oxidation reactions have been studied well not only with enzymes and but also with their model compounds.[2-9] In the proposed catalytic cycle of oxidation reaction by cytochromes P450, high-valent iron(IV)-oxo porphyrin π- radical cations (compound I) are believed as a key intermediate.[2-9] As a model of the key intermediate, various high-valent iron(IV)-oxo radical species have been synthesized and characterized with various spectroscopic methods, and their reactivities have also been investigated in a number of oxidation reactions, including alkane hydroxylation and olefin epoxidation, in an effort to unveil mechanistic details of oxygen atom transfer reaction by cytochromes P450.[2,9]

High-valent iron(IV)-oxo species have also been involved as key reactive intermediates in nonheme iron(IV)-oxo enzyme.[6,10,11] Our understanding of the catalytic mechanisms in enzymes, especially the active species, has been improved by intensive mechanistic studies of the enzymes and their model compounds. In the catalytic cycles of *Escherichia coli* taurine: α-ketogultarate dioxygenase (TauD), a nonheme iron(IV)-oxo species is regarded as an important intermediate.[12-14] The intermediate has been characterized with various spectroscopic methods, such as Mössbauer, *r*-Raman, and X-ray crystallography, showing that the iron(IV)-oxo intermediate is in a high-spin state (S = 2) with double bond character of Fe-O.[13,14]

In 2003, the first crystal structure of synthetic mononuclear nonheme iron(IV)-oxo complex, $[(TMC)Fe^{IV}(O)]^{2+}$ (TMC = 1,4,8,11-tetramethyl-1,4,8,11-tetraazacyclo tetradecane), bearing a macrocyclic ligand was reported as a model of the high-valent nonheme iron(IV)-oxo intermediate.[15] This complex was well characterized with various spectroscopic methods and X-ray crystallography (Figure 2), indicate that the complex has an iron(IV)-oxo unit with Fe-O double bond and a low-spin state (S =1).[15]

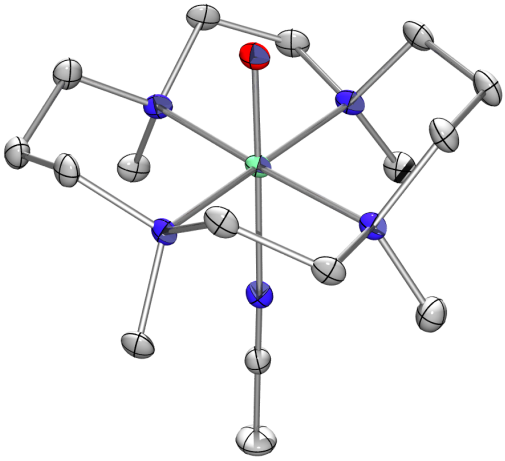

Figure 2. X-ray crystal structure of $[(TMC)Fe^{IV}(O)(NCCH_3)]^{2+}$.

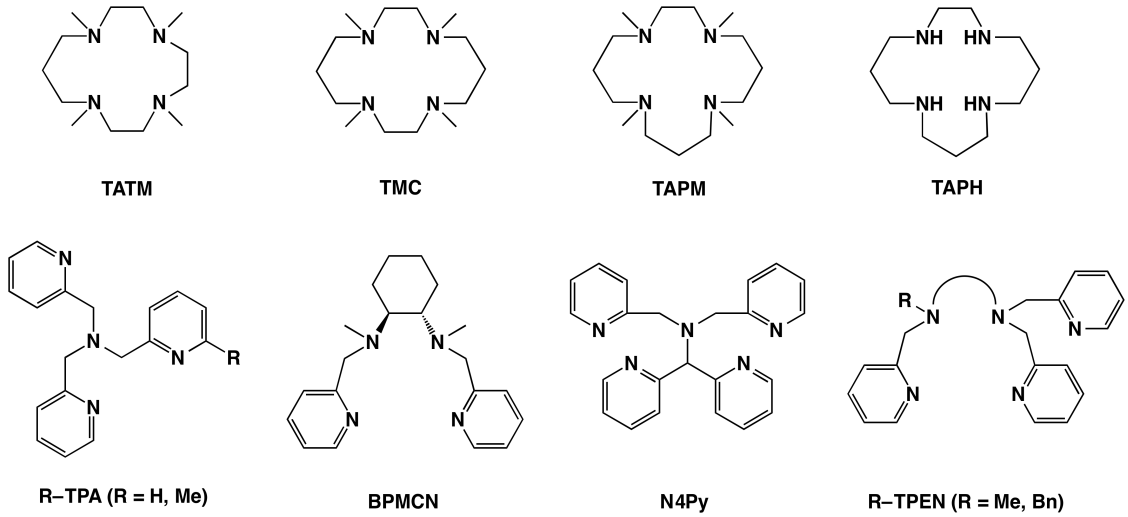

Figure 3. Structure of various nonheme ligands.

A number of nonheme iron(IV)-oxo complexes bearing tetradentate N4 and pentadentate N5 and N4S ligands have so far been synthesized (Figure 3) and characterized with various spectroscopic methods including X-ray crystallography.[10,15-21] Over the past decades, the reactivities of the biomimetic iron(IV)-oxo complexes have been extensively investigated in various oxidation reactions, such as C–H bond activation, oxidation of olefins, alcohols, sulfides, and aromatic compounds, and *N*-dealkylation (Figure 4).[15-21] It has been demonstrated that the reactivities of the iron(IV)-oxo species are markedly affected by supporting and axial ligands, solvent systems, and other conditions.[22-26] Understanding factors that

control reactivities of nonheme iron complexes in oxidation reactions is of significant importance in designing efficient biomimetic catalysts with high reactivity and selectivity.

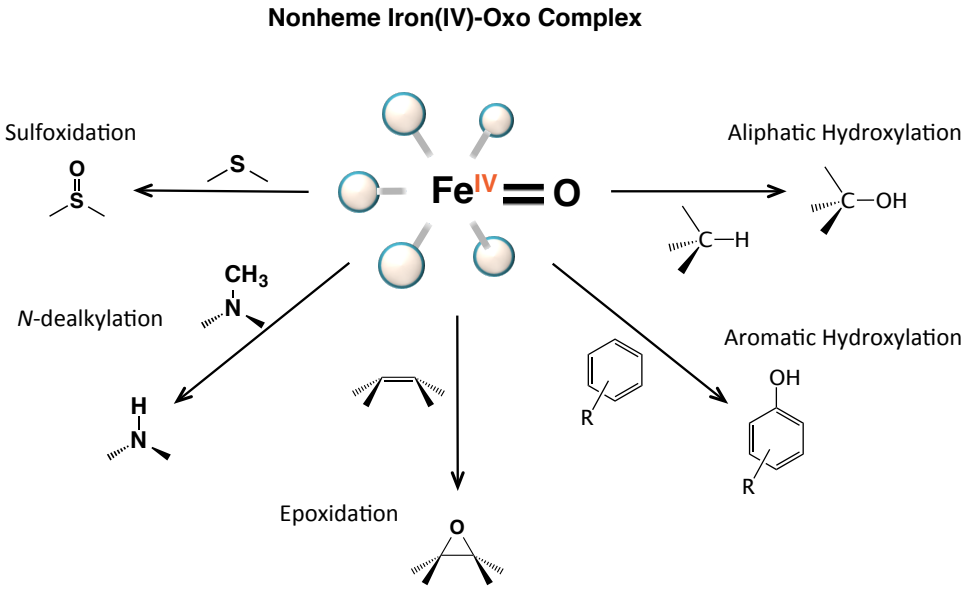

Figure 4. Oxidation reactions mediated by mononuclear nonheme iron(IV)-oxo complexes.

The reactivities of the iron(IV)-oxo species can also be affected by their interaction with Lewis acids, i.e. metal ions.[27] A metal ion binding to oxygen and nitrogen atoms of C=O and C=N bonds has been reported to enhance their electron-acceptor ability.[28-33] Such enhancement of the electron-acceptor ability can be expected not only for organic compounds with carbon-oxygen double bonds (C=O) but also for high-valent metal-oxo species with metal-oxygen double bonds (M=O). [28-33] The binding of Lewis acids to high-valent metal-oxo species has been proposed to enhance the catalytic activity of high-valent metal-oxo species in natural systems.[34]

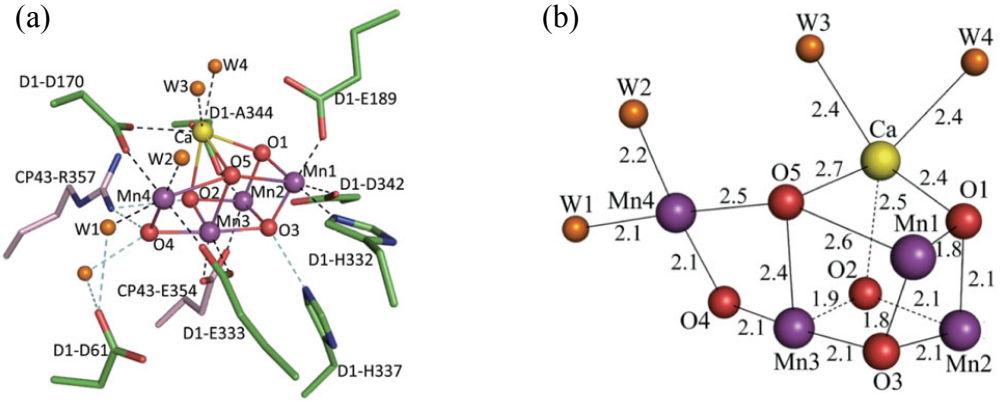

Figure 5. (a) Stereo view of the Mn_4CaO_5 cluster. (b) X-ray crystal structure of Mn_4CaO_5 cluster.[40]

The metal-oxo cluster, Mn_4O_5, with one Ca^{2+} ion which is located in the oxygen-evolving complex (OEC) in photosystem II (PS II) in nature (Figure 5) catalyzes biological water oxidation.[35-40] To understand the catalytic function of the cluster for water oxidation, the structure of cluster and the mechanism of water oxidation have been investigated in various ways, such as synthesis, computation, X-ray crystallography and so on. [35-40] It should be noted that the Ca^{2+} ion has been identified as an essential cofactor in the OEC. [35-41] Unfortunately, the function of Ca^{2+} ion in OEC has yet to be clarified. However, The synthesis of potentially biomimetic manganese oxide clusters as chemical models of the OEC has merited increasing attention.[42-47] The rational synthesis of a $[Mn_3CaO_4]^{6+}$ cubane that structurally models the trimanganese-calcium–cubane subsite of the OEC has recently been reported by Agapie and coworkers.[48] Structural and electrochemical comparison between Mn_3CaO_4 and a related Mn_4O_4 cubane alongside characterization of an intermediate calcium-manganese multinuclear complex has revealed the potential roles of calcium in facilitating high oxidation states at manganese and in the assembly of the biological cluster. [48]

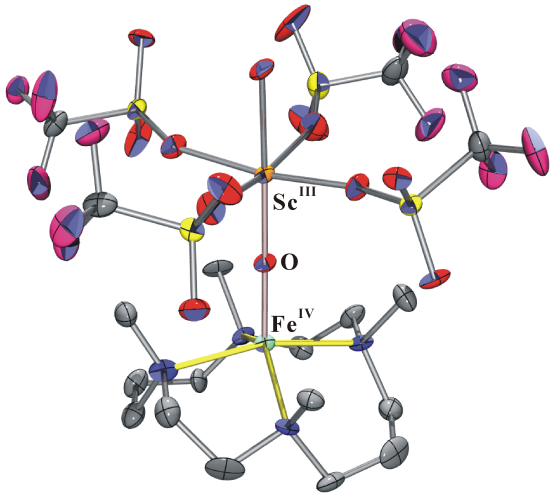

Figure 6. X-ray crystal structure of Sc^{3+} ion bound $[(TMC)Fe^{IV}(O)]^{2+}$.[49]

Binding of a redox-inactive metal ion acting as a Lewis acid to a high-valent metal-oxo complex has been demonstrated for the first time by the crystal structure of a Sc^{3+} ion–bound nonheme iron(IV)-oxo complex, $[(TMC)Fe^{IV}(O)]^{2+}$ (Figure 6).[49] The binding of Sc^{3+} to $[(TMC)Fe^{IV}(O)]^{2+}$ resulted in change in the number of electrons transferred from ferrocene (Fc) to $[(TMC)Fe^{IV}(O)]^{2+}$ in a solution: two-electron reduction of $[(TMC)Fe^{IV}(O)]^{2+}$ by Fc occurs with Sc^{3+} binding, whereas only

single-electron reduction of $[(TMC)Fe^{IV}(O)]^{2+}$ by Fc occurs in the absence of Sc^{3+}.[48] The change in the number of electrons transferred form Fc to $[(TMC)Fe^{IV}(O)]^{2+}$ in the presence of redox-inactive Sc^{3+} ion is brought about by binding of Sc^{3+} to the oxo group. This implies a possible key role that the auxiliary Lewis acid metal ion could play in the manganese cluster in photosystem II.[50]

Such control of the electron–transfer reactivity via metal-ion binding has been a general phenomenon when metal ions bind to the one–electron reduced species of electron acceptors.[51-61] Binding redox inactive metal ions to electron acceptors results in a positive shift of the one-electron reduction potentials of electron acceptors, because the binding of metal ions to the one-electron reduced species, *i.e.*, the radical anions of electron acceptors, is stronger as compared to the electron acceptors due to stronger electrostatic interaction.[62-67] Thus, endergonic electron transfer from electron donors (D) to electron acceptors (A) without metal ions has often been made possible in the presence of metal ions by strong binding of metal ions to the radical anions ($A^{\bullet-}$).[60-64] Such electron transfer involving metal ion binding is defined as metal ion-coupled electron transfer (MCET).[63]

Scheme1.

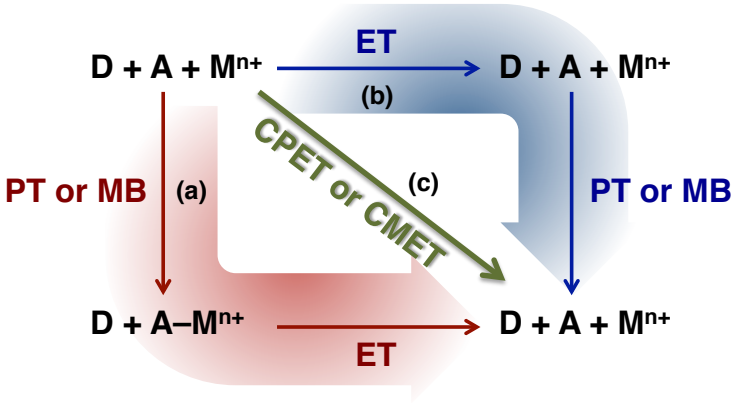

There are difference types of mechanisms of MCET as shown in scheme 1; (a) binding of metal ions (M^{n+}) to A followed by electron transfer from D to $A–M^{n+}$ (MBET), electron transfer from D to $A–M^{n+}$ occur when M^{n+} binding to A,[63] (b) electron transfer from D to A followed by M^{n+} binding to $A^{\bullet-}$ (ETMB), and (c) binding of M^{n+} to A and electron transfer from D to A occurs in a concerted manner.[68]

Rates of electron transfer from a series of one-electron reductants to an iron(IV)-oxo complex, $[(N4Py)Fe^{IV}(O)]^{2+}$ (N4Py: *N*,*N*-bis(2-pyridylmethyl)-*N*-bis(2-pyridyl)methyl amine), are enhanced as much as 10^8-fold in the presence of metal ions, such as Sc^{3+}, Zn^{2+}, Mg^{2+} and Ca^{2+}, as compared with the rates in the absence of metal ions.[69] The rate enhancement by metal ions exhibits a good correlation with the Lewis acidity of metal ions. The one-electron reduction potential of $[(N4Py)Fe^{IV}(O)]^{2+}$ has been demonstrated to be shifted in a positive direction by as much as 0.84 V in the presence of Sc^{3+} ions.[69] These results indicate a possible key role of the auxiliary Lewis acid in the manganese cluster of OEC in photosystem II.

Not only metal ions but also Brønsted acids, such as perchloric acid ($HClO_4$) and triflic acid (HOTf), are known to accelerate electron transfer from various electron donors to electron acceptors when the radical anions, which are based, are protonated or bound to metal ions (Lewis acids). However, the acceleration effects of metal ions and protons on reactivity of high-valent metal-oxo complexes toward various substrates in relation with the metal ion–coupled electron transfer (MCET) and proton coupled electron transfer (PCET) have yet to be clarified.

In this thesis, remarkable acceleration effects of Lewis acids, such as a $Sc(OTf)_3$ ($OTf = CF_3SO_3^-$), perchloric acid ($HClO_4$) and triflic acid (HOTf), on the reactivity of a nonheme iron(IV)-oxo complex, $[(N4Py)Fe^{IV}(O)]^{2+}$ toward various organic substrates such as thioanisole derivatives and toluene derivatives have been systematically investigated in relation with the MCET and PCET reactions of $[(N4Py)Fe^{IV}(O)]^{2+}$. Chapter 1 describes the switch of a reaction mechanism from direct oxygen atom transfer to MCET by the addition of a metal ion (Sc^{3+} ion) to the reaction system of sulfoxidation of thioanisole derivatives by a $[(N4Py)Fe^{IV}(O)]^{2+}$. In Chapter 2, the mechanism of oxidative dimerization and *N*-demethylation of *N*,*N*-dimethylaniline, which was enhanced in the presence of Sc^{3+} ions, has been clarified. Chapter 3 describes a PCET pathway for sulfoxidation of thioanisole derivatives by $[(N4Py)Fe^{IV}(O)]^{2+}$. In Chapter 4, remarkable acceleration effects of $HClO_4$ on the reactivity of $[(N4Py)Fe^{IV}(O)]^{2+}$ in the C–H bond cleavage of toluene derivatives are shown to result from PCET from toluene derivatives to protonated $Fe^{IV}(O)$ species with no deuterium kinetic isotope effect. The reactivity of $[(N4Py)Fe^{IV}(O)]^{2+}$ in the oxidation of toluene and thioanisole derivatives in the presence of HOTf and $Sc(OTf)_3$ has been well analyzed as unified PCET and MCET driving force dependence of the rate constants of PCET and MCET pathways in light of the Marcus theory of electron

transfer (Chapter 5). Such a unified PCET driving force dependence of the rate constant is also applied for oxidation of styrene derivatives by $[(N4Py)Fe^{IV}(O)]^{2+}$ (Chapter 6).

References

(1) Nelson, D. R.; Koymans, L.; Kamimataki, T.; Stegeman, J. J.; Feyereisen, R.; Waxman, D. J.; Waterman, M. R.; Gotoh, O.; Coon, M. J.; Estabrook, R. W.; Gunsalus, I. C.; Nebert, D. W. *Pharmacogenetics*, **1996**, *6*, 1.

(2) (a) Ortiz de Montelloano, P. R. *Cytochrome P450: Structure, Mechanism and biochemistry*, 3rd ed.; Kluwer Academic/Plenum Publisher: New York, **2005**. . (b) Meunier, B., Ed. *Biomimetic Oxidations Catalyzed by Transition Metal Complexes*; Imperial College Press: London, 2000. (c) *The Ubiquitous Role of Cytochrome P450 Proteins In Metal Ions in Life Sciences*; Sigel, A., Sigel, H., Sigel, R. K. O., Eds.; John Wiley & Sons Ltd: Chichester, England, 2007; Vol. 3.

(3) Ullrich, V. *Topics in Current Chemistry*, **1979**, *83*, 67.

(4) Dnisov, I. G.; Makris, T. M.; Sligar, S. G.; Schilchting, I. *Chem. Rev*. **2005**, *105*, 2253.

(5) Meunier, B.; de Visser, S. P.; Shaik, S. *Chem. Rev*. **2004**, *104*, 3947.

(6) Abu-Omar, M. M.; Loaiza, A.; Hontzeas, N. *Chem. Rev*. **2005**, *105*, 2227.

(7) Costas, M.; Mehn, M. P.; Jensen, M. P.; Que, L. Jr. *Chem. Rev*. **2004**, *104*, 939.

(8) Taube, H. *J. Gen. Physiol*. **1965**, *49*, 29.

(9) Groves, J. T. *J. Inorg. Biochem*. **2006**, *100*, 434.

(10) Shan, X.; Que, L. Jr. *J. Inorg. Biochem.* **2006**, *100*, 421.

(11) Kryatov. S. V.; Rybak-Akomova, E. V.; Schindler, S. *Chem. Rev*. **2005**, *105*, 2175.

(12) Bollinger, J. M., Jr.; Krebs, C. *J. Inorg. Biochem*. **2006**, *100*, 586.

(13) Hoffart, L. M.; Barr, E. W.; Guyer, R. B.; Bollinger, J. M., Jr.; Krebs, C. *Proc. Natl. Acad. Sci. U. S. A*. **2006**, *103*, 4738.

(14) Galonic, D. P.; Barr, E. W.; Walshm C. T.; Bollinger, J. M., Jr.; Krebs, C. *Nat. Chem. Biol*. **2007**, *3*, 113.

(15) Rohde, J.-U.; In, J.-H.; Lim, M. H.; Brennessel, W. W.; Bukowski, M. R.; Stubna, A.; Münck, E.; Nam, W.; Que, L., Jr. *Science*, **2003**, *299*, 1037.

(16) Lim, M. H.; Rohde, J.-U.; Stubna, A.; Bukowski, M. R.; Cosras, M.; Ho, R. Y. N.; Münck, E.; Nam, W.; Que, L., Jr. *Proc. Natl. Acd. Sci. U. S. A*. **2003**, *100*, 3665.

(17) (a) Kaizer, J.; Klinker, E. J.; Oh, N. Y. Rohde, J.-U.; Song, W. J.; Stubna, A.; Kim, J.; Münck, E.; Nam, W.; Que, L., Jr. *J. Am. Chem. Soc*. **2004**, *126*, 472. (b) Sastri, C. V.; Seo, M. S.; Park, M. J.; Kim, K. M.; Nam, W. *Chem. Commun*. **2005**, 1405. (c) Kim, S. O.; Sastri, C. V.; Seo, M. S.; Kim, J.; Nam, W. *J. Am. Chem. Soc*. **2005**, *127*, 4179.

(18) (a) Oh N. Y.; Suh, Y. Park, M. J.; Seo, M. S.; Kim, J.; Nam, W. *Angew. Chem., Int. Ed.* **2005**, *44*, 4235. (b) Sastri, C. V.; Park, M. J.; Ohta, T.; Jackson, T. A.; Stubna, A.; Seo, M. S.; Lee, J.; Kim, J.; Kitagawa, T.; Münck, E.; Que, L., Jr.; Nam, W. *J. Am. Chem. Soc*. **2005**, *127*, 12494.

(19) Bukowski, M. R.; Koehntop, K. D.; Stubna, A.; Bominaar, E. L.; Halfen, J. A.; Münck, E.; Nam, W.; Que, L., Jr. *Science* **2005**, *310*, 1000.

(20) (a) Klinker, E. J.; Kaizer, J.; Brennessel, W. W.; Woodrum, N. L.; Cramer, C. J.; Que, L., Jr. *Angew. Chem., Int. Ed*. **2005**, *44*, 3690. (b) Sastri, C. V.; Oh, K.; Lee, Y. J.; Seo, M. S.; Shin, W.; Nam, W. *Angew. Chem., Int. Ed*. **2006**, *45*, 3992. (c) Suh, Y.; Seo, M. S.; Kim, K. M.; Kim, Y. S.; Jang, H. G.; Tosha, T.; Kitagawa, T.; Kim, J.; Nam, W. J. *Inorg. Biochem*. **2006**, *100*, 627.

(21) (a) Nehru, K.; Seo, M. S.; Kim, J.; Nam, W. *Inorg. Chem*. **2007**, *46*, 293. (b) Balland, V.; Charlot, M.-F.; Banse, F.; Girerd, J.-J.; Mattioli, T. A.; Bill, E.; Bartoli, J.-F.; Battioni, P.; Mansuy, D. *Eur, J. Inorg. Chem*. **2004**, 301. (c) Martinho, M.; Banse, F.; Bartoli, J.-F.; Mattioli, T. A.; Battioni, P.; Horner, O.; Boucier, S.; Girerd, J.-J. *Inorg. Chem*. **2005**, *44*, 9592.

(22) (a) Groves, J. T.; Shalyaev, K.; Lee, J. In *The Porphyrin Handbook*; Kadish, K. M., Smith, K. M., Guilard, R., Eds.; Academic Press: Elsevier Science (USA), 2000, Vol. 4, pp 17-40. (b) Watanabe, Y. In *The Porphyrin Handbook*; Kadish, K. M., Smith, K. M., Guilard, R., Eds.; Academic Press: Elsevier Science (USA), 2000, Vol. 4, pp 97-117. (c) Groves, J. T. *J. Inorg. Biochem*. **2006**, *100*, 434.

(23) (a) Meunier, B.; de Visser, S. P.; Shaik, S. *Chem. Rev.* **2004**, *104*, 3947. (b)

Shaik, S.; Cohen, S.; Wang, Y.; Chen, H.; Kumar, D.; Thiel, W. *Chem. Rev*. **2010**, *110*, 949. (c) Abu-Omar, M. M.; Loaiza, A.; Hontzeas, N. *Chem. Rev.* **2005**, *105*, 2227. (d) Denisov, I. G.; Makris, T. M.; Sligar, S. G.; Schlichting, I. *Chem. Rev.* **2005**, *105*, 2253. (e) Ortiz de Montellano, P. R. *Chem. Rev*. **2010**, *110*, 932.

(24) (a) Krebs, C.; Fujimori, D. G.; Walsh, C. T.; Bollinger, J. M., Jr. *Acc. Chem. Res.* **2007**, *40*, 484. (b) Que, L., Jr. *Acc. Chem. Res*. **2007**, *40*, 493. (c) Nam, W. *Acc. Chem. Res.* **2007**, *40*, 522. (d) Borovik, A. S. *Acc. Chem. Res.* **2005**, *38*, 54. (e) Shaik, S.; Lai, W.; Chen, H.; Wang, Y. *Acc. Chem. Res*. **2010**, *43*, 1154.

(25) (a) Comba, P.; Kerscher, M.; Schiek, W. *Prog. Inorg. Chem.* **2007**, *55*, 613. (b) Bakac, A. *Coord. Chem. Rev.* **2006**, *250*, 2046. (c) Espenson, J. H. *Coord. Chem. Rev.* **2005**, *249*, 329. (d) Fujii, H. *Coord. Chem. Rev*. **2002**, *226*, 51.

(26) (a) Costas, M.; Mehn, M. P.; Jensen, M. P.; Que, L., Jr. *Chem. Rev*. **2004**, *104*, 939. (b) Tshuva, E. Y.; Lippard, S. J. *Chem. Rev*. **2004**, *104*, 987. (c) Que, L., Jr.; Ho, R. Y. N. *Chem. Rev*. **1996**, *96*, 2607. (d) Solomon, E. I.; Brunold, T. C.; Davis, M. I.; Kemsley, J. N.; Lee, S.-K.; Lehnert, N.; Neese, F.; Skulan, A. J.; Yang, Y.-S.; Zhou, J. *Chem. Rev*. **2000**, *100*, 235. (e) Decker, A.; Solomon, E. I. *Curr. Opin. Chem. Biol*. **2005**, *9*, 152.

(27) (a) Yiu, S.-M.; Man, W.-L.; Lau, T.-C. *J. Am. Chem. Soc.* **2008**, *130*, 10821. (b) Lam, W. W. Y.; Yiu, S.-M.; Lee, J. M. N.; Yau, S. K. Y.; Kwong, H.-K.; Lau, T.-C.; Liu, D.; Lin, Z. *J. Am. Chem. Soc.* **2006**, *128*, 2851. (c) Yiu, S.-M.; Wu, Z.-B.; Mak, C.-K.; Lau, T.-C. *J. Am. Chem. Soc.* **2004**, *126*, 14921. (d) Miller, C. G.; Gordon-Wylie, S. W.; Horwitz, C. P.; Strazisar, S. A.; Peraino, D. K.; Clark, G. R.; Weintraub, S. T.; Collins, T. J. *J. Am. Chem. Soc.* **1998**, *120*, 11540.

(28) (a) *Selectivities in Lewis Acid Promoted Reactions*; Schinzer, D. Ed.; Kluwer Academic: Dordrecht, 1989. (b) *Lewis Acids in Organic Synthesis*; Yamamoto, H. Ed.; Wiley-VCH: Weinheim, 2000. (c) Abell, J. P.; Yamamoto, H. *Chem. Soc. Rev*. **2010**, *39*, 61.

(29) (a) Kobayashi, S.; Ishitani, H. *Chem. Rev.* **1999**, *99*, 1069. (b) Akiyama, R.; Kobayashi, S. *Chem. Rev*. **2009**, *109*, 594. (c) Kobayashi, S.; Yamashita, Y. *Acc. Chem. Res*. **2011**, *44*, 58.

(30) (a) Johnson, J. S.; Evans, D. A. *Acc. Chem. Res*. **2000**, *33*, 325. (b) Rovis, T.;

Evans, D. A. *Prog. Inorg. Chem*. **2001**, *50*, 1.

(31) (a) Pohlhaus, P. D.; Bowman, R. K.; Johnson, J. S. *J. Am. Chem. Soc.* **2004**, *126*, 2294. (b) Fukuzumi, S.; Fujita, M.; Otera, J.; Fujita, Y. *J. Am. Chem. Soc.* **1992**, *114*, 10271.

(32) (a) Mukaiyama, T.; Ishida, A. *Chem. Lett*. **1975**, 319. (b) Ishida, A.; Mukaiyama, T. *Chem. Lett*. **1975**, 1167. (c) Ishida, A.; Mukaiyama, T. *Bull. Chem. Soc. Jpn*. **1977**, *50*, 1161. (d) Ishida, A.; Mukaiyama, T. *Chem. Lett*. **1977**, 467. (e) Ishida, A.; Mukaiyama, T. *Bull. Chem. Soc. Jpn*. **1978**, *51*, 2077. (f) Mukaiyama, T.; Ishida, A. *Chem. Lett*. **1975**, 1201.

(33) (a) Casiraghi, G.; Battistini, L.; Curti, C.; Rassu, G.; Zanardi, F. *Chem. Rev*. **2011**, *111*, 3076. (b) Denmark, S. E.; Heemstra, J. R., Jr.; Beutner, G. L. *Angew. Chem., Int. Ed.* **2005**, *44*, 4682. (c) Casiraghi, G.; Zanardi, F.; Appendino, G.; Rassu, G. *Chem. Rev.* **2000**, *100*, 1929. (d) Kalesse, M. *Top. Curr. Chem*. **2005**, *244*, 43.

(34) (a) Pecoraro, V. L.; Baldwin, M. J.; Caudle, M. T.; Hsieh, W.; Law, N. A. *Pure Appl. Chem*. **1998**, *70*, 925. (b) Limburg, J.; Szalai, V. A.; Brudvig, G. W. *J. Chem. Soc. Dalton Trans.* **1999**, 1353. (c) Cady, C. W.; Crabtree, R. H.; Brudvig, G. W. *Coord. Chem. Rev.* **2008**, *252*, 444.

(35) Najafpour, M. M.; Moghaddam, A. N.; Allakhverdiev, S. I.; Govindjee, *Biochim. Biophys. Acta Bioenerg.* **2012**, *1817*, 1110.

(36) Loll, B.; Kern, J.; Saenger, W.; Zouni, A. Biesiadka, J. *Nature* **2005**, *438*, 1040.

(37) (a) Aromi, G.; Brechin, E. K. *Struct. Bonding* **2006**, *122*, 1. (b) Bagai, R.; Christou, G. *Chem. Soc. Rev.* **2009**, *38*, 1011.

(38) (a) Mullins, C. S.; Pecoraro, V. L. *Coord. Chem. Rev.* **2008**, *252*, 416. (b) Iwata, S.; Barber, *J. Curr. Opin. Struct. Biol.* **2004**, *14*, 447.

(39) J. Barber, *Philos. Trans. R. Soc. B* **2008**, *363*, 2665.

(40) Umena, Y.; Kawakami, K.; Shen, J.-R.; Kamiya, N. *Nature* **2011**, *473*, 55.

(41) Kawakami, K.; Umena, Y.; Kamiya, N.; Shen, J.-R. *J. Photochem. Photobiol. B* **2011**, *104*, 9.

(42) Dismukes, G. C.; Brimblecombe, R.; Felton, G. A. N.; Pryadun, R. S.; Sheats, J. E.; Spiccia, L.; Swiegers, G. F. *Acc. Chem. Res.* **2009**, *42*, 1935.

(43) Yagi, M.; Kaneko, M. *Chem. Rev.* **2001**, *101*, 21.

(44) (a) McEvoy, J. P.; Brudvig, G. W. *Chem. Rev.* **2006**, *106*, 4455. (b) Sproviero, E. M.; Gascon, J. A.; McEvoy, J. P.; Brudvig, G. W.; Batista, V. S. *J. Am. Chem. Soc.* **2008**, *130*, 3428. (c) Siegbahn, P. E. M. *Acc. Chem. Res.* **2009**, *42*, 1871.

(45) (a) Nayak, S.; Nayek, H. P.; Dehnen, S.; Powell, A. K.; Reedijk, J. *Dalton Trans.* **2011**, *40*, 2699. (b) Kotzabasaki, V.; Siczek, M.; Lis, T.; Milios, C. J. *Inorg. Chem. Commun.* **2011**, *14*, 213. (c) Koumousi, E. S.; Mukherjee, S.; Beavers, C. M.; Teat, S. J.; Christou, G.; Stamatatos, T. C. *Chem. Commun.* **2011**, *47*, 11128.

(46) Mukherjee, S.; Stull, J. A.; Yano, J.; Stamatatos, T. C.; Pringouri, K.; Stich, T. A.; Abboud, K. A.; Britt, R. D.; Yachandra, V. K.; Christou, G. *Proc. Natl. Acad. Sci. U.S.A.* **2012**, *109*, 2257.

(47) Lacy, D. C.; Park, Y. J.; Ziller, J. W.; Yano, J. Borovik, A. S. *J. Am. Chem. Soc.* **2012**, *134*, 17526.

(48) Kanady, J. S.; Tsui, E. Y.; Day, M. W.; Agapie, T. *Science* **2011**, *333*, 733.

(49) Fukuzumi, S.; Morimoto, Y.; Kotani, H.; Naumov, P.; Lee, Y.-M.; Nam, W. *Nat. Chem*. **2010**, *2*, 756.

(50) Karlin, K. D. *Nat. Chem*. **2010**, *22*, 711.

(51) (a) Fukuzumi, S.; Nishizawa,N.; Tanaka, T. *J. Chem. Soc. Perkin Trans. 2* **1985**, *371*. (b) Fukuzumi,S.; Kuroda, S.; Tanaka, T. *J. Am. Chem. Soc.* 1985, *107*, 3020.

(52) (a) Itoh, S.; Taniguchi, M.; Takada, N.; Nagatomo, S.; Kitagawa, T.; Fukuzumi, S. *J. Am. Chem. Soc.* **2000**, *122*, 12087. (b) Fukuzumi, S.; Yasui, K.; Suenobu, T.; Ohkubo, K.; Fujitsuka, M.; Ito, O. *J. Phys. Chem. A* **2001**, *105*, 10501. (c) Fukuzumi, S.; Satoh, N.; Okamoto, T.; Yasui, K.; Suenobu, T.; Seko, Y.; Fujitsuka, M.; Ito, O. *J. Am. Chem. Soc.* **2001**, *123*, 7756.

(53) (a) Fukuzumi, S.; Ohkubo, K.; Okamoto, T. *J. Am. Chem. Soc*. **2002**, *124*, 14147. (b) Fukuzumi, S.; Itoh, S. *Antioxid. Redox Signal*. **2004**, *3*, 807. (c) Fukuzumi, S.; Okamoto, K.; Imahori, H. *Angew. Chem. Int. Ed*. **2002**, *41*, 620. (d) Fukuzumi, S.; Okamoto, K.; Yoshida, Y.; Imahori, H.; Araki, Y.; Ito, O. *J. Am. Chem. Soc*.

2003, *125*, 1007. (e) Okamoto, K.; Imahori, H.; Fukuzumi, S. *J. Am. Chem. Soc.* **2003**, *125*, 7014.

(54) Yuasa, J.; Suenobu, T; Fukuzumi, S. *ChemPhysChem* **2006**, *7*, 942.

(55) Wu, H.; Zhang, D.; Su, L.; Ohkubo, K.; Zhang, C.; Yin, S.; Mao, L.; Shuai, S.; Fukuzumi, S.; Zhu, D. *J. Am. Chem. Soc.* **2007**, *129*, 6839.

(56) Fukuzumi, S.; Ohtsu, H.; Ohkubo, K. *Coord. Chem. Rev.* **2002**, *226*, 71.

(57) Yuasa, J.; Yamada, S.; Fukuzumi, S. *Chem. Eur. J.* **2008**, *14*, 1866.

(58) Tan, L.; Zhang, G.; Zhang, D.; Zhu, D. *J. Org. Chem.* **2011**, *76*, 904.

(59) Kawashima, T.; Ohkubo, K.; Fukuzumi, S. *Phys. Chem. Chem. Phys*. **2011**, *13*, 3344.

(60) Yang, G.; Zhang, G.; Sheng, P.; Sun, F.; Xu, W.; Zhang, D. J. *Mater. Chem*. **2012**, *22*, 4391.

(61) Fukuzumi, S. *Pure Appl. Chem*. **2003**, *75*, 577.

(62) Fukuzumi, S. Kojima, T. *J. Biol. Inorg. Chem*. **2008**, *13*, 321.

(63) Yocum, C. F. *Coord. Chem. Rev*. **2008**, *252*, 296.

(64) (a) Fukuzumi, S. *Prog. Inorg. Chem.* **2009**, *56*, 49. (b) Fukuzumi, S. *Bull. Chem. Soc. Jpn.* **1997**, *70*, 1.

(65) (c) Fukuzumi, S.; Ohkubo, K. *Coord. Chem. Rev.* **2010**, *254*, 372. (d) Fukuzumi, S. *Chem. Lett.* **2008**, *37*, 808.

(66) (a) Fukuzumi, S.; Ohtsu, H.; Ohkubo, K.; Itoh, S.; Imahori, H. *Coord. Chem. Rev.* **2002**, *226*, 71. (b) Fukuzumi, S.; Itoh, S. *Antioxid. Redox Signal.* **2001**, *3*, 807.

(67) (a) Fukuzumi, S. *Pure Appl. Chem.* **2003**, *75*, 577. (b) Fukuzumi, S. ; *Electron Transfer in Chemistry*, vol. 4, ed. V. Balzani; Wiley-VCH: Weinheim, Germany, 2001, pp. 3–59.

(68) Fukuzumi, S.; Ohkubo, K.; Morimoto, Y. *Phys. Chem. Chem. Phys*. **2012**, *14*, 8472.

(69) Morimoto, Y.; Kotani, H.; Park, J.; Lee, Y.-M.; Nam, W.; Fukuzumi, S. *J. Am Chem. Soc*. **2011**, *133*, 403.

Chapter 1. Metal Ion Effect on the Switch of Mechanism form Direct Oxygen Transfer to Metal Ion–Coupled Electron Transfer in the Sulfoxidation of Thioanisoles by a Nonheme Iron(IV)-Oxo Complex

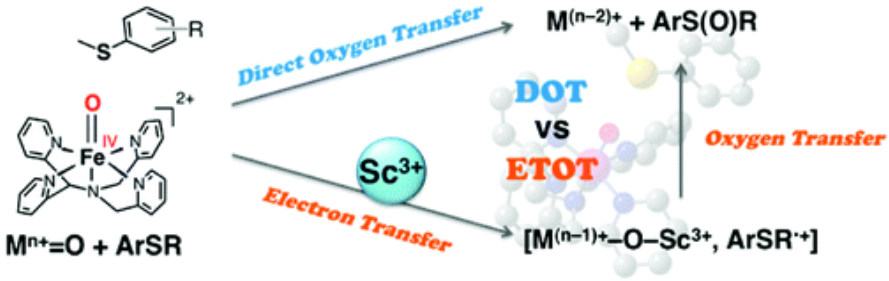

Abstract: The mechanism of sulfoxidation of thioaniosoles by a nonheme iron(IV)-oxo complex is switched from direct oxygen transfer to metal ion–coupled electron transfer by the presence of scandium ion, Sc^{3+}; the switch of the sulfoxidation mechanism is dependent on one-electron oxidation potentials of thioanisoles. The rate of sulfoxidation is accelerated as much as 10^2-fold by the addition of Sc^{3+}.

Introduction

Oxygen atom transfer from high-valent metal-oxo species to organic or inorganic substrates is ubiquitous in biological and catalytic oxygenation processes.[1] Extensive efforts have been devoted to clarify mechanisms of the oxygen atom transfer reactions by iron(IV)-oxo complexes bearing heme and nonheme ligands as chemical models of cytochromes P450 (CYP 450) and nonheme iron oxygenases, respectively.[2] In sulfoxidation reactions, two plausible mechanisms have been proposed for the oxidation of sulfides by high-valent metal-oxo complexes,[3-5] such as direct oxygen transfer (DOT) and electron transfer followed by oxygen transfer (ETOT). Sulfoxide (ArS(O)R) is formed either by the direct oxygen atom transfer from a metal-oxo species ($M^{n+}(O)$) to sulfide (ArSR) or by the electron transfer from ArSR to $M^{n+}(O)$ followed by the oxygen atom transfer from $M^{(n-1)+}(O)$ to the radical cation ($ArSR^{\bullet+}$).

Although mechanisms of the oxidation of sulfides by high-valent iron-oxo intermediates of CYP 450 and model compounds have been extensively investigated experimentally and theoretically,[4,6] nonheme iron(IV)-oxo species have been rarely explored in the mechanistic studies of sulfoxidation reactions.[7] We report herein remarkable effects of a metal ion (i.e., Sc^{3+}) on the acceleration of the reaction rate and the change of the mechanism from DOT to ETOT in the sulfoxidation of thioanisoles by a nonheme iron(IV)-oxo complex, $[(N4Py)Fe^{IV}(O)]^{2+}$ (N4Py = *N*,*N*-bis(2-pyridyl methyl)-*N*-bis(2-pyridyl)methylamine).[8-10] The role of the metal ion on the sulfoxidation reactions has been discussed as well.

Experimental Section

Materials and Reaction Conditions. Commercially available chemicals were used without further purification unless otherwise indicated. Solvents were dried according to published procedures and distilled under Ar prior to use.[11] N4Py (*N*,*N*-bis(2-pyridyl-methyl)-*N*-bis(2-pyridyl)methylamine) ligand, $[(N4Py)Fe^{II}(CH_3CN)](ClO_4)_2$ complex and its oxoiron(IV) species, $[(N4Py)Fe^{IV}(O)]^{2+}$, were prepared by literature methods.[12] Thioanisole derivatives and scandium triflate, $Sc^{III}(OTf)_3$ (OTf = $CF_3SO_3^-$), were purchased from Aldrich Chemical Co. and used as received. One-electron reductants, $[Ru^{II}(bpy)_3](PF_6)_2$ (bpy = 2,2'-bipyridine), $[Ru^{II}(Me_2bpy)_3](PF_6)_2$ (Me_2bpy = 4,4'-dimethyl-2,2'-bipyridine), $[Fe^{II}(bpy)_3](PF_6)_2$, $[Fe^{II}(Ph_2phen)_3](PF_6)_2$ (Ph_2phen =

4,7-diphenyl-1,10-phenanthroline), and $[Fe(Clphen)_3](PF_6)_2$ (Clphen = 5-chloro-1,10-phenanthroline) were prepared according to the published procedures.[13]

Instrumentation. UV/Vis spectra were recorded on a Hewlett Packard Agilent 8453 UV-visible spectrophotometer equipped with a circulating water bath or an UNISOKU RSP-601 stopped-flow spectrometer equipped with a MOS-type highly sensitive photodiode-array in CH_3CN at 298 K. Product analysis was performed with a Bruker model digital AVANCE III 400 FT-NMR spectrometer.

Kinetic Studies and Product Analysis. Kinetic measurements of sulfoxidation of thioanisoles by $[(N4Py)Fe^{IV}(O)]^{2+}$ were performed on a Hewlett Packard 8453 spectrophotometer or an UNISOKU RSP-601 stopped-flow spectrometer in MeCN at 298 K. Rates of sulfoxidation of thioanisoles by $[(N4Py)Fe^{IV}(O)]^{2+}$ were monitored by the decay of absorption bands at 695 nm due to $[(N4Py)Fe^{IV}(O)]^{2+}$. All kinetic measurements were carried out under pseudo-first-order conditions where the concentrations of thioanisoles were maintained to be more than 10-folds excess of that of $[(N4Py)Fe^{IV}(O)]^{2+}$ (2.0×10^{-4} M or 5.0×10^{-4} M) in the presence of Sc^{3+} (0 - 5.0×10^{-2} M).

Kinetic measurements of electron transfer (ET) from one-electron reductants to $[(N4Py)Fe^{IV}(O)]^{2+}$ in the presence of Sc^{3+} were also performed on a Hewlett Packard 8453 spectrophotometer or an UNISOKU RSP-601 stopped-flow spectrometer in CH_3CN at 298 K. These ET reactions were monitored by the decay of absorption band at 695 nm due to $[(N4Py)Fe^{IV}(O)]^{2+}$. Typically, a deaerated MeCN solution containing $[(N4Py)Fe^{IV}(O)]^{2+}$ (2.0×10^{-4} M) was injected with a microsyringe to a deaerated MeCN solution (2 mL) containing one electron reductants (2.0 - 8.0×10^{-3} M) in the presence of Sc^{3+} (0 - 5.0×10^{-2} M). All kinetic measurements were carried out under pseudo-first-order conditions where the concentrations of one electron reductants were maintained to be more than 10-folds excess of that of $[(N4Py)Fe^{IV}(O)]^{2+}$ (2.0×10^{-4} M) in the presence of Sc^{3+} (0 - 5.0×10^{-2} M).

Products formed in sulfoxidation reactions of thioanisole by $[(N4Py)Fe^{IV}(O)]^{2+}$, which were carried out in the absence and presence of Sc^{3+} under Ar atmosphere in CD_3CN at 298 K, were analyzed by ^1H NMR spectroscopy. Quantitative analyses were made on the basis of comparison of NMR peak integration between products and authentic samples. Methyl phenyl sulfoxide was obtained as a sole product with 96 %

and 94 % of yield (based on the intermediate generated) in the absence and presence of Sc^{3+} (10 mM), respectively.

Results and Discussion

Sulfoxidaton of *para*-substituted thioanisoles by $[(N4Py)Fe^{IV}(O)]^{2+}$ has been suggested to occur via an electrophilic reaction, giving the corresponding methyl phenyl sulfoxides and Fe^{II} complex quantitatively as products.[7] As shown in Figure 1a, the time course of the reaction of $[(N4Py)Fe^{IV}(O)]^{2+}$ with *p*-methylthioanisole was readily monitored by the decrease in absorbance due to $[(N4Py)Fe^{IV}(O)]^{2+}$ (λ_{max} = 695 nm).[8] In the presence of $Sc(OTf)_3$ (scandium triflate, OTf = $CF_3SO_3^-$), the reaction was remarkably accelerated and the time course was monitored by a stopped-flow spectrometer (Figure 1b).[10] The rate obeyed pseudo-first-order kinetics (Figure 2), and the pseudo-first-order rate constant increased linearly with increasing concentration of *p*-methylthioanisole (Figure 3). The second-order rate constants (k_{obs}) were obtained from the slope of the linear correlation between the pseudo-first-order rate constant and concentration of *p*-methylthioanisole.

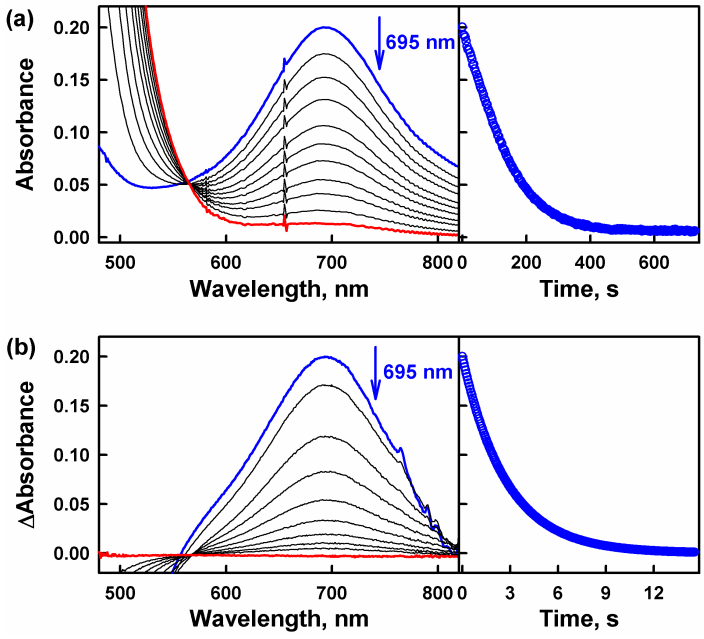

Figure 1. Visible spectral changes observed in the sufoxidation of *p*-methylthioanisole (5.0 mM) by $[(N4Py)Fe^{IV}(O)]^{2+}$ (0.50 mM) in the (a) absence and (b) presence of Sc^{3+} (10 mM) in MeCN at 298 K (left panels). Right panels show time courses monitored at 695 nm.

The dependence of k_{obs} on $[Sc^{3+}]$ for the sulfoxidation of *p*-methylthioanisole by $[(N4Py)Fe^{IV}(O)]^{2+}$ is shown in Figure 4a. The k_{obs} value increased with increasing $[Sc^{3+}]$, exhibiting a first-order dependence on $[Sc^{3+}]$ at low concentrations, whereas a second-order dependence was observed at high concentrations (eq 1):

$$k_{obs} = k_0 + [Sc^{3+}](k_1 + k_2[Sc^{3+}]) \quad (1)$$

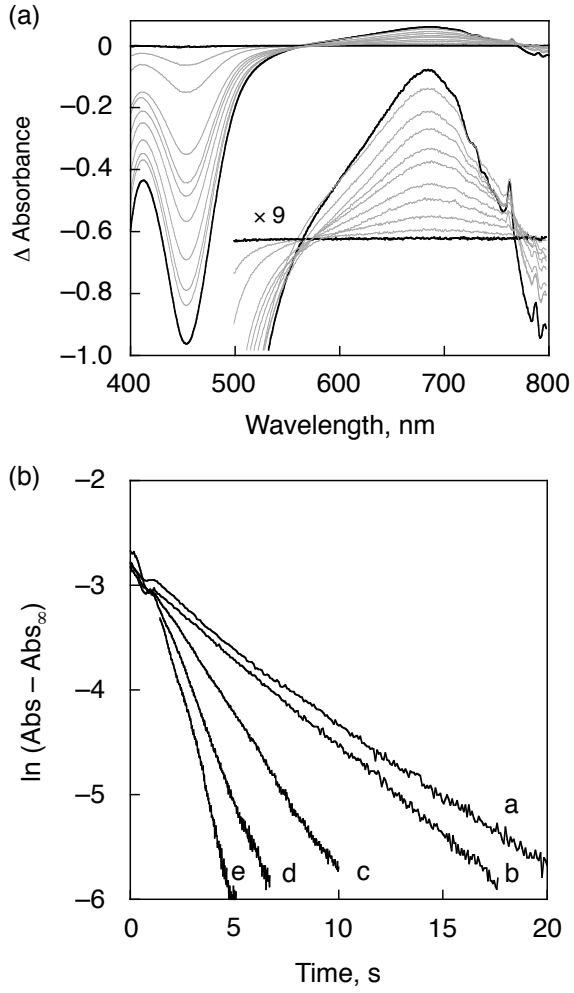

Figure 2. (a) UV-vis spectral changes in the sulfoxidation of *p*-methylthioanisole (2.0×10^{-3} M) by $[(N4Py)Fe^{IV}(O)]^{2+}$ (2.0×10^{-4} M) in presence of Sc^{3+} (1.0×10^{-2} M) in MeCN at 298 K. (b) First-order plots monitored by absorbance decay at 695 nm due to $[(N4Py)Fe^{IV}(O)]^{2+}$ in the sulfoxidation of *p*-methylthioanisole (2.0×10^{-3} M) by $[(N4Py)Fe^{IV}(O)]^{2+}$ (2.0×10^{-4} M) in the presence of various concentrations of Sc^{3+} (a, 5.0×10^{-3}; b, 1.0×10^{-2}; c, 2.0×10^{-2}; d, 3.0×10^{-2}; e, 4.0×10^{-2} M) in MeCN at 298 K.

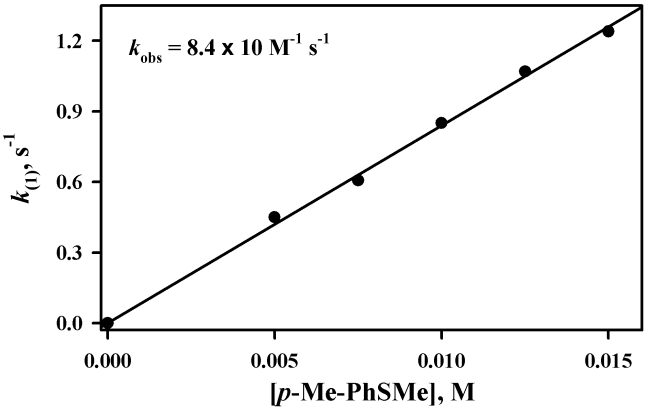

Figure 3. Plot of the first-order rate constant ($k_{(1)}$) vs *p*-methylthioanisole concentration to determine a second-order rate constant (k_{obs}) for the sulfoxidation of *p*-methylthioanisole by $[(N4Py)Fe^{IV}(O)]^{2+}$ (5.0×10^{-4} M) in the presence of Sc^{3+} (1.0×10^{-2} M) in MeCN at 298 K.

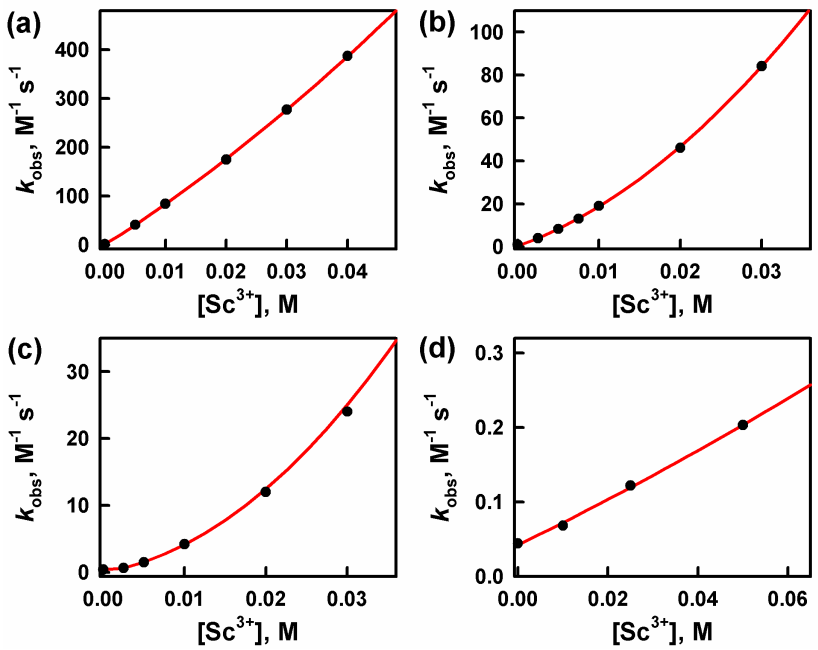

Figure 4. Plots of k_{obs} vs Sc^{3+} concentration in the sulfoxidation of *para*-X-substituted thioanisoles (X = (a) Me, (b) H, (c) Cl, and (d) CN) by $[(N4Py)Fe^{IV}(O)]^{2+}$ in MeCN at 298 K.

where k_0 is the rate constant for the sulfoxidation of *p*-substituted thioanisole derivatives by $[(N4Py)Fe^{IV}(O)]^{2+}$ (5.0×10^{-4} M) in the absence of Sc^{3+}. The k_1 and k_2 values were determined from the intercept and the slope of the linear plot of $(k_{obs} - k_0)/ [Sc^{3+}]$ vs $[Sc^{3+}]$, respectively (Figure 5). The k_{obs} value in the presence of 10 mM of Sc^{3+} is 8.4×10 M^{-1} s^{-1}, which is ~10^2-fold larger than the value determined in the absence of Sc^{3+}. The dependence of the first-order and second-order rate constants on concentration of

Sc^{3+} was reported for metal ion-coupled electron transfer from one-electron reductants to $[(N4Py)Fe^{IV}(O)]^{2+}$, and this was ascribed to binding of one Sc^{3+} ion and two Sc^{3+} ions to $[(N4Py)Fe^{IV}(O)]^{2+}$, respectively.[14-17]

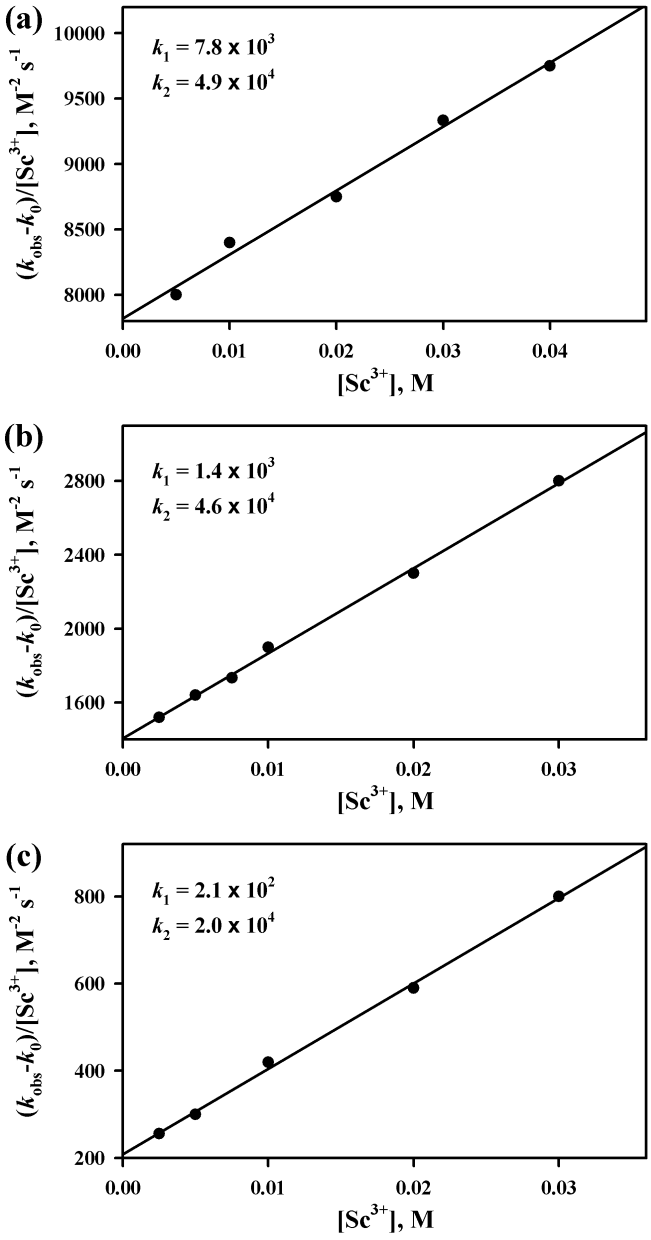

Figure 5. Plot of $(k_{obs}–k_0)/[Sc^{3+}]$ vs $[Sc^{3+}]$ to determine the k_1 and k_2 values from the intercept and the slope of the linear equation, $k_{obs} = k_0 + [Sc^{3+}](k_1 + k_2[Sc^{3+}])$ for the sulfoxidation of *p*-X-substituted thioanisole (X = (a) Me, (b) H, and (c) Cl) by $[(N4Py)Fe^{IV}(O)]^{2+}$ (5.0×10^{-4} M) depending on concentration of Sc^{3+} ($2.5 \times 10^{-3} – 4.0 \times 10^{-2}$ M) in MeCN at 298 K.

Similar remarkable acceleration effects of Sc^{3+} were observed in the sulfoxidation of *para*-X-substituted thioanisoles (X = H, Cl and Br) by $[(N4Py)Fe^{IV}(O)]^{2+}$ (Figure 6). When a strongly electron-withdrawing substituent (X = CN and NO_2) is employed, however, only little acceleration was observed as shown in Figures 2d and 6b, respectively.

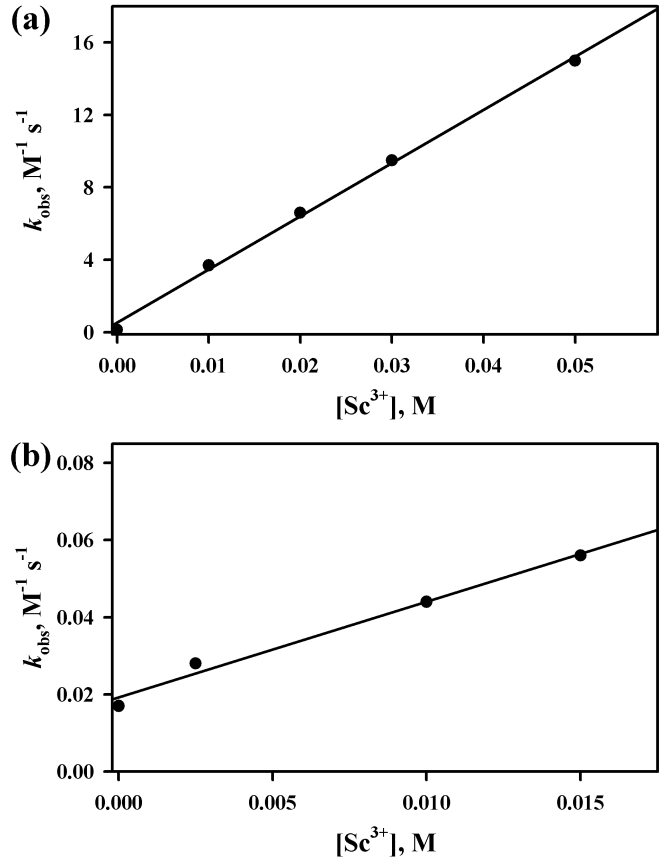

Figure 6. Plots of k_{obs} vs Sc^{3+} concentration in the sulfoxidation of *p*-X-substituted thioanisoles (X = (a) Br and (b) NO_2) by $[(N4Py)Fe^{IV}(O)]^{2+}$ in the presence of Sc^{3+} in MeCN at 298 K.

The reason why the acceleration effect of Sc^{3+} is quite different depending on the substituent X can be explained by plots of log k_{obs} vs the driving force of electron transfer from thioanisols to $[(N4Py)Fe^{IV}(O)]^{2+}$ ($-\Delta G_{et}$) in the absence and presence of Sc^{3+}, as shown in Figure 7. The ΔG_{et} values are obtained from the difference between the one-electron oxidation potentials of thioanisoles (E_{ox} vs SCE)[4a] and the one-electron reduction potentials of $[(N4Py)Fe^{IV}(O)]^{2+}$ (E_{red} vs SCE) in the absence and presence of Sc^{3+}.[14,18] It should be noted that the E_{ox} values of thioanisoles are not changed in the

presence of Sc^{3+}, whereas the E_{red} value of $[(N4Py)Fe^{IV}(O)]^{2+}$ is significantly shifted to the positive direction from 0.51 V vs SCE in the absence of Sc^{3+} to 1.19 V vs SCE in the presence of 10 mM of Sc^{3+}.[14,18a] In the absence of Sc^{3+}, the driving force of electron transfer ($-\Delta G_{et}$) is largely negative. This indicates that electron transfer from thioanisoles to $[(N4Py)Fe^{IV}(O)]^{2+}$ is highly endergonic and therefore it is quite unlikely to occur. In such a case, direct oxygen atom transfer (Scheme 1a) predominates over an electron-transfer pathway (Scheme 1b) and the k_{obs} values are only slightly dependent on the $-\Delta G_{et}$ values.

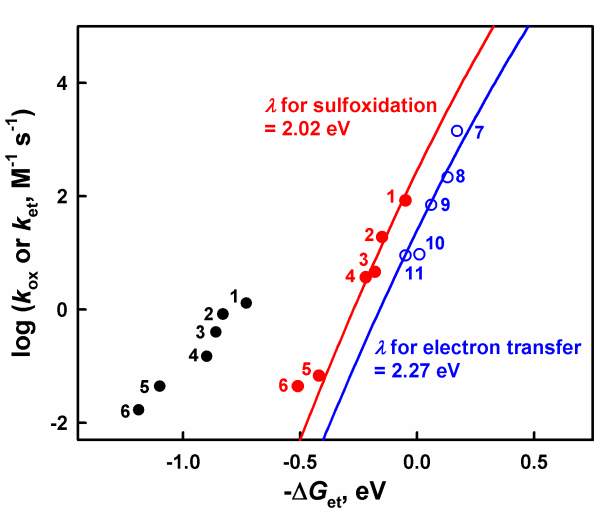

Figure 7. Plot of log k_{obs} for oxidation of *para*-X-substituted thioanisoles (X = Me for 1, H for 2, Cl for 3, Br for 4, CN for 5, NO_2 for 6) by $[(N4Py)Fe^{IV}(O)]^{2+}$ in the absence of Sc^{3+} (closed black circles) and in the presence of Sc^{3+} (10 mM, closed red circles) in MeCN at 298 K vs the driving force of electron transfer [$-\Delta G_{et} = e(E_{red} - E_{ox})$] from *para*-X-substituted thioanisoles to $[(N4Py)Fe^{IV}(O)]^{2+}$. Open blue circles show the driving force of rate constants (log k_{et}) for electron transfer from one-electron reductants (7, $[Fe^{II}(Ph_2phen)_3]^{2+}$; 8, $[Fe^{II}(bpy)_3]^{2+}$; 9, $[Ru^{II}(Me_2bpy)_3]^{2+}$; 10, $[Fe^{II}(Clphen)_3]^{2+}$; 11, $[Ru^{II}(bpy)_3]^{2+}$) to $[(N4Py)Fe^{IV}(O)]^{2+}$ in the presence of Sc^{3+} (10 mM) in MeCN at 298 K.

In contrast, the log k_{obs} values obtained in the presence of Sc^{3+} increase remarkably with increasing the driving force of electron transfer. In the case of *p*-methylthioanisole, the free energy change of electron transfer becomes negative. In such a case, an electron-transfer pathway (Scheme 1b) becomes dominant over a direct oxygen atom transfer pathway (Scheme 1a). The dependence of log k_{obs} on the driving force of electron transfer ($-\Delta G_{et}$) in the presence of Sc^{3+} (red line in Figure 7) is remarkably in parallel with that of log k_{et} of actual electron transfer from one-electron reductants to

$[(N4Py)Fe^{IV}(O)]^{2+}$ (blue line in Figure 7). The driving force dependence of both the rate constants of sulfoxidation of thioanisoles by $[(N4Py)Fe^{IV}(O)]^{2+}$ and electron transfer from one-electron reductants to $[(N4Py)Fe^{IV}(O)]^{2+}$ in the presence of 10 mM of Sc^{3+} is well fitted in light of the Marcus theory of adiabatic outer-sphere electron transfer (eq 2):

$$k_{et} = Z\exp[-(\lambda/4)(1 + \Delta G_{et}/\lambda)^2/k_B T] \quad (2)$$

where Z is the collision frequency taken as 1×10^{11} M^{-1} s^{-1}, λ is the reorganization energy of electron transfer, k_B is the Boltzmann constant, and T is the absolute temperature.[18,19] The best fit λ value of electron transfer in sulfoxidation of thioanisols is determined to be 2.02 eV, which agrees reasonably well with the λ value of electron transfer from one-electron reductants (2.27 eV).[20] Such an agreement with the Marcus equation indicates that the sulfoxidation of thioanisoles by $[(N4Py)Fe^{IV}(O)]^{2+}$ in the presence of Sc^{3+} proceeds via Sc^{3+} ion–coupled electron transfer from thioanisoles to $[(N4Py)Fe^{IV}(O)]^{2+}$, which is the rate-determining step, followed by rapid transfer of the oxygen atom from $[(N4Py)Fe^{III}(O)]^{+}$ to the radical cation ($ArSR^{\bullet+}$), as described in Scheme 1, pathways b and c.

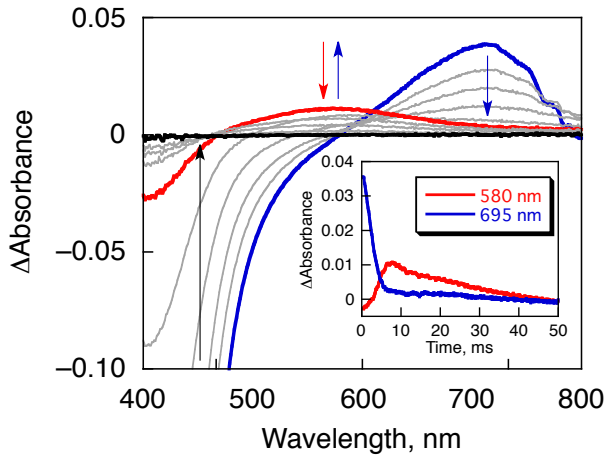

Figure 8. Difference UV-vis spectral changes in the reaction of $[(N4Py)Fe^{IV}(O)]^{2+}$ (1.0×10^{-4} M) with *p*-methoxythioanisole (4.0×10^{-3} M) in presence of Sc^{3+} (4.0×10^{-3} M) in MeCN at 298 K. Inset shows the time courses monitored at 580 nm due to *p*-methoxy-thioanisole radical cation and 695 nm due to $[(N4Py)Fe^{IV}(O)]^{2+}$.

When the ΔG_{et} value becomes more negative than 0.4 eV, the k_{et} value becomes smaller than the k_{obs} value for direct oxygen atom transfer. Thus, the borderline between a direct oxygen atom transfer pathway (Scheme 1a) and an electron-transfer pathway (Scheme 1b) may be determined by the E_{ox} value of *p*-X-substituted thioanisoles, ca. 1.6 V vs SCE that corresponds to *p*-cyanothioanisole.

The occurrence of electron transfer is clearly shown in the case of *p*-methoxythioanisole in the presence of Sc^{3+} (4 mM), when the driving force of electron transfer is positive ($-\Delta G_{et}$ = 0.01 eV) as shown in Figure 8, where the transient absorption band at 580 nm due to *p*-methoxythioanisole radical cation appears accompanied by a decrease in the absorption band at 695 nm due to $[(N4Py)Fe^{IV}(O)]^{2+}$ (see Figure 9 where the reference spectrum of *p*-methoxyanisole radical cation is shown).[21] This result clearly demonstrates that an electron-transfer pathway becomes dominant over a direct oxygen atom transfer pathway when the sulfoxidation by the iron(IV)-oxo complex is carried out in the presence of a metal ion (Scheme 1).

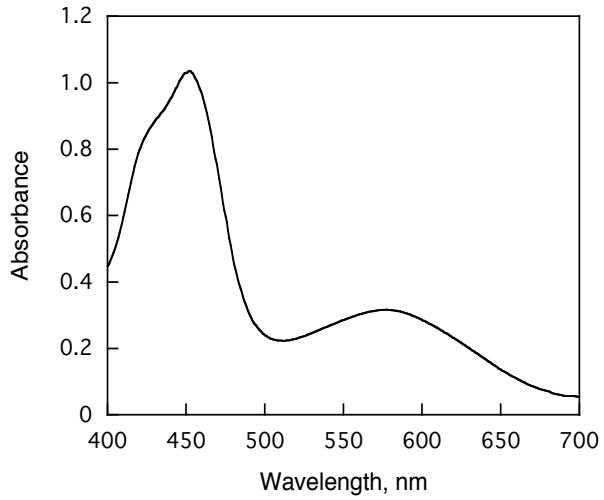

Figure 9. Visible spectrum observed in the oxidation of *p*-methylthioanisole (4.0×10^{-3} M) by one-electron oxidant, $[Ru^{III}(bpy)_3]^{3+}$ (bpy = 2,2'-bipyridine) (7.5×10^{-5} M) by stopped-flow technique just after mixing in MeCN at 298 K. Absorption band around at 450 nm and 580 nm are due to $[Ru^{II}(bpy)_3]^{2+}$ and *p*-methylthioanisole radical cation, respectively.[21]

In summary, we have demonstrated that Sc^{3+} ion promotes sulfoxidation of thioanisols significantly via Sc^{3+} ion-coupled electron transfer and the border line between a direct oxygen atom transfer pathway (Scheme 1a) and an electron-transfer pathway (Scheme 1b) is determined by the E_{ox} value of thioanisoles that is ca. 1.6 V vs

SCE. Thus, the present study provides a new and rational way to enhance the reactivity of high-valent metal-oxo species by binding of redox-inactive metal ions such as Sc^{3+}. The generality of this idea is under investigation.

Scheme 1

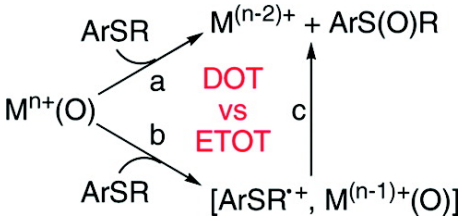

Conclusion

Effects Sc^{3+} ion on sulfoxidation of thioanisole derivatives by $[(N4Py)Fe^{IV}(O)]^{2+}$ were observed, showing largerly enhancement of reaction rates. The rate of sulfoxidation was accelerated as much as 10^2-fold by the addition of Sc^{3+}. The switch of a reaction mechanism was demonstrated in the oxidation of thioanisole derivatives by $[(N4Py)Fe^{IV}(O)]^{2+}$ from direct oxygen atom transfer to MCET by addition of $Sc(OTf)_3$ in acetonitrile depending on the oxidation potentials of thioanisole derivatives. This is the first example of a new reaction pathway to enhance the reactivity of the nonheme iron(IV) complex by binding of redox-inactive metal ions such as Sc^{3+} ion.

References

(1) (a) Bertini, I.; Gray, H. B.; Stiefel, E. I.; Valentine, J. S., Eds. *Biological Inorganic Chemistry: Structure & Reactivity*; University Science Books: Sausalito, California, 2007. (b) Ortiz. de Montellano, P. R. *Cytochrome P450: Structure, Mechanism, and Biochemistry*, 3rd ed., Kluwer Academic/Plenum Publishers, New York, 2005. (c) Meunier, B., Ed. *Biomimetic Oxidations Catalyzed by Transition Metal Complexes*; Imperial College Press: London, 2000.

(2) (a) Nam, W. *Acc. Chem. Res.* **2007**, *40*, 465, and review articles in the special issue. (b) Meunier, B.; de Visser, S. P.; Shaik, S. *Chem. Rev.* **2004**, *104*, 3947. (c) Abu-Omar, M. M.; Loaiza, A.; Hontzeas, N. *Chem. Rev.* **2005**, *105*, 2227. (d) Espenson, J. H. *Coord. Chem. Rev.* **2005**, *249*, 329. (e) Denisov, I. G.; Makris, T. M.; Sligar, S. G.; Schlichting, I. *Chem. Rev.* **2005**, *105*, 2253. (f) Borovik, A. S.

Acc. Chem. Res. **2005**, *38*, 54. (g) Bakac, A. *Coord. Chem. Rev.* **2006**, *250*, 2046. (h) Krebs, C.; Fujimori, D. G.; Walsh, C. T.; Bollinger, J. M., Jr. *Acc. Chem. Res.* **2007**, *40*, 484. (i) Nam, W. *Acc. Chem. Res.* **2007**, *40*, 522. (j) Comba, P.; Kerscher, M.; Schiek, W. *Prog. Inorg. Chem.* **2007**, *55*, 613.

(3) (a) Arias, J.; Newlands, C. R.; Abu-Omar, M. M. *Inorg. Chem.* **2001**, *40*, 2185. (b) Fertinger, C.; Hessenauer-Ilicheva, N.; Franke, A.; van Eldik, R. *Chem.–Eur. J.* **2009**, *15*, 13435. (c) Arunkumar, C.; Lee, Y.-M.; Lee, J. Y.; Fukuzumi, S.; Nam, W. *Chem.–Eur. J.* **2009**, *15*, 11482. (d) Kumar, A.; Goldberg, I.; Botoshansky, M.; Buchman, Y.; Gross, Z. *J. Am. Chem. Soc.* **2010**, *132*, 15233. (e) Benet-Buchholz, J.; Comba, P.; Llobet, A.; Roeser, S.; Vadivelu, P.; Wiesner, S. *Dalton Trans.* **2010**, *39*, 3315.

(4) (a) Goto, Y.; Matsui, T.; Ozaki, S.; Watanabe, Y.; Fukuzumi, S. *J. Am. Chem. Soc.* **1999**, *121*, 9497. (b) Baciocchi, E.; Gerini, M. F.; Lanzalunga, O.; Lapi, A.; Lo Piparo, M. G. *Org. Biomol. Chem.* **2003**, *1*, 422.

(5) Khenkin, A. M.; Leitus, G.; Neumann, R. *J. Am. Chem. Soc.* **2010**, *132*, 11446.

(6) (a) Shaik, S.; Wang, Y.; Chen, H.; Song, J.; Meir, R. *Faraday Discuss.* **2010**, *145*, 49. (b) Porro, C. S.; Sutcliffe, M. J.; de Visser, S. P. *J. Phys. Chem. A* **2009**, *113*, 11635. (c) Kumar, D.; de Visser, S. P.; Sharma, P. K.; Hirao, H.; Shaik, S. *Biochemistry* **2005**, *44*, 8148. (d) Sharma, P. K.; de Visser, S. P.; Shaik, S. *J. Am. Chem. Soc.* **2003**, *125*, 8698.

(7) Park, M. J.; Lee, J.; Suh, Y.; Kim, J.; Nam, W. *J. Am. Chem. Soc.* **2006**, *128*, 2630.

(8) Kaizer, J.; Klinker, E. J.; Oh, N. Y.; Rohde, J.–U.; Song, W. J.; Stubna, A.; Kim, J.; Münck, E.; Nam, W.; Que, L., Jr. *J. Am. Chem. Soc.* **2004**, *126*, 472.

(9) An acceleration effect of metal ions including Sc^{3+} on OAT from high-valent manganese-oxo complexes to triphenylphosphine and to olefins has been reported, although the acceleration mechanism has yet to be clarified; see: Miller, C. G.; Gordon-Wylie, S. W.; Horwitz, C. P.; Strazisar, S. A.; Peraino, D. K.; Clark, G. R.; Weintraub, S. T.; Collins, T. J. *J. Am. Chem. Soc.* **1998**, *120*, 11540.

(10) The products and product yields formed in the presence of Sc^{3+} were the same as those reported in the reactions carried out in the absence of Sc^{3+} (see ref 7 and SI, Experimental Section).

(11) Armarego, W. L. F.; Chai, C. L. L. Eds., *Purification of Laboratory Chemicals*, 6th ed; Pergamon Press: Oxford, 2009.

(12) (a) Lubben, M; Meetsma, A.; Wilkinson, E. C.; Feringa, B.; Que, L., Jr. *Angew. Chem., Int. Ed.* **1995**, *34*, 1512-1514; b) Kaizer, J.; Klinker, E. J.; Oh, N. Y.; Rohde, J.-U.; Song, W. J.; Stubna, A.; Kim, J.; Münck, E.; Nam, W.; Que, Jr., L. *J. Am. Chem. Soc.* **2004**, *126*, 472-473

(13) (a) Lin, C-T.; Bottcher, W.; Chou, M.; Creutz, C.; Sutin, N. *J. Am. Chem. Soc.* **1976**, *98*, 6536. (b) Fussa-Rydel, O.; Zhang, H. T.; Hupp, J. T.; Leidnert C. R. *Inorg. Chem.* **1989**, *28*, 1533. (c) Leidner C. R.; Murray, R. W. *J. Am. Chem. Soc.* **1984**, *106*, 1606-1614.

(14) Morimoto, M.; Kotani, H.; Park, J.; Lee, Y.-M.; Nam, W.; Fukuzumi, S. *J. Am. Chem. Soc.* **2011**, *133*, 403.

(15) An X-ray crystal structure of Sc^{3+}-bound iron(IV)-oxo complex has been reported: (a) Fukuzumi, S.; Morimoto, Y.; Kotani, H.; Naumov, P.; Lee, Y.-M.; Nam, W. *Nature Chem.* **2010**, *2*, 756. (b) Karlin, K. D. *Nature Chem.* **2010**, *2*, 711.

(16) For metal ion-coupled electron transfer, see: (a) Fukuzumi, S. *Prog. Inorg. Chem.* **2009**, *56*, 49. (b) Fukuzumi, S. *Bull. Chem. Soc. Jpn.* **1997**, *70*, 1. (c) Fukuzumi, S.; Ohkubo, K. *Coord. Chem. Rev.* **2010**, *254*, 372.

(17) Sc^{3+} ion is known to be most the effective for metal ion-coupled electron transfer; see: Fukuzumi, S.; Ohkubo, K. *Chem.–Eur. J.* **2000**, *6*, 4532.

(18) (a) Lee, Y.-M.; Kotani, H.; Suenobu, T.; Nam, W.; Fukuzumi, S. *J. Am. Chem. Soc.* **2008**, *130*, 434. (b) Fukuzumi, S.; Kotani, H.; Suenobu, T.; Hong, S.; Lee, Y.-M.; Nam, W. *Chem.–Eur. J.* **2010**, *16*, 354.

(19) (a) Marcus, R. A. *Annu. Rev. Phys. Chem.* **1964**, *15*, 155. (b) Marcus, R. A. *Angew. Chem., Int. Ed. Engl.* **1993**, *32*, 1111.

(20) The slightly smaller *l* value of thioanisoles as compared with the *l* value of metal complexes may be ascribed to the delocalization of the charge in the *p*-radical cations; see: Eberson, L. *Electron-Transfer Reactions in Organic Chemistry; Reactivity and Structure*; Springer: Heidelberg, 1987; Vol. 25.

(21) Yokoi, H.: Hatta, A.: Ishiguro, K.: Sawaki, Y. *J. Am. Chem. Soc.* **1998**, *120*, 12728.

Chapter 2. Scandium Ion–Enhanced Oxidative Dimerization and *N*-Demethylation of *N,N*-Dimethylanilines by a Nonheme Iron(IV)-Oxo Complex

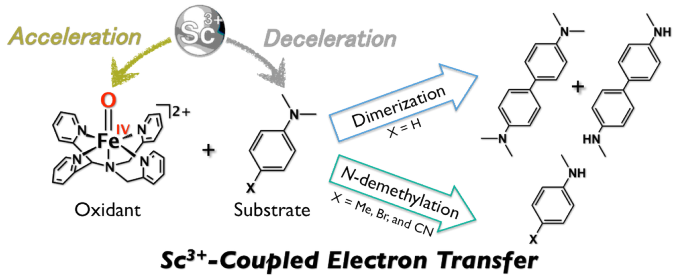

Abstract: Oxidative dimerization of *N*,*N*-dimethylaniline (DMA) occurs with a nonheme iron(IV)-oxo complex, $[(N4Py)Fe^{IV}(O)]^{2+}$ (N4Py = *N*,*N*-bis(2-pyridylmethyl)-*N*-bis(2- pyridyl)methylamine), to yield the corresponding dimer, tetramethylbenzidine (TMB), in acetonitrile. The rate of the oxidative dimerization of DMA by $[Fe^{IV}(O)(N4Py)]^{2+}$ is markedly enhanced by the presence of scandium triflate, $Sc(OTf)_3$ (OTf = $CF_3SO_3^-$), when TMB is further oxidized to the radical cation ($TMB^{\bullet+}$). In contrast, we have observed the oxidative *N*-demethylation with *para*-substituted DMA substrates, since the position of the C–C bond formation to yield the dimer is blocked. The rate of the oxidative *N*-demethylation of *para*-substituted DMA by $[(N4Py)Fe^{IV}(O)]^{2+}$ is also markedly enhanced by the presence of $Sc(OTf)_3$. In the case of *para*-substituted DMA derivatives with electron-donating substituents, radical cations of DMA derivatives are initially formed by Sc^{3+} ion-coupled electron transfer from DMA derivatives to $[(N4Py)Fe^{IV}(O)]^{2+}$, giving demethylated products. Binding of Sc^{3+} to $[(N4Py)Fe^{IV}(O)]^{2+}$ enhances the Sc^{3+} ion-coupled electron transfer from DMA derivatives to $[(N4Py)Fe^{IV}(O)]^{2+}$, whereas binding of Sc^{3+} to DMA derivatives retards the electron–transfer reaction. The complicated kinetics of the Sc^{3+} ion–coupled electron transfer from DMA derivatives to $[(N4Py)Fe^{IV}(O)]^{2+}$ are analyzed by competition between binding of Sc^{3+} to DMA derivatives and to $[(N4Py)Fe^{IV}(O)]^{2+}$. The binding constants of Sc^{3+} to DMA derivatives increase with the increase of the electron–donating ability of the *para*-substituent. The rate constants of Sc^{3+} ion–coupled electron transfer from DMA derivatives to $[(N4Py)Fe^{IV}(O)]^{2+}$, which are estimated from the binding constants of Sc^{3+} to DMA derivatives, agree well with those predicted from the driving force dependence of the rate constants of Sc^{3+} ion–coupled electron transfer from one-electron reductants to $[(N4Py)Fe^{IV}(O)]^{2+}$. Thus, oxidative dimerization of

DMA and *N*-demethylation of *para*-substituted DMA derivatives proceed via Sc^{3+} ion–coupled electron transfer from DMA derivatives to $[(N4Py)Fe^{IV}(O)]^{2+}$.

Introduction

High-valent iron-oxo complexes of heme and nonheme ligands play key roles as reactive intermediates in biological and chemical oxidation reactions.[1,2] The reactivities of the iron-oxo complexes have been extensively investigated over the past several decades, and it has been demonstrated that the reactivities can be controlled by many factors, such as the oxidation state of iron centers and ligand structures.[1,2] In addition, the reactivities of synthetic nonheme iron(IV)-oxo complexes have been intensively investigated in various oxidation reactions,[3] since the first crystal structure of a mononuclear nonheme iron(IV)-oxo complex was reported in 2003.[4] The factors affecting the formation and reactivities of nonheme iron(IV)-oxo complexes in the C-H bond activation and oxo transfer reactions have also been discussed in detail (e.g., supporting and axial ligands and solvents).[5] The reactivities of metal-oxo complexes in the oxidation reactions of alkanes and oxygen atom transfer reactions are controlled not only by the oxidation state of the metal and the ligands,[1-7] but also by metal ions acting as Lewis acids.[8] We have shown that the reactivities of the nonheme iron-oxo complexes are markedly affected by the binding of redox inactive metal ions at the iron-oxo centers.[9-11] For example, a crystal structure of Sc^{3+}–bound $[(TMC)Fe^{IV}(O)]^{2+}$ (TMC = 1,4,8,11-tetramethyl-1,4,8,11-tetraazacyclo- tetradecane) was determined by X-ray crystallography.[9] In the study, binding of Sc^{3+} to $[(TMC)Fe^{IV}(O)]^{2+}$ has been shown to change the number of electrons transferred from one-electron reductants (e.g., ferrocene) to $[(TMC)Fe^{IV}(O)]^{2+}$.[9] More recently, it has been demonstrated that rates of electron transfer from one-electron reductants to a nonheme iron(IV)-oxo complex, $[(N4Py)Fe^{IV}(O)]^{2+}$ (N4Py = *N*,*N*-bis(2-pyridylmethyl)-*N*-bis(2-pyridyl)- methylamine), are enhanced as much as 10^8-fold by addition of Sc^{3+} ion.[10] Such an enhancement of the oxidizing power of nonheme iron(IV)-oxo complexes by metal ions results from strong binding of metal ions to the electron acceptors, which causes large positive shifts in the one-electron reduction potentials, as observed in metal ion–coupled electron–transfer reduction of various electron acceptors.[9-18] On the other hand, binding of metal ions to electron donors results in retardation of electron–transfer reactions of electron donors, because the one-electron oxidation potentials of electron donors are positively shifted by binding of metal ions that results in decreasing the driving force of electron transfer.[19] Thus, there are two opposite effects of metal ion binding on electron transfer: One is acceleration of electron transfer by binding of metal ions to electron acceptors

(e.g., metal-oxo complex) and the other is deceleration of electron transfer by binding of metal ions to electron donors (e.g., substrate).[20] However, to the best of our knowledge, there has been no report on such competing effects of redox-inactive metal ions on the oxidation of substrates by metal-oxo complexes.

We report herein that competition between binding of Sc^{3+} ion to *N*,*N*-dimethylaniline (DMA) and $[(N4Py)Fe^{IV}(O)]^{2+}$ results in overall enhancement of electron transfer from DMA to a nonheme iron(IV)-oxo complex, $[(N4Py)Fe^{IV}(O)]^{2+}$. The present study also provides the definitive evidence for the occurrence of electron transfer from DMA to high-valent metal-oxo complexes, although there have been extensive studies on the mechanism of the oxidation of DMA by various oxidants including a possible electron-transfer pathway.[21-28] The complicated kinetics caused by competitive binding of Sc^{3+} ion to DMA and $[(N4Py)Fe^{IV}(O)]^{2+}$ are analyzed as well. While we have observed the formation of a radical cation of DMA dimer, tetramethylbenzidine ($TMB^{\bullet+}$), in the oxidation of DMA by the $[(N4Py)Fe^{IV}(O)]^{2+}$ complex when the reaction is performed in the presence of Sc^{3+} ion, the oxidative *N*-demethylation reaction takes place with *para*-substituted DMA derivatives and the oxidative *N*-demethylation is accelerated by the presence of Sc^{3+} ion. The rate constants of oxidative dimerization and *N*-demethylation of DMA and its derivatives by $[(N4Py)Fe^{IV}(O)]^{2+}$ in the presence of Sc^{3+} ion are compared with the driving force dependence of Sc^{3+} ion–coupled electron transfer from one-electron reductants to $[(N4Py)Fe^{IV}(O)]^{2+}$ to clarify the oxidation mechanism of DMA derivatives by $[(N4Py)Fe^{IV}(O)]^{2+}$. The extensive analysis on competing effects of binding of Sc^{3+} ion to DMA and its derivatives and to $[(N4Py)Fe^{IV}(O)]^{2+}$ will expand the scope of metal ion–coupled electron transfer on the oxidation of a variety of substrates by high-valent metal-oxo complexes.

Experimental Section

Materials. All chemicals were purchased from Sigma-Aldrich, Wako, Nacalai Tesque, and Lancaster Co., Ltd. and used without further purification unless otherwise noted. $[(N4Py)Fe^{II}(MeCN)](ClO_4)_2$ was prepared in a glovebox according to the literature method.[29] Acetonitrile (MeCN) and ether were dried according to the literature procedures and distilled under Ar prior to use.[30] Iodosylbenzene (PhIO) was prepared by a literature method.[31] $[(N4Py)Fe^{IV}(O)]^{2+}$ was prepared by the literature

method.[29] Deuterated *N*,*N*-dimethylaniline (DMA-d_6) was prepared by alkylating aniline with CD_3I.[22a] The purities of the compounds were checked by ^1H NMR spectroscopy. Tetra-*n*-butylammonium hexafluorophosphate was purchased from Sigma Chemical Co., recrystallized from ethyl alcohol, and dried under vacuum at 40 °C for at least 1 week prior to use.

Caution: Perchlorate salts are potentially explosive and should be handled with care.

General Reaction Procedures. Typically, DMA (4.0×10^{-3} M) was added to a CD_3CN solution (0.50 mL) containing $[(N4Py)Fe^{IV}(O)]^{2+}$ (4.0×10^{-3} M) in the absence and presence of $Sc(OTf)_3$ in an NMR tube. The reaction was complete within 10 min under these conditions. The products in the absence and presence of $Sc(OTf)_3$ were identified as TMB and $[(N4Py)Fe^{II}]^{2+}$ by comparing the ^1H NMR spectra with those of authentic samples. In the case of *para*-substituted DMA derivatives, the demethylated products were formed in the absence and presence of $Sc(OTf)_3$ and they were identified and quantitized by comparing the ^1H NMR spectra with those of authentic samples.

Spectral and Kinetic Measurement. Reactions of DMA and its derivatives with $[(N4Py)Fe^{IV}(O)]^{2+}$ (5.0×10^{-5} M) were examined by monitoring spectral changes in the presence of various concentrations of DMA or its derivatives ($1.0 \times 10^{-3} - 5.0 \times 10^{-2}$ M) in the absence and presence of $Sc(OTf)_3$ in MeCN at 298 K, with a Hewlett Packard 8453 photodiode-array spectrophotometer and a quartz cuvette (path length = 10 mm). Kinetic measurements were performed on a UNISOKU RSP-601 stopped-flow spectrometer equipped with a MOS-type highly sensitive photodiode array or a Hewlett Packard 8453 photodiode-array spectrophotometer at 298 K. Rates of reactions of DMA and its derivatives with $[(N4Py)Fe^{IV}(O)]^{2+}$ were monitored by the decrease of the absorption band due to $[(N4Py)Fe^{IV}(O)]^{2+}$ (λ_{max} = 695 nm) in the absence and presence of $Sc(OTf)_3$ in MeCN. When TMB radical cation ($TMB^{\bullet+}$) was formed in the reaction of DMA with $[(N4Py)Fe^{IV}(O)]^{2+}$ in the presence of $Sc(OTf)_3$ in MeCN, the rate was determined from the increase in the NIR absorption band (λ_{max} = 900 nm) due to $TMB^{\bullet+}$.[32] The concentration of DMA or its derivative was maintained at least more than 10-fold excess of the other reactant to attain pseudo-first-order conditions. Pseudo-first-order rate constants were determined by a least-squares curve fit. The first-order plots were linear for three or more half-lives with the correlation coefficient

$\rho > 0.999$. In each case, it was confirmed that the rate constants derived from at least five independent measurements agreed within an experimental error of ±5%.

Electrochemical Measurements. Measurements of cyclic voltammetry (CV) were performed at 298 K using a BAS 630B electrochemical analyzer in a deaerated solvent containing 0.10 M TBAP as a supporting electrolyte at 298 K. A conventional three-electrode cell was used with a platinum working electrode and a platinum wire as a counter electrode. The measured potentials were recorded with respect to the $Ag/AgNO_3$ (1.0×10^{-2} M). The E_{ox} and E_{red} values (vs $Ag/AgNO_3$) are converted to those vs SCE by adding 0.29 V.[33] All electrochemical measurements were carried out under an Ar atmosphere.

EPR Measurements. EPR detection of $TMB^{\bullet+}$ was performed as follows: Typically, a MeCN solution of $[(N4Py)Fe^{IV}(O)]^{2+}$ (3.0×10^{-4} M) in the presence of $Sc(OTf)_3$ (3.0×10^{-4} M) in an EPR cell (3.0 mm i.d.) was purged with Ar for 5 min. Then, DMA (8.0×10^{-4} M) was added to the solution. The EPR spectrum of $TMB^{\bullet+}$ was recorded on a JEOL JES-RE1XE spectrometer at 243 K. The magnitude of modulation was chosen to optimize the resolution and signal-to-noise (S/N) ratio of the observed spectra under nonsaturating microwave power conditions. The g value was calibrated using a Mn^{2+} marker (g = 2.034, 1.981). Computer simulation of the EPR spectra was carried out by using Calleo EPR version 1.2 (Calleo Scientific Publisher) on a personal computer.

Results and Discussion

Three-Electron Oxidation of DMA by $[(N4Py)Fe^{IV}(O)]^{2+}$ in the Presence of Sc^{3+}. DMA has been suggested to be oxidized by nonheme iron(IV)-oxo complexes such as $[(N4Py)Fe^{IV}(O)]^{2+}$ to yield the demethylated product (*N*-methylaniline) via an electron transfer-proton transfer (ET-PT) mechanism,[27] as shown in Scheme 1. Electron transfer from DMA to $[(N4Py)Fe^{IV}(O)]^{2+}$ is followed by proton transfer from $DMA^{\bullet+}$ and $[(N4Py)Fe^{III}(O)]^{+}$ to yield the DMA radical and $[(N4Py)Fe^{III}(OH)]^{2+}$, because $DMA^{\bullet+}$ and $[(N4Py)Fe^{III}(O)]^{+}$ are a strong acid and base, respectively. The rebound between DMA radical and $[(N4Py)Fe^{III}(OH)]^{2+}$ results in formation of the demethylated product. However, the intermediate $DMA^{\bullet+}$ formed in the ET-PT mechanism cannot be detected because the initial ET process is the rate-determining step.[27]

Scheme 1

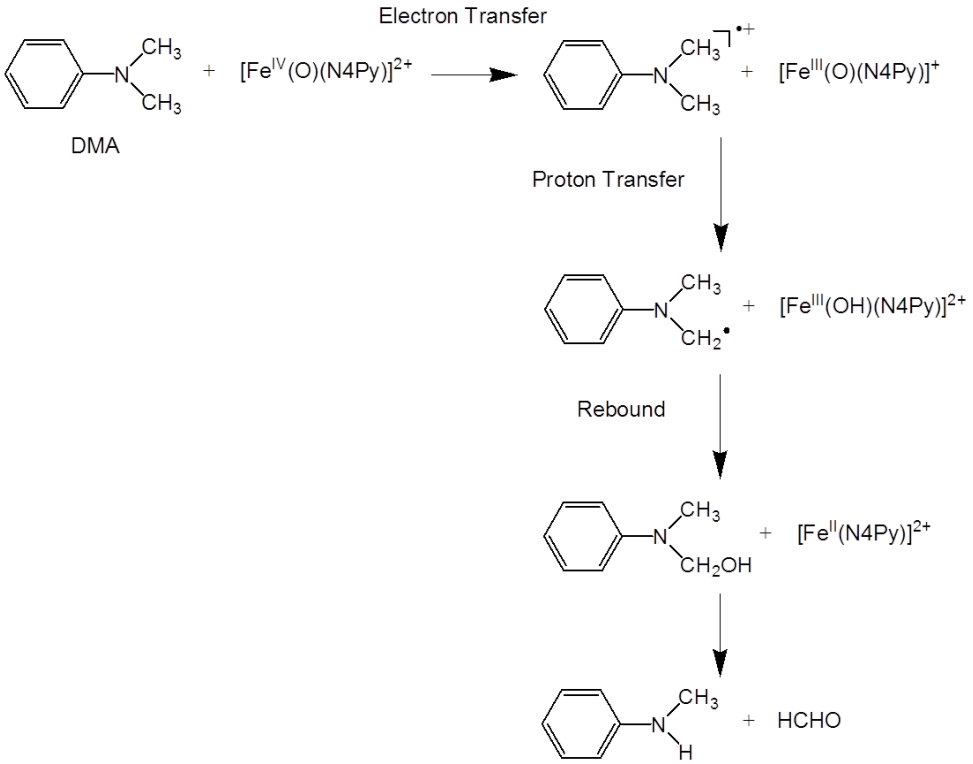

In the presence of $Sc(OTf)_3$, however, the oxidized product of DMA by $[(N4Py)Fe^{IV}(O)]^{2+}$ was changed from the demethylated product in the absence of $Sc(OTf)_3$ to the dimer radial cation, i.e., tetramethylbenzidine radical cation ($TMB^{\bullet+}$). The quantitative formation of $TMB^{\bullet+}$ in the reaction of DMA with $[(N4Py)Fe^{IV}(O)]^{2+}$ in the presence of $Sc(OTf)_3$ in MeCN is shown in Figure 1a, where the absorption bands at 470, 900 and 1000 nm are assigned due to $TMB^{\bullet+}$.[32,34] The same absorption bands due to $TMB^{\bullet+}$ are observed in the one-electron oxidation of TMB by a strong one-electron oxidant $[Ru^{III}(bpy)_3]^{3+}$ and cerium(IV) ammonium nitrate (Figure 1b and 1c). The $TMB^{\bullet+}$ produced by the one-electron oxidation of TMB by one equiv of $[Ru^{III}(bpy)_3]^{3+}$ was oxidized to TMB^{2+} by further addition of $[Ru^{III}(bpy)_3]^{3+}$ (bpy = 2,2'-bipyridine) in Figure 1b (right panel), because the second one-electron oxidation potential of TMB (0.68 V vs SCE)[35] is still lower than the one-electron reduction potential of $[Ru(bpy)_3]^{3+}$ (1.24 V vs SCE). The concentration of $TMB^{\bullet+}$ was determined using the *e* value at 900 nm (2.0×10^4 M^{-1} cm^{-1}; see Figure 1b, right panel) to be 1.0×10^{-4} M, which is one-third of the initial concentration of $[(N4Py)Fe^{IV}(O)]^{2+}$ (3.0×10^{-4} M). Thus, three-electron oxidation of DMA occurs with $[(N4Py)Fe^{IV}(O)]^{2+}$ to yield $TMB^{\bullet+}$. The formation of $TMB^{\bullet+}$ was also confirmed by the EPR spectrum (Figure 2).[36]

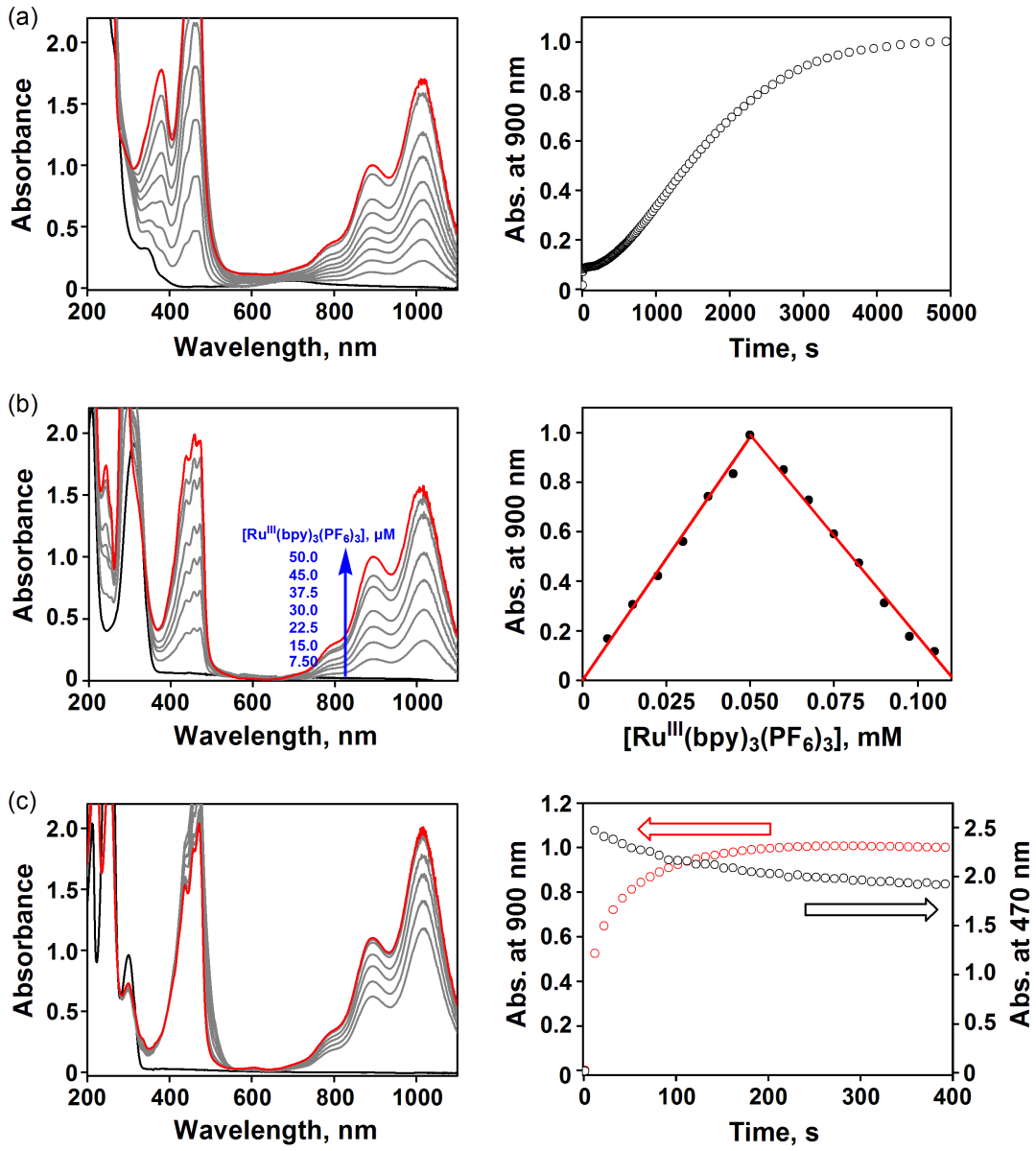

Figure 1. (a) Visible spectral changes observed in the reaction of $[(N4Py)Fe^{IV}(O)]^{2+}$ (0.15 mM) with DMA (0.44 mM) in the presence of $Sc(OTf)_3$ (0.15 mM) in MeCN at 298 K (left panel). Right panel shows time course monitored at 900 nm. (b) Visible spectral changes observed in the formation of $TMB^{\bullet+}$ by titration of TMB (0.050 mM) with $[Ru^{III}(bpy)_3](ClO_4)_3$ (0 – 0.050 mM) in MeCN at 298 K (left panel). Right panel shows Job's plot of absorbance changes monitored at 900 nm due to $TMB^{\bullet+}$ upon addition of $[Ru^{III}(bpy)_3](PF_6)_3$ (0 – 0.105 mM) into the solution of TMB (0.050 mM) in MeCN at 298 K. (c) Visible spectral changes observed in the reaction of DMA (0.30 mM) with cerium(IV) ammonium nitrate (0.20 mM) in MeCN at 298 K (left panel). Right panel shows time courses monitored at 470 and 900 nm.

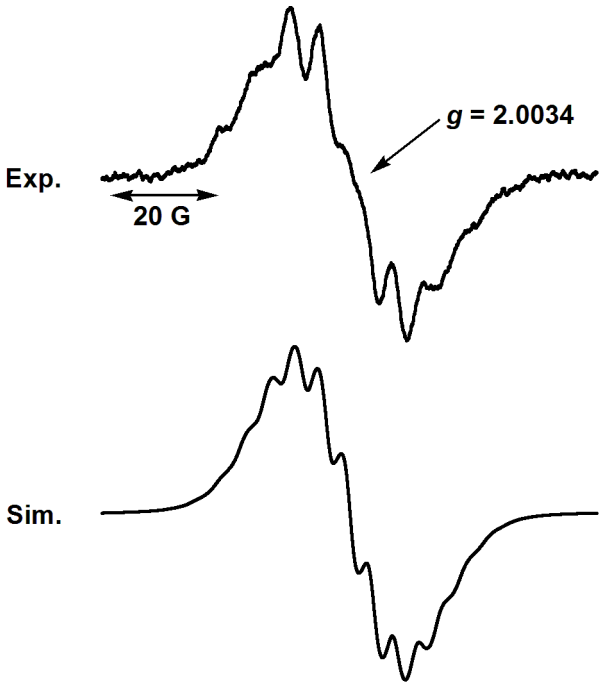

Figure 2. X-band EPR spectra of $TMB^{\bullet+}$ produced in the oxidation reaction of DMA (0.6 mM) by $[(N4Py)Fe^{IV}(O)]^{2+}$ (0.3 mM) in the presence of Sc^{3+} (0.1 mM) in deaerated MeCN at 243 K and the computational simulation spectrum prepared with reported hyperfine coupling constants of $TMB^{\bullet+}$ (A_N = 4.81 G, A_{CH3} = 4.7 G, A_{2H} = 0.76 G, and A_{3H} = 1.65 G; see Stenland, C.; Kevan, L. *J. Phys. Chem.* **1993**, *97*, 5177).

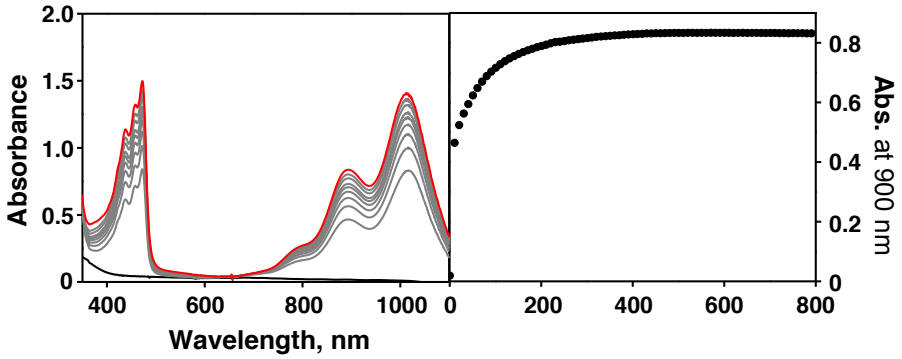

Figure 3. Visible spectral change observed in the reaction of $[(N4Py)Fe^{IV}(O)]^{2+}$(0.050 mM) with TMB (0.13 mM) in MeCN at 298 K.

The drastic change of the oxidized product of DMA with $[(N4Py)Fe^{IV}(O)]^{2+}$ upon addition of $Sc(OTf)_3$ is well understood as shown in Scheme 2, which is in line with Scheme 1. The initial electron transfer from DMA to $[(N4Py)Fe^{IV}(O)]^{2+}$ is much enhanced by Sc^{3+} ion, as observed in Sc^{3+} ion–coupled electron transfer from one-electron reductants to $[(N4Py)Fe^{IV}(O)]^{2+}$, to yield $DMA^{\bullet+}$ and the Sc^{3+} ion–bound Fe(III)-oxo complex. The proton transfer from $DMA^{\bullet+}$ to the Fe(III)-oxo complex may be prohibited by the strong binding of Sc^{3+} to the Fe(III)-oxo complex. In such a case, $DMA^{\bullet+}$ undergoes the dimerization to produce TMB, via the reaction with DMA that acts as a nucleophile, accompanied by the oxidation and removal of two protons (Scheme 2).[32] Judging from the significantly lower one-electron oxidation potential of TMB (E_{ox} = 0.43 V vs SCE)[37] as compared with DMA (E_{ox} = 0.76 V vs SCE),[38] TMB is further oxidized by $[(N4Py)Fe^{IV}(O)]^{2+}$ (E_{red} = 0.51 V vs SCE)[10] to produce $TMB^{\bullet+}$. The formation of $TMB^{\bullet+}$ by the one-electron oxidation of TMB by $[(N4Py)Fe^{IV}(O)]^{2+}$ in the presence of Sc^{3+} was confirmed as shown in Figure 3. Thus, Sc^{3+} ion–coupled electron transfer from DMA to $[(N4Py)Fe^{IV}(O)]^{2+}$ results in the three-electron oxidation of DMA by $[(N4Py)Fe^{IV}(O)]^{2+}$ to yield $TMB^{\bullet+}$ rather than the demethylated product in the presence of Sc^{3+}. At prolonged reaction time, deprotonation of $TMB^{\bullet+}$ occurs slowly to yield the demethylated product of TMB, *N*,*N*-dimethylbenzidine (DMB), together with the Fe(II) complex (Figures 4 and 5).[39] The right panel of Figure 1c indicates the rapid formation of $DMA^{\bullet+}$ (rise in absorbance at 900 nm) and the subsequent slow conversion to $TMB^{\bullet+}$ (decay in absorbance at 470 nm).

According to Scheme 2, once Sc^{3+} ion–coupled electron transfer from DMA to $[(N4Py)Fe^{IV}(O)]^{2+}$ occurs, protons are produced in the radical coupling reaction of $DMA^{\bullet+}$ to yield TMB. In such a case, proton–coupled electron transfer from DMA to $[(N4Py)Fe^{IV}(O)]^{2+}$ may occur, leading to formation of $TMB^{\bullet+}$ as shown in Scheme 3. The $TMB^{\bullet+}$ concentration formed in the reaction of DMA with $[(N4Py)Fe^{IV}(O)]^{2+}$ was confirmed by the titration of Sc^{3+} concentration as shown in Figure 6. Only a catalytic amount of $Sc(OTf)_3$ (e.g., 1/9 of $[(N4Py)Fe^{IV}(O)]^{2+}$) is enough to obtain the stoichiometric amount of $TMB^{\bullet+}$ (Figure 7).[40] The careful re-examination of the products of the reaction of DMA with $[(N4Py)Fe^{IV}(O)]^{2+}$ in the absence of $Sc(OTf)_3$ revealed formation of DMB, demethylated product of TMB, (9% based on the initial concentration of $[(N4Py)Fe^{IV}(O)]^{2+}$) as well as *N*-methylaniline (62%) and TMB (1%) as the final products (Figure 8). Because DMB and TMB are the six-electron and four-electron oxidized products of DMA, respectively, the overall yield based on

$[(N4Py)Fe^{IV}(O)]^{2+}$ (a two-electron oxidant) will be 9 × 3 + 1 × 2 + 62 = 90%. Thus, even in the absence of $Sc(OTf)_3$, the dimerization of $DMA^{\bullet+}$ competes with proton transfer from $DMA^{\bullet+}$ to the Fe(III)-oxo complex.

Scheme 2

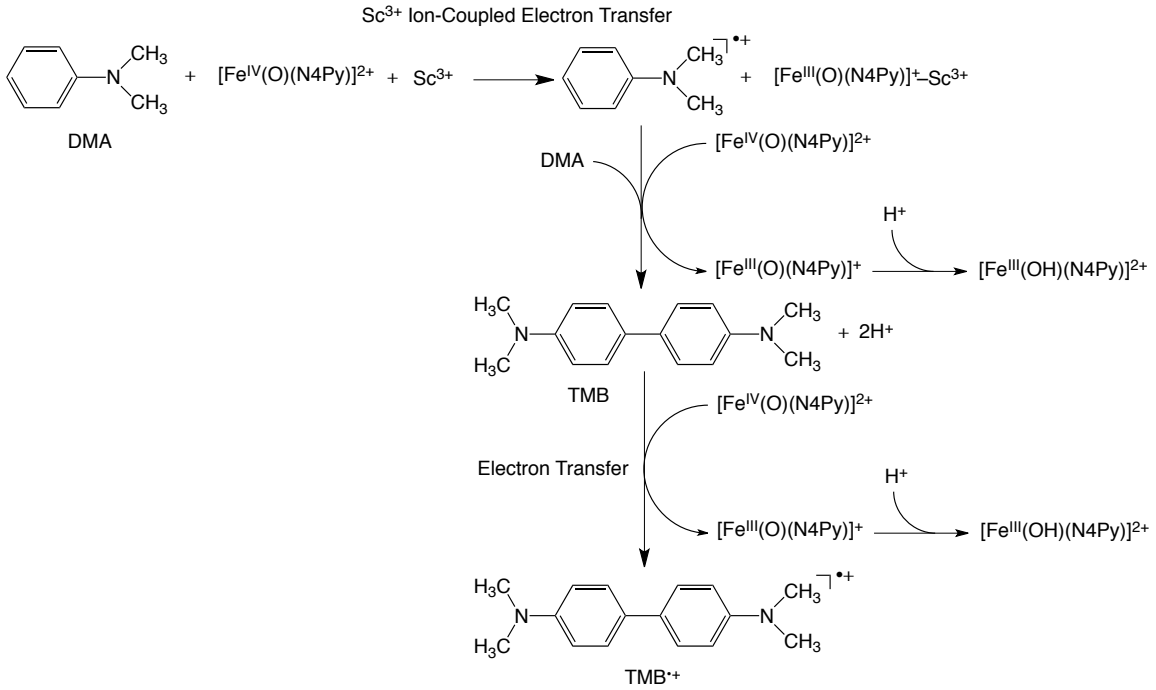

Scheme 3

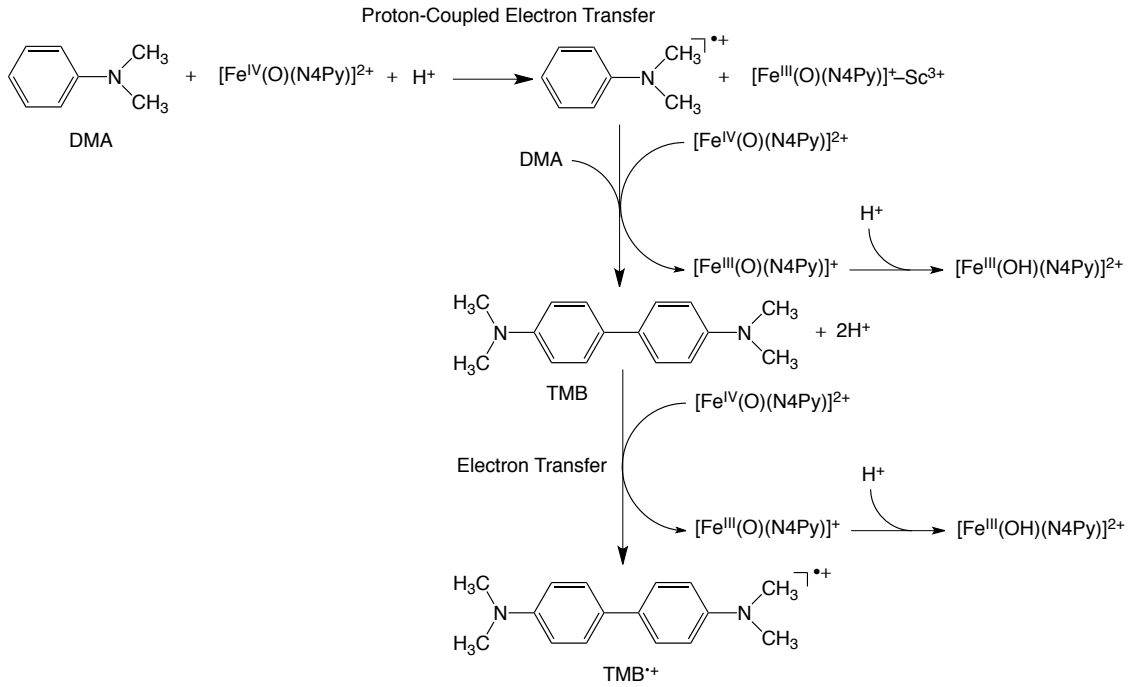

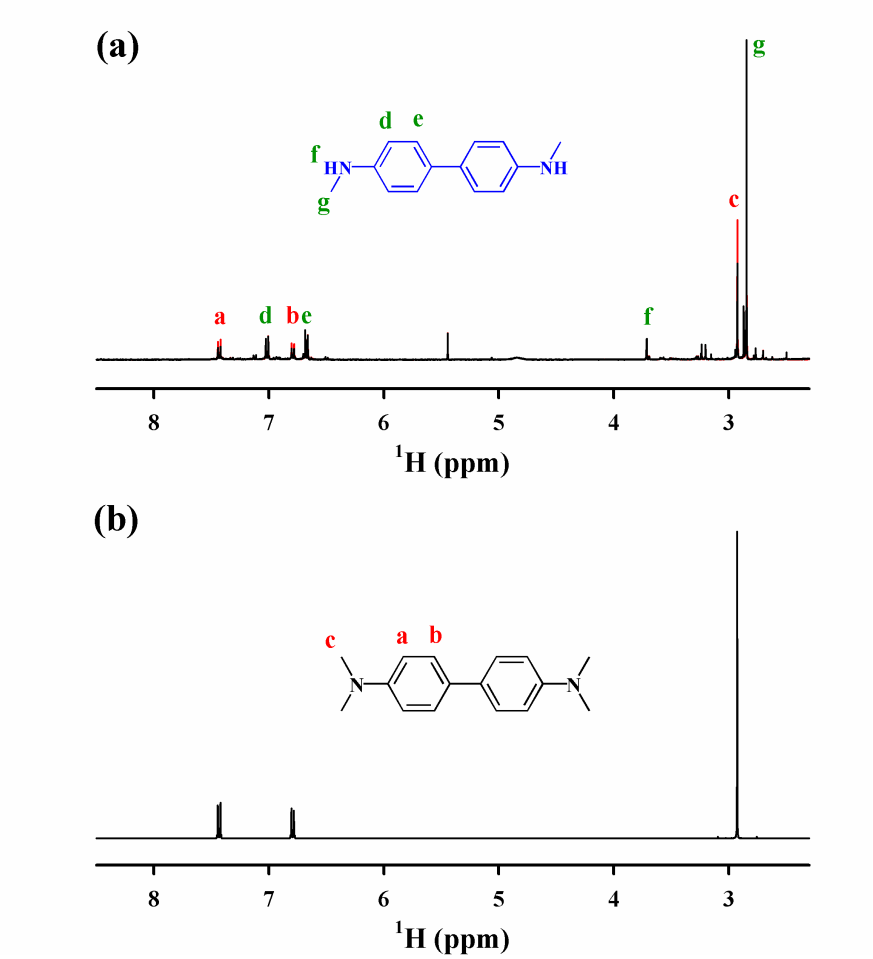

Figure 4. (a) ^{1}H NMR spectrum (400 MHz) of the products (black line) obtained in the reaction of $[(N4Py)Fe^{IV}(O)]^{2+}$ (2 mM) and DMA (1.5 equiv) in the presence of Sc^{3+} (0.11 equiv) in CD_3CN at 298 K. The products were obtained after column chromatography, which was packed with silicagel 60 and eluted by 96% CH_2Cl_2 and 4% methanol. Red line shows ^{1}H NMR spectrum of the products with *N*,*N*,*N*',*N*'-tetramethylbenzidine (TMB, 0.4 mM) as an internal standard. The peak integration ratios of a : b : c and d : e : f : g are 4 : 4 : 12 and 4 : 4 : 2 : 6, respectively. These ratios indicate that the products are TMB and *N*,*N*'-dimethylbenzidine (DMB) (see also Figure 5 for assignment of DMB). Yields of TMB and DMB based on the concentration of $[(N4Py)Fe^{IV}(O)]^{2+}$ were 8.0% and 32%, respectively. A trace amount of *N*-methylaniline was also obtained. (b) ^{1}H NMR spectrum (400 MHz) of TMB as an authentic reference.

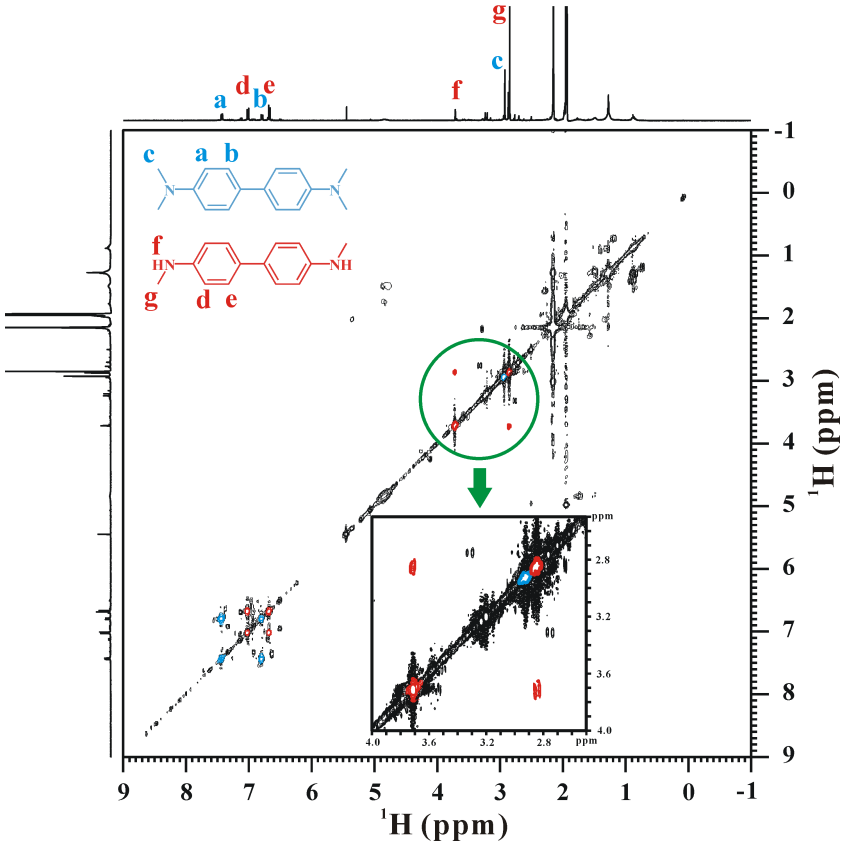

Figure 5. 2D ^{1}H–^{1}H COSY spectrum (400 MHz) of the products obtained in the reaction of $[(N4Py)Fe^{IV}(O)]^{2+}$ (2 mM) and DMA (1.5 equiv) in the presence of Sc^{3+} (0.11 equiv) in CD_3CN at 298 K. The products were obtained after column chromatography, which was packed with silicagel 60 and eluted by 96% CH_2Cl_2 and 4% methanol. The peak integration ratios of a : b : c and d : e : f : g are 4 : 4 : 12 and 4 : 4 : 2 : 6, respectively. There are good correlations between peaks a and b, d and e, and f and g, respectively. These ratios with correlation peaks indicate that the products are TMB and DMB.

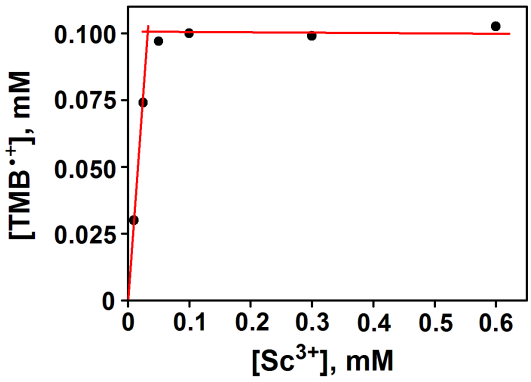

Figure 6. Plot of concentration of $TMB^{\bullet+}$ produced in the reaction of $[(N4Py)Fe^{IV}(O)]^{2+}$(0.30 mM) with DMA (0.6 – 1.4 mM) in the presence of Sc^{3+} in MeCN at 298 K vs Sc^{3+} concentration.

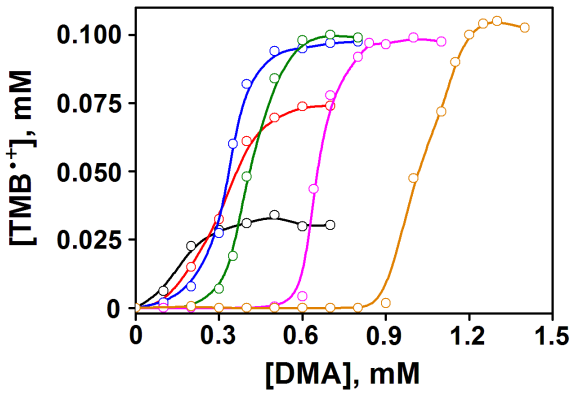

Figure 7. Plot of the concentration of $TMB^{\bullet+}$ generated vs DMA concentration depending on Sc^{3+} ion concentrations (0.010 mM, black open circle; 0.025 mM, red open circle; 0.050 mM, blue open circle; 0.10 mM, green open circle; 0.30 mM, pink open circle; 0.60 mM, yellow open circle) in the reaction of $[(N4Py)Fe^{IV}(O)]^{2+}$(0.30 mM) with DMA in MeCN at 298K.

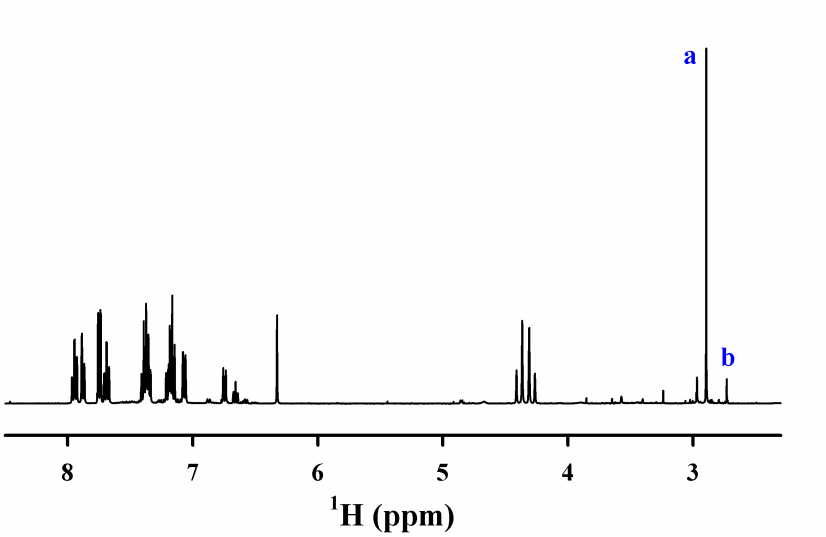

Figure 8. ^1H NMR spectra (400 MHz) of the products obtained in the reaction of $[(N4Py)Fe^{IV}(O)]^{2+}$ (2.0 mM) and DMA (40 mM, 20 equiv) in the absence of Sc^{3+} in CD_3CN at 298 K. Peaks a and b correspond to *N*-Me groups of DMA and *N*-methylaniline, respectively. Yield of *N*-methyl aniline based on the concentration of $[(N4Py)Fe^{IV}(O)]^{2+}$ was 62%. After column chromatography, TMB and DMB were also obtained, but yields of those compounds were just ~1.0% and 8.5%, respectively (see Figures 4 and 5 for experimental conditions).

Sc^{3+}-Enhanced Demethylation of X-DMA with $[(N4Py)Fe^{IV}(O)]^{2+}$. When DMA is replaced by *para*-cyano-*N*,*N*-dimethylaniline (CN-DMA), no dimer radical cation was formed even in the presence of $Sc(OTf)_3$, because the *para*-position is blocked by the

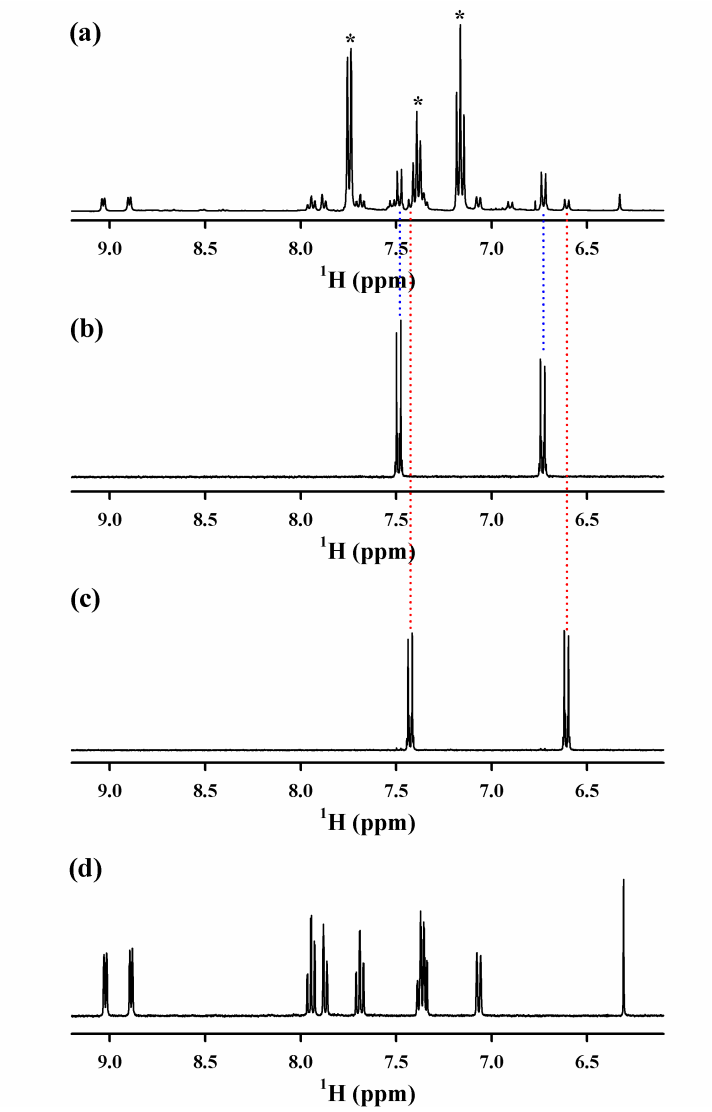

Figure 9. ^{1}H NMR spectra (400 MHz) of the reaction products and the authentic reference samples in the absence of Sc^{3+} in CD_3CN at 298 K. (a) shows ^{1}H NMR spectrum of the reaction products obtained in the reaction of $[(N4Py)Fe^{IV}(O)]^{2+}$ (4 mM) and CN-DMA (20 mM). The peaks marked with * are from PhI formed in the reaction of $[(N4Py)Fe^{II}]^{2+}$ and PhIO. According to the ratio between the peak integrations of the residual CN-DMA and generated *para*-CN-*N*-CH_3-aniline, yield of *para*-CN-*N*-CH_3-aniline based on the concentration of $[(N4Py)Fe^{IV}(O)]^{2+}$ was more than 95 %. (b), (c) and (d) show ^{1}H NMR spectra of the authentic samples, such as CN-DMA, *para*-CN-*N*-CH_3-aniline, $[(N4Py)Fe^{II}](ClO_4)_2$, respectively.

CN group and the demethylated product was obtained predominantly as identified by the ^{1}H NMR spectrum (Figures 9 and 10). The absorption spectral change in the reaction of CN-DMA with $[(N4Py)Fe^{IV}(O)]^{2+}$ in the absence and the presence of $Sc(OTf)_3$ in MeCN is shown in Figure 11a and 11b, respectively. In the presence of $Sc(OTf)_3$, the reaction rate was much enhanced as compared with that in the absence of

$Sc(OTf)_3$ and therefore the spectra in Figure 3b were measured using a stopped-flow spectrophotometer.[41] $Sc(OTf)_3$ is known to exist as a free ion (Sc^{3+}) in solution.[10] In each case only the decay of absorbance at 695 nm due to $[(N4Py)Fe^{IV}(O)]^{2+}$ was observed (i.e., no formation of dimer radical cation was observed). The decay rate of $[(N4Py)Fe^{IV}(O)]^{2+}$ with large excess CN-DMA and Sc^{3+} obeyed first-order kinetics (Table 1). Under the conditions in Figure 1a, the reaction was slowed down because of small concentration of DMA (0.44 mM) and $Sc(OTf)_3$ (0.15 mM). In such a case the proton-coupled electron transfer in Scheme 3 becomes playing a major role as the reaction proceed. This may be the reason why an induction period is observed in Figure 1a (right panel). In order to avoid the contribution of the proton–coupled electron transfer, the kinetic measurements were performed using a large concentration of Sc^{3+} (e.g., 10 mM). For the kinetic measurements no induction period was observed as shown in Figure 3b. The observed first-order rate constant (k_{obs}) in the presence of $Sc(OTf)_3$ becomes much larger than that in the absence of $Sc(OTf)_3$. Similar results are obtained for other *para*-substituted DMA derivatives (Figure 12).

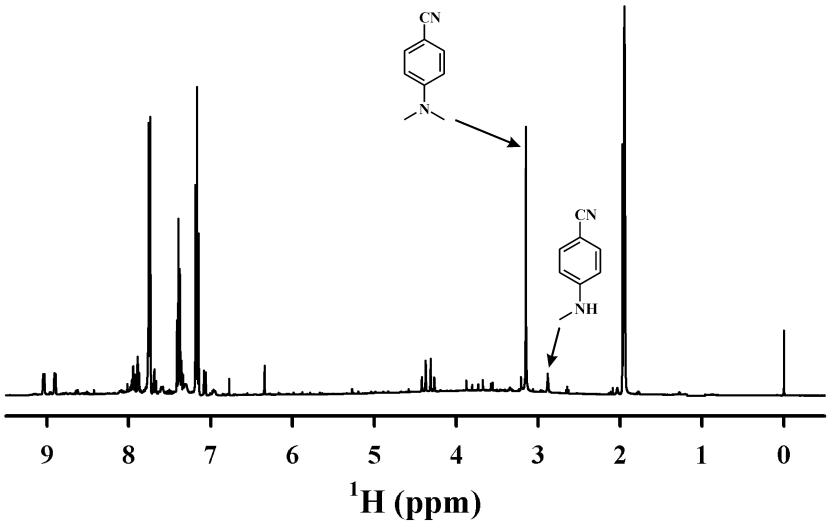

Figure 10. ^{1}H NMR spectrum (400 MHz) of the products obtained in the reaction of $[(N4Py)Fe^{IV}(O)]^{2+}$ (4 mM) and CN-DMA (20 mM) in the presence of Sc^{3+} (40 mM) in CD_3CN at 298 K. According to the ratio between the peak integrations of *N,N*-dimethyl group of the residual CN-DMA and *N*-methyl group of the generated para-CN-*N*-CH_3-aniline, yield of para-CN-*N*-CH_3-aniline based on the concentration of $[(N4Py)Fe^{IV}(O)]^{2+}$ was 75 %. Peak assignments were done by the titrations of CN-DMA and para-CN-*N*-CH_3-aniline with Sc^{3+} (see also Figure 21) because the chemical shifts of the peaks were dependent on the ratios of [CN-DMA]:[Sc^{3+}] and [para-CN-*N*-CH_3-aniline]:[Sc^{3+}] due to their binding constants.

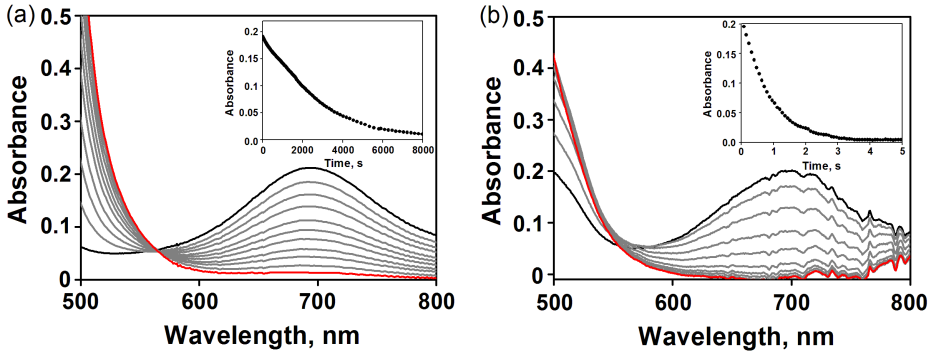

Figure 11. Visible spectral changes observed in the reaction of $[(N4Py)Fe^{IV}(O)]^{2+}$ (0.50 mM) with CN-DMA (5.0 mM) in the absence (a) and presence (b) of Sc^{3+} (15 mM) in MeCN at 298 K. Insets show time courses monitored at 695 nm.

Table 1. The k_{obs} Values Determined in the Reaction of $[(N4Py)Fe^{IV}(O)]^{2+}$ (0.50 mM) and X-DMA (5mM) Depending on Sc^{3+} Concentration in MeCN at 298 K

$[Sc^{3+}]$,	k_{obs}, s^{-1}			
mM	Me	H	Br	CN
5.0	$(6.6 \pm 0.2) \times 10^{-2}$	$(3.0 \pm 0.2) \times 10^{-2}$	$(1.3 \pm 0.1) \times 10^{-1}$	$(1.2 \pm 0.1) \times 10^{-1}$
10	$(1.5 \pm 0.2) \times 10^{-1}$	$(2.1 \pm 0.2) \times 10^{-1}$	$(3.1 \pm 0.2) \times 10^{-1}$	$(7.9 \pm 0.3) \times 10^{-1}$
15	$(3.0 \pm 0.2) \times 10^{-1}$	$(3.6 \pm 0.2) \times 10^{-1}$	$(4.6 \pm 0.2) \times 10^{-1}$	1.2 ± 0.1
20	$(3.8 \pm 0.2) \times 10^{-1}$	$(5.5 \pm 0.2) \times 10^{-1}$	$(6.3 \pm 0.2) \times 10^{-1}$	1.7 ± 0.2
25	$(5.3 \pm 0.3) \times 10^{-1}$	$(6.7 \pm 0.2) \times 10^{-1}$	$(7.2 \pm 0.2) \times 10^{-1}$	2.0 ± 0.2

Figure 13 shows the dependence of k_{obs} on concentration of $Sc(OTf)_3$. The k_{obs} values increase lineary with increasing Sc^{3+} concentration in the region where Sc^{3+} concentrations are larger than the concentration of DMA derivatives (X-DMA). Plots of k_{obs} versus $[Sc(OTf)_3]$ - [X-DMA] afford linear correlations (Figure 13, right panels). This indicates that Sc^{3+} forms a 1:1 complex with X-DMA and that Sc^{3+}-bound X-DMA is inert toward oxidation.

On the other hand, the k_{obs} value increases with increasing concentration of CN-DMA to reach a constant value in the region where concentrations of CN-DMA are larger than Sc^{3+} concentration as shown in Figure 14. This also indicates that Sc^{3+} binds with CN-DMA to form a 1:1 complex and the acceleration of the rate requires Sc^{3+} ion, which is not bound to CN-DMA. Similar results were obtained for other *para*-substituted DMA (X-DMA). Thus, the enhanced reactivity of X-DMA observed in

the presence of Sc^{3+} is ascribed to Sc^{3+} ion–coupled electron transfer from X-DMA to $[(N4Py)Fe^{IV}(O)]^{2+}$, as shown in Scheme 4. Because Sc^{3+} ions bound to X-DMA and $[(N4Py)Fe^{IV}(O)]^{2+}$ are in equilibrium with free Sc^{3+} ions in Scheme 4, there may be exchange equilibria among them.

Scheme 4

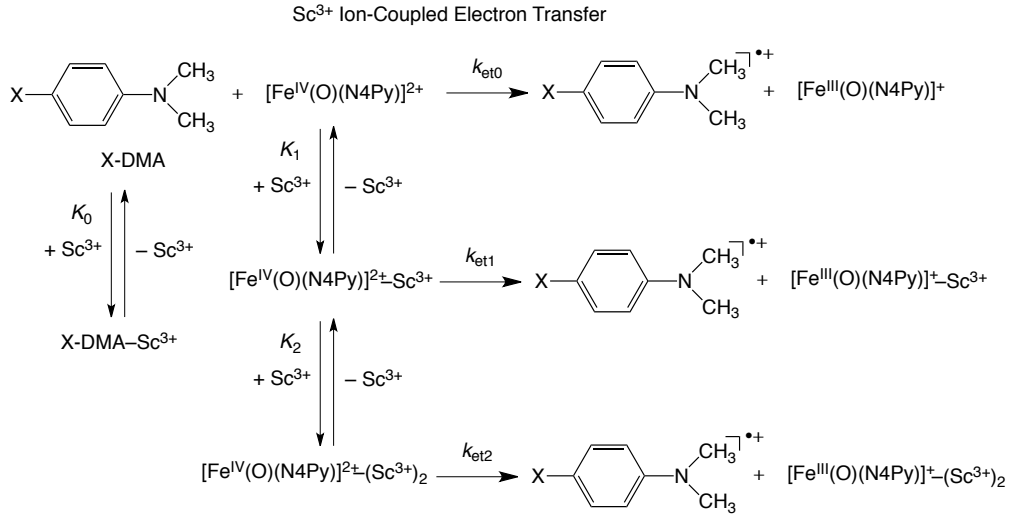

Electron transfer from X-DMA to $[(N4Py)Fe^{IV}(O)]^{2+}$ is enhanced by binding of Sc^{3+} to $[(N4Py)Fe^{IV}(O)]^{2+}$, which competes with the binding of Sc^{3+} to X-DMA. It has been reported that one Sc^{3+} ion or two Sc^{3+} ions can bind to $[(N4Py)Fe^{IV}(O)]^{2+}$ to enhance the electron–transfer reduction of $[(N4Py)Fe^{IV}(O)]^{2+}$.[10] In the case of DMA, the dimerization of $DMA^{\bullet+}$ may occur much more rapidly than proton transfer from $DMA^{\bullet+}$ to the Sc^{3+} ion–bound Fe(III)-oxo complex (Scheme 2). In the case of X-DMA, however, the dimerization of $X\text{-}DMA^{\bullet+}$ is prohibited by the *para*-substituent and proton transfer from $X\text{-}DMA^{\bullet+}$ to the Sc^{3+} ion–bound Fe(III)-oxo complex occurs that leads to the formation of the demethylated product, as shown in Scheme 1.

The results in Figure 13 and Figure 14 can be explained by Scheme 4. It should be emphasized that only uncomplexed Sc^{3+} and DMA are involved in Sc^{3+}ion–coupled electron transfer in Scheme 4, where two Sc^{3+} ions are involved as reported previously.[10] Under the conditions ($[Sc^{3+}] > [X\text{-}DMA]$) in Figure 13, Sc^{3+} ion–coupled electron transfer from free X-DMA to free Sc^{3+} is accelerated showing the second-order dependence on $[Sc^{3+}]$. At a constant concentration of X-DMA (5 mM), the concentration of free DMA decreases with increasing $[Sc^{3+}]$. For example, by using K_0 value (620 M^{-1}), the ratio of free DMA concentration to the total concentration (5 mM)

at 20 mM Sc^{3+} is only 9.1%. Thus, the concentration of free DMA is inversely proportional to concentration of Sc^{3+}: $[Sc^{3+}]^{-1}$. The second-order acceleration of the rate $[Sc^{3+}]^2$ is cancelled by the dependence of the ratio of free DMA on $[Sc^{3+}]^{-1}$. As a result, we can observe the apparent linear acceleration of the first-order rate constant with increasing concentration of Sc^{3+} in the region where $[Sc^{3+}] > [DMA]$ in Figure 13. On the other hand, under the conditions ($[Sc^{3+}] = 50$ mM) in Figure 14, the first-order rate constant increases with increasing concentration of DMA, but reaches a constant value

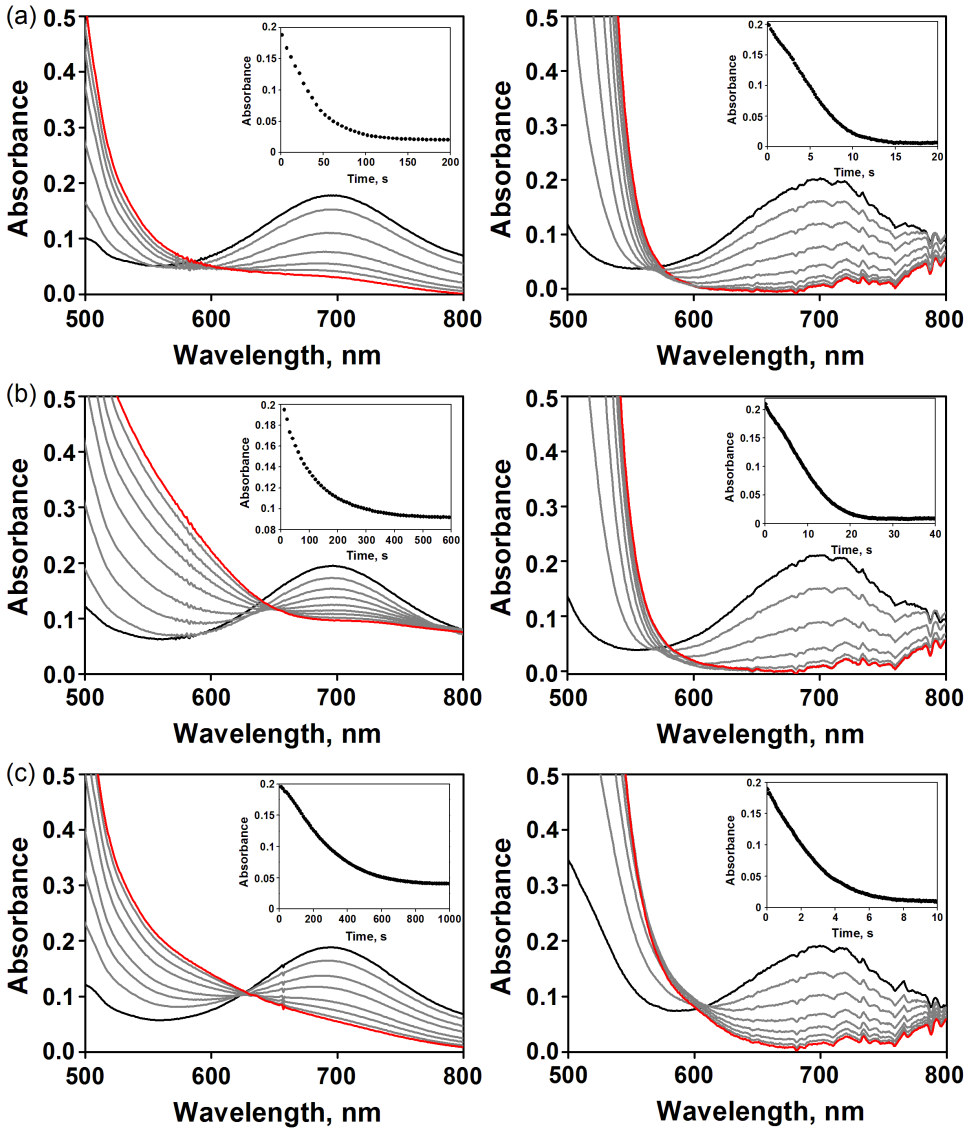

Figure 12. Visible spectral changes observed in the reactions of $[(N4Py)Fe^{IV}(O)]^{2+}$ (0.5 mM) with X-DMA (X = Me (a), H (b) and Br (c); 5.0 mM) in the absence (left panels) and presence (right panels) of free Sc^{3+} (10 mM) in MeCN at 298 K. Insets show time courses monitored at 695 nm.

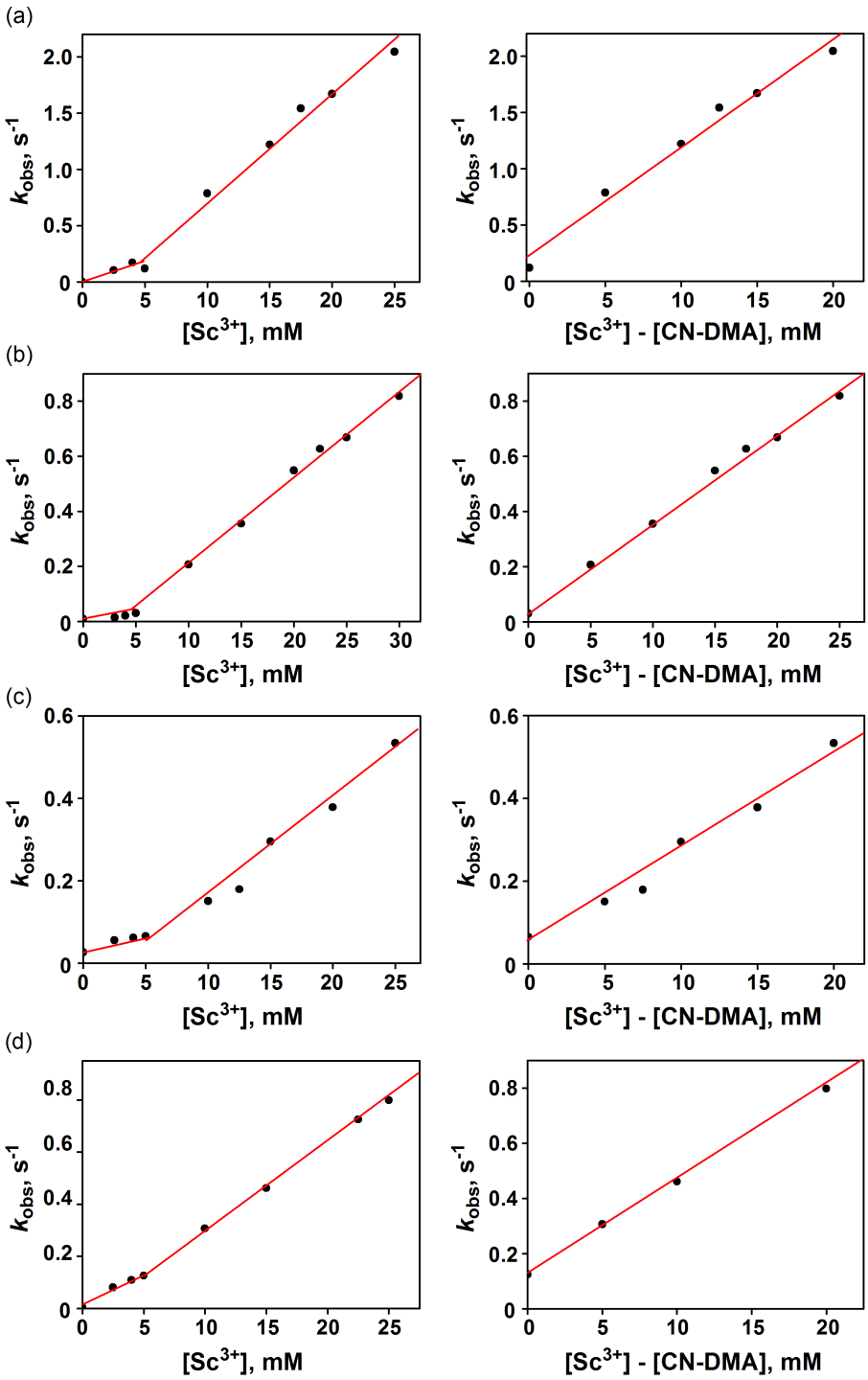

Figure 13. Plots of k_{obs} vs [Sc^{3+}] (left panels) and [Sc^{3+}] – [X-DMA] (right panels) in the reaction of $[(N4Py)Fe^{IV}(O)]^{2+}$ (0.50 mM) and X-DMA (5.0 mM) (X = CN (a), H (b), Me (c) and Br (d)) in the presence of Sc^{3+} in MeCN at 298 K.

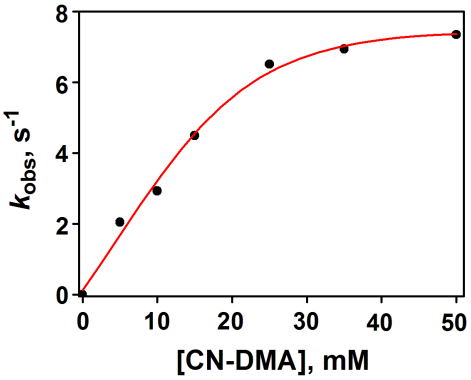

Figure 14. Plot of k_{obs} vs [CN-DNA] in the reaction of $[(N4Py)Fe^{IV}(O)]^{2+}$ (0.50 mM) and CN-DNA in the presence of Sc^{3+} (50 mM) in MeCN at 298 K.

in the region where [X-DMA] > $[Sc^{3+}]$, because the concentration of free Sc^{3+} is inversely proportional to concentration of DMA: $[DMA]^{-1}$. As a result, the first-order dependence of the rate on [X-DMA] is cancelled by the dependence of the concentration of free Sc^{3+} on $[X\text{-}DMA]^{-1}$ to be a constant value in the region where [X-DMA] > $[Sc^{3+}]$ in Figure 14. More quantitative analysis on Figure 13 and Figure 14 is given below.

According to Scheme 4, the reaction rate ($-d[Fe^{IV}(O)]/dt$ where $[Fe^{IV}(O)]$ = $[[(N4Py)Fe^{IV}(O)]^{2+}]$) is given by eqs 1 and 2,

$$-d[Fe^{IV}(O)]/dt = k_{et}\,[Fe^{IV}(O)][X\text{-}DMA] \quad (1)$$

$$k_{et} = (k_{et0} + k_{et1}K_1[Sc^{3+}] + k_{et2}K_1K_2[Sc^{3+}]^2) \quad (2)$$

where k_{et0}, k_{et1} and k_{et2} are the rate constants of electron transfer from X-DMA to $[(N4Py)Fe^{IV}(O)]^{2+}$, $[(N4Py)Fe^{IV}(O)]^{2+}$–Sc^{3+} and $[(N4Py)Fe^{IV}(O)]^{2+}$–$(Sc^{3+})_2$, respectively. K_1 and K_2 are the binding constants of Sc^{3+} to $[(N4Py)Fe^{IV}(O)]^{2+}$ and $[(N4Py)Fe^{IV}(O)]^{2+}$–Sc^{3+}, respectively. On the other hand, the concentration of Sc^{3+}-bound X-DMA [X-DMA–Sc^{3+}] is given by eq 3,

$$[X\text{-}DMA\text{–}Sc^{3+}] = K_0[X\text{-}DMA][Sc^{3+}] \quad (3)$$

where K_0 is the binding constant of Sc^{3+} to X-DMA.

When $[Sc^{3+}]_0 << [X\text{-}DMA]_0$ and $1 << K_0[DMA]$ (the subscript 0 denotes the initial

concentration), [X-DMA] ≅ [X-DMA]$_0$, [Sc^{3+}] ≅ [Sc^{3+}]$_0$/K_0[X-DMA]$_0$. In such a case, the binding of Sc^{3+} to [(N4Py)Fe^{IV}(O)]$^{2+}$–Sc^{3+} may be negligible because of the small concentration of free Sc^{3+} and the observed first-order rate constant (k_{obs}) is given from eqs 1-3 by eq 4, where k_{et0} is neglected. This equation agrees with the constant dependence of k_{obs} on [X-DMA] in the region where [Sc^{3+}] << [X-DMA] in Figure 14.

$$k_{obs} \cong k_{et1}K_1[Sc^{3+}]_0/K_0 \quad (4)$$

When [Sc^{3+}] >> [X-DMA] and K_0[Sc^{3+}] >> 1, [Sc^{3+}] ≅ [Sc^{3+}]$_0$, [X-DMA] ≅ [X-DMA]$_0$/K_0[Sc^{3+}]$_0$. In such a case the binding of Sc^{3+} to [(N4Py)Fe^{IV}(O)]$^{2+}$–Sc^{3+} (K_2) may be dominant as compared to the binding of Sc^{3+} to [(N4Py)Fe^{IV}(O)]$^{2+}$ (K_1) and k_{obs} is given by eq 5, which agrees with the linear dependence of k_{obs} on [Sc^{3+}] in the region where [Sc^{3+}] > [X-DMA] in Figure 13 and also the linear dependence of k_{obs} on [X-DMA] in the region where [X-DMA] << [Sc^{3+}] in Figure 14.

$$k_{obs} \cong k_{et2}K_1K_2[Sc^{3+}]_0[X\text{-}DMA]_0/K_0 \quad (5)$$

The complex formation of X-DMA with Sc^{3+} is also indicated by the UV-vis spectral change of X-DMA in the presence of $Sc(OTf)_3$. As shown in Figure 15, the absorption band at 293 nm due to CN-DMA is changed due to formation of the CN-DMA–Sc^{3+} complex with a clean isosbestic point. The K_0 value is determined from the intercept and slope of the linear plot of $(\Delta A)^{-1}$ vs [Sc^{3+}]$^{-1}$ (Figure 15c) to be 6.2×10^2 M^{-1}. The UV-vis spectral titrations of other DMA derivatives with Sc^{3+} are shown in Figure 16. The spectral titration of X-DMA with $Sc(OTf)_3$ indicates that Sc^{3+} forms a 1:1 complex with X-DMA. The 1:1 complex formation between X-DMA and Sc^{3+} was also confirmed by the ^{1}H NMR spectra (Figures 17-21). The change in the chemical shift of the *N*-Me group by binding of Sc^{3+} indicates that Sc^{3+} ion binds to the nitrogen of the *N*-Me group of X-DMA. The binding constants K_0 were determined from the spectral change of X-DMA with Sc^{3+} and the K_0 values thus determined are listed in Table 2 together with the one-electron oxidation potentials of X-DMA (E_{ox}). The K_0 value increases with decreasing the E_{ox} value. This indicates that the stronger is the electron donor ability of X-DMA, the larger becomes the binding constant of Sc^{3+} to X-DMA.

The k_{obs} values with 5.0 mM X-DMA and 15 mM Sc^{3+} are also listed in Table 2 together with k_{obs} values in the absence of $Sc(OTf)_3$ in MeCN at 298 K. The k_{obs} values

in the presence of Sc^{3+} (15 mM) are significantly larger than those in the absence of Sc^{3+} for each X-DMA. In the absence of Sc^{3+}, the k_{obs} value increases with decreasing the E_{ox} value of X-DMA and Me-DMA with an electron-donating *para*-substituent affords the largest k_{obs} value, whereas CN-DMA with an electron-withdrawing substituent affords the largest k_{obs} value in the presence of Sc^{3+}. This results from the binding of Sc^{3+} to X-DMA. As mentioned above, Sc^{3+}–bound DMA derivatives exhibit negligible reactivity as compared with Sc^{3+}–free DMA derivatives.

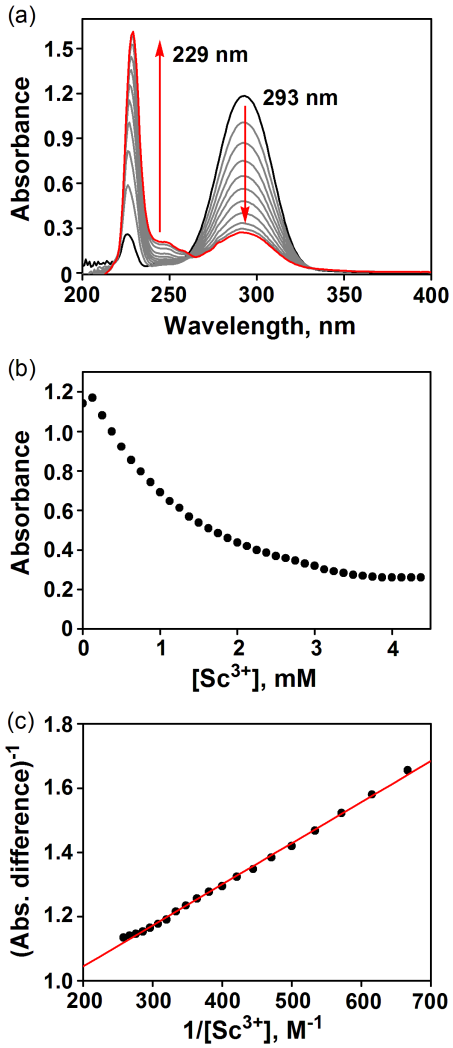

Figure 15. (a) Visible spectral changes observed in the titration of CN-DMA with Sc^{3+} upon addition of Sc^{3+} (0.0 – 4.0 mM) into the CN-DMA solution (0.050 mM) in MeCN at 298 K. (b) Plot of the absorbance at 293 nm vs $[Sc^{3+}]$ in the titration of CN-DMA with Sc^{3+} upon addition of Sc^{3+} (0.0 – 4.0 mM) into the CN-DMA solution (0.050 mM) in MeCN at 298 K. (c) Plot of reciprocal absorbance difference vs $1/[Sc^{3+}]$ for the determination of the binding constant between *p*-CN-DMA and Sc^{3+} (see Figure 16 for other case of X-DMA).

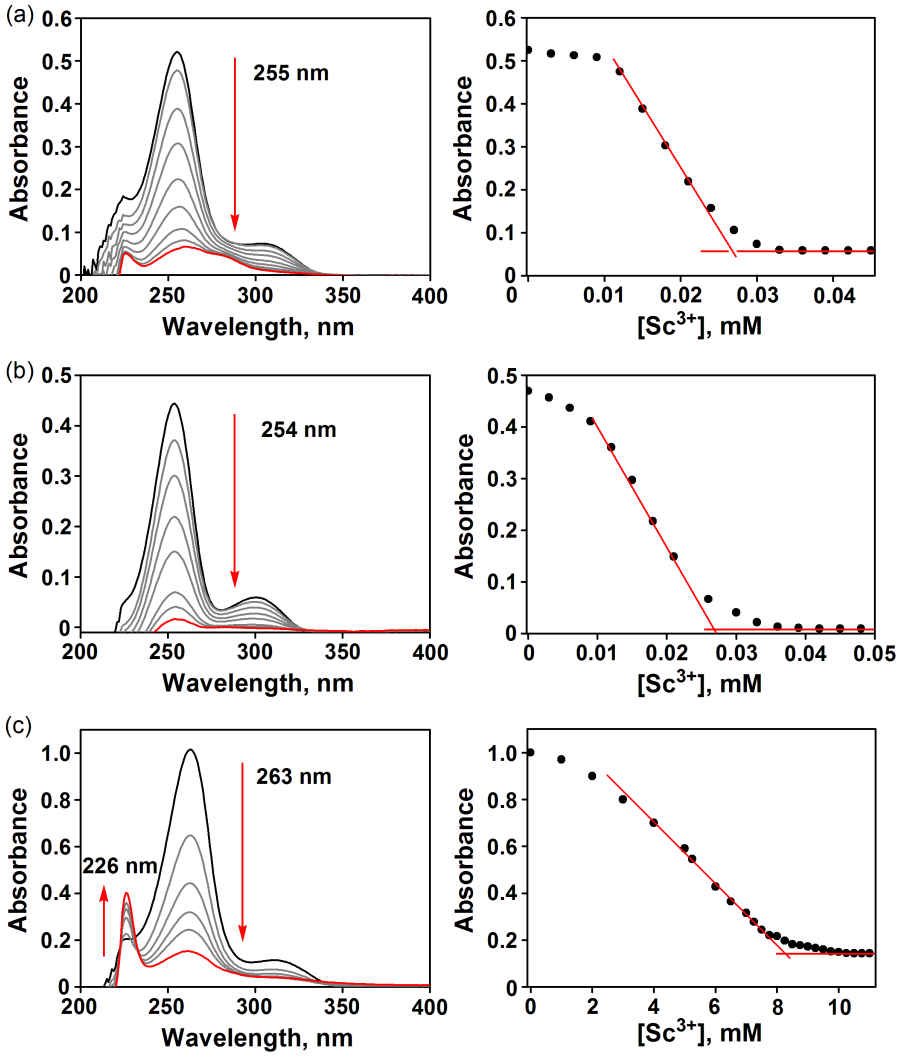

Figure 16. Visible spectral changes (left panels) and plots of the absorbance of X-DMA vs [Sc^{3+}] (right panels) observed in the titration of X-DMA (X = Me (0.03mM) (a), H (0.03 mM) (b), and Br (0.05mM) (c)) with Sc^{3+} for the determination of binding constants of X-DMA and Sc^{3+} in CH_3CN at 298 K.

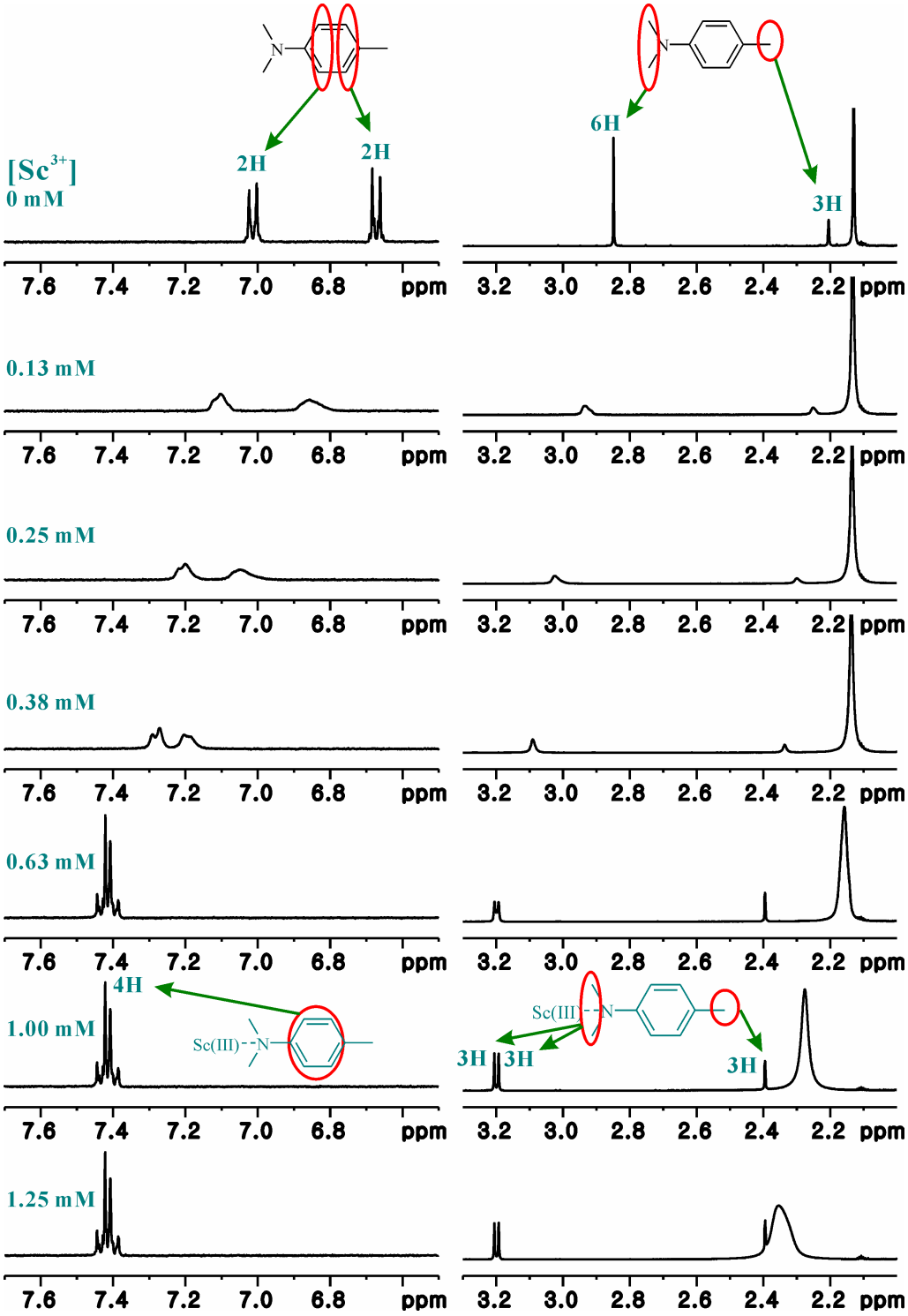

Figure 17. ^{1}H NMR spectral changes of Me-DMA (1.0 mM) upon addition of Sc^{3+} (0 – 1.25 mM) in CD_3CN at 298 K.

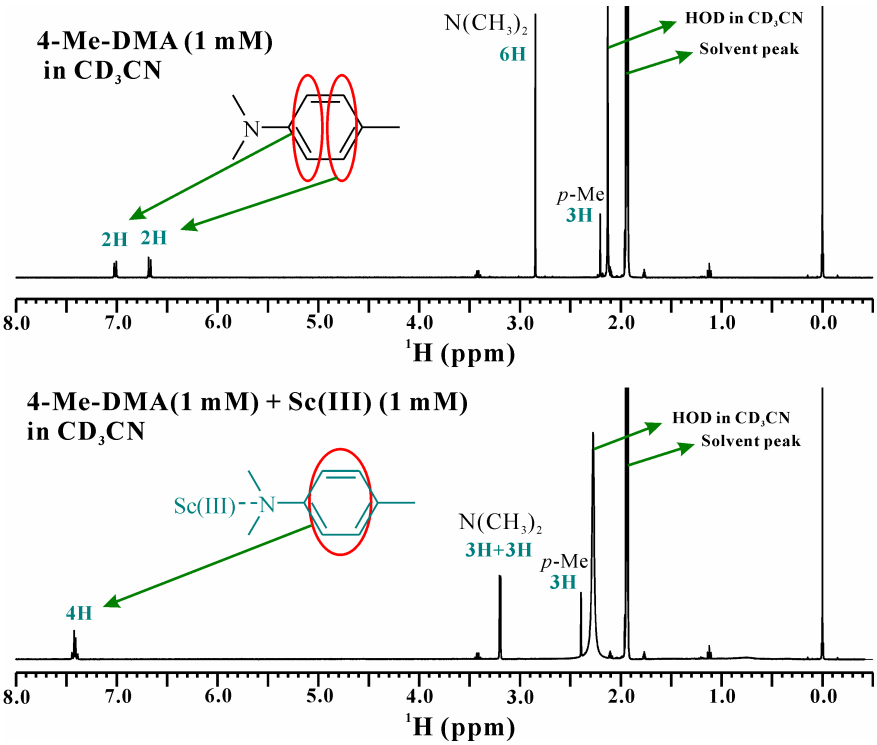

Figure 18. ^{1}H NMR spectra of Me-DMA (1.0 mM) and Me-DMA-Sc^{3+} (1.0 mM) in CD_3CN at 298 K.

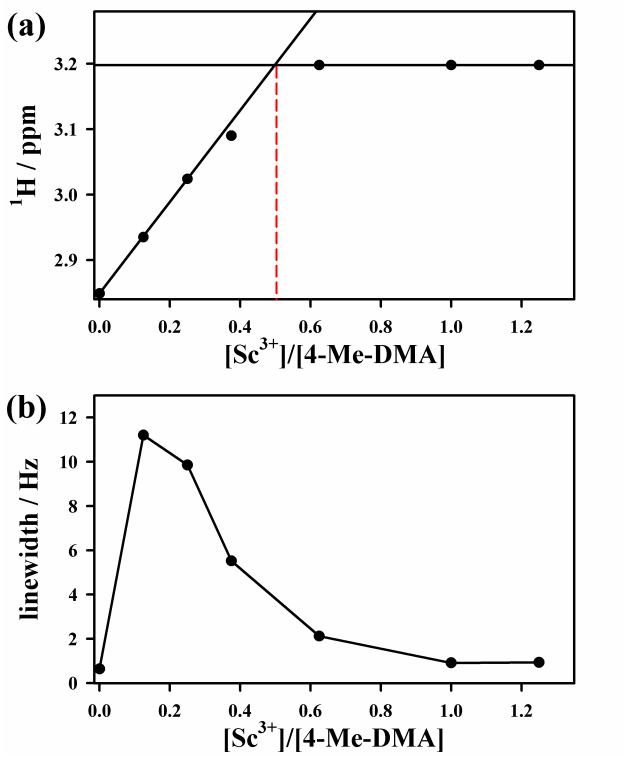

Figure 19. Chemical shift (a) and spectral line width (b) profiles of ^{1}H NMR signal for *N*,*N*-dimethyl group of Me-DMA as a function of increasing [Sc^{3+}]:[Me-DMA] ratio in CD_3CN at 298K.

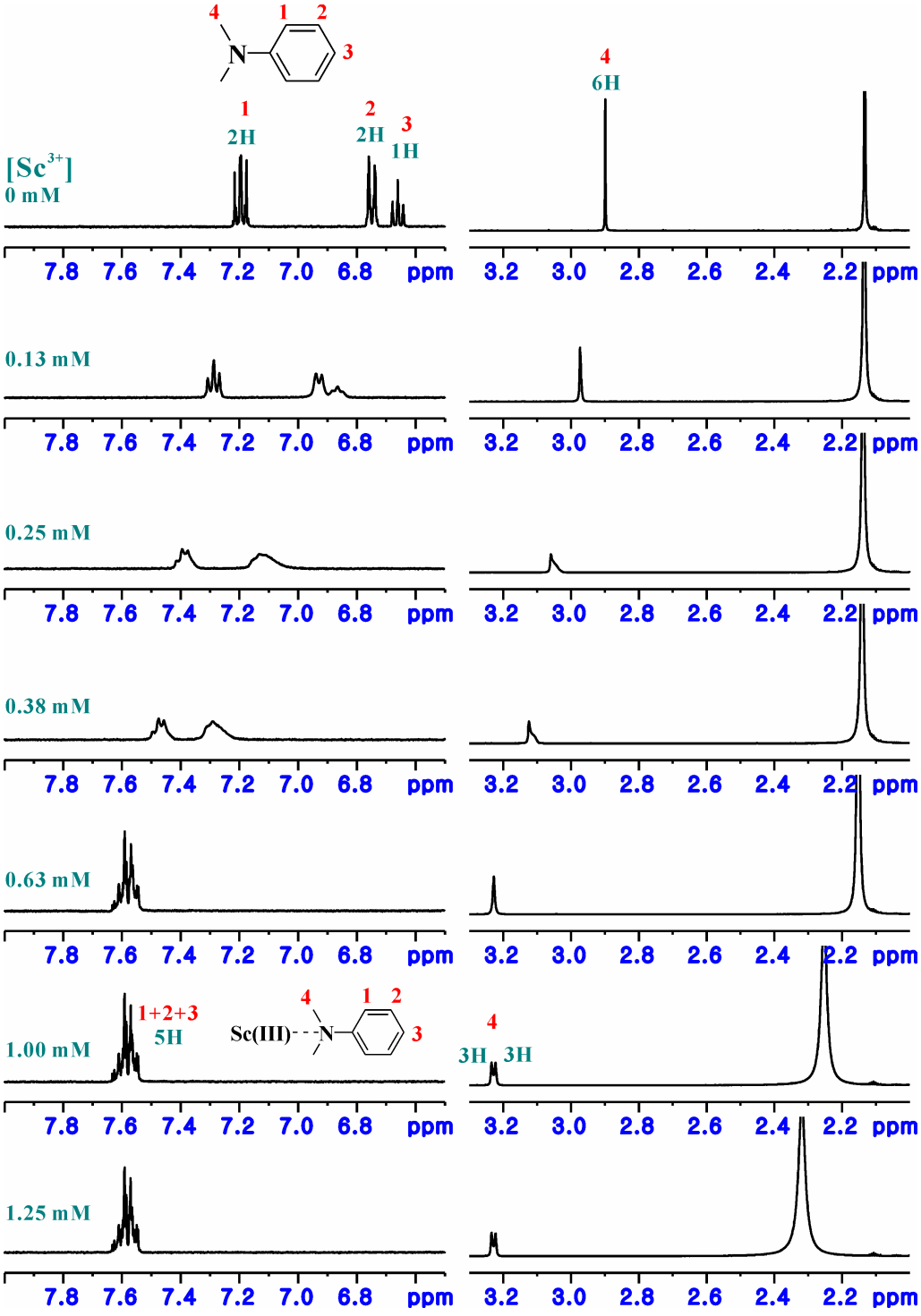

Figure 20. ^{1}H NMR spectral changes of DMA (1.0 mM) upon addition of Sc^{3+} (0 – 1.25 mM) in CD_3CN at 298 K.

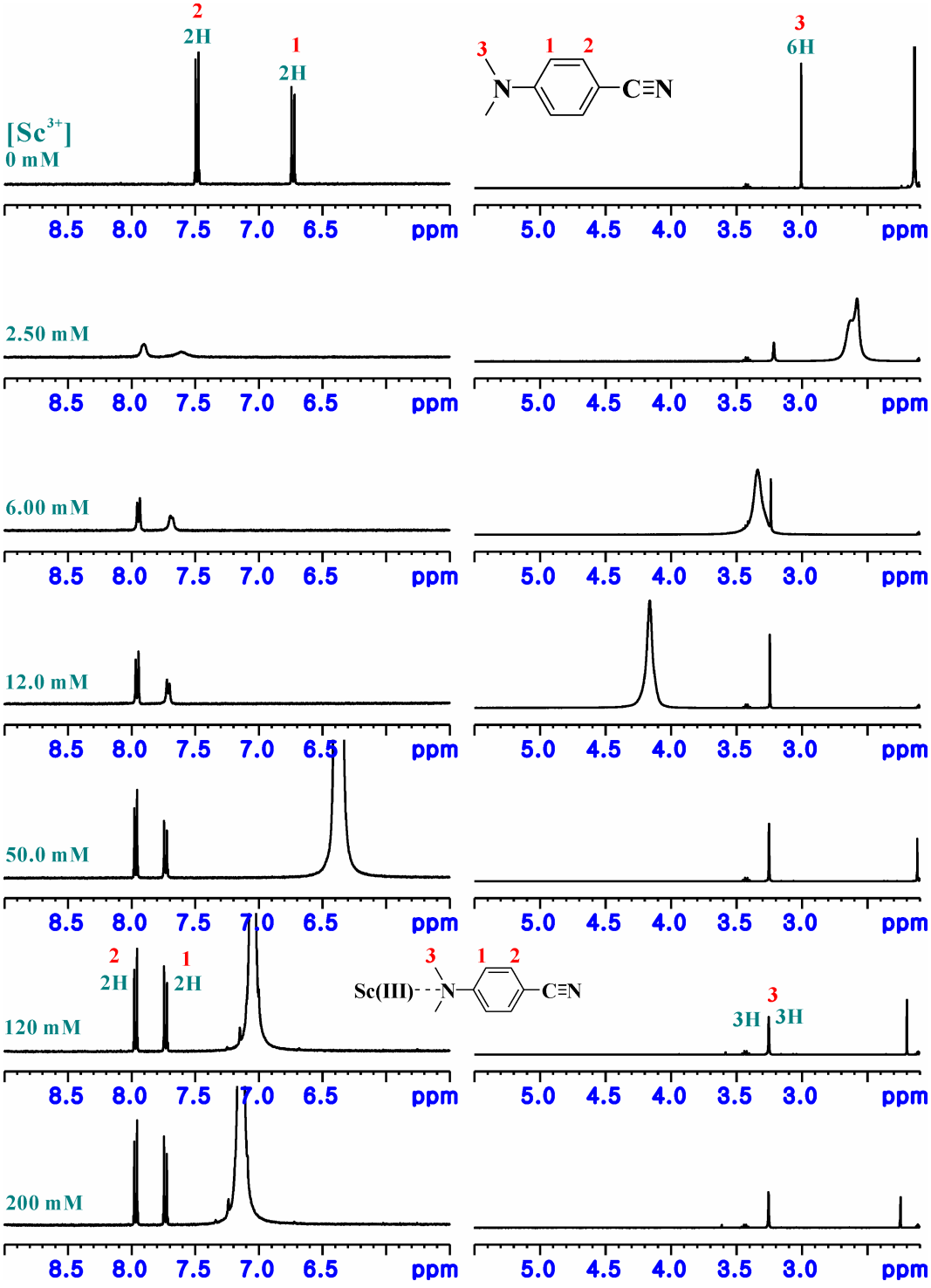

Figure 21. ^{1}H NMR spectral changes of CN-DMA (1.0 mM) upon addition of Sc^{3+} (0 – 200 mM) in CD_3CN at 298 K.

This was confirmed by the change in the one-electron oxidation potential (E_{ox}) of X-DMA in the presence of $Sc(OTf)_3$ as shown in Figure 22, where the redox couple of CN-DMA in the absence of Sc^{3+} at $E_{1/2}$ = 1.13 V (vs SCE) disappears as concentration of Sc^{3+} increases. No anodic peak of CN-DMA is observed in the presence of large excess $Sc(OTf)_3$ (10 mM). This indicates that the E_{ox} value of CN-DMA (1.13 V vs SCE)[36] is positively shifted to the value larger than 2.0 V (vs SCE) when Sc^{3+} is bound to CN-DMA. Thus, once Sc^{3+} is bound to X-DMA, the X-DMA–Sc^{3+} complex cannot act as an electron donor and only free X-DMA is involved in the Sc^{3+} ion–coupled electron transfer to $[(N4Py)Fe^{IV}(O)]^{2+}$ (E_{red} = 1.19 V vs SCE in the presence of 10 mM of Sc^{3+})[10] as shown in Scheme 4.

Table 2. Binding Constants (K_0) of Sc^{3+} with X-DMA, One-Electron Oxidation Potentials (E_{ox} vs SCE) of X-DMA, Rate Constants of Reactions of $[(N4Py)Fe^{IV}(O)]^{2+}$ (0.50 mM) with X-DMA (5.0 mM) in the Absence and Presence of Sc^{3+} (15 mM) in MeCN at 298 K

X	E_{ox} (vs SCE, V)	K_0[a], M^{-1}	k_{obs}[b], s^{-1}	k_{obs}[c], s^{-1}	k_{et}[d], M^{-1} s^{-1}
M	0.69	$(3.0 \pm 0.3) \times 10^7$	$(2.6 \pm 0.2) \times 10^{-2}$	$(3.0 \pm 0.2) \times 10^{-1}$	$(1.8 \pm 0.2) \times 10^7$
H	0.76	$(7.3 \pm 0.4) \times 10^6$	$(8.9 \pm 0.3) \times 10^{-3}$	$(3.6 \pm 0.2) \times 10^{-1}$	$(5.3 \pm 0.2) \times 10^6$
Br	0.92	$(3.6 \pm 0.2) \times 10^5$	$(4.1 \pm 0.2) \times 10^{-3}$	$(4.6 \pm 0.3) \times 10^{-1}$	$(3.3 \pm 0.2) \times 10^5$
C	1.15	$(6.2 \pm 0.2) \times 10^2$	$(3.9 \pm 0.2) \times 10^{-4}$	1.2 ± 0.1	$(1.5 \pm 0.1) \times 10^3$

[a] The K_0 values were determined by the UV-vis spectral titration of X-DMA with Sc^{3+}. [b] Rate constants in the absence of Sc^{3+}. [c] Rate constants determined in the presence of 15 mM of Sc^{3+}. [d] Rate constants of reactions of $[(N4Py)Fe^{IV}(O)]^{2+}$ with free X-DMA which is not bound to Sc^{3+}, determined by eq 6, when the concentration of free Sc^{3+} ($[Sc^{3+}]_0 - [X\text{-}DMA]_0$) is 10 mM.[42]

The second-order rate constant (k_{et}) of Sc^{3+} ion-coupled electron transfer from free X-DMA, which is not bound to Sc^{3+}, to $[(N4Py)Fe^{IV}(O)]^{2+}$ is derived from the observed pseudo-first-order rate constant (k_{obs}) with large excess X-DMA as given by eq 6,

$$k_{et} \cong k_{obs}(K_0[Sc^{3+}] + 1)/[X\text{-}DMA]_0 \quad (6)$$

because $[X\text{-}DMA] = [X\text{-}DMA]_0/(1 + K_0[Sc^{3+}])$ according to eq 3 (note that $[X\text{-}DMA]_0 = [X\text{-}DMA] + [X\text{-}DMA\text{–}Sc^{3+}]$). The k_{et} values thus evaluated from the k_{obs} values are

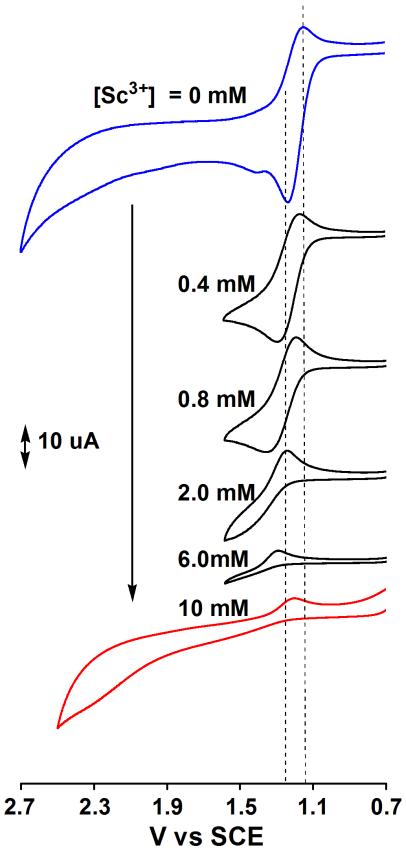

Figure 22. Cyclic voltammograms of CN-DMA (2.0 mM) upon addition of $Sc(OTf)_3$ into an MeCN solution of CN-DMA containing $TBAPF_6$ (0.10 M) at 298 K with a Pt working electrode. Scan rate was 0.10 V s^{-1}.

listed in Table 2, where the concentration of free Sc^{3+}, which is not bound to X-DMA, is 10 mM ($[Sc^{3+}]_0 - [X\text{-}DMA]_0$). For example, the k_{et} value of DMA was determined from the k_{obs} value (0.36 s^{-1} in Table 2) using eq 6 to be 5.3×10^6 M^{-1} s^{-1} ($= 0.36 \times (7.3 \times 10^6 \times 1.0 \times 10^{-2} + 1)/(5.0 \times 10^{-3})$).

Driving Force of Sc^{3+}–Coupled Electron Transfer. The driving force dependence of the rate constants (k_{et0}) of the demethylation reactions of X-DMA with $[(N4Py)Fe^{IV}(O)]^{2+}$ in the absence of Sc^{3+} is shown in Figure 23 together with the driving force dependence of the rate constants (k_{et}) of Sc^{3+} ion–coupled electron transfer from free X-DMA, which is not bound to Sc^{3+}, and various one-electron reductants to $[(N4Py)Fe^{IV}(O)]^{2+}$. The driving force dependence of k_{et} is well fitted in light of the Marcus theory of adiabatic outer-sphere electron transfer (eq 7),

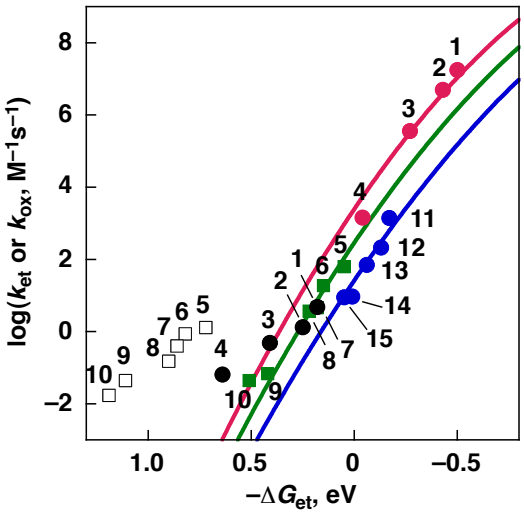

Figure 23. Plots of log k_{et} for electron transfer from X-DMA (X = Me for 1, H for 2, Br for 3, CN for 4) to $[(N4Py)Fe^{IV}(O)]^{2+}$ in the absence of Sc^{3+} (closed black circles) and in the presence of free Sc^{3+} (10 mM, closed pink circles) in MeCN at 298 K vs the driving force of electron transfer [$-\Delta G_{et} = e(E_{red} - E_{ox})$] from X-DMA to $[(N4Py)Fe^{IV}(O)]^{2+}$. Squares show the driving force dependence of rate constants (log k_{ox} for oxygenation reaction of *para*-X-substituted thioanisoles (X = Me for 5, H for 6, Cl for 7, Br for 8, CN for 9, NO_2 for 10) by $[(N4Py)Fe^{IV}(O)]^{2+}$ in the absence of Sc^{3+} (open black squares) and in the presence of Sc^{3+} (10 mM, closed green squares) in MeCN at 298 K. Closed blue circles show the driving force dependence of rate constants (log k_{et}) for electron transfer from one-electron reductants (11, $[Fe^{II}(Ph_2phen)_3]^{2+}$ (Ph_2phen = 4,7-diphenyl-1,10-phenanthroline); 12, $[Fe^{II}(bpy)_3]^{2+}$ (bpy = 2,2'-bipyridine); 13, $[Ru^{II}(Me_2bpy)_3]^{2+}$ (Me_2bpy = 4,4'-dimethyl-2,2'-bipyridine); 14, $[Fe^{II}(Clphen)_3]^{2+}$ (Clphen = 5-chloro-1,10-phenanthroline); 15, $[Ru^{II}(bpy)_3]^{2+}$) to $[(N4Py)Fe^{IV}(O)]^{2+}$ in the presence of Sc^{3+} (10 mM). The fitting to the Marcus theory of the electron transfer are shown by the pink line with λ = 1.79 eV, green line with λ = 2.02 eV and blue line with λ = 2.27 eV, respectively.

$$k_{et} = Z\exp[-(\lambda/4)(1 + \Delta G_{et}/\lambda)^2/k_B T] \quad (7)$$

where Z is the collision frequency taken as 1×10^{11} M^{-1} s^{-1}, λ is the reorganization energy of electron transfer, k_B is the Boltzmann constant, and T is the absolute temperature.[43] The best fit λ value of Sc^{3+} ion–coupled electron transfer from X-DMA, which is not bound to Sc^{3+}, to $[(N4Py)Fe^{IV}(O)]^{2+}$ is determined to be 1.79 eV, which is smaller than the λ value of electron transfer from one-electron reductants (2.27 eV).[10] The smaller λ value Sc^{3+} ion–coupled electron transfer from X-DMA to $[(N4Py)Fe^{IV}(O)]^{2+}$ may result from the smaller λ value of electron exchange between X-DMA and $X\text{-DMA}^{\bullet+}$ as compared with the λ values of metal complexes used as

one-electron reductants. Thus, the demethylation of X-DMA with $[(N4Py)Fe^{IV}(O)]^{2+}$ in the presence of Sc^{3+} proceeds via Sc^{3+} ion–coupled electron transfer from X-DMA to $[(N4Py)Fe^{IV}(O)]^{2+}$ as shown in Scheme 4.

In the absence of Sc^{3+}, the k_{et0} values of Me-DMA and DMA agree with those predicted by the Marcus plot of electron transfer with λ = 2.02 eV. With increasing the E_{ox} values of X-DMA with electron withdrawing *para*-substituents (Br and CN), the deviation of the observed rate constant from the predicted value by the Marcus plot of electron transfer becomes larger, when the $-\Delta G_{et}$ value becomes more positive than 0.4 eV. Thus, the borderline between a direct hydrogen atom transfer pathway and an electron-transfer pathway (Scheme 1) may be determined by the E_{ox} value of X-DMA, ca. 1.2 V vs SCE that corresponds to Br-DMA. It is interesting to note that this border line is virtually the same as reported between oxygen atom transfer pathway and an electron transfer pathway for the oxygenation of thioanisole derivatives with $[(N4Py)Fe^{IV}(O)]^{2+}$ as shown in Figure 23 (no. 5-10).[11]

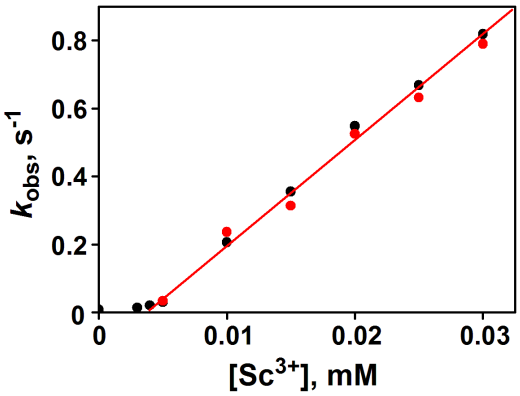

Figure 24. Plot of k_{obs} vs Sc^{3+} concentration in the reaction $[(N4Py)Fe^{IV}(O)]^{2+}$ (0.50 mM) with DMA (5.0 mM, black circle) and DMA–d_6 (5.0 mM, red circle) in MeCN at 298 K. Kinetic isotope effect (KIE) value was determined to be 1.0.

It is also important to note that through the use of DMA and deuterated DMA (*N*,*N*-dimetyl-d_6-aniline; DMA-d_6) as a substrate in the presence of Sc^{3+}, the k_{obs} values increase linearly with increasing Sc^{3+} concentration in the region where Sc^{3+} concentrations are larger than concentration of DMA and DMA-d_6, respectively, and no deuterium kinetic isotope effect (KIE) was observed, i.e., KIE = 1.0 (Figure 24). This result confirms that the initial Sc^{3+} ion–coupled electron transfer from DMA and DMA-d_6 to $[(N4Py)Fe^{IV}(O)]^{2+}$ is the rate-determining step.

Conclusion

Rates of oxidation of X-DMA with $[(N4Py)Fe^{IV}(O)]^{2+}$ were significantly accelerated by the presence of $Sc(OTf)_3$ in MeCN at 298 K. In the case of DMA, the demethylation of DMA occurs via electron transfer from DMA to $[(N4Py)Fe^{IV}(O)]^{2+}$, followed by proton transfer from $DMA^{\bullet+}$ to $[(N4Py)Fe^{III}(O)]^{+}$. The initial electron transfer is remarkably accelerated by Sc^{3+} ion–coupled electron transfer. However, the subsequent proton transfer is prohibited by the binding of Sc^{3+} to $[(N4Py)Fe^{III}(O)]^{+}$, when $DMA^{\bullet+}$ dimerizes to form TMB, which is further oxidized by $[(N4Py)Fe^{IV}(O)]^{2+}$ to yield $TMB^{\bullet+}$ as the final three-electron oxidized product. When *para*-substituted DMA derivatives (X-DMA: X = Me, Br and CN) are employed, the initial electron transfer is also remarkably accelerated by Sc^{3+} ion–coupled electron transfer. The resulting $X\text{-}DMA^{\bullet+}$ cannot dimerize because of the blockage of *para*-position, leading to the demethylation. The complicated kinetics of Sc^{3+} ion–coupled electron transfer from X-DMA to $[(N4Py)Fe^{IV}(O)]^{2+}$ is well analyzed by the competition of binding of Sc^{3+} to X-DMA and $[(N4Py)Fe^{IV}(O)]^{2+}$. The rate constants of Sc^{3+} ion–coupled electron transfer from uncomplexed X-DMA to $[(N4Py)Fe^{IV}(O)]^{2+}$, which were evaluated using the binding constants (K_0) of Sc^{3+} to X-DMA, agree well with those predicted by the Marcus plot of the rate constants of Sc^{3+} ion–coupled electron transfer from one-electron reductants to $[(N4Py)Fe^{IV}(O)]^{2+}$. Thus, the present study provides a general way to enhance the reactivity of high-valent metal-oxo species by binding of redox-inactive metal ions such as Sc^{3+} towards substrates which also bind with metal ions.

References

(1) (a) Ortiz de Montellano, P. R. *Cytochrome P450: Structure, Mechanism, and Biochemistry*, 3rd ed.; Kluwer Academic/Plenum Publishers: New York, 2005. (b) Meunier, B., Ed. *Biomimetic Oxidations Catalyzed by Transition Metal Complexes*; Imperial College Press: London, 2000. (c) *The Ubiquitous Role of Cytochrome P450 Proteins In Metal Ions in Life Sciences*; Sigel, A., Sigel, H., Sigel, R. K. O., Eds.; John Wiley & Sons Ltd: Chichester, England, 2007; Vol. 3.

(2) (a) Sono, M.; Roach, M. P.; Coulter, E. D.; Dawson, J. H. *Chem. Rev*. **1996**, *96*, 2841. (b) Watanabe, Y. *J. Biol. Inorg. Chem*. **2001**, *6*, 846. (c) Jung, C. *Biochim. Biophys. Acta* **2011**, *1814*, 46.

(3) (a) Groves, J. T.; Shalyaev, K.; Lee, J. In *The Porphyrin Handbook*; Kadish, K. M., Smith, K. M., Guilard, R., Eds.; Academic Press: Elsevier Science (USA), 2000, Vol. 4, pp 17-40. (b) Watanabe, Y. In *The Porphyrin Handbook*; Kadish, K. M., Smith, K. M., Guilard, R., Eds.; Academic Press: Elsevier Science (USA), 2000, Vol. 4, pp 97-117. (c) Groves, J. T. *J. Inorg. Biochem*. **2006**, *100*, 434.

(4) (a) Meunier, B.; de Visser, S. P.; Shaik, S. *Chem. Rev.* **2004**, *104*, 3947. (b) Shaik, S.; Cohen, S.; Wang, Y.; Chen, H.; Kumar, D.; Thiel, W. *Chem. Rev*. **2010**, *110*, 949. (c) Abu-Omar, M. M.; Loaiza, A.; Hontzeas, N. *Chem. Rev.* **2005**, *105*, 2227. (d) Denisov, I. G.; Makris, T. M.; Sligar, S. G.; Schlichting, I. *Chem. Rev.* **2005**, *105*, 2253. (e) Ortiz de Montellano, P. R. *Chem. Rev*. **2010**, *110*, 932.

(5) (a) Krebs, C.; Fujimori, D. G.; Walsh, C. T.; Bollinger, J. M., Jr. *Acc. Chem. Res.* **2007**, *40*, 484. (b) Que, L., Jr. *Acc. Chem. Res*. **2007**, *40*, 493. (c) Nam, W. *Acc. Chem. Res.* **2007**, *40*, 522. (d) Borovik, A. S. *Acc. Chem. Res.* **2005**, *38*, 54. (e) Shaik, S.; Lai, W.; Chen, H.; Wang, Y. *Acc. Chem. Res*. **2010**, *43*, 1154.

(6) (a) Comba, P.; Kerscher, M.; Schiek, W. *Prog. Inorg. Chem.* **2007**, *55*, 613. (b) Bakac, A. *Coord. Chem. Rev.* **2006**, *250*, 2046. (c) Espenson, J. H. *Coord. Chem. Rev.* **2005**, *249*, 329. (d) Fujii, H. *Coord. Chem. Rev*. **2002**, *226*, 51.

(7) (a) Costas, M.; Mehn, M. P.; Jensen, M. P.; Que, L., Jr. *Chem. Rev*. **2004**, *104*, 939. (b) Tshuva, E. Y.; Lippard, S. J. *Chem. Rev*. **2004**, *104*, 987. (c) Que, L., Jr.; Ho, R. Y. N. *Chem. Rev*.**1996**, *96*, 2607. (d) Solomon, E. I.; Brunold, T. C.; Davis, M. I.; Kemsley, J. N.; Lee, S.-K.; Lehnert, N.; Neese, F.; Skulan, A. J.; Yang, Y.-S.; Zhou, J. *Chem. Rev*. **2000**, *100*, 235. (e) Decker, A.; Solomon, E. I. *Curr. Opin. Chem. Biol*. **2005**, *9*, 152.

(8) (a) Yiu, S.-M.; Man, W.-L.; Lau, T.-C. *J. Am. Chem. Soc.* **2008**, *130*, 10821. (b) Lam, W. W. Y.; Yiu, S.-M.; Lee, J. M. N.; Yau, S. K. Y.; Kwong, H.-K.; Lau, T.-C.; Liu, D.; Lin, Z. *J. Am. Chem. Soc.* **2006**, *128*, 2851. (c) Yiu, S.-M.; Wu, Z.-B.; Mak, C.-K.; Lau, T.-C. *J. Am. Chem. Soc.* **2004**, *126*, 14921. (d) Miller, C. G.; Gordon-Wylie, S. W.; Horwitz, C. P.; Strazisar, S. A.; Peraino, D. K.; Clark, G. R.; Weintraub, S. T.; Collins, T. J. *J. Am. Chem. Soc.* **1998**, *120*, 11540.

(9) (a) Fukuzumi, S.; Morimoto, Y.; Kotani, H.; Naumov, P.; Lee, Y.-M.; Nam, W. *Nature Chem.* **2010**, *2*, 756. (b) Karlin, K. D. *Nature Chem.* **2010**, *2*, 711.

(10) Morimoto, M.; Kotani, H.; Park, J.; Lee, Y.-M.; Nam, W.; Fukuzumi, S. *J. Am. Chem. Soc.* **2011**, *133*, 403.

(11) Park, J.; Morimoto, M.; Lee, Y.-M.; Nam, W.; Fukuzumi, S. *J. Am. Chem. Soc.* **2011**, *133*, 5236.

(12) (a) Fukuzumi, S. *Prog. Inorg. Chem.* **2009**, *56*, 49. (b) Fukuzumi, S. *Bull. Chem. Soc. Jpn.* **1997**, *70*, 1. (c) Fukuzumi, S.; Ohtsu, H.; Ohkubo, K.; Itoh, S.; Imahori, H. *Coord. Chem. Rev*. **2002**, *226*, 71. (d) Fukuzumi, S.; Ohkubo, K. *Coord. Chem. Rev.* **2010**, *254*, 372. (e) Fukuzumi, S.; Itoh, S. *Antioxid. Redox Sign.* **2001**, *3*, 807.

(13) (a) Fukuzumi, S.; Kuroda, S.; Tanaka, T. *J. Am. Chem. Soc*. **1985**, *107*, 3020. (b) Itoh, S.; Taniguchi, M.; Takada, N.; Nagatomo, S.; Kitagawa, T.; Fukuzumi, S. *J. Am. Chem. Soc.* **2000**, *122*, 12087. (c) Fukuzumi, S.; Yasui, K.; Suenobu, T.; Ohkubo, K.; Fujitsuka, M.; Ito, O. *J. Phys. Chem. A* **2001**, *105*, 10501.

(14) (a) Fukuzumi, S.; Ohkubo, K. *Chem.–Eur. J*. **2000**, *6*, 4532. (b) Fukuzumi, S.; Ohkubo, K. *J. Am. Chem. Soc*. **2002**, *124*, 10270. (c) Ohkubo, K.; Menon, S. C.; Orita, A.; Otera, J.; Fukuzumi, S. *J. Org. Chem.* **2003**, *68*, 4720.

(15) (a) Itoh, S.; Kumei, H.; Nagatomo, S.; Kitagawa, T.; Fukuzumi, S. *J. Am. Chem. Soc*. **2001**, *123*, 2165. (b) Fukuzumi, S.; Satoh, N.; Okamoto, T.; Yasui, K.; Suenobu, T.; Seko, Y.; Fujitsuka, M.; Ito, O. *J. Am. Chem. Soc*. **2001**, *123*, 7756. (c) Fukuzumi, S.; Ohkubo, K.; Okamoto, T. *J. Am. Chem. Soc*. **2002**, *124*, 14147.

(16) (a) Fukuzumi, S.; Okamoto, K.; Imahori, H. *Angew. Chem., Int. Ed*. **2002**, *41*, 620. (b) Okamoto, K. Imahori, H.; Fukuzumi, S. *J. Am. Chem. Soc*. **2003**, *125*, 7014. (c) Fukuzumi, S.; Okamoto, K.; Yoshida, Y.; Imahori, H.; Araki, Y.; Ito, O. *J. Am. Chem. Soc*. **2003**, *125*, 1007. (d) Savéant, J.-M. *J. Am. Chem. Soc*. **2008**, *130*, 4732.

(17) (a) Chen, X.; Bu, Y. *J. Am. Chem. Soc*. **2007**, *129*, 9713. (b) Wu, H.; Zhang, D.; Su, L.; Ohkubo, K.; Zhang, C.; Yin, S.; Mao, L.; Shuai, Z.; Fukuzumi, S.; Zhu, D. *J. Am. Chem. Soc*. **2007**, *129*, 6839. (c) Zeng, Y.; Zhang, G.; Zhang, D.; Zhu, D. *J. Org. Chem*. **2009**, *74*, 4375. (d) Jia, L.; Zhang, G.; Zhang, D.; Xiang, J.; Xu, W.; Zhu, D. *Chem. Commun*. **2011**, *47*, 322.

(18) (a) Yuasa, J.; Suenobu, T.; Fukuzumi, S. *J. Am. Chem. Soc*. **2003**, *125*, 12090. (b) Yuasa, J.; Suenobu, T.; Fukuzumi, S. *ChemPhysChem* **2006**, *7*, 942. (c) Yuasa, J.; Yamada, S.; Fukuzumi, S. *Chem.–Eur. J*. **2008**, *14*, 1866.

(19) (a) Fukuzumi, S.; Koumitsu, S.; Hironaka, K.; Tanaka, T. *J. Am. Chem. Soc*. **1987**, *109*, 305. (b) Fukuzumi, S.; Kondo, Y.; Tanaka, T. *J. Chem. Soc., Perkin Trans*. 2 **1984**, 673. (c) Fukuzumi, S.; Kondo, Y.; Tanaka, T. *Chem. Lett*. **1983**, 485.

(20) (a) Fukuzumi, S.; Nishizawa, N.; Tanaka, T. *J. Chem. Soc., Perkin Trans, 2* **1985**, 371. (b) Fukuzumi, S.; Fujii, Y.; Suenobu, T. *J. Am. Chem. Soc*. **2001**, *123*, 10191.

(21) (a) Miwa, G. T.; Walsh, J. S.; Kedderis, G. L.; Hollenberg, P. F. *J. Biol. Chem*. **1983**, *258*, 14445. (b) Guengerich, F. P.; Yun, C.-H.; Macdonald, T. L. *J. Biol. Chem*. **1996**, *271*, 27321. (c) Lindsay Smith, J. R.; Mortimer, D. N. *J. Chem. Soc., Perkin Trans. 2* **1986**, 1743.

(22) (a) Dinnocenzo, J. P.; Karki, S. B.; Jones, J. P. *J. Am. Chem. Soc*. **1993**, *115*, 7111 (b) Manchester, J. I.; Dinnocenzo, J. P.; Higgins, L.; Jones, J. P. *J. Am. Chem. Soc*. **1997**, *119*, 5069. (c) Karki, S. B.; Dinnocenzo, J. P.; Jones, J. P.; Korzekwa, K. R. *J. Am. Chem. Soc*. **1995**, *117*, 3657.

(23) (a) Goto, Y.; Watanabe, Y.; Fukuzumi, S.; Jones, J. P.; Dinnocenzo, J. P. *J. Am. Chem. Soc*. **1998**, *120*, 10762. (b) Goto, Y.; Matsui, T.; Ozaki, S.; Watanabe, Y.; Fukuzumi, S. *J. Am. Chem. Soc.* **1999**, *121*, 9497. (c) Fukuzumi, S.; Shimoosako, K.; Suenobu, T.; Watanabe, Y. *J. Am. Chem. Soc*. **2003**, *125*, 9074.

(24) (a) Shaffer, C. L.; Morton, M. D.; Hanzlik, R. P. *J. Am. Chem. Soc*. **2001**, *123*, 8502. (b) Bhakta, M. N.; Wimalasena, K. *J. Am. Chem. Soc*. **2002**, *124*, 1844. (c) Shaffer, C. L.; Harriman, S.; Koen, Y. M.; Hanzlik, R. P. *J. Am. Chem. Soc*. **2002**, *124*, 8268. (d) Bhakta, M.; Hollenberg, P. F.; Wimalasena, K. *Chem. Commun*. **2005**, 265. (e) Bhakta, N.; Hollenberg, P. F.; Wimalasena, K. *J. Am. Chem. Soc*. **2005**, *127*, 1376. (f) Bhakta, M. N.; Wimalasena, K. *Eur. J. Org. Chem.* **2005**, 4801. (g) Cerny, M. A.; Hanzlik, R. P. *J. Am. Chem. Soc*. **2006**, *128*, 3346.

(25) (a) Baciocchi, E.; Lanzalunga, O.; Lapi, A.; Manduchi, L. *J. Am. Chem. Soc*. **1998**, *120*, 5783. (b) Baciocchi, E.; Gerini, M. F.; Lanzalunga, O.; Lapi, A.; Lo Piparo, M. G. *Org. Biomol. Chem.* **2003**, *1*, 422.

(26) Baciocchi, E.; Bietti, M.; Lanzalunga, O.; Lapi, A.; Raponi, D. *J. Org. Chem*. **2010**, *75*, 1378.

(27) Nehru, K.; Seo, M. S.; Kim, J.; Nam, W. *Inorg. Chem*. **2007**, *46*, 293.

(28) (a) Shearer, J.; Zhang, C. X.; Hatcher, L. Q.; Karlin, K. D. *J. Am. Chem. Soc*. **2003**, *125*, 12670. (b) Wang, Y.; Kumar, D.; Yang, C.; Han, K.; Shaik, S. *J. Phys. Chem. B* **2007**, *111*, 7700. (c) Chiavarino, B.; Cipollini, R.; Crestoni, M. E.; Fornarini, S.; Lanucara, F.; Lapi, A. *J. Am. Chem. Soc*. **2008**, *130*, 3208.

(29) Lubben, M.; Meetsma, A.; Wilkinson, E. C.; Feringa, B.; Que, L., Jr. *Angew. Chem., Int. Ed*. **1995**, *34*, 1512.

(30) Armarego, W. L. F.; Chai, C. L. L. *Purification of Laboratory Chemicals*, 5th ed.; Butterworth Heinemann: Amsterdam, 2003.

(31) *Organic Syntheses*; Saltzman, H.; Sharefkin, J. G., Eds.; Wiley: New York, 1973; Vol. V, p 658.

(32) Kirchgessner, M.; Sreenath, K.; Gopidas, K. R. *J. Org. Chem*. **2006**, *71*, 9849.

(33) Mann, C. K.; Barnes, K. K. In *Electrochemical Reactions in Non-aqueous Systems*; Mercel Dekker: New York, 1970.

(34) For $DMA^{\bullet+}$ see: (a) Sumalekshmy, S.; Gopidas, K. R. *Chem. Phys. Lett*. **2005**, *413*, 294. (b) Murakami, M.; Ohkubo, K.; Fukuzumi, S. *Chem.–Eur. J*. **2010**, *16*, 7820. (c) Amada, I.; Yamaji, M.; Tsunoda, S.; Shizuka, H. *J. Photochem. Photobiol. A: Chem.* **1996**, *95*, 27. (d) Shida, T. In *Electronic Absorption Spectra of Radical Ions*; Elsevier: Amsterdam, 1988, p 209.

(35) Akutagawa, T.; Saito, G. *Bull. Chem. Soc. Jpn*. **1995**, *68*, 1753.

(36) (a) Streeter, I.; Wain, A. J.; Thompson, M.; Compton, R. G. *J. Phys. Chem. B* **2005**, *109*, 12636. (b) Josephy, P. D.; Eling, T.; Mason, R. P. *J. Biol. Chem*. **1982**, *257*, 3669.

(37) (a) Siegman, H. In *Technique of Electroorganic Synthesis; Technique of Chemistry*; Weinberg, N. L., Ed.; John Wiley: New York, 1975; Vol. 5, Part II, pp 667-1056. (b) Sekiguchi, S.; Kobori, Y.; Akiyama, K.; Tero-Kubota, S. *J. Am. Chem. Soc*. **1998**, *120*, 1325.

(38) Fukuzumi, S.; Shimoosako, K.; Suenobu, T.; Watanabe, Y. *J. Am. Chem. Soc*. **2003**, *125*, 9074.

(39) The yield of DMB was also one-third of the initial concentration of $[Fe^{IV}(O)(N4Py)]^{2+}$ (Figure 4).

(40) It should be noted that formation of $TMB^{\bullet+}$ is prohibited under the conditions such that concentrations of DMA are smaller than that of Sc^{3+}, because of the binding of Sc^{3+} to DMA (Figure 5).

(41) The spectra measured with a stopped-flow spectrometer in Figure 3b become noisy as compared with those measured with a photodiode-array UV-vis spectrophotometer in Figure 3a. The scandium(III) triflate salt used in Figure 3b was completely soluble in MeCN.

(42) In the case of CN-DMA, concentration of free Sc^{3+} is 10.7 mM due to the relatively small K_0 value.

(43) (a) Marcus, R. A. *Annu. Rev. Phys. Chem*. **1964**, *15*, 155. (b) Marcus, R. A. *Angew. Chem., Int. Ed. Engl*. **1993**, *32*, 1111.

Chapter 3. Proton–Promoted Oxygen Atom Transfer vs Proton–Coupled Electron Transfer of a Nonheme Iron(IV)-Oxo Complex

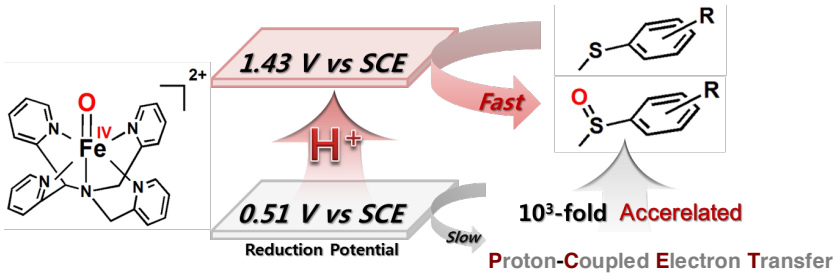

Abstract: Sulfoxidation of thioanisoles by a nonheme iron(IV)-oxo complex, $[(N4Py)Fe^{IV}(O)]^{2+}$ (N4Py = *N*,*N*-bis(2-pyridylmethyl)-*N*-bis(2-pyridyl)methylamine), was remarkably enhanced by perchloric acid (70% $HClO_4$). The observed second-order rate constant (k_{obs}) of sulfoxidation of thioaniosoles by $[(N4Py)Fe^{IV}(O)]^{2+}$ increases linearly with increasing concentration of $HClO_4$ (70%) in acetonitrile (MeCN) at 298 K. In contrast to sulfoxidation of thioanisoles by $[(N4Py)Fe^{IV}(O)]^{2+}$, the observed second-order rate constant (k_{et}) of electron transfer from one-electron reductants such as $[Fe^{II}(Me_2bpy)_3]^{2+}$ (Me_2bpy = 4,4-dimehtyl-2,2'-bipyridine) to $[(N4Py)Fe^{IV}(O)]^{2+}$ increases with increasing concentration of $HClO_4$, exhibiting second-order dependence on $HClO_4$ concentration. This indicates that the proton–coupled electron transfer (PCET) involves two protons associated with electron transfer from $[Fe^{II}(Me_2bpy)_3]^{2+}$ to $[(N4Py)Fe^{IV}(O)]^{2+}$ to yield $[Fe^{III}(Me_2bpy)_3]^{3+}$ and $[(N4Py)Fe^{III}(OH_2)]^{3+}$. The one-electron reduction potential (E_{red}) of $[(N4Py)Fe^{IV}(O)]^{2+}$ in the presence of 10 mM $HClO_4$ (70%) in MeCN is determined to be 1.43 V vs SCE. Plot of E_{red} vs log[$HClO_4$] also indicates involvement of two protons in the PCET reduction of $[(N4Py)Fe^{IV}(O)]^{2+}$. The PCET driving force dependence of log k_{et} is fitted in light of the Marcus theory of outer-sphere electron transfer to afford the reorganization of PCET (λ = 2.74 eV). The comparison of the k_{obs} values of acid–promoted sulfoxidation of thioanisoles by $[(N4Py)Fe^{IV}(O)]^{2+}$ with the k_{et} values of PCET from one-electron reductants to $[(N4Py)Fe^{IV}(O)]^{2+}$ at the same PCET driving force reveals that the acid–promoted sulfoxidation proceeds by one-step oxygen atom transfer from $[(N4Py)Fe^{IV}(O)]^{2+}$ to thioanisoles rather than outer-sphere PCET.

Introduction

Brønsted acid is well known to enhance the electrophilicity of electrophiles by interaction, making them possible to react with nucleophiles, which would otherwise exhibit no reactivity.[1-3] Metal ion salts, which act as Lewis acids, are also known to enhance the electrophilicty of electrophiles by interacting with Lewis acids to facilitate the reactions with nucleophiles.[4-9] The promoting effects of Brønsted acid and Lewis acids result from the activation of the C=X bond (X = O, NR, CR_2), thereby decreasing the LUMO energy and promoting the reactions with nucleophiles.[1-9] On the other hand, both Brønsted acid and metal ions acting as Lewis acids promote electron-transfer reactions from various electron donors to electron acceptors provided that the one-electron reduced species of electron acceptors can bind with Brønsted acid (protonation) and Lewis acids, respectively. The former is classified as proton–coupled electron transfer (PCET),[10-14] whereas the latter is regarded as metal ion–promoted electron transfer.[15-24] It should be noted that the term of PCET has also been used for the case when an electron and a proton are transferred from the same molecule.[25-28]

Not only C=O bond but also M=O (M = metal) bond can be activated by Brønsted acid and Lewis acids. In this context, we have recently reported the first example of binding of metal ions, such as Sc^{3+} and Ca^{2+}, to a nonheme iron(IV)-oxo complex, $[(TMC)Fe^{IV}(O)]^{2+}$ (TMC = 1,4,8,11-tetramethyl-1,4,8,11-tetraazacyclotetradecane), and the crystal structure of Sc^{3+}–bound $[(TMC)Fe^{IV}(O)]^{2+}$ was successfully determined by X-ray crystallography.[29] The binding of Sc^{3+} to $[(TMC)Fe^{IV}(O)]^{2+}$ resulted in change in the number of electrons transferred from ferrocene (Fc) to $[(TMC)Fe^{IV}(O)]^{2+}$ from one electron in the absence of Sc^{3+} to two electrons in the presence of Sc^{3+}.[29] Rates of electron transfer from a series of one-electron reductants to an iron(IV)-oxo complex, $[(N4Py)Fe^{IV}(O)]^{2+}$ (N4Py: *N*,*N*-bis(2-pyridylmethyl)-*N*-bis(2-pyridyl)methylamine), were enhanced as much as 10^8-fold in the presence of metal ions, such as Sc^{3+}, Zn^{2+}, Mg^{2+} and Ca^{2+}, as compared with the rates in the absence of metal ion.[30] The rate enhancement by metal ions exhibits a good correlation with Lewis acidity of metal ions.[30] The one-electron reduction potential of $[(N4Py)Fe^{IV}(O)]^{2+}$ has been demonstrated to be shifted to a positive direction by as large as 0.84 V in the presence of Sc^{3+} ion.[30-32]

In contrast to the extensive studies on Brønsted acid–promoted reactions of organic electrophiles containing C=O bonds,[1-9] there have been only a few reports on Brønsted

aid–promoted reactions of metal-oxo (M=O) complexes.[33] In particular, the fundamental properties of high-valent metal-oxo complexes such as the one-electron reduction potentials and the reorganization energies in PCET have yet to be reported. In addition, the relation between Brønsted acid–promoted reactions of high-valent metal-oxo complexes with nucleophiles and the PCET with one-electron reductants has yet to be clarified.

We report herein Brønsted acid–promoted oxygen atom transfer from nonheme iron(IV)-oxo complex, $[(N4Py)Fe^{IV}(O)]^{2+}$ to thioanisoles[34] in comparison with PCET from one-electron reductants to $[(N4Py)Fe^{IV}(O)]^{2+}$. The PCET rate constants were evaluated in light of the Marcus theory of outer-sphere electron transfer[35,36] to determine the one-electron reduction potential and the reorganization energy of PCET reactions of $[(N4Py)Fe^{IV}(O)]^{2+}$ in the presence of perchloric acid ($HClO_4$, 70 wt. % in H_2O) in acetonitrile (MeCN). The detailed kinetic analyses on both acid–promoted oxygen atom transfer from $[(N4Py)Fe^{IV}(O)]^{2+}$ to thioanisoles and the PCET reactions from one-electron reductants to $[(N4Py)Fe^{IV}(O)]^{2+}$ provide valuable insight into the important mechanistic difference between direct oxygen atom-transfer[37] and outer-sphere PCET pathways, both of which are enhanced by Brønsted acid.

Experimental Section

Materials. All chemicals, which were the best available purity, were purchased from Aldrich Chemical Co. and used without further purification unless otherwise noted. Solvents, such as MeCN and diethyl ether, were dried according to the literature procedures and distilled under Ar prior to use.[38] Iodosylbenzene (PhIO) was prepared by a literature method.[39] Nonheme iron(II) complex $[(N4Py)Fe^{II}(MeCN)](ClO_4)_2$ and its iron(IV)-oxo, $[(N4Py)Fe^{IV}(O)]^{2+}$, were prepared by the literature methods.[34] Perchloric acid (70 wt. % in H_2O) was purchased from Wako Pure Chemical Ind. Ltd..

Caution: Perchlorate salts are potentially explosive and should be handled with care.

Kinetic Studies and Product Analyses. Kinetic measurements were performed on a UNISOKU RSP-601 stopped-flow spectrometer equipped with a MOS-type highly sensitive photodiode array or a Hewlett Packard 8453 photodiode-array spectrophotometer using a 10 mm quartz cuvette (10 mm path length) at 298 K.

Sulfoxidation reactions of thioanisole and its *para*-substituted derivatives (2.5×10^{-3} – 1.0×10^{-2} M) by $[(N4Py)Fe^{IV}(O)]^{2+}$ (2.5×10^{-4} M) were carried out and the rates were monitored by the decay of the absorption band at 695 nm due to $[(N4Py)Fe^{IV}(O)]^{2+}$ in the absence and presence of $HClO_4$ in MeCN at 298 K. The concentration of thioanisole derivatives was maintained at least more than 10-fold excess of $[(N4Py)Fe^{IV}(O)]^{2+}$ to attain pseudo-first-order conditions. First-order fitting of the kinetic data allowed us to determine the pseudo-first-order rate constants. The first-order plots were linear for three or more half-lives with the correlation coefficient $\rho > 0.999$. In each case, it was confirmed that the rate constants derived from at least five independent measurements agreed within an experimental error of ±5%. The pseudo-first-order rate constants increased proportionally with increase in concentrations of substrates, from which second-order rate constants were determined.

Typically, thioanisole (1.0×10^{-2} M) was added to an MeCN solution (0.50 mL) containing $[(N4Py)Fe^{IV}(O)]^{2+}$ (1.0×10^{-3} M) in the absence and presence of $HClO_4$ (1.0×10^{-2} M) in a vial. The reaction was complete within 1 h under these conditions. Products formed in the oxidation reactions of thioanisole by $[(N4Py)Fe^{IV}(O)]^{2+}$, which were carried out in the absence and presence of $HClO_4$ under Ar atmosphere in MeCN at 298 K, were analyzed by HPLC. Quantitative analyses were made on the basis of comparison of HPLC peak integration between products and their authentic samples. In the case of thioanisole, methyl phenyl sulfoxide was obtained as a sole product with 96% and 93% of yield (based on the intermediate generated) in the absence and presence of $HClO_4$ (10 mM), respectively. In the cases of *para*-substituted thioanisoles, methyl *para*-substituted phenyl sulfoxides were obtained quantitatively by HPLC, as the case of thioanisole.

Instrumentation. UV-vis spectra were recorded on a UNISOKU RSP-601 stopped-flow spectrometer equipped with a MOS-type highly sensitive photodiode array or a Hewlett Packard 8453 photodiode-array spectrophotometer. X-band EPR spectra were taken at 5 K using a X-band Bruker EMX-plus spectrometer equipped with a dual mode cavity (ER 4116DM). Low temperatures were achieved and controlled with an Oxford Instruments ESR900 liquid He quartz cryostat with an Oxford Instruments ITC503 temperature and gas flow controller. The experimental parameters for EPR spectra were as follows: Microwave frequency = 9.65 GHz, microwave power = 1 mW, modulation amplitude = 10 G, gain = 5×10^3, time constant = 40.96 ms, conversion

time = 81.00 ms. Electrospray ionization mass spectra (ESI MS) were collected on a Thermo Finnigan (San Jose, CA, USA) LCQ^{TM} Advantage MAX quadrupole ion trap instrument, by infusing samples directly into the source using a manual method. The spray voltage was set at 3.7 kV and the capillary temperature at 100 °C. Product analysis for oxidation reactions was performed on DIONEX Summit Pump Series P580 equipped with a variable wavelength UV-200 detector (HPLC). Products were separated on Hypersil GOLD column (4.6 × 250 mm), and product yields were determined with a UV Detector at 215 and 254 nm. ^{1}H NMR spectra were measured with Bruker model digital AVANCE III 400 FT-NMR spectrometer. Cyclic voltammetry (CV) measurements were performed on a BAS 630B electrochemical analyzer in a deaerated MeCN solution containing 0.10 M TBA(PF_6) as a supporting electrolyte at 298 K. A conventional three-electrode cell was used with a platinum working electrode, a platinum wire as a counter electrode and an $Ag/AgNO_3$ reference electrode. The measured potentials were recorded with respect to the $Ag/AgNO_3$ (1.0×10^{-2} M). The E_{ox} and E_{red} values (vs $Ag/AgNO_3$) are converted to those vs SCE by adding 0.29 V.[40] All electrochemical measurements were carried out under an Ar atmosphere.

Results and Discussion

Brønsted Acid–Promoted Oxygen Atom Transfer from $[(N4Py)Fe^{IV}(O)]^{2+}$ to Thioanisoles. It has been well established that oxygen atom transfer from a nonheme iron(IV)-oxo complex ($[(N4Py)Fe^{IV}(O)]^{2+}$) to thioanisole occurs to yield the sulfoxide and $[(N4Py)Fe^{II}]^{2+}$ in MeCN (Figure 1).[39] The UV-visible spectral change observed in the reaction of oxygen atom transfer from $[(N4Py)Fe^{IV}(O)]^{2+}$ to thioanisole is shown in Figure 2a (left panel), where the absorption band at 695 nm due to $[(N4Py)Fe^{IV}(O)]^{2+}$ decreases, accompanied by increase in absorbance due to $[(N4Py)Fe^{II}]^{2+}$.

$$PhSMe + [(N4Py)Fe^{IV}(O)]^{2+} \longrightarrow PhS(O)Me + [(N4Py)Fe^{II}]^{2+} \quad (1)$$

Addition of $HClO_4$ (70%, 10 mM) to an MeCN solution of $[(N4Py)Fe^{IV}(O)]^{2+}$ resulted in remarkable enhancement of the reaction rate as indicated by the comparison of the time profile in the absence of $HClO_4$ (right panel in Figure 2a) vs that in the

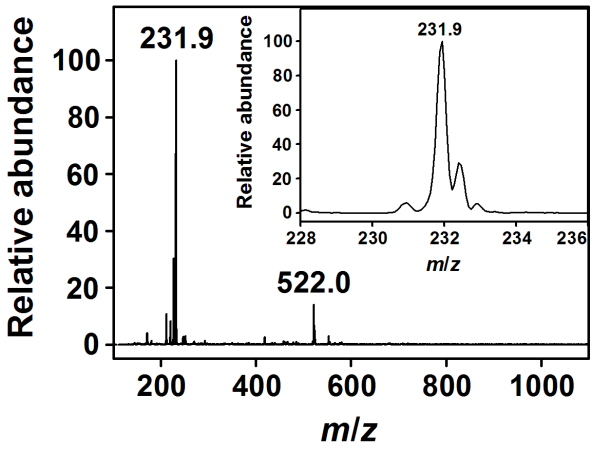

Figure 1. ESI-MS spectrum of the final products obtained in the reaction of $[(N4Py)Fe^{IV}(O)]^{2+}$ (0.5 mM) with thioanisole (5.0 mM) in the presence of $HClO_4$ (10 mM) in MeCN at 298 K. Peaks at *m/z* of 231.9 and 522.0 correspond to $[(N4Py)Fe^{II}(MeCN)]^{2+}$ (calcd *m/z* 232.1) and $[(N4Py)Fe^{II}(ClO_4)]^{+}$ (calcd *m/z* 522.1), respectively. Inset shows the observed isotope distribution patterns for $[(N4Py)Fe^{II}(MeCN)]^{2+}$.

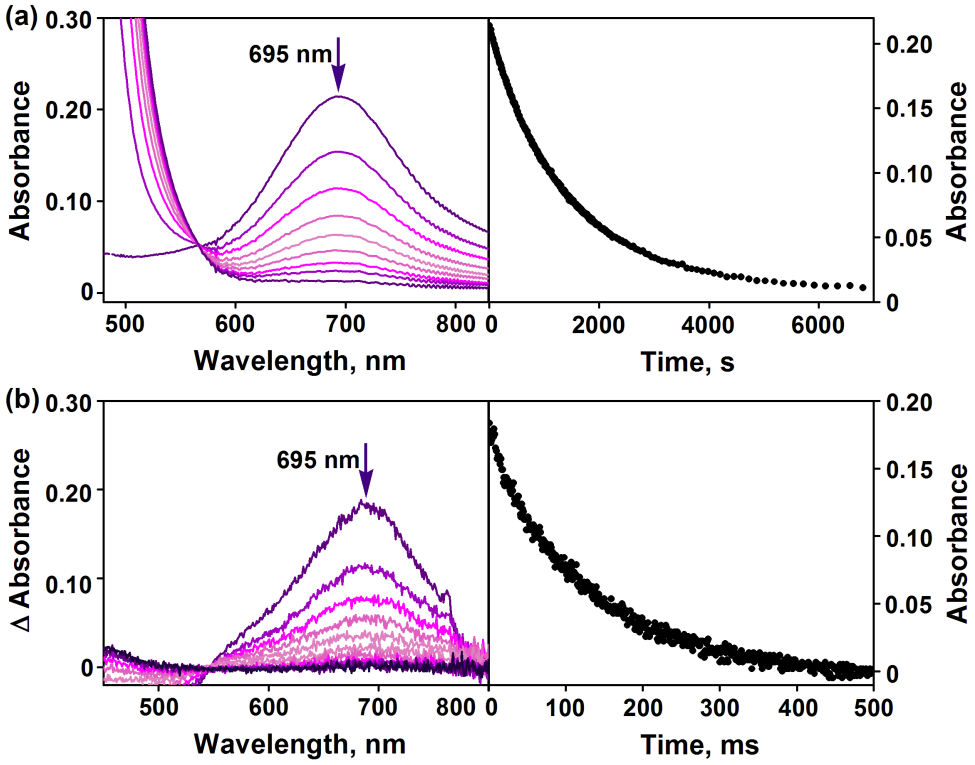

Figure 2. Visible spectral changes observed in the reaction of $[(N4Py)Fe^{IV}(O)]^{2+}$ (0.50 mM) with 10 equiv of thioanisole (5.0 mM) in the absence (a) and presence (b) of $HClO_4$ (10.0 mM) in MeCN at 298 K (left panel). Right panels show time courses monitored at 695 nm due to the decay of $[(N4Py)Fe^{IV}(O)]^{2+}$.

presence of $HClO_4$ (right panel in Figure 2b). In the presence of $HClO_4$, the reaction rate was too fast to follow by a conventional spectroscopic method, therefore, the rate was followed by using a stopped-flow technique (see Experimental Section). The rapid decrease in absorbance at 695 nm due to $[(N4Py)Fe^{IV}(O)]^{2+}$ in the presence of $HClO_4$ was accompanied by an increase in absorbance due to $[(N4Py)Fe^{II}]^{2+}$, which was observed as the recovery of the bleaching as shown in Figure 2b (right panel), where the spectrum after the reaction was subtracted from the observed spectra in the stopped flow measurements. The yield of the sulfoxide in the presence of $HClO_4$ was quantitative as the case in the absence of $HClO_4$ (see Experimental Section).

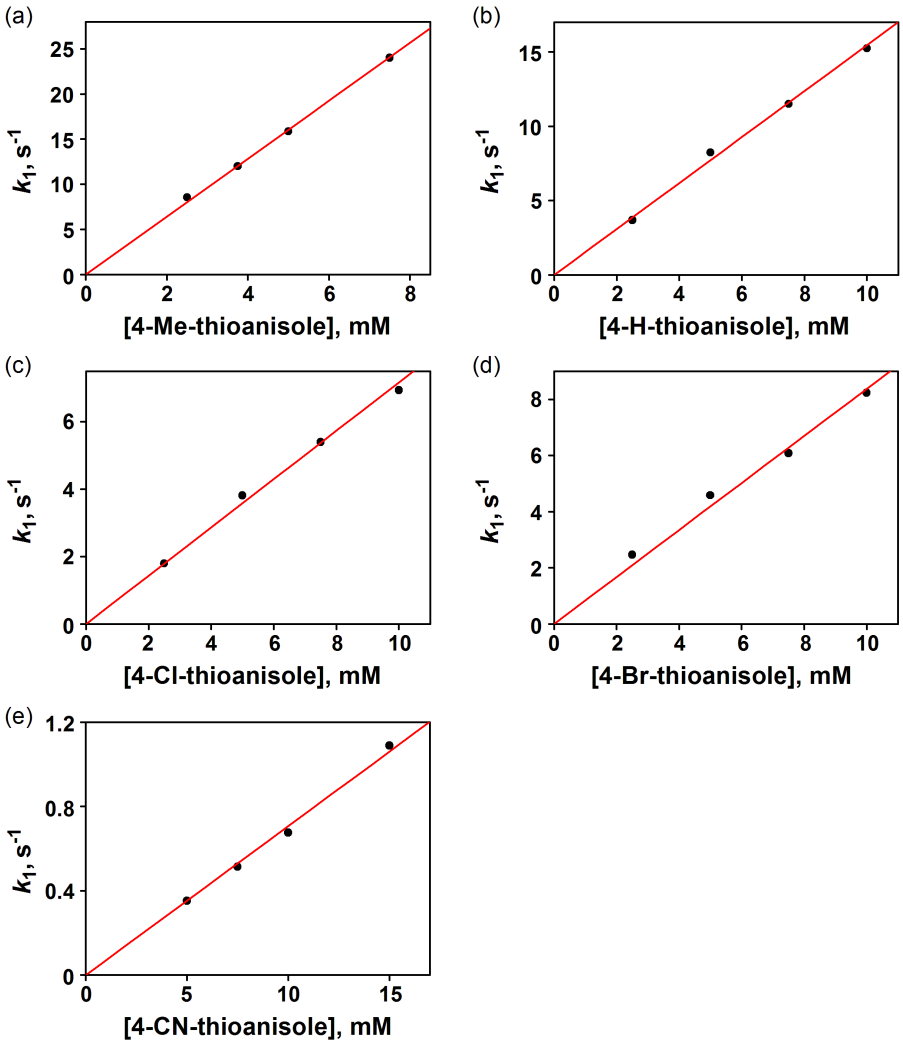

Figure 3. Plots of the pseudo-first-order rate constants (k_1) vs concentrations of *para*-X-thioanisoles to determine the second-order rate constants (k_{obs}) in the sulfoxidation of *para*-X-thioanisoles by $[(N4Py)Fe^{IV}(O)]^{2+}$ (0.25 mM) in the presence of $HClO_4$ (10 mM) in MeCN at 298 K.

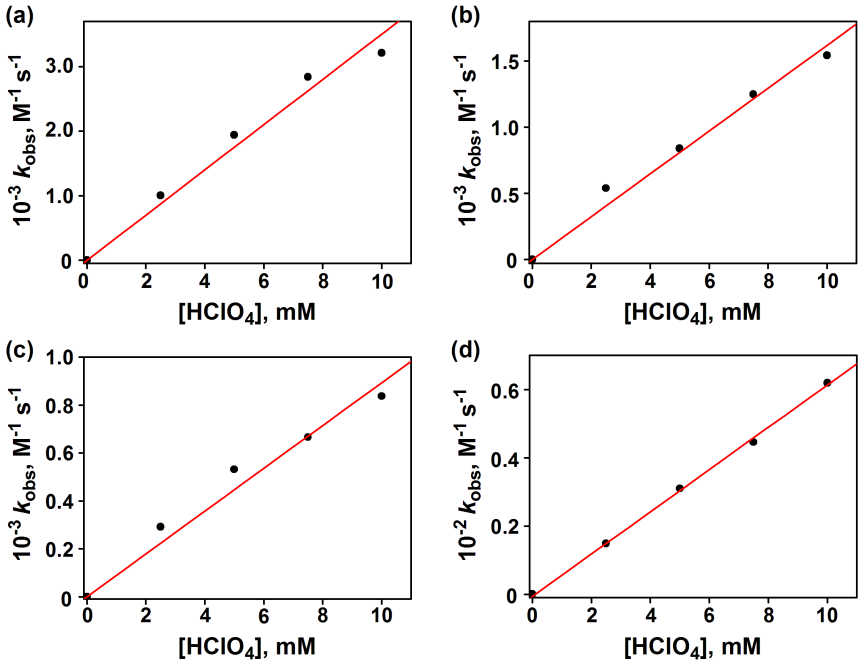

Figure 4. Plots of k_{obs} vs $HClO_4$ concentration in acid–promoted sulfoxidation of *para*-X-substituted thioanisoles (X = (a) Me, (b) H, (c) Br and (d) CN) by $[(N4Py)Fe^{IV}(O)]^{2+}$ in MeCN at 298 K.

Table 1. One-Electron Oxidation Potentials (E_{ox}) of *para*-X-Substituted Thioanisoles and Second-Order Rate Constants of the Sulfoxidation by $[(N4Py)Fe^{IV}(O)]^{2+}$ in the Absence and Presence of $HClO_4$ (10 mM) in MeCN at 298 K

X	E_{ox} (vs SCE, V)	k_{obs}, M^{-1} s^{-1}	
		without $HClO_4$	with $HClO_4$ (10 mM)
Me	1.24	1.3 ± 0.1	$(3.2 \pm 0.2) \times 10^{3}$
H	1.34	$(8.7 \pm 0.4) \times 10^{-1}$	$(1.5 \pm 0.1) \times 10^{3}$
Cl	1.37	$(8.7 \pm 0.4) \times 10^{-1}$	$(7.2 \pm 0.4) \times 10^{2}$
Br	1.41	$(1.5 \pm 0.1) \times 10^{-1}$	$(8.4 \pm 0.4) \times 10^{2}$
CN	1.61	$(4.4 \pm 0.2) \times 10^{-2}$	$(6.2 \pm 0.3) \times 10$

Decay rates of the absorption band at 695 nm due to $[(N4Py)Fe^{IV}(O)]^{2+}$ in oxygen atom transfer from $[(N4Py)Fe^{IV}(O)]^{2+}$ to large excess thioanisole in the absence and presence of large excess $HClO_4$ obeyed pseudo-first-order kinetics (Figure 2). The pseudo-first-order rate constant increased linearly with increasing concentration of thioanisole (Figure 3).[41] The observed second-order rate constant (k_{obs}) obtained from

the slope of a linear plot of the pseudo-first-order rate constant vs concentration of thioanisole increased proportionally with increasing concentration of $HClO_4$ as shown in Figure 4a. The dependence of k_{obs} of other thioanisole derivatives on concentration of $HClO_4$ also exhibited linear relations (Figures 4b-d) as given by eq 2, where k_0 and k_1 are the rate constant of oxygen atom transfer from $[(N4Py)Fe^{IV}(O)]^{2+}$ to *para*-X-substituted thioanisoles in the absence and presence of $HClO_4$, respectively.

$$k_{obs} = k_0 + k_1 [HClO_4] \quad (2)$$

The observed second-order rate constants (k_{obs}) of sulfoxidation of thioanisoles by $[(N4Py)Fe^{IV}(O)]^{2+}$ in the absence and presence of $HClO_4$ (10 mM) are listed in Table 1.

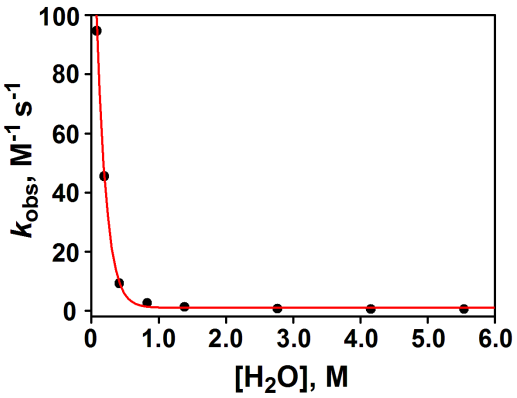

Figure 5. Plot of k_{obs} vs additional H_2O concentration in sulfoxidation of thioanisoles by $[(N4Py)Fe^{IV}(O)]^{2+}$ in the presence of $HClO_4$ (10 mM) in MeCN at 298 K.

It should be noted that the k_{obs} values of thioanisoles in the presence of $HClO_4$ (10 mM) is more than 10^3-fold larger than the corresponding values in the absence of $HClO_4$. The enhanced reactivity of $[(N4Py)Fe^{IV}(O)]^{2+}$ by the presence of $HClO_4$ (70%) remarkably decreased by addition of H_2O. The k_{obs} value of acid–promoted sulfoxidation of thioanisole by $[(N4Py)Fe^{IV}(O)]^{2+}$ decreased significantly with increasing concentration of added water due to the decrease in the acidity of $HClO_4$ by H_2O,[12a,42] as shown in Figure 5. Because 70 wt. % $HClO_4$ in H_2O is employed in this work, the use of 100% $HClO_4$ may enhance the reactivity of $[(N4Py)Fe^{IV}(O)]^{2+}$ drastically. However, the possible explosion of 100% $HClO_4$ has precluded the examination of the enhancement of reactivity of $[(N4Py)Fe^{IV}(O)]^{2+}$ by $HClO_4$ without water.

PCET from One-Electron Reductants to $[(N4Py)Fe^{IV}(O)]^{2+}$. When $[Ru^{II}(Clphen)_3]^{2+}$ (Clphen: 5-chlorophenathrene) was employed as an electron donor, no electron transfer from $[Ru^{II}(Clphen)_3]^{2+}$ (E_{ox} = 1.36 V vs SCE)[30] to $[(N4Py)Fe^{IV}(O)]^{2+}$ (E_{red} = 0.51 V)[36] occurred in MeCN, because the free energy change of electron transfer is highly positive (ΔG_{et} = 0.85 eV), i.e., endergonic. In the presence of $HClO_4$, however, the electron transfer occurred efficiently as shown in Figure 6, where the absorption band due to $[Ru^{II}(Clphen)_3]^{2+}$ (λ_{max} = 450 nm) and $[(N4Py)Fe^{IV}(O)]^{2+}$ (λ_{max} = 695 nm) decrease to be changed to an absorption band due to $[Ru^{III}(Clphen)_3]^{3+}$ (λ_{max} = 640 nm) with an isosbestic point at 548 nm.

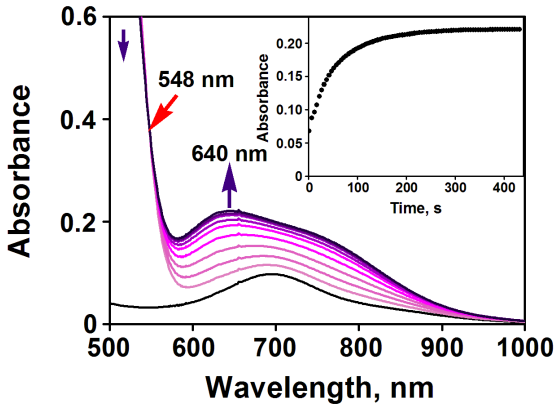

Figure 6. Visible spectral changes observed in PCET from $[Ru^{II}(Clphen)_3]^{2+}$ (12.5 mM) to $[(N4Py)Fe^{IV}(O)]^{2+}$ (0.25 mM) in the presence of $HClO_4$ (10 mM) in MeCN at 298 K. Inset shows time course monitored at 640 nm due to the formation of $[Ru^{III}(Clphen)_3]^{3+}$.

Formation of $[Ru^{III}(Clphen)_3]^{3+}$ and $[(N4Py)Fe^{III}(OH_2)]^{3+}$ in the PCET reaction was confirmed by EPR measurements. In the absence of $HClO_4$, as shown in Figure 7a, no electron transfer occurred because both reactants $[Ru^{II}(Clphen)_3]^{2+}$ and $[(N4Py)Fe^{IV}(O)]^{2+}$ are EPR silent. In the presence of $HClO_4$, PCET from $[Ru^{II}(Clphen)_3]^{2+}$ to $[(N4Py)Fe^{IV}(O)]^{2+}$ occurred to produce $[Ru^{III}(Clphen)_3]^{3+}$ and $[(N4Py)Fe^{III}(OH_2)]^{3+}$ as indicated by EPR signals observed at g_1 = 2.70, g_2 = 2.46 and g_3 = 1.65 after the PCET reaction (Figure 7b). The observed EPR signals agree with the superposition of EPR signals of $[Ru^{III}(Clphen)_3]^{3+}$ (Figure 7c)[43] and $[(N4Py)Fe^{III}(OH_2)]^{3+}$ (Figure 7d), which were produced by the photosensitized oxidation of $[Ru^{II}(Clphen)_3]^{2+}$ with sodium persulfate and by PCET from ferrocene to $[(N4Py)Fe^{IV}(O)]^{2+}$ in the presence of $HClO_4$ in MeCN at 298 K, respectively. It was

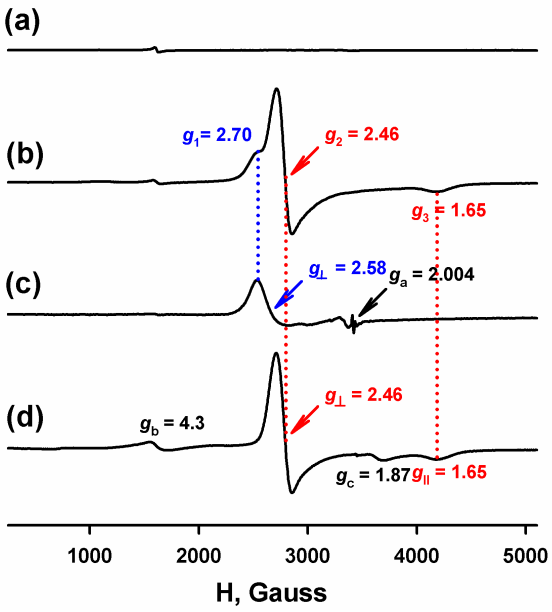

Figure 7. EPR spectra of the products obtained in the reaction of $[(N4Py)Fe^{IV}(O)]^{2+}$ (1.0 mM) with $[Ru^{II}(Clphen)_3]^{2+}$ (2.0 mM) (a) in the absence and (b) presence of $HClO_4$ (10 mM). (c) EPR spectrum of $[Ru^{III}(Clphen)_3]^{3+}$ generated in the photocatalytic oxidation of $[Ru^{II}(Clphen)_3]^{2+}$ (1.0 mM) with sodium persulfate (50 mM) in the presence of $HClO_4$ (50 mM) in MeCN at 298 K. The EPR signal intensity observed at g = 2.004, which is attributed an organic radical species, is negligible as compared with the intensity due to $[Ru^{III}(Clphen)_3]^{3+}$. (d) EPR spectrum of $[(N4Py)Fe^{III}(OH_2)]^{3+}$ generated by PCET from ferrocene (1.0 mM) to $[(N4Py)Fe^{IV}(O)]^{2+}$ (1.0 mM) in the presence of $HClO_4$ (10 mM) in MeCN at 298 K. The low spin $[(N4Py)Fe^{III}(OH_2)]^{3+}$ observed at $g_\perp$ = 2.46 and $g_{//}$ = 1.65 was converted to a high spin species at g_b = 4.3 and g_c = 1.87 at prolonged reaction time.

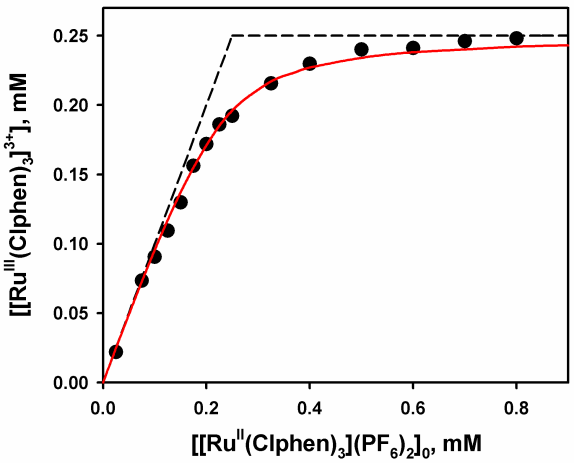

Figure 8. Plot of concentration of $[Ru^{III}(Clphen)_3]^{3+}$ produced in PCET from $[Ru^{II}(Clphen)_3]^{2+}$ to $[(N4Py)Fe^{IV}(O)]^{2+}$ (2.5×10^{-4} M) in the presence of $HClO_4$ (1.0×10^{-2} M) in deaerated MeCN at 298 K vs initial concentration of $[Ru^{II}(Clphen)_3](PF_6)_2$, $[[Ru^{II}(Clphen)_3](PF_6)_2]_0$.

observed that the low spin EPR signals due to $[(N4Py)Fe^{III}(OH_2)]^{3+}$ were converted to the high spin EPR signals (g_b and g_c), which can be assigned to $[(N4Py)Fe^{III}]^{3+}$.

The concentration of $[Ru^{III}(Clphen)_3]^{3+}$ produced in PCET from $[Ru^{II}(Clphen)_3]^{2+}$ to $[(N4Py)Fe^{IV}(O)]^{2+}$ (2.5×10^{-4} M) in the presence of $HClO_4$ (10 mM) increased with increasing the initial concentration of $[Ru^{II}(Clphen)_3]^{2+}$ to reach the initial concentration of $[(N4Py)Fe^{IV}(O)]^{2+}$ as shown in Figure 8. Such a titration curve indicates that PCET from $[Ru^{II}(Clphen)_3]^{2+}$ (E_{ox} = 1.36 V vs SCE)[30] to $[(N4Py)Fe^{IV}(O)]^{2+}$ in the presence of $HClO_4$ (10 mM) is in equilibrium as shown in eq 3. The PCET equilibrium constant (K_{et}) was determined to be 14.0 by fitting curve based on the PCET equilibrium (eq 3).

$$[(N4Py)Fe^{IV}(O)]^{2+} + [Ru^{II}(Clphen)_3]^{2+} + 2H^{+} \overset{K_{et}}{\rightleftarrows} [(N4Py)Fe^{III}(OH_2)]^{3+} + [Ru^{III}(Clphen)_3]^{3+} \quad (3)$$

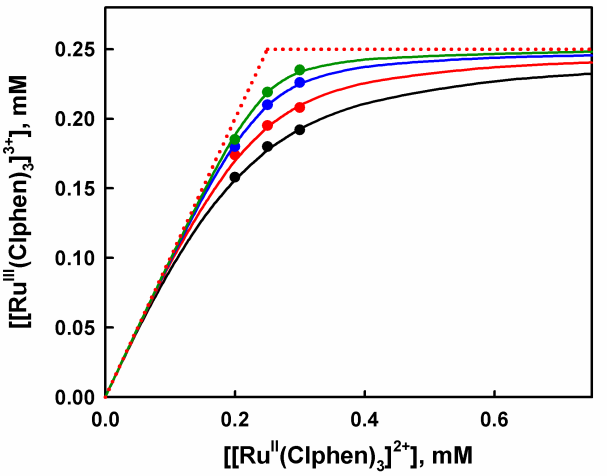

Figure 9. Plots of concentration of $[Ru^{III}(Clphen)_3]^{3+}$ produced in PCET from $[Ru^{II}(Clphen)_3]^{2+}$ to $[(N4Py)Fe^{IV}(O)]^{2+}$ (0.25 mM) in the presence of various $HClO_4$ concentrations (black line; 5.0 mM, red line; 7.5 mM, blue line; 15 mM and green line; 20 mM) in deaerated MeCN at 298 K vs initial concentration of $[Ru^{II}(Clphen)_3](PF_6)_2$, $[[Ru^{II}(Clphen)_3](PF_6)_2]_0$.

The reduction potential (E_{red}) of $[(N4Py)Fe^{IV}(O)]^{2+}$ in the presence of $HClO_4$ (10 mM) in MeCN at 298 K was then determined from the K_{et} value and E_{ox} value of $[Ru^{II}(Clphen)_3]^{2+}$ (E_{ox} = 1.36 V vs SCE)[30] using an Nernst equation (eq 4, where R is the gas constant, T is absolute temperature, and F is the Faraday constant) to be 1.43 V vs SCE. The K_{et} values in the presence of various concentrations of $HClO_4$ were determined by global fitting of plots of concentrations of $[Ru^{III}(Clphen)_3]^{3+}$ vs initial

concentrations of $[Ru^{II}(Clphen)_3]^{2+}$ (Figure 9). The one-electron reduction potentials of $[(N4Py)Fe^{IV}(O)]^{2+}$ (E_{red}) in the presence of various concentrations of $HClO_4$ were also determined from the K_{et} values and the E_{ox} value of $[Ru^{II}(Clphen)_3]^{2+}$ using eq 4.

$$E_{red} = E_{ox} + (RT/F)\ \ln K_{et} \tag{4}$$

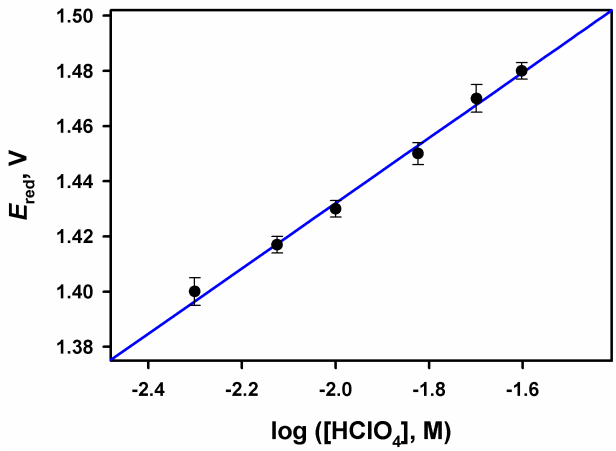

Figure 10. Dependence of E_{red} of $[(N4Py)Fe^{IV}(O)]^{2+}$on log($[HClO_4]$) in deaerated MeCN at 298 K. The blue line is fitted by eq 6.

The dependence of E_{red} of $[(N4Py)Fe^{IV}(O)]^{2+}$ on log($[HClO_4]$) is shown in Figure 10, where the slope is of the apparent linear correlation is close to 120 mV/log($[HClO_4]$). This slope indicates that two protons are involved in the PCET reduction of $[(N4Py)Fe^{IV}(O)]^{2+}$ according to the Nernst equation for the dependence of E_{red} on $[HClO_4]$ (eq 5),

$$E_{red} = E^{o}_{red} + (2.3RT/F)\log((K_{red1}[HClO_4](1 + K_{red2}[HClO_4])) \tag{5}$$

where K_{red1} and K_{red2} are the equilibrium constants for the first protonation and the second protonation of the one-electron reduced complex, $[(N4Py)Fe^{III}(O)]^{+}$.[44] The plot of E_{red} of $[(N4Py)Fe^{IV}(O)]^{2+}$ vs log($[HClO_4]$) in Figure 10 is well fitted by eq 5 with the best fit values of K_{red1} and K_{red2} (1.2×10^{13} and 3.0×10^{6} M^{-1}, respectively) as shown in the solid line (Figure 10). Under the conditions such that $K_{red2}[HClO_4]$ >>1, eq 5 is rewritten by eq 6,

$$E_{red} = E^{o}_{red} + 2(2.3RT/F)\log(K_{red}\ K_{red2}[HClO_4]) \tag{6}$$

when the slope of a linear colleration between E_{red} and log[$HClO_4$] corresponds to $2(2.3RT/F)$ = 118 mV at 298 K as observed in Figure 10.

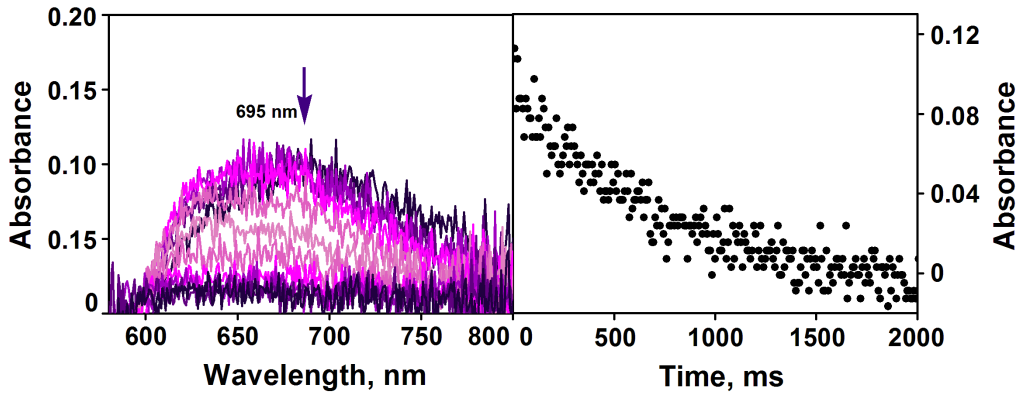

Figure 11. Visible spectral changes observed in the reaction of $[(N4Py)Fe^{IV}(O)]^{2+}$ (0.25 mM) with $[Fe^{II}(Me_2bpy)]^{2+}$ (5.0 mM) in the presence of $HClO_4$ (10.0 mM) in MeCN at 298 K (left panel). Right panel shows time course monitored at 695 nm due to the decay of $[(N4Py)Fe^{IV}(O)]^{2+}$.

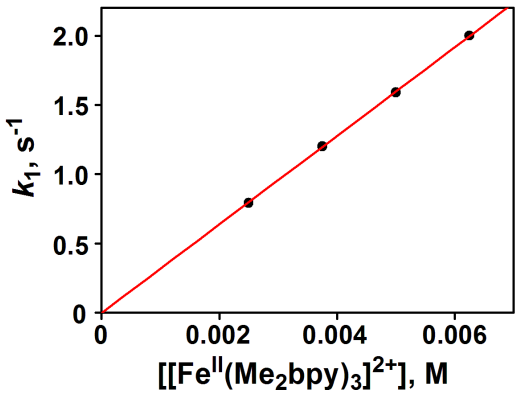

Figure 12. Plot of the pseudo-first-order rate constant (k_1) vs concentration of $[Fe^{II}(Me_2bpy)]^{2+}$ to determine the second-order rate constant (k_{obs}) of PCET from $[Fe^{II}(Me_2bpy)]^{2+}$ to $[(N4Py)Fe^{IV}(O)]^{2+}$ (0.25 mM) in the presence of $HClO_4$ (10 mM) in MeCN at 298 K.

The protonation of two protons to $[(N4Py)Fe^{III}(O)]^{+}$ is also supported by the kinetic measurements (vide infra).[21] The rate of PCET from $[Fe^{II}(Me_2bpy)_3]^{2+}$ to $[(N4Py)Fe^{IV}(O)]^{2+}$ was determined by monitoring a decrease in absorbance at 695 nm due to $[(N4Py)Fe^{IV}(O)]^{2+}$. The rate obeyed pseudo-first-order kinetics in the presence of large excess $[Fe^{II}(Me_2bpy)_3]^{2+}$ and $HClO_4$ (Figure 11). The pseudo-first-order rate constant increased linearly with increasing at the high concentration of $HClO_4$ as shown in Figure 12. This result shows sharp contrast to the case of proton–promoted oxygen

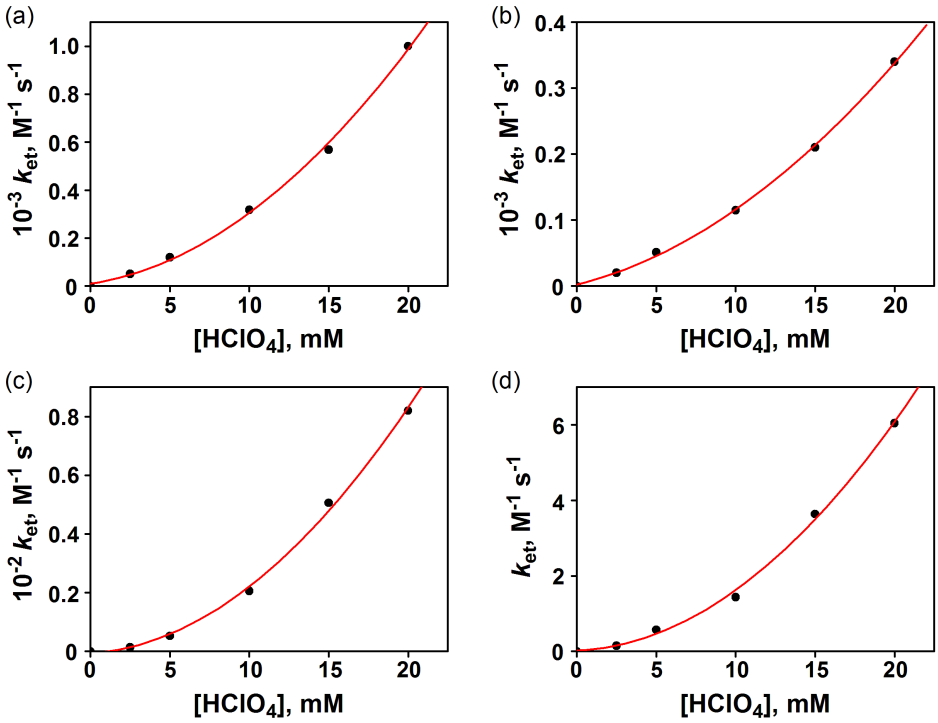

Figure 13. Plots of k_{et} vs concentrations of $HClO_4$ in PCET from (a) $[Fe^{II}(Me_2bpy)_3](PF_6)_2$, (b) $[Ru^{II}(Me_2bpy)_3](PF_6)_2$, (c) $[Fe^{II}(Clphen)_3](PF_6)_2$ and (d) $[Ru^{II}(Clphen)_3](PF_6)_2$ to $[(N4Py)Fe^{IV}(O)]^{2+}$ in the presence of $HClO_4$ (70%) in MeCN at 298 K.

atom transfer from $[(N4Py)Fe^{IV}(O)]^{2+}$ to thioanisoles in Figure 2, where the k_{obs} values increased linearly with increasing concentration of $HClO_4$.

The results in Figure 13 are well analyzed by eq 7, where k_{et1} is the rate constant of electron transfer from a one-electron reductant to the monoprotonated complex ($[(N4Py)Fe^{IV}(OH)]^{3+}$) and k_{et2} is the rate constant of electron transfer to the diprotonated complex ($[(N4Py)Fe^{IV}(OH_2)]^{4+}$). Eq 7 is written by eq 8, which predicts a linear relation between $k_{et}/([HClO_4])$ and $[HClO_4]$. Linear plots of $k_{et}/([HClO_4])$ and $[HClO_4]$ were confirmed as shown in Figure 14, indicating the involvement of two-protons in the PCET reactions.

$$k_{et} = k_{et1}[HClO_4] + k_{et2}[HClO_4]^2 \quad (7)$$

$$k_{et}/[HClO_4] = k_{et1} + k_{et2}[HClO_4] \quad (8)$$

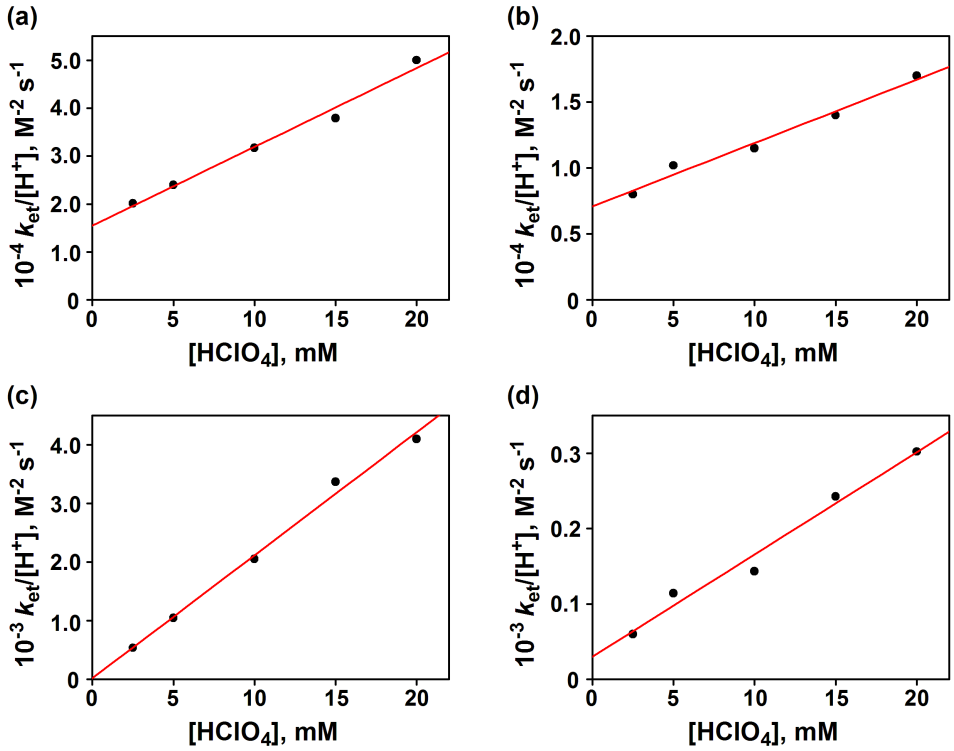

Figure 14. Plots of $k_{et}/[HClO_4]$ vs $[HClO_4]$ in PCET from (a) $[Fe^{II}(Me_2bpy)_3](PF_6)_2$, (b) $[Ru^{II}(Me_2bpy)_3](PF_6)_2$, (c) $[Fe^{II}(Clphen)_3](PF_6)_2$ and (d) $[Ru^{II}(Clphen)_3](PF_6)_2$ to $[(N4Py)Fe^{IV}(O)]^{2+}$ in the presence of $HClO_4$ in MeCN at 298 K.

Direct Oxygen Atom Transfer vs Electron Transfer in Proton–Promoted Sulfoxidation of Thioanisoles by $[(N4Py)Fe^{IV}(O)]^{2+}$. The PCET deriving force ($-\Delta G_{et}$) was obtained from the difference between the one-electron oxidation potentials of thioanisoles (E_{ox} vs SCE)[45] and the one–electron reduction potentials of $[(N4Py)Fe^{IV}(O)]^{2+}$ (E_{red} vs SCE) in the absence and presence of $HClO_4$ at 298 K.[36] It should be noted that the E_{ox} values of thioanisoles are not changed in the presence of $HClO_4$, whereas the E_{red} value of $[(N4Py)Fe^{IV}(O)]^{2+}$ is significantly shifted to the positive direction from 0.51 V vs SCE in the absence of $HClO_4$ to 1.43 V vs SCE in the presence of 10 mM of $HClO_4$ (vide supra).[36]

The driving force dependence of rate constants of PCET from one-electron reductants to $[(N4Py)Fe^{IV}(O)]^{2+}$ in the presence of 10 mM of $HClO_4$ is well fitted in light of the Marcus theory of adiabatic outer-sphere electron transfer (eq 9),

$$k_{et} = Z\exp[-(\lambda/4)(1 + \Delta G_{et}/\lambda)^2/k_B T] \quad (9)$$

where Z is the collision frequency taken as 1×10^{11} M^{-1} s^{-1}, λ is the reorganization energy of electron transfer, k_B is the Boltzmann constant, and T is the absolute temperature.[35] The best fit λ value of PCET from one-electron reductants to $[(N4Py)Fe^{IV}(O)]^{2+}$ in the presence of 10 mM of $HClO_4$ is determined to be 2.74 eV, which is the same as the λ value of electron transfer from one-electron reductants to $[(N4Py)Fe^{IV}(O)]^{2+}$ (2.74 eV) as shown in Figure 15.[36] The same value of the reorganization energy (2.74 eV) obtained from electron transfer from one-electron reductants to $[(N4Py)Fe^{IV}(O)]^{2+}$ ($[(N4Py)Fe^{IV}(OH_2)]^{4+}$) in the presence and absence of $HClO_4$ indicates that the large reorganization energy results from the one-electron reduction of the Fe^{IV} center to the Fe^{III} center. In fact, a large reorganization energy (2.34 eV) was reported for the electron-transfer oxidation of an organoiron(III) porphyrin to the corresponding organoiron(IV) porphyrin.[46]

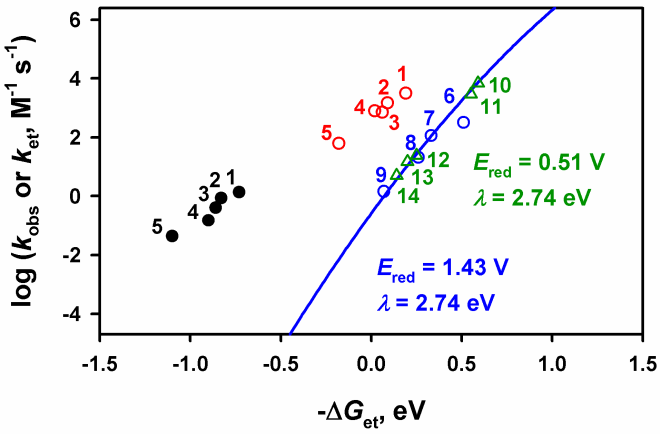

Figure 15. Plots of log k_{obs} for sulfoxidation of *para*-X-substituted thioanisoles (X = (1) Me, (2) H, (3) Cl, (4) Br and (5) CN) by $[(N4Py)Fe^{IV}(O)]^{2+}$ in the absence and presence of $HClO_4$ (70%, 10 mM) MeCN at 298 K vs the driving force of electron transfer [$-\Delta G = e(E_{red} - E_{ox})$] from thioanisoles to $[(N4Py)Fe^{IV}(O)]^{2+}$ in the absence (black closed circles) and the presence of $HClO_4$ (10 mM) (red open circles). The blue open circles show the driving force dependence of the rate constants (log k_{et}) of PCET from one-electron reductants ((6) $[Fe^{II}(Me_2bpy)_3](PF_6)_2$, (7) $[Ru^{II}(Me_2bpy)_3](PF_6)_2$, (8) $[Fe^{II}(Clphen)_3](PF_6)_2$ and (9) $[Ru^{II}(Clphen)_3](PF_6)_2$) to $[(N4Py)Fe^{IV}(O)]^{2+}$ in the presence of $HClO_4$ (10 mM) in MeCN at 298 K (see Table S1 in SI). The green open triangles show the driving force dependence of the rate constants (log k_{et}) of electron transfer from one-electron reductants ((10) decamethylferrocene, (11) octamethylferrocene, (12) 1.1'-dimethylferrocene, (13) *n*-amylferrocene and (14) ferrocene) to $[(N4Py)Fe^{IV}(O)]^{2+}$ in the absence of $HClO_4$ in MeCN at 298 K.[34]

It is interesting to note that two Sc^{3+} ions are involved in Sc^{3+}–promoted electron transfer from one-electron reductants to $[(N4Py)Fe^{IV}(O)]^{2+}$ as the case of the PCET reactions of $[(N4Py)Fe^{IV}(O)]^{2+}$, in which two protons are also involved. The observed second-order rate constants of Sc^{3+}–promoted oxygen atom transfer from $[(N4Py)Fe^{IV}(O)]^{2+}$ to thioanisoles fit well with the driving force dependence of k_{et} for Sc^{3+}–promoted electron-transfer reactions using the Marcus equation (eq 9). Such an agreement with the Marcus equation indicates that the Sc^{3+}–promoted oxygen atom transfer from $[(N4Py)Fe^{IV}(O)]^{2+}$ to thioanisoles in the presence of Sc^{3+} proceeds via Sc^{3+} ion-coupled electron transfer from thioanisoles to $[(N4Py)Fe^{IV}(O)]^{2+}$, which is the rate-determining step, followed by rapid transfer of the oxygen atom from $[(N4Py)Fe^{III}(O)]^{+}$ to the radical cation ($ArSR^{\bullet+}$).[31]

Scheme 1

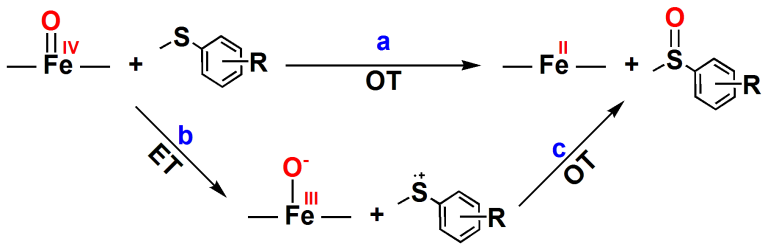

In the absence of $HClO_4$, the driving force of electron transfer ($-\Delta G_{et}$) is largely negative. This indicates that electron transfer from thioanisoles to $[(N4Py)Fe^{IV}(O)]^{2+}$ is highly endergonic and thereby the electron transfer is thermodynamically infeasible. The k_{obs} values in the absence of $HClO_4$ are more than 10 orders magnitude larger than the expected k_{et} values of outer-sphere electron transfer from thioanisoles to $[(N4Py)Fe^{IV}(O)]^{2+}$ without $HClO_4$ (extrapolated blue line in Figure 15). In such a case, direct oxygen atom transfer (Scheme 1a) occurs rather than an outer-sphere electron-transfer pathway (Scheme 1b).[31]

In the presence of $HClO_4$ (10 mM), the k_{obs} values are still two to four orders magnitude larger than the expected k_{et} values of outer-sphere PCET from thioanisoles to $[(N4Py)Fe^{IV}(O)]^{2+}$ in the presence of $HClO_4$ (10 mM) (blue line in Figure 15), exhibiting parallel correlation with driving force dependence of k_{et} for outer-sphere PCET. Thus, the proton–promoted sulfoxidation of thioanisoles by $[(N4Py)Fe^{IV}(O)]^{2+}$ also occurs via outer-sphere PCET from thioanisoles to monoprotonated complex

($[(N4Py)Fe^{IV}(OH)]^{3+}$) rather than direct oxygen atom transfer from the monoprotonated complex ($[(N4Py)Fe^{IV}(OH)]^{3+}$) to thioanisoles. The difference in the reactivity between proton–coupled electron transfer and Sc^{3+} ion–coupled electon transfer may result from the steric effect.

In both the Sc^{3+} ion–coupled electron transfer and PCET from one-electron reductants to $[(N4Py)Fe^{IV}(O)]^{2+}$, two Sc^{3+} ions and two protons are involved in the electron–transfer reactions, exhibiting the second-order dependence of the rate constant on concentrations of $Sc(OTf)_3$ and $HClO_4$, respectively. In the case of proton–promoted direct oxygen transfer, only the monoprotonated complex ($[(N4Py)Fe^{IV}(OH)]^{3+}$) is involved and the diprotonated complex ($[(N4Py)Fe^{IV}(OH_2)]^{4+}$) is less reactive due to the steric effect of two protons, whereas in the PCET reaction, the diprotonated complex ($[(N4Py)Fe^{IV}(OH_2)]^{4+}$) is the most reactive species because of the much high reduction potential as indicated by eq 5. The proton–promoted direct oxygen transfer from thioanisoles to $[(N4Py)Fe^{IV}(OH)]^{3+}$ may be regarded as inner-sphere electron transfer,[47-49] in which electron transfer is accompanied by the oxygen-ligand transfer.[50]

Conclusion

We have found that sulfoxidation of thioanisoles by a nonheme iron(IV)-oxo complex ($[(N4Py)Fe^{IV}(O)]^{2+}$) is remarkably promoted by a Brønsted acid ($HClO_4$). The comparison of the observed second-order rate constants of acid–promoted sulfoxidation of thioanisoles by $[(N4Py)Fe^{IV}(O)]^{2+}$ with those of PCET from one-electron reductants to $[(N4Py)Fe^{IV}(O)]^{2+}$ in light of the Marcus theory of outer-sphere electron transfer has allowed us to conclude that acid–promoted sulfoxidation of thioanisoles by $[(N4Py)Fe^{IV}(O)]^{2+}$ proceeds via outer-sphere PCET from thioanisoles to $[(N4Py)Fe^{IV}(OH)]^{3+}$ s rather than direct oxygen atom transfer from the monoprotonated complex ($[(N4Py)Fe^{IV}(OH)]^{3+}$) to thioanisole. Such an activation of Fe^{IV}=O species by the protonation will expand the scope of acid–promoted reactions of high-valent metal-oxo complexes as the case of organic compounds containing C=O bond.

References

(1) (a) Akiyama, T. *Chem. Rev.* **2007**, *107*, 5744. (b) Akiyama, T.; Itoh, J.; Fuchibe, K. *Adv. Synth. Catal.* **2006**, *348*, 999. (c) Cheon, C.-H.; Yamamoto, H. *Chem.*

Commun. **2011**, *47*, 3043.

(2) (a) Yu, J.; Shi, F.; Gong, L.-Z. *Acc. Chem. Res.* Articles ASAP. (b) Sun, J.; Kozmin, S. A. *J. Am. Chem. Soc.* **2005**, *127*, 13512. (c) Zhang L.; Kozmin, S. A. *J. Am. Chem. Soc.* **2004**, *126*, 10204.

(3) (a) Schreiner, P. R. *Chem. Soc. Rev.* **2003**, *32*, 289. (b) Pihko, P. M. *Angew. Chem.*, *Int. Ed.* **2004**, *43*, 2062. (c) Bolm, C.; Rantanen, T.; Schiffers, I.; Zani, L. *Angew. Chem.*, *Int. Ed.* **2005**, *44*, 1758. (d) Pihko, P. M. *Lett. Org. Chem*. **2005**, *2*, 398. (e) Taylor, M. S.; Jacobsen, E. N. *Angew. Chem*., *Int. Ed*. **2006**, *45*, 1520. (f) Mahoney, J. M.; Smith, C. R.; Johnston, J. N. *J. Am. Chem. Soc*. **2005**, *127*, 1354.

(4) (a) *Selectivities in Lewis Acid Promoted Reactions*; Schinzer, D. Ed.; Kluwer Academic: Dordrecht, 1989. (b) *Lewis Acids in Organic Synthesis*; Yamamoto, H. Ed.; Wiley-VCH: Weinheim, 2000. (c) Abell, J. P.; Yamamoto, H. *Chem. Soc. Rev*. **2010**, *39*, 61.

(5) (a) Kobayashi, S.; Ishitani, H. *Chem. Rev.* **1999**, *99*, 1069. (b) Akiyama, R.; Kobayashi, S. *Chem. Rev*. **2009**, *109*, 594. (c) Kobayashi, S.; Yamashita, Y. *Acc. Chem. Res*. **2011**, *44*, 58.

(6) (a) Johnson, J. S.; Evans, D. A. *Acc. Chem. Res*. **2000**, *33*, 325. (b) Rovis, T.; Evans, D. A. *Prog. Inorg. Chem*. **2001**, *50*, 1.

(7) (a) Pohlhaus, P. D.; Bowman, R. K.; Johnson, J. S. *J. Am. Chem. Soc.* **2004**, *126*, 2294. (b) Fukuzumi, S.; Fujita, M.; Otera, J.; Fujita, Y. *J. Am. Chem. Soc.* **1992**, *114*, 10271.

(8) (a) Mukaiyama, T.; Ishida, A. *Chem. Lett*. **1975**, 319. (b) Ishida, A.; Mukaiyama, T. *Chem. Lett*. **1975**, 1167. (c) Ishida, A.; Mukaiyama, T. *Bull. Chem. Soc. Jpn*. **1977**, *50*, 1161. (d) Ishida, A.; Mukaiyama, T. *Chem. Lett*. **1977**, 467. (e) Ishida, A.; Mukaiyama, T. *Bull. Chem. Soc. Jpn*. **1978**, *51*, 2077. (f) Mukaiyama, T.; Ishida, A. *Chem. Lett*. **1975**, 1201.

(9) (a) Casiraghi, G.; Battistini, L.; Curti, C.; Rassu, G.; Zanardi, F. *Chem. Rev*. **2011**, *111*, 3076. (b) Denmark, S. E.; Heemstra, J. R., Jr.; Beutner, G. L. *Angew. Chem., Int. Ed.* **2005**, *44*, 4682. (c) Casiraghi, G.; Zanardi, F.; Appendino, G.; Rassu, G. *Chem. Rev.* **2000**, *100*, 1929. (d) Kalesse, M. *Top. Curr. Chem*. **2005**, *244*, 43.

(10) (a) Fukuzumi, S.; *Bull. Chem. Soc. Jpn*. **1997**, *70*, 1. (b) Fukuzumi, S. *Org.*

Biomol. Chem. **2003**, *1*, 609. (c) Fukuzumi, S. *Bull. Chem. Soc. Jpn.* **2006**, *79*, 177. (d) Fukuzumi, S. *Pure Appl. Chem.* **2007**, *79*, 981. (e) Fukuzumi, S. *Pure Appl. Chem.* **2003**, *75*, 577.

(11) (a) Fukuzumi, S.; Ishikawa, K.; Hironaka, K.; Tanaka, T. *Perkin Trans. 2*, **1987**, 751. (b) Fukuzumi, S.; Ishikawa, M.; Tanaka, T. *Chem. Commun.* **1985**, 1069. (c) Fukuzumi, S.; Ishikawa, M.; Tanaka, T. *Perkin Trans. 2*, **1989**, 1811. (d) Ishikawa, M.; Fukuzumi, S. *Chem. Commun.* **1990**, 1353. (e) Ishikawa, M.; Fukuzumi, S. *J. Chem. Soc., Faraday Trans.1* **1990**, *86*, 3531. (f) Fukuzumi, S.; Mochizuki, S.; Tanaka, T. *J. Am. Chem. Soc.* **1989**, *111*, 1497. (g) Yuasa, J.; Yamada, S.; Fukuzumi, S. *J. Am. Chem. Soc.* **2008**, *130*, 5808.

(12) (a) Fukuzumi, S.; Kuroda, S. *Res. Chem. Int.* **1999**, *25*, 789. (b) Fukuzumi, S.; Tokuda, Y. *J. Phys. Chem.* **1993**, *97*, 3737. (c) Fukuzumi, S.; Chiba, M. *J. Chem. Soc., Perkin Trans. 2* **1991**, 1393. (d) Fukuzumi, S.; Mochizuki, S.; Tanaka, T. *J. Phys. Chem.* **1990**, *94*, 722.

(13) (a) Hayashi, H.; Ogo, S.; Fukuzumi, S. *Chem. Commun.* **2004**, 2714. (b) Hayashi, H.; Ogo, S.; Abura, T.; Fukuzumi, S. *J. Am. Chem. Soc.* **2003**, *125*, 14266.

(14) (a) Halime, Z.; Kotani, H.; Li, Y.; Fukuzumi, S.; Karlin, K. D. *Proc. Natl. Acad. Sci. U.S.A.* **2011**, *108*, 13990. (b) Fukuzumi, S.; Okamoto, K.; Gros, C. P.; Guilard, R. *J. Am. Chem. Soc.* **2004**, *126*, 10441. (c) Fukuzumi, S.; Mochizuki, S.; Tanaka, T. *Inorg. Chem.* **1989**, *28*, 2459.

(15) (a) Fukuzumi, S. *Prog. Inorg. Chem.* **2009**, *56*, 49. (b) Fukuzumi, S. *Bull. Chem. Soc. Jpn.* **1997**, *70*, 1. (c) Fukuzumi, S.; Ohtsu, H.; Ohkubo, K.; Itoh, S.; Imahori, H. *Coord. Chem. Rev.* **2002**, *226*, 71. (d) Fukuzumi, S.; Ohkubo, K. *Coord. Chem. Rev.* **2010**, *254*, 372.

(16) (a) Fukuzumi, S.; Itoh, S. in *Advances in Photochemistry*; Neckers, D. C.; Volman, D. H.; von Bünau, G., Eds.; Wiley: New York, 1998, Vol. 25, pp. 107-172. (b) Fukuzumi, S.; Itoh, S. *Antioxidants and Redox Signaling*, **2001**, *3*, 807.

(17) (a) Fukuzumi, S.; Ohkubo, K. *Chem.–Eur. J.* **2000**, *6*, 4532. (b) Ohkubo, K.; Menon, S. Orita, C. A.; Otera, J.; Fukuzumi, S. *J. Org. Chem.* **2003**, *68*, 4720.

(18) (a) Fukuzumi, S.; Okamoto, T. *J. Am. Chem. Soc.* **1993**, *115*, 11600. (b) Fukuzumi, S.; Nishizawa, N.; Tanaka, T. *Perkin Trans. 2*, **1985**, 371. (c) Fukuzumi, S.; Suenobu, T.; Patz, M.; Hirasaka, T.; Itoh, S.; Fujitsuka, M.; Ito, O.

J. Am. Chem. Soc. **1998**, *120*, 8060.

(19) (a) Fukuzumi, S.; Kuroda, S.; Tanaka, T. *J. Am. Chem. Soc*. **1985**, *107*, 3020. (b) Itoh, S.; Taniguchi, M.; Takada, N.; Nagatomo, S.; Kitagawa, T.; Fukuzumi, S. *J. Am. Chem. Soc*. **2000**, *122*, 12087. (c) Fukuzumi, S.; Yasui, K.; Suenobu, T.; Ohkubo, K.; Fujitsuka, M.; Ito, O. *J. Phys. Chem. A* **2001**, *105*, 10501.

(20) (a) Fukuzumi, S.; Okamoto, T.; Otera, J. *J. Am. Chem. Soc.* **1994**, *116*, 5503. (b) Fukuzumi, S.; Fujii, Y.; Suenobu, T. *J. Am. Chem. Soc.* **2001**, *123*, 10191.

(21) (a) Itoh, S.; Kumei, H.; Nagatomo, S.; Kitagawa, T.; Fukuzumi, S. *J. Am. Chem. Soc*. **2001**, *123*, 2165. (b) Fukuzumi, S.; Satoh, N.; Okamoto, T.; Yasui, K.; Suenobu, T.; Seko, Y.; Fujitsuka, M.; Ito, O. *J. Am. Chem. Soc*. **2001**, *123*, 7756. (c) Fukuzumi, S.; Ohkubo, K.; Okamoto, T. *J. Am. Chem. Soc*. **2002**, *124*, 14147.

(22) (a) Fukuzumi, S.; Okamoto, K.; Imahori, H. *Angew. Chem., Int. Ed*. **2002**, *41*, 620. (b) Okamoto, K. Imahori, H.; Fukuzumi, S. *J. Am. Chem. Soc*. **2003**, *125*, 7014. (c) Fukuzumi, S.; Okamoto, K.; Yoshida, Y.; Imahori, H.; Araki, Y.; Ito, O. *J. Am. Chem. Soc*. **2003**, *125*, 1007. (d) Savéant, J.-M. *J. Am. Chem. Soc*. **2008**, *130*, 4732.

(23) (a) Chen, X.; Bu, Y. *J. Am. Chem. Soc*. **2007**, *129*, 9713. (b) Wu, H.; Zhang, D.; Su, L.; Ohkubo, K.; Zhang, C.; Yin, S.; Mao, L.; Shuai, Z.; Fukuzumi, S.; Zhu, D. *J. Am. Chem. Soc*. **2007**, *129*, 6839. (c) Zeng, Y.; Zhang, G.; Zhang, D.; Zhu, D. *J. Org. Chem*. **2009**, *74*, 4375. (d) Jia, L.; Zhang, G.; Zhang, D.; Xiang, J.; Xu, W.; Zhu, D. *Chem. Commun*. **2011**, *47*, 322.

(24) (a) Yuasa, J.; Suenobu, T.; Fukuzumi, S. *J. Am. Chem. Soc*. **2003**, *125*, 12090. (b) Yuasa, J.; Suenobu, T.; Fukuzumi, S. *ChemPhysChem* **2006**, *7*, 942. (c) Yuasa, J.; Yamada, S.; Fukuzumi, S. *Chem.–Eur. J*. **2008**, *14*, 1866.

(25) (a) Dempsey, J. L.; Winkler, J. R.; Gray, H. B. *Chem. Rev.* **2010**, *110*, 7024. (b) Warren, J. J.; Tronic, T. A.; Mayer, J. M. *Chem. Rev*. **2010**, *110*, 6961. (c) Huynh, M. H. V.; Meyer, T. J. *Chem. Rev*. **2007**, *107*, 5004.

(26) (a) Reece, S. Y.; Nocera, D. G. *Annu. Rev. Biol. Chem*. **2009**, *78*, 673. (b) Chang, C. J.; Chang, M. C. Y.; Damrauer, N. H.; Nocera, D. G. *Biochim. Biophys. Acta* **2004**, *1655*, 13. (c) Cukier, R. I.; Nocera, D. G. *Annu. Rev. Phys. Chem*. **1998**, *49*, 337.

(27) (a) Mayer, J. M.; Rhile, I. J. *Biochim. Biophys. Acta* **2004**, *1655*, 51. (b) Mayer, J. M. *Annu. Rev. Phys. Chem.* **2004**, *55*, 363.

(28) Fukuzumi, S. *Helv. Chim. Acta* **2006**, *89*, 2425.

(29) (a) Fukuzumi, S.; Morimoto, Y.; Kotani, H.; Naumov, P.; Lee, Y.-M.; Nam, W. *Nature Chem.* **2010**, *2*, 756. (b) Karlin, K. D. *Nature Chem*. **2010**, *2*, 711.

(30) Morimoto, Y.; Kotani, H.; Park, J.; Lee, Y.-M.; Nam, W.; Fukuzumi, S. *J. Am. Chem. Soc.* **2011**, *133*, 403.

(31) Park, J.; Morimoto, Y.; Lee, Y.-M.; Nam, W.; Fukuzumi, S. *J. Am. Chem. Soc.* **2011**, *133*, 5236.

(32) Park, J.; Morimoto, Y.; Lee, Y.-M.; You, Y.; Nam, W.; Fukuzumi, S. *Inorg. Chem*. **2011**, *50*, 11612.

(33) (a) Fukuzumi, S.; Kotani, H.; Suenobu, T.; Hong, S.; Lee, Y.-M.; Nam, W. *Chem.–Eur. J*. **2010**, *16*, 354. (b) Fukuzumi, S.; Kotani, H.; Prokop, K. A.; Goldberg, D. P. *J. Am. Chem. Soc.* **2011**, *133*, 1859.

(34) (a) Lubben, M; Meetsma, A.; Wilkinson, E. C.; Feringa, B.; Que, L., Jr. *Angew. Chem., Int. Ed.* **1995**, *34*, 1512. (b) Kaizer, J.; Klinker, E. J.; Oh, N. Y.; Rohde, J.-U.; Song, W. J.; Stubna, A.; Kim, J.; Münck, E.; Nam, W.; Que, Jr., L. *J. Am. Chem. Soc.* **2004**, *126*, 472. (c) Klinker, E., J.; Kaizer, J.; Brennessel, W., W.; Woodrum, N., L.; Cramer, C., J.; Que, L., Jr. *Angew. Chem. Int. Ed*. **2005**, *44*, 3690.

(35) (a) Marcus, R. A. *Annu. Rev. Phys. Chem*. **1964**, *15*, 155. (b) Marcus, R. A. *Angew. Chem., Int. Ed. Engl*. **1993**, *32*, 1111.

(36) Lee, Y.-M.; Kotani, H.; Suenobu, T.; Nam, W.; Fukuzumi, S. *J. Am. Chem. Soc.* **2008**, *130*, 434.

(37) (a) Arias, J.; Newlands, C. R.; Abu-Omar, M. M. *Inorg. Chem.* **2001**, *40*, 2185. (b) Prokop, K. A.; New, H. M.; de Visser, S. P.; Goldberg, D. P. J. *Am. Chem. Soc*. **2011**, *133*, 15874. (c) Fertinger, C.; Hessenauer-Ilicheva, N.; Franke, A.; van Eldik, R. *Chem.–Eur. J.* **2009**, *15*, 13435. (d) Arunkumar, C.; Lee, Y.-M.; Lee, J. Y.; Fukuzumi, S.; Nam, W. *Chem.–Eur. J.* **2009**, *15*, 11482. (e) Kumar, A.; Goldberg, I.; Botoshansky, M.; Buchman, Y.; Gross, Z. *J. Am. Chem. Soc.* **2010**, *132*, 15233. (f) Benet-Buchholz, J.; Comba, P.; Llobet, A.; Roeser, S.; Vadivelu,

P.; Wiesner, S. *Dalton Trans.* **2010**, *39*, 3315.

(38) Armarego, W. L. F.; Chai, C. L. L. *Purification of Laboratory Chemicals*, 5th ed.; Butterworth Heinemann: Amsterdam, 2003.

(39) Park, M. J.; Lee, J.; Suh, Y.; Kim, J.; Nam, W. *J. Am. Chem. Soc.* **2006**, *128*, 2630.

(40) Mann, C. K.; Barnes, K. K. in *Electrochemical Reactions in Non-aqueous Systems*; Mercel Dekker: New York, 1970.

(41) Thioanisoles can be protonated by in the presence of large excess $HClO_4$ (see Figure S1 in SI). The plots of k_1 vs concentrations exhibit a saturation behavior in the region of high concentrations of thioanisoles due to the protonation of thioanisoles. Under the present experimental conditions in Figure 3, the effect of the protonation of thioanisoles can be neglected.

(42) (a) Fukuzumi, S.; Chiba, M.; Ishikawa, M.; Ishikawa, K.; Tanaka, T. *J. Chem. Soc., Perkin Trans. 2* **1989**, 1417. (b) Fukuzumi, S.; Ishikawa, M.; Tanaka, T. *Tetrahedron* **1986**, *42*, 1021. (c) Fukuzumi, S.; Chiba, M.; Tanaka, T. *Chem. Lett*. **1989**, 31.

(43) The observed $g_{\perp}$ value (2.58) is in a good agreement with the value reported for $[Ru^{III}(bpy)_3]^{3+}$ in which the $g_{\parallel}$ component was not observed because of its weak intensity; see: (a) Matsuura, K.; Kevan, L. *J. Chem. Soc., Faraday Trans.* **1997**, *93*, 1763. (b) Kotani, H.; Suenobu, T.; Lee, Y.-M.; Nam, W.; Fukuzumi, S. *J. Am. Chem. Soc.* **2011**, *133*, 3249.

(44) For similar Nernst analysis, see: (a) Yuasa, J.; Suenobu, T.; Fukuzumi, S. *J. Am. Chem. Soc.* **2003**, *125*, 12090. (b) Okamoto, K.; Imahori, H.; Fukuzumi, S. *J. Am. Chem. Soc*. **2003**, *125*, 7014.

(45) Goto, Y.; Matsui, T.; Ozaki, S.; Watanabe, Y.; Fukuzumi, S. *J. Am. Chem. Soc*. **1999**, *121*, 9497.

(46) Fukuzumi, S.; Nakanishi, I.; Tanaka, K.; Suenobu, T.; Tabard, A.; Guilard, R.; Caemelbecke, E.; Kadish, K. M. *J. Am. Chem. Soc*. **1999**, *121*, 785.

(47) For the difference between the inner-sphere and outer-sphere electron-transfer pathways, see: (a) Fukuzumi, S.; Wong, C. L.; Kochi, J. K. *J. Am. Chem. Soc*. **1980**, *102*, 2928–2939. (b) Fukuzumi, S.; Kochi, J. K. *Bull. Chem. Soc. Jpn*. **1983**,

56, 969–979.

(48) (a) Fukuzumi, S.; Kochi J. K. *J. Am. Chem. Soc*. **1981**, *103*, 2783. (b) Fukuzumi, S.; Kochi J. K. *J. Am. Chem. Soc*. **1981**, *103*, 7240. (c) Fukuzumi, S.; Kochi, J. K. *J. Am. Chem. Soc*. **1982**, *104*, 7599.

(49) Rosokha, S. V.; Kochi, J. K. *Acc. Chem. Res*. **2008**, *41*, 641.

(50) For the classical definition of inner-sphere electron transfer, see: (a) Taube, H.; Myers, H. J.; Rich, R. L. *J. Am. Chem. Soc*. **1953**, *75*, 4118. (b) Taube, H. *Science* **1984**, *226*, 1028.

Supporting Information

for Chapter 3

Table S1. One-Electron Oxidation Potentials (E_{ox}) of *para*-X-Substituted Thioanisoles and One-Electron Reductants and Second-Order Rate Constants of Sulfoxidation and Electron- Transfer Reactions with $[(N4Py)Fe^{IV}(O)]^{2+}$ in MeCN at 298K

thioanisole or one-electron reductant	E_{ox} (V vs SCE)	k_2 or k_{et}, M^{-1} s^{-1}		10 mM $HClO_4$
		without $HClO_4$	10 mM $HClO_4$	log (k_2, M^{-1} s^{-1})
para-X-thioanisoles				
p-Me	1.24	1.3 ± 0.1	$(3.2 \pm 0.2) \times 10^3$	3.5
p-H	1.34	$(8.7 \pm 0.4) \times 10^{-1}$	$(1.5 \pm 0.1) \times 10^3$	3.2
p-Cl	1.37	$(8.7 \pm 0.4) \times 10^{-1}$	$(7.2 \pm 0.4) \times 10^2$	2.8
p-Br	1.41	$(1.5 \pm 0.1) \times 10^{-1}$	$(8.4 \pm 0.4) \times 10^2$	2.9
p-CN	1.61	$(4.4 \pm 0.2) \times 10^{-2}$	$(6.2 \pm 0.3) \times 10$	1.8
one-electron reductant				
$[Fe^{II}(Me_2bpy)_3]^{2+}$	0.92	NR[a]	$(3.2 \pm 0.2) \times 10^2$	2.5
$[Ru^{II}(Me_2bpy)_3]^{2+}$	1.10	NR[a]	$(1.2 \pm 0.1) \times 10^2$	2.1
$[Fe^{II}(Clphen)_3]^{2+}$	1.17	NR[a]	$(2.1 \pm 0.1) \times 10$	1.3
$[Ru^{II}(Clphen)_3]^{2+}$	1.36	NR[a]	1.4 ± 0.1	1.6×10^{-1}

[a]NR : No Reaction

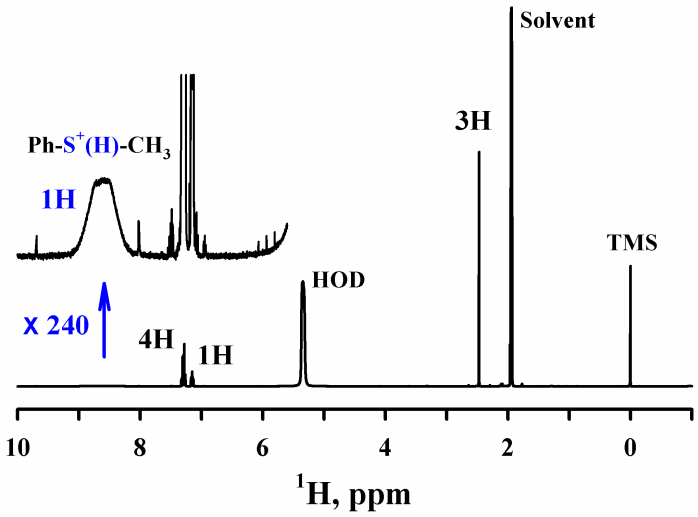

Figure S1. ^1H NMR spectrum of thioanisole (5.0 mM) in the presence of $HClO_4$ (20 mM) in CD_3CN at 298 K. A broadened Ph-S^+(H)-CH_3 peak appeared in the range of 8.1 – 9.1 ppm, indicating that there is an equilibrium between thioanisole and protonated thioanisole in the presence of $HClO_4$. Number of scan was 2048.

Chapter 4. C–H Bond Cleavage via Proton–Coupled Electron Transfer from Toluene Derivaitves to a Protonated Nonheme Iron(IV)-Oxo Complex with No Kinetic Isotope Effect

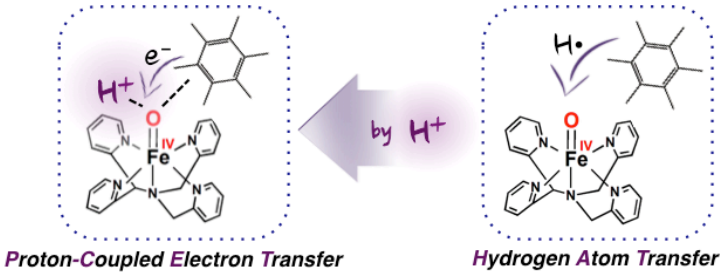

Abstract: The reactivity of a nonheme iron(IV)-oxo complex, $[(N4Py)Fe^{IV}(O)]^{2+}$ (N4Py = *N*,*N*-bis(2-pyridylmethyl)-*N*-bis(2-pyridyl)methylamine), was markedly enhanced by perchloric acid (70% $HClO_4$) in the oxidation of toluene derivatives. Toluene, which has a high one-electron oxidation potential (E_{ox} = 2.20 V vs SCE), was oxidized by $[(N4Py)Fe^{IV}(O)]^{2+}$ in the presence of $HClO_4$ in acetonitrile (MeCN) to yield a stoichiometric amount of benzyl alcohol, in which $[(N4Py)Fe^{IV}(O)]^{2+}$ was reduced to $[(N4Py)Fe^{III}(OH_2)]^{3+}$. The second-order rate constant (k_{obs}) of the oxidation of toluene derivatives by $[(N4Py)Fe^{IV}(O)]^{2+}$ increased with increasing concentration of $HClO_4$, showing the first-order dependence on $[HClO_4]$. A significant kinetic isotope effect (KIE) was observed when mesitylene was replaced by mesitylene-d_{12} in the oxidation with $[(N4Py)Fe^{IV}(O)]^{2+}$ in the absence of $HClO_4$ in MeCN at 298 K. The KIE value drastically decreased from KIE = 31 in the absence of $HClO_4$ to KIE = 1.0 with increasing concentration of $HClO_4$, accompanied by the large acceleration of the oxidation rate. The absence of KIE suggests that electron transfer from a toluene derivative to the protonated iron(IV)-oxo complex ($[(N4Py)Fe^{IV}(OH)]^{3+}$) is the rate-determining step in the acid–promoted oxidation reaction. The detailed kinetic analysis in light of the Marcus theory of electron transfer has revealed that the acid–promoted C–H bond cleavage proceeds via the rate-determining electron transfer from toluene derivatives to $[(N4Py)Fe^{IV}(OH)]^{3+}$ through formation of strong precursor complexes between toluene derivatives and $[(N4Py)Fe^{IV}(OH)]^{3+}$.

Introduction

High-valent iron-oxo complexes with heme and nonheme ligands play pivotal roles as reactive intermediates in biological and chemical oxidation reactions.[1,2] Extensive efforts have been devoted to synthesize various nonheme iron(IV)-oxo complexes, which were characterized by various spectroscopic methods and X-ray crystallography.[3-13] Over the past several decades, the reactivity of the biomimetic iron(IV)-oxo complexes have been investigated in various oxidation reactions such as oxygen atom transfer and C–H bond cleavage.[7-17] It has been demonstrated that the reactivity of iron(IV)-oxo complexes are affected by supporting and axial ligands, solvents and other various reaction conditions.[8-17] Understanding factors that control reactivity of nonheme iron complexes in oxidation reactions is indispensable in designing efficient biomimetic catalysts with high reactivity and selectivity. One important factor that controls the reactivity of iron(IV)-oxo complexes is Brønsted acids, which can protonate iron(IV)-oxo complexes to enhance the reacitivity.[18]

We have previously reported that Brønsted acids promote oxygen atom transfer from a nonheme iron(IV)-oxo complex and also electron transfer from one-electron reductants such as ferrocene derivatives.[18,19] With regard to C–H bond cleavage, nonheme iron(IV)-oxo complexes reported to date are capable of activating weak C–H bonds of activated alkanes (e.g., alkylaromatics such as xanthene, 9,10-dihydroanthracene, and fluorene).[15] In the presence of $Sc(OTf)_3$ (OTf^- = triflate anion), a nonheme iron(IV)-oxo complex becomes capable of oxidizing benzyl alcohol derivatives with electron-donating substituents via outer-sphere electron transfer from the benzyl alcohol derivatives to a nonheme iron(IV)-oxo complex, which is coupled with binding of $Sc(OTf)_3$.[20] In such an outer-sphere electron-transfer pathway, the reactivity of nonheme iron(IV)-oxo complexes is determined by the one-electron reduction potentials when no further enhancement of the reactivity is possible because interactions between substrates and Sc^{3+} ion–bound iron(IV)-oxo complexes are prohibited due to the steric effect of Sc^{3+} ion.[21] In contrast to the case of Sc^{3+} ion–coupled electron transfer reactions of nonheme iron(IV)-oxo complexes, it is possible to have strong interactions between substrates and protonated non-hem iron(IV)-oxo complexes in proton–coupled electron-transfer (PCET) reactions.[19] However, C–H bond cleavage via PCET from substrates to nonheme iron(IV)-oxo complexes has yet to be reported.

We report herein remarkable acceleration effects of Brønsted acid (i.e., $HClO_4$) on C–H bond cleavage of toluene derivatives by a nonheme iron(IV)-oxo complex, $[(N4Py)Fe^{IV}(O)]^{2+}$ (N4Py = *N*,*N*-bis(2-pyridylmethyl)-*N*-bis(2-pyridyl)methylamine), via electron transfer from toluene derivatives to a protonated iron(IV)-oxo complex, $[(N4Py)Fe^{IV}(OH)]^{3+}$. Strong precursor complexes were formed between toluene derivatives and $[(N4Py)Fe^{IV}(OH)]^{3+}$ prior to electron transfer. Although C–H bond cleavage of mesitylene with $[(N4Py)Fe^{IV}(O)]^{2+}$ without $HClO_4$ is sluggish to exhibit a significant deuterium kinetic isotope effect (KIE = 31), the rate of C–H bond cleavage with $[(N4Py)Fe^{IV}(O)]^{2+}$ is 10^3–fold faster in the presence of $HClO_4$ (10 mM) to show no KIE (KIE = 1.0). The rate constants of C–H bond cleavage of toluene derivatives with $[(N4Py)Fe^{IV}(O)]^{2+}$ and $[(N4Py)Fe^{IV}(OH)]^{3+}$ are quantitatively compared with those of outer-sphere electron-transfer reactions from coordinatively saturated metal complexes (one-electron reductants) to $[(N4Py)Fe^{IV}(OH)]^{3+}$ in light of the Marcus theory of electron transfer. The present study provides valuable mechanistic insights into the switch of the C–H bond cleavage mechanism from hydrogen atom transfer from toluene derivatives to $[(N4Py)Fe^{IV}(O)]^{2+}$ in the absence of $HClO_4$ to electron transfer from toluene derivatives to $[(N4Py)Fe^{IV}(OH)]^{3+}$ in the presence of $HClO_4$.

Experimental section

Materials. All chemicals, which were the best available purity, were purchased from Aldrich Chemical Co. and Tokyo Chemical Industry, used without further purification unless otherwise noted. Solvents, such as acetonitrile (MeCN) and diethyl ether, were dried according to the literature procedures and distilled under Ar prior to use.[22] Nonheme iron(II) complex $[(N4Py)Fe^{II}(MeCN)](ClO_4)_2$ and its corresponding iron(IV)-oxo $[(N4Py)Fe^{IV}(O)]^{2+}$ were prepared by the literature methods.[15,23] Iodosylbenzene (PhIO) was prepared by the literature method.[24] Perchloric acid (70 wt. % in H_2O) was purchased from Sigma Aldrich Chemical Co.

Caution: Perchlorate salts are potentially explosive and should be handled with care.

Kinetic Studies. Kinetic measurements were performed on a Hewlett Packard 8453 photodiode-array spectrophotometer using a 10 mm quartz cuvette (10 mm path length) at 298 K. C–H bond cleavage of toluene derivatives by $[(N4Py)Fe^{IV}(O)]^{2+}$ was examined by monitoring the spectral change due to $[(N4Py)Fe^{IV}(O)]^{2+}$ (2.5×10^{-5} M)

with various concentrations of alkylbenzenes (2.5×10^{-3} – 1.0×10^{-1} M) in the absence and presence of $HClO_4$ in MeCN at 298 K. Rates of C–H bond cleavage of toluene derivatives by $[(N4Py)Fe^{IV}(O)]^{2+}$ were monitored by the decay of the absorption band at 695 nm due to $[(N4Py)Fe^{IV}(O)]^{2+}$ (λ_{max} = 695 nm) in the absence and presence of $HClO_4$ in MeCN. The concentration of toluene derivatives was maintained at least more than 10-fold excess of $[(N4Py)Fe^{IV}(O)]^{2+}$ to attain pseudo-first-order conditions. First-order fitting of the kinetic data allowed us to determine the pseudo-first-order rate constants. The first-order plots were linear for three or more half-lives with the correlation coefficient $\rho > 0.999$. In each case, it was confirmed that the rate constants derived from at least five independent measurements agreed within an experimental error of ±5%. The pseudo-first-order rate constants increased proportionally with increase in concentrations of substrates, from which second-order rate constants were determined.

Product Analysis. Typically, hexamethylbenzene (2.0×10^{-2} M) was added to an MeCN solution (0.50 mL) containing $[(N4Py)Fe^{IV}(O)]^{2+}$ (4.0×10^{-3} M) in the presence of $HClO_4$ (10 mM) in a vial. The reaction was complete within 5 min under these conditions. Products formed in the oxidation reactions of toluene derivatives by $[(N4Py)Fe^{IV}(O)]^{2+}$, which were carried out in the presence of $HClO_4$ under Ar atmosphere in MeCN-d_3 at 298 K, were analyzed by ^{1}H NMR. Quantitative analyses were made on the basis of comparison of ^{1}H NMR spectral integration between products and their authentic samples. In the case of hexamethylbenzene, pentamethyl benzyl alcohol was obtained as a product with 50% of yield (based on the intermediate generated) in the presence of $HClO_4$ (10 mM). In the cases of other toluene derivatives, $(methyl)_n$benzene, $(methyl)_{n-1}$benzyl alcohols were obtained in quantitative amounts[17,31] by ^{1}H NMR, as the case of hexamethylbenzene (HMB).

Instrumentation. UV-vis spectra were recorded on a Hewlett Packard 8453 photodiode-array spectrophotometer. X-band EPR spectra were taken at 5 K using a X-band Bruker EMX-plus spectrometer equipped with a dual mode cavity (ER 4116DM). Low temperatures were achieved and controlled with an Oxford Instruments ESR900 liquid He quartz cryostat with an Oxford Instruments ITC503 temperature and gas flow controller. The experimental parameters for EPR spectra were as follows: Microwave frequency = 9.648 GHz, microwave power = 1 mW and modulation

amplitude = 10 G. ^{1}H NMR spectra were measured with Bruker model digital AVANCE III 400 FT-NMR spectrometer. GC-MS spectra were monitored using a Shimadzu GC-17A gas chromatograph and Shimadzu MS-QP5000 mass spectrometer.

Results and Discussion

Brønsted Acid–Promoted C–H Bond Cleavage of Toluene Derivatives by $[(N4Py)Fe^{IV}(O)]^{2+}$ with $HClO_4$. Although oxidation of hexamethylbenzene by $[(N4Py)Fe^{IV}(O)]^{2+}$ in acetonitrile (MeCN) is sluggish, the reaction with $HClO_4$ (10 mM) occurred efficiently to afford pentamethylbenzyl alcohol as the sole oxidized product, when $[(N4Py)Fe^{IV}(O)]^{2+}$ was reduced to yield $[(N4Py)Fe^{III}]^{3+}$ as indicated by the EPR spectrum (Figure 1). The stoichiometry of the oxidation of hexamethylbenzene by $[(N4Py)Fe^{IV}(O)]^{2+}$ with $HClO_4$ is given by eq 1. In such a case the observed 50% yield of pantametheylbenzyl alcohol (Figure 2) indicates the quantitative conversion because

$$PhCH_3 + 2[(N4Py)Fe^{IV}(O)]^{2+} + 2H^+ \longrightarrow PhCH_2{-}OH + 2[(N4Py)Fe^{III}]^{3+} + H_2O \quad (1)$$

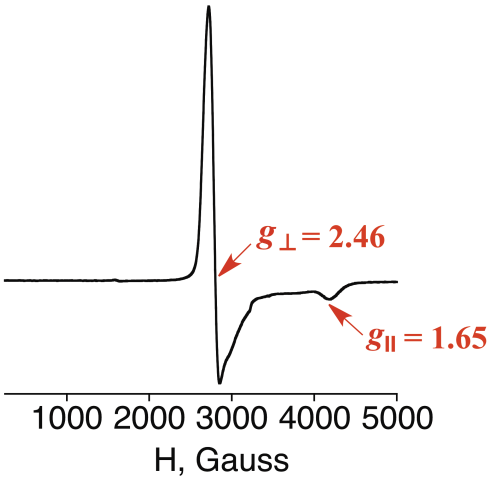

Figure 1. EPR spectrum of the complete reaction solution obtained in oxidation of hexamethylbenzene (5.0 mM) with $[(N4Py)Fe^{IV}(O)]^{2+}$ (1.0 mM) in the presence of $HClO_4$ (10 mM) in MeCN at 77K under Ar. The *g* values of EPR active species indicates that the Fe(III) species was formed.

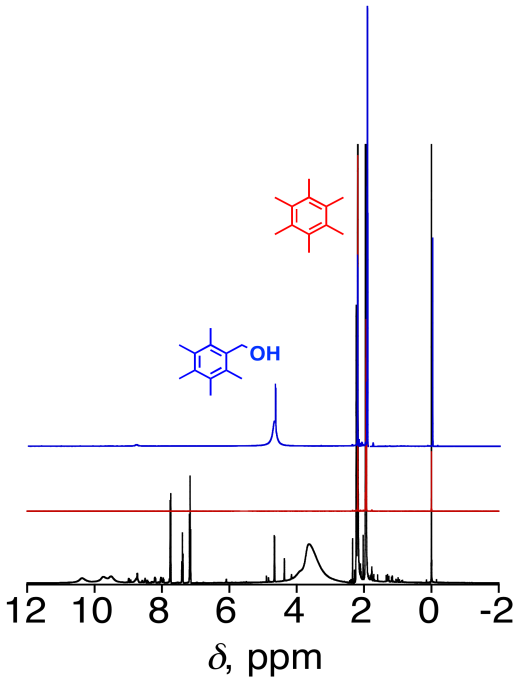

Figure 2. ^{1}H NMR spectrum of the complete reaction solution obtained in oxidation of hexamethylbenzene (20 mM) with $[(N4Py)Fe^{IV}(O)]^{2+}$ (4.0 mM) in the presence of $HClO_4$ (10 mM) in CD_3CN at 298 K (black line). The peak at 4.7 ppm due to $–CH_2–$ group in 1,2,3,4,5-pentamethylbenzyl alcohol was formed. Red and blue lines show ^{1}H NMR spectra of hexamethylbenzene (4.0 mM) and 1,2,3,4,5-pentamethylbenzyl alcohol (4.0 mM) as authentic references, respectively.

$[(N4Py)Fe^{IV}(O)]^{2+}$ in the presence of $HClO_4$ acts as a one-electron oxidant without oxygen in contrast to the case in the absence of $HClO_4$.[15,25-27] No further oxidation of pantametheylbenzyl alcohol was observed. The one-electron oxidation potential of pentamethylbenzyl alcohol in the presence of an acid in MeCN is higher than that of hexamethylbenzene (1.49 V vs SCE).[20] Thus, PCET from petamethylbenzyl alcohol to $[(N4Py)Fe^{IV}(O)]^{2+}$ is expected to be slower than that from hexamethylbenzene as discussed later. In addition, much excess hexamethybenzene relative to $[(N4Py)Fe^{IV}(O)]^{2+}$ was employed to analyze the product. This is the reason why no further oxidation of pentamethylbenzyl alcohol was observed in this study.

In the presence of $HClO_4$ (10 mM), the one-electron reduction potential of $[(N4Py)Fe^{IV}(O)]^{2+}$ is reported to be shifted to a positive direction from 0.51 V vs SCE to 1.43 V vs SCE,[18,19,28] which is much more positive than the one-electron oxidation potential of $[(N4Py)Fe^{II}(MeCN)]^{2+}$ (E_{ox} = 1.00 V vs SCE).[29] Thus, $[(N4Py)Fe^{II}(MeCN)]^{2+}$ is oxidized by $[(N4Py)Fe^{IV}(O)]^{2+}$ in the presence of $HClO_4$ to produce $[(N4Py)Fe^{III}]^{3+}$ (Figure 1).

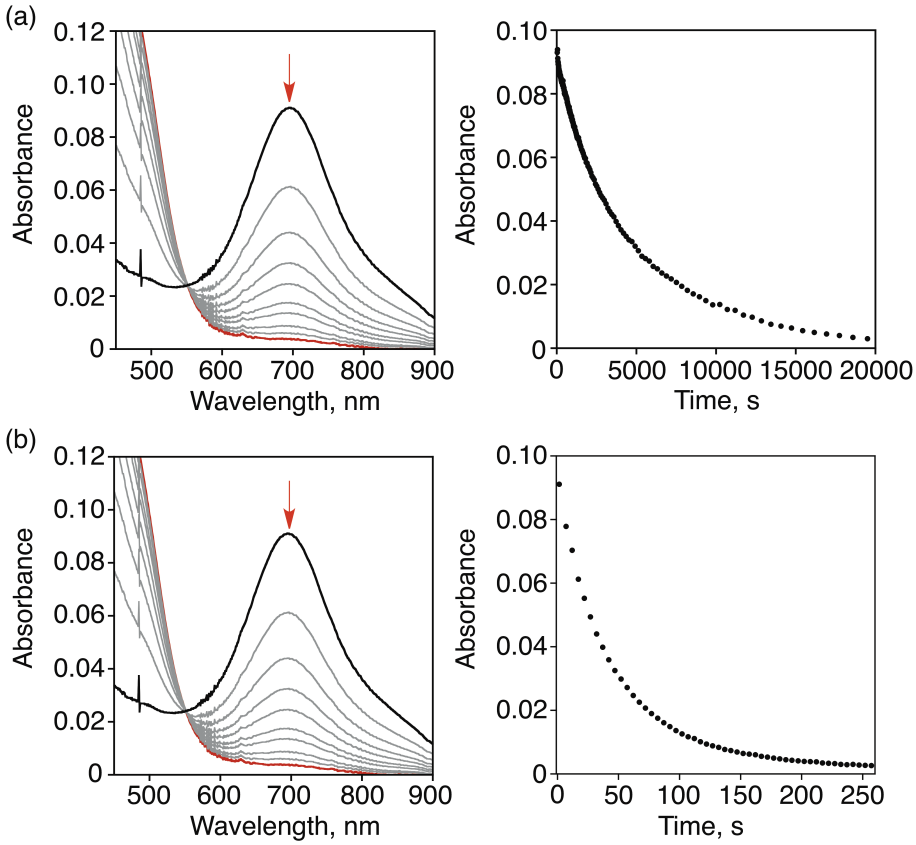

Figure 3. Visible spectral changes observed in the reaction of $[(N4Py)Fe^{IV}(O)]^{2+}$ (0.25 mM) with 1,2,4,5-Tetramethylbenzene (TMB) ((a) 25 mM and (b) 6.3 mM) in the absence (a) and presence (b) of $HClO_4$ (10 mM) in MeCN at 298 K (left panel). Right panels show time courses monitored at 695 nm due to the decay of $[(N4Py)Fe^{IV}(O)]^{2+}$.

Rates of oxidation of toluene derivatives by $[(N4Py)Fe^{IV}(O)]^{2+}$ were remarkably enhanced by the presence of $HClO_4$. A typical example is shown in Figure 3, where the absorption band at 695 nm due to $[(N4Py)Fe^{IV}(O)]^{2+}$ decays in the course of oxidation of 1,2,4,5-tetramethylbenzene (TMB) by $[(N4Py)Fe^{IV}(O)]^{2+}$. The decay rate of $[(N4Py)Fe^{IV}(O)]^{2+}$ becomes much faster in the presence of $HClO_4$ (10 mM) (Figures 3a vs 3b). Decay rates of $[(N4Py)Fe^{IV}(O)]^{2+}$ with large excess of TMB in the absence and presence of large excess $HClO_4$ obeyed pseudo- first-order kinetics. The pseudo-first-order rate constant increased proportionally with increasing TMB concentration (Figure 4). The second-order rate constant (k_{obs}) was determined from the slope of the linear plot of the pseudo-first-order rate constant vs TMB concentration. The observed second-order rate constant (k_{obs}) increased linearly with increasing $HClO_4$ concentration (Figure 5). The k_{obs} values of other toluene derivatives also exhibited linear correlations with $HClO_4$ concentration as given by eq 2,

$$k_{obs} = k_0 + k_1[HClO_4] \quad (2)$$

where k_0 is the rate constant in the absence of $HClO_4$. A similar correlation between the rate constant of PCET from the excited state of $[Ru^{II}(bpy)_3]^{2+}$ to aromatic carbonyl compounds and $[HClO_4]$ has been established by using 70 wt% $HClO_4$ in MeCN.[27] The PCET rate constants are known to decrease significantly by the addition of water at constant $[HClO_4]$.[28] Although the k_{obs} values oxidation of 1,2,4,5-tetramethylbenzene with $[(N4Py)Fe^{IV}(O)]^{2+}$ in the presence of 10 mM and 20 mM of $HClO_4$ (70%) in MeCN at 298 K decrease significantly with increasing added H_2O concentration, the ratio of k_{obs} with 20 mM vs 10 mM remains constant (two) irrespective of added H_2O

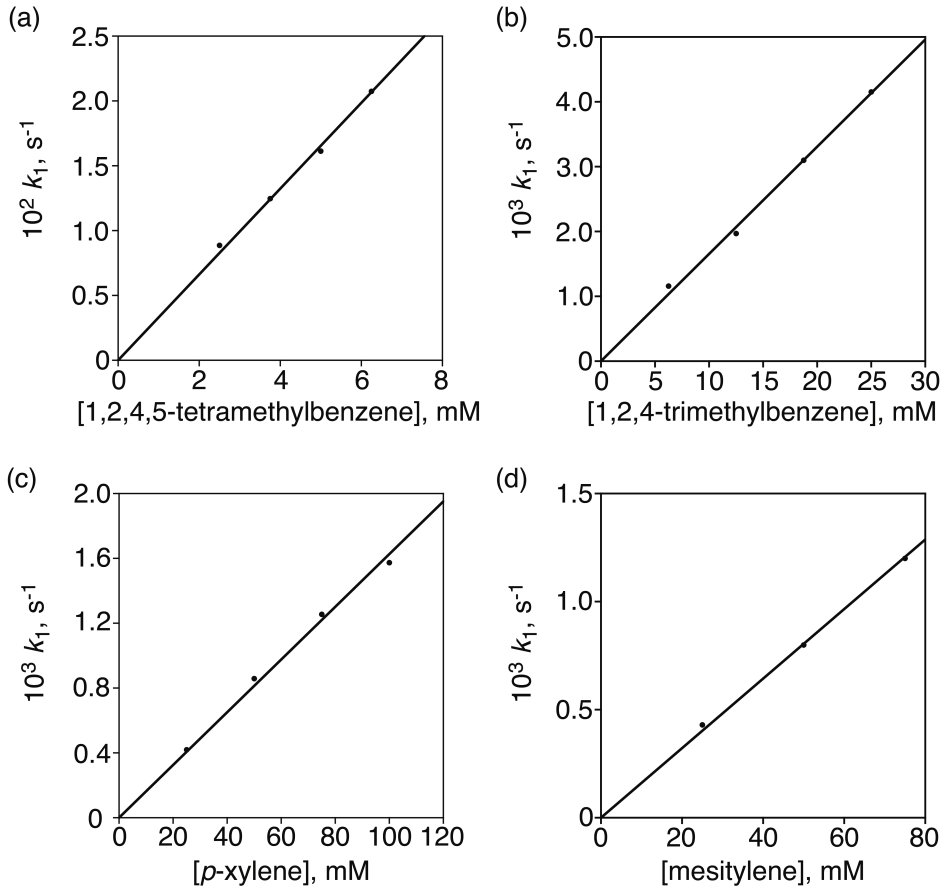

Figure 4. Plots of pseudo-first-order rate constants (k_1) vs concentrations of toluene derivatives to determine the second-order rate constants (k_{obs}) in oxidation of toluene derivatives with $[(N4Py)Fe^{IV}(O)]^{2+}$ (0.25 mM) in the presence of $HClO_4$ (10 mM) in MeCN at 298 K (*p*-xylene = 1,4-dimethylbenzene; mesitylene = 1,3,5-trimethyl- benzene).

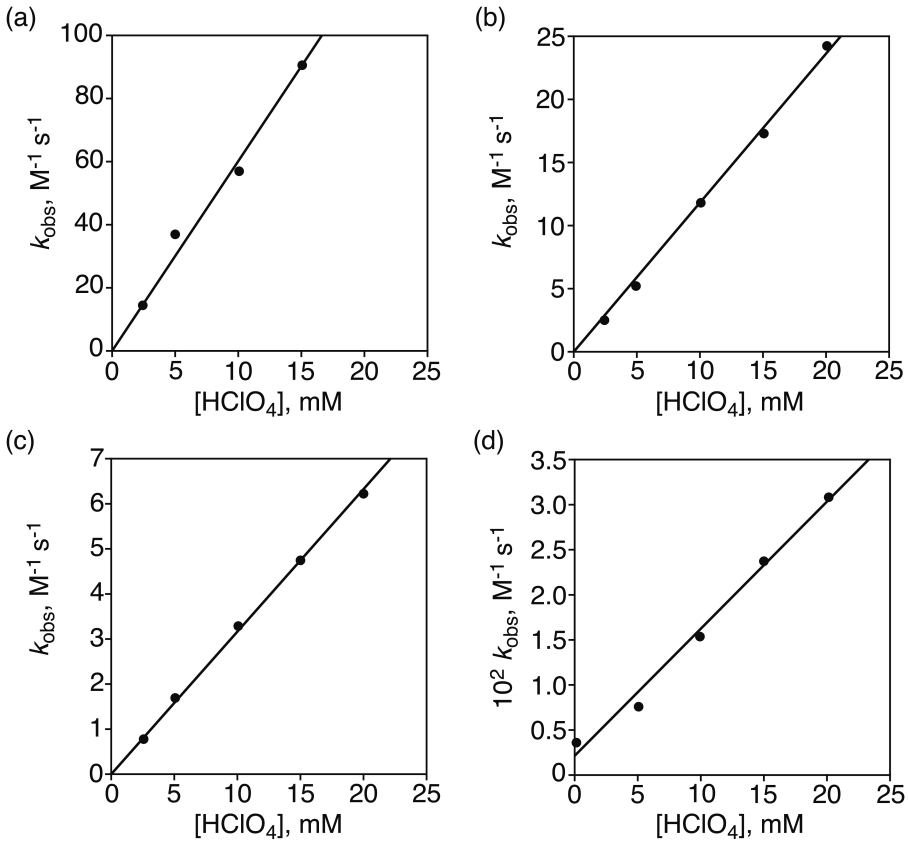

Figure 5. Plots of k_{obs} vs $HClO_4$ concentration in oxidation of (a) hexamethylbenzene, (b) 1,2,3,4,5-pentamethylbenzene, (c) 1,2,4,5-tetramethyl-benzene and (d) 1,3,5-trimethylbenzene) with $[(N4Py)Fe^{IV}(O)]^{2+}$ in the presence of $HClO_4$ in MeCN at 298 K.

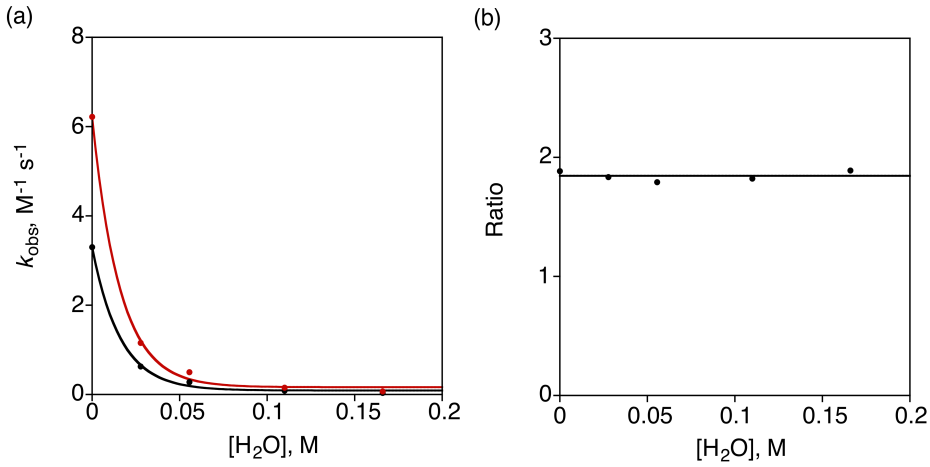

Figure 6. (a) Plots of second-order rate constant (k_2) vs concentration of H_2O in oxidation of 1,2,4,5-tetramethylbenzene with $[Fe^{IV}(O)(N4Py)]^{2+}$ (0.25 mM) in the presence of 10 mM (black) and 20 mM (red) of $HClO_4$ in MeCN at 298 K. (b) Plot of ratio ($k_{2,\ 20\ mM}$ / $k_{2,\ 10\ mM}$) vs concentration of H_2O.

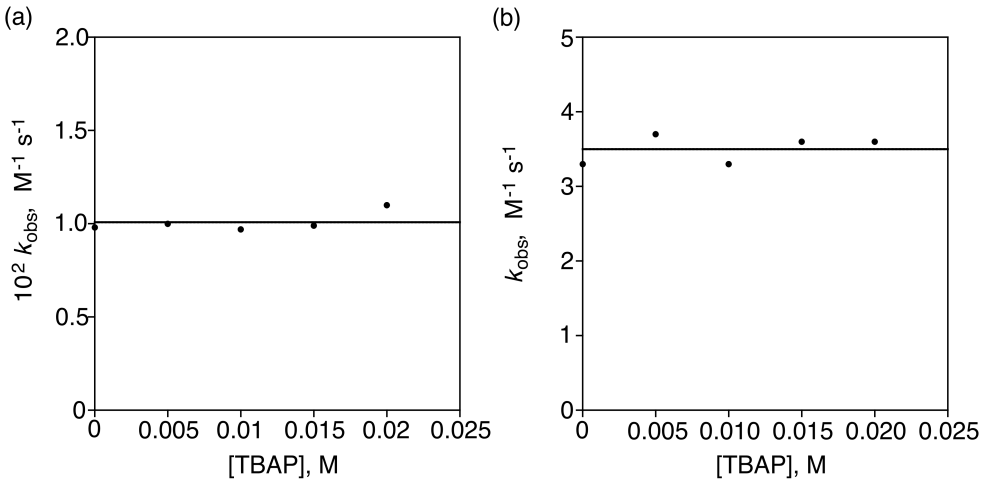

Figure 7. Plots of second-order rate constant (k_{obs}) vs concentration of tetrabutylammonium perchlorate in oxidation of 1,2,4,5-tetramethylbenzene with $[(N4Py)Fe^{IV}(O)]^{2+}$ (0.25 mM) (a) in the absence and (b) presence of 10 mM of $HClO_4$ in MeCN at 298 K.

Table 1. One-Electron Oxidation Potentials (E_{ox}) of Toluene Derivatives and Second-Order Rate Constants of the C–H Bond Cleavage by $[(N4Py)Fe^{IV}(O)]^{2+}$ in the Presence of $HClO_4$ (10 mM) in MeCN at 298 K

toluene derivative	E_{ox} (vs SCE, V)[a]	k_{obs}, $M^{-1} s^{-1}$	
		without $HClO_4$	with $HClO_4$ (10 mM)
hexamethylbenzene	1.49	$(5.1 \pm 0.2) \times 10^{-2}$	$(5.7 \pm 0.2) \times 10$
1,2,3,4,5-pentamehtylbenzene	1.58	$(1.0 \pm 0.1) \times 10^{-2}$	$(1.2 \pm 0.1) \times 10$
1,2,4,5-tetramethylbenzene	1.63	$(9.8 \pm 0.4) \times 10^{-3}$	3.3 ± 0.2
1,2,4-trimethylbenzene	1.79	$(5.5 \pm 0.2) \times 10^{-3}$	$(1.9 \pm 0.1) \times 10^{-1}$
1,4-dimethylbenzene	1.93	$(4.0 \pm 0.1) \times 10^{-3}$	$(1.6 \pm 0.1) \times 10^{-2}$
1,3,5-trimethylbenzene	1.98	$(3.7 \pm 0.1) \times 10^{-3}$	$(1.6 \pm 0.2) \times 10^{-2}$
toluene	2.20	$(1.5 \pm 0.1) \times 10^{-4}$	$(5.3 \pm 0.2) \times 10^{-4}$

[a] Taken from ref 36.

concentration (Figure 6). This indicates that the acidity of $HClO_4$ (70%) decreases with increasing added H_2O but that the k_{obs} values are proportional to concentration of $HClO_4$ (70%) irrespective of added H_2O concentration. If we could use $HClO_4$ (100%), the acidity would be much higher. However, $HClO_4$ without H_2O may explode. Thus, we have used $HClO_4$ (70%) in this study to utilize the high acidity safely. We have also confirmed that the k_{obs} values of oxidation of 1,2,4,5-tetramethylbenzene with

$[(N4Py)Fe^{IV}(O)]^{2+}$ both in the absence and presence or 10 mM of $HClO_4$ remain constant irrespective of concentration of tetra-*n*-butylammonium perchlorate (TBAP) as shown in Figure 7. This indicates that the ionic strength does not affect the k_{obs} values.

The observed second-order rate constants (k_{obs}) of C–H bond cleavage of toluene derivatives with $[(N4Py)Fe^{IV}(O)]^{2+}$ in the absence and presence of $HClO_4$ (10 mM) are listed in Table 1. The k_{obs} values in the presence of $HClO_4$ (10 mM) relative to those in the absence of $HClO_4$ increase with increasing the number of methyl groups on benzene, and the enhancement is as large as 10^3-fold in the case of hexamethylbenzene.

In the absence of $HClO_4$, C–H bond cleavage of toluene derivatives with $[(N4Py)Fe^{IV}(O)]^{2+}$ proceeds via the rate-determining hydrogen atom transfer from toluene derivatives to $[(N4Py)Fe^{IV}(O)]^{2+}$. It was evidenced by observation of a large deuterium kinetic isotope effect (KIE) as shown in Figure 8a, where the rate constant of mesitylene (1,3,5-trimethylbenzene) is about 30 times larger than that of fully deuterated mesitylene (KIE = 31). Such a large KIE value suggests that the hydrogen atom transfer occurs via tunneling.[32-35]

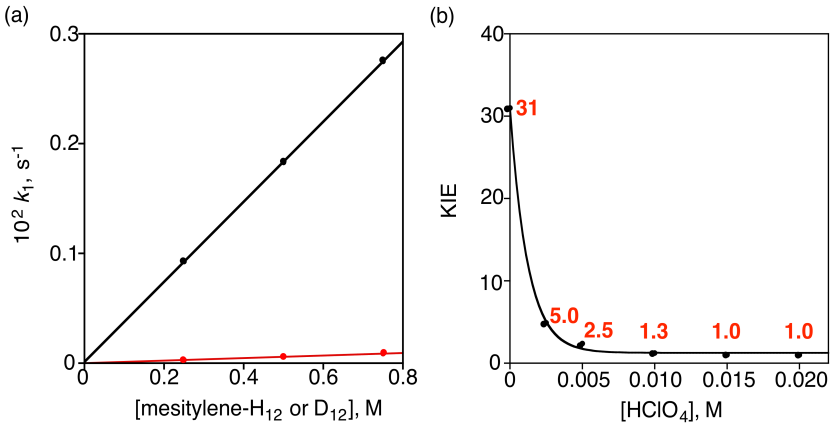

Figure 8. (a) Plots of first-order rate constants vs concentration of mesitylene in oxidation of mesitylene (black circle) and mesitylene-d_{12} (red circle) with $[(N4Py)Fe^{IV}(O)]^{2+}$ (0.25 mM) in the absence of $HClO_4$ in MeCN at 298 K. (b) Plot of KIE vs concentration of $HClO_4$ in MeCN at 298 K. Red numbers show the KIE values obtained experimentally.

In the presence of $HClO_4$, the k_{obs} value of oxidation of mesitylene with $[(N4Py)Fe^{IV}(O)]^{2+}$ increased with increasing concentration of $HClO_4$ (Figure 5d). However, the KIE value decreased significantly with increasing concentration of $HClO_4$ as shown in Figure 8b, where the large KIE value of 31 in the absence of $HClO_4$ is

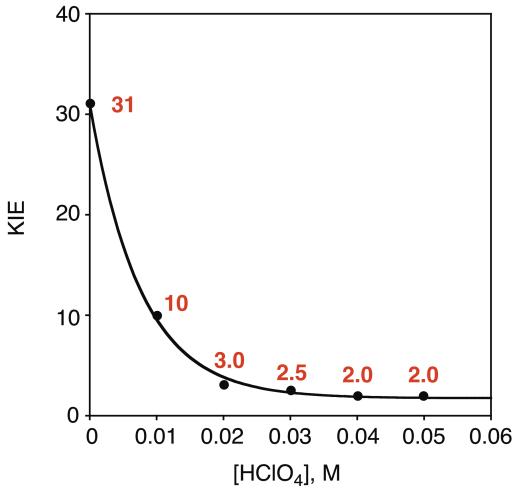

Figure 9. Plot of KIE vs concentration of $HClO_4$ in oxidation reaction of toluene and toluene-d_8 with $[(N4Py)Fe^{IV}(O)]^{2+}$ (0.25 mM) in MeCN at 298 K. Red numbers show the KIE values obtained experimentally.

changed to no KIE (KIE = 1.0) in the presence of large concentrations of $HClO_4$ (>10 mM). The absence of KIE in the presence of $HClO_4$ (>10 mM) indicates the change of the mechanism from a rate-determining hydrogen atom transfer pathway in the absence of $HClO_4$ (eq 3) to an electron–transfer pathway from toluene derivatives to the monoprotonated iron(IV)-oxo complex ($[(N4Py)Fe^{IV}(OH)]^{3+}$) in the presence of $HClO_4$ (eq 4).

The change in the KIE values in the presence of $HClO_4$ was also observed in the oxidation reaction of toluene vs toluene-d_8 as shown in Figure 9. The large KIE value (31) in the absence of $HClO_4$ decreased with increasing concentration of $HClO_4$. In this case, however, a small KIE value (2.0) was observed in the presence of large excess $HClO_4$. This indicates that an hydrogen atom transfer pathway (eq 3) is still competing with an electron-transfer pathway from toluene to the monoprotonated iron(IV)-oxo complex ($[(N4Py)Fe^{IV}(OH)]^{3+}$) in the presence of $HClO_4$ (eq 4) under the conditions in Figure 9.

$$PhCH_3 + [(N4Py)Fe^{IV}(O)]^{2+} \longrightarrow PhCH_2^{\bullet} + [(N4Py)Fe^{III}(OH)]^{2+} \quad (3)$$

$$PhCH_3 + [(N4Py)Fe^{IV}(O)]^{2+} + H^+ \longrightarrow PhCH_3^{\bullet+} + [(N4Py)Fe^{III}(OH)]^{2+} \quad (4)$$

In the presence of $HClO_4$, PCET from toluene derivatives to $[(N4Py)Fe^{IV}(OH)]^{3+}$

may become much faster than the hydrogen atom transfer reaction. Radical cations of toluene derivatives are known to undergo rapid deprotonation, producing benzyl radical derivatives, which may react with $[(N4Py)Fe^{IV}(O)]^{2+}$ with H^+ to yield benzyl alcohol derivatives and $[(N4Py)Fe^{III}]^{3+}$ to be consistent with the stoichiometry in eq 1. The more detailed mechanism of C–H bond cleavage of toluene derivatives with $[(N4Py)Fe^{IV}(O)]^{2+}$ in the presence of $HClO_4$ is discussed after comparison of the reactivity with that of outer-sphere PCET reactions of $[(N4Py)Fe^{IV}(O)]^{2+}$ (vide infra).

Outer-Sphere PCET Reactions of $[(N4Py)Fe^{IV}(O)]^{2+}$. In order to compare the reactivity of C–H bond cleavage reactions, which proceed via PCET of toluene derivatives with $[(N4Py)Fe^{IV}(OH)]^{3+}$, the reactivity of outer-sphere PCET reactions of $[(N4Py)Fe^{IV}(OH)]^{3+}$ was examined using coordinatively saturated metal complexes, $[Fe^{II}(Me_2bpy)_3]^{2+}$ (Me_2bpy = 4,4'-dimethyl-2,2'-bipyridine), $[Ru^{II}(Me_2bpy)_3]^{2+}$, $[Fe^{II}(Clphen)_3]^{2+}$ (Clphen = 5-chloro-1,10-phenanthroline) and $[Ru^{II}(Clphen)_3]^{2+}$, as electron donors.[19] In contrast to the case of PCET reactions of $[(N4Py)Fe^{IV}(OH)]^{3+}$ with

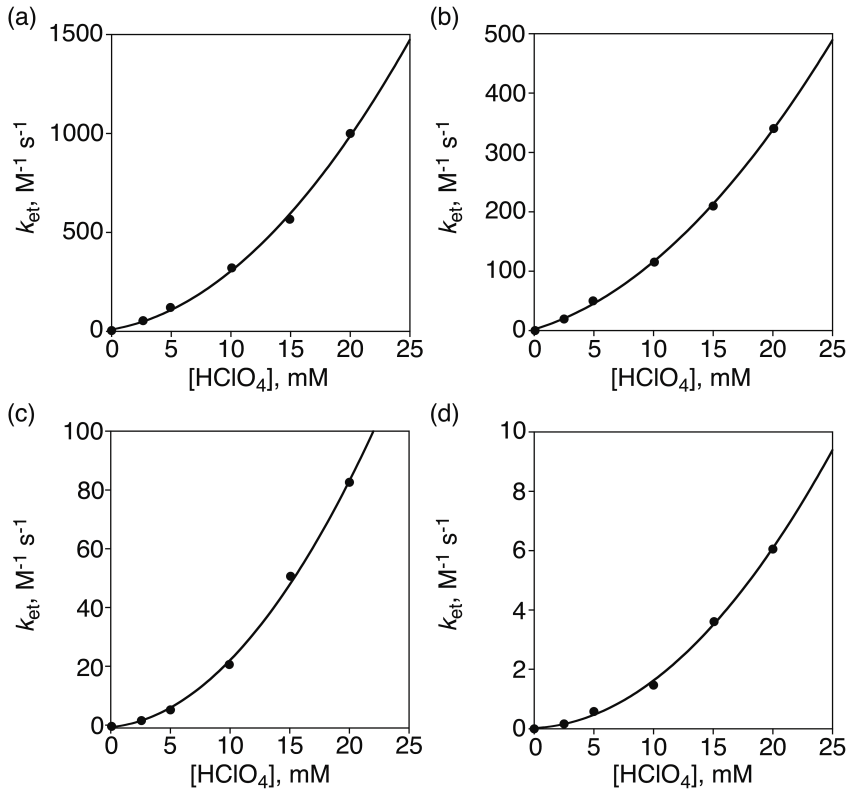

Figure 10. Plots of k_{et} vs concentration of $HClO_4$ in PCET from (a) $[Fe^{II}(Me_2bpy)_3](PF_6)_2$, (b) $[Ru^{II}(Me_2bpy)_3](PF_6)_2$, (c) $[Fe^{II}(Clphen)_3](PF_6)_2$ and (d) $[Ru^{II}(Clphen)_3](PF_6)_2$ to $[(N4Py)Fe^{IV}(O)]^{2+}$ in the presence of $HClO_4$ (70 %) in MeCN at 298 K.

toluene derivatives as shown in Figure 5, where the second-order rate constants (k_{obs}) show linear correlations with [$HClO_4$], the k_{obs} values of PCET reactions of [(N4Py)Fe^{IV}(OH)]$^{3+}$ with coordinatively saturated metal complexes show the first-order dependence on [$HClO_4$] at lower concentrations that changes to the second-order dependence on [$HClO_4$] at higher concentrations (Figure 10). Such mixture of the first- and second-order dependence of k_{obs} on [$HClO_4$] is given by eq 5,

$$k_{obs} = k'_0 + k'_1[HClO_4] + k'_2[HClO_4]^2 \quad (5)$$

$$k_{obs}/[HClO_4] = k'_1 + k'_2[HClO_4] \quad (6)$$

where k'_0, k'_1 and k'_2 are the rate constants for the zero-, first- and second-order dependence on [$HClO_4$], respectively. Because the k'_0 value in the absence of $HClO_4$ is negligible as compared with k'_1 and k'_2, eq 5 is rewritten by eq 6, which predicts a

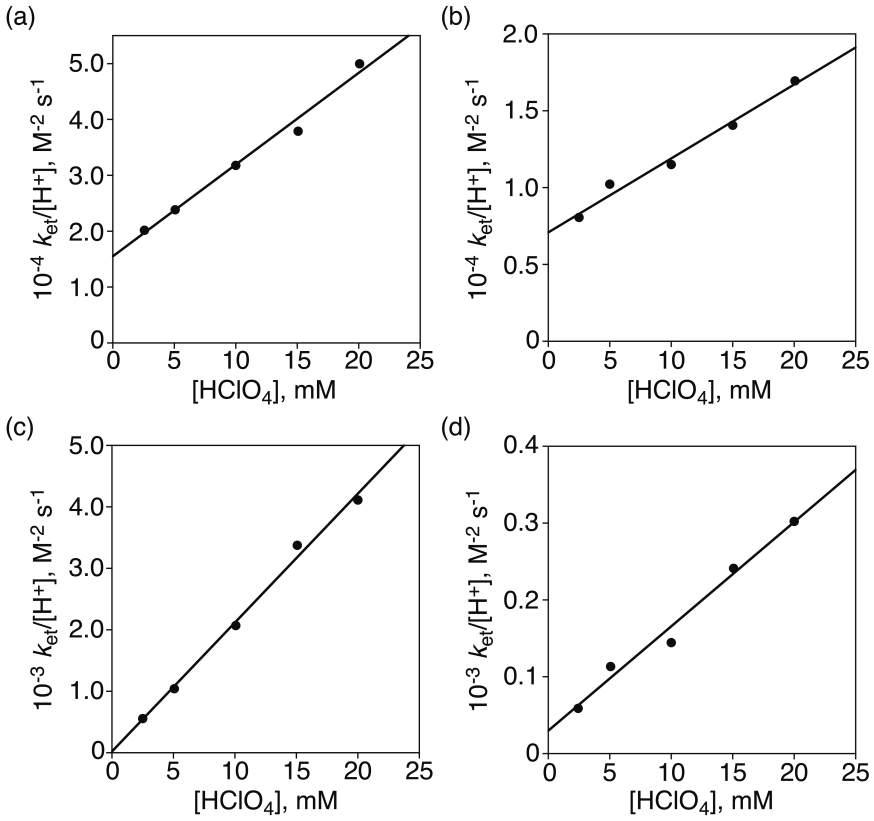

Figure 11. Plots of k_{et}/[$HClO_4$] vs concentration of $HClO_4$ in PCET from (a) [$Fe^{II}(Me_2bpy)_3$]$(PF_6)_2$, (b) [$Ru^{II}(Me_2bpy)_3$]$(PF_6)_2$, (c) [$Fe^{II}(Clphen)_3$]$(PF_6)_2$ and (d) [$Ru^{II}(Clphen)_3$]$(PF_6)_2$ to [(N4Py)Fe^{IV}(O)]$^{2+}$ upon addition of $HClO_4$ (70 %) in MeCN at 298 K.

Scheme 1

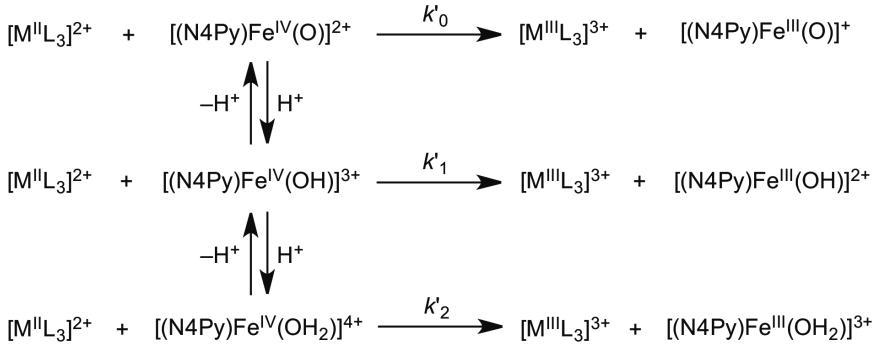

linear correlation between $k_{obs}/[HClO_4]$ vs $[HClO_4]$. Linear plots of $k_{obs}/[HClO_4]$ vs $[HClO_4]$ are shown in supporting information (Figure 11). The first- and second-order dependence of k_{obs} on $[HClO_4]$ suggests that PCET occurs from the metal complexes not only to the monoprotonated iron(IV)-oxo complex ($[(N4Py)Fe^{IV}(OH)]^{3+}$) but also to the diprotonated iron(IV)-oxo complex ($[(N4Py)Fe^{IV}(OH_2)]^{4+}$), both of which exist in equilibrium with $[(N4Py)Fe^{IV}(O)]^{2+}$ as shown in Scheme 1.[18] It should be noted that concentrations of $[(N4Py)Fe^{IV}(OH)]^{3+}$ and $[(N4Py)Fe^{IV}(OH_2)]^{4+}$ were too small to be detected by the change in absorption spectrum of $[(N4Py)Fe^{IV}(O)]^{2+}$ in the presence of large excess $HClO_4$ in MeCN at 298 K. This is the reason for the dependence of k_{obs} on $[HClO_4]$ (eq 2) without exhibiting any saturation behavior.

Comparison of Reactivity of C–H Bond Cleavage via PCET vs Outer-Sphere PCET. We now compare the reactivity of PCET of $[(N4Py)Fe^{IV}(O)]^{2+}$ in C–H bond cleavage vs outer-sphere electron-transfer in light of the Marcus theory of adiabatic electron transfer.[37,38] The driving forces ($-\Delta G_{et}$) of PCET are obtained from the one-electron oxidation potentials (E_{ox}) of electron donors (toluene derivatives and coordinatively saturated metal complexes) and the one-electron reduction potentials (E_{red}) of $[(N4Py)Fe^{IV}(O)]^{2+}$ in the presence of $HClO_4$ as given by eq 7,

$$-\Delta G_{et} = e(E_{red} - E_{ox}) \tag{7}$$

$$E_{red} = E^0_{red} + RT\ln(K_1[HClO_4] + K_1K_2[HClO_4]^2) \tag{8}$$

where e is the elementary charge. The E_{red} values are shifted to a positive direction with increasing concentration of $HClO_4$ according to the Nernst equation (eq 8),[19] where K_1

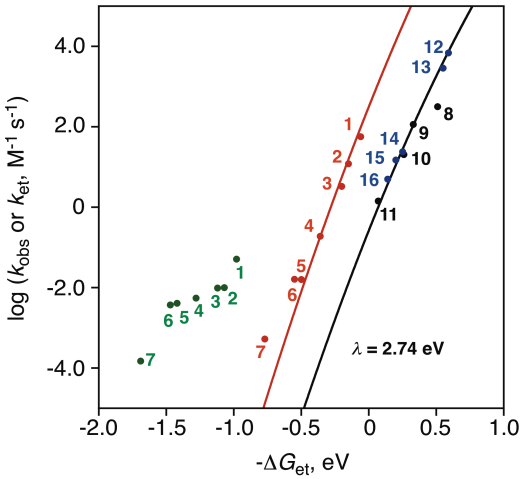

Figure 12. Plots of log k_{obs} for C–H bond cleavage of toluene derivatives ((1) hexamethylbenzene, (2) 1,2,3,4,5-pentamethylbenzene, (3) 1,2,4,5-tetramethylbenzene, (4) 1,2,4-trimethylbenzene, (5) 1,2-dimethylbenzene, (6) 1,3,5-trimethylbenzene, and (7) toluene) by $[(N4Py)Fe^{IV}(O)]^{2+}$ in the presence of $HClO_4$ (70%, 10 mM) MeCN at 298 K vs the driving force of electron transfer [$-\Delta G = e(E_{red} - E_{ox})$] from toluene derivatives to $[(N4Py)Fe^{IV}(O)]^{2+}$ in the absence (green closed circles) and presence of $HClO_4$ (10 mM) (red closed circles). The black closed circles show the driving force dependence of the rate constants (log k_{et}) of PCET from one-electron reductants ((8) $[Fe^{II}(Me_2bpy)_3](PF_6)_2$, (9) $[Ru^{II}(Me_2bpy)_3]$-$(PF_6)_2$, (10) $[Fe^{II}(Clphen)_3](PF_6)_2$ and (11) $[Ru^{II}(Clphen)_3](PF_6)_2$) to $[(N4Py)Fe^{IV}(O)]^{2+}$ in the presence of $HClO_4$ (10 mM) in MeCN at 298 K (see Table S1 in SI).[19] The blue closed circles show the driving force dependence of the rate constants (log k_{et}) of electron transfer from one-electron reductants ((12) decamethylferrocene, (13) octamethylferrocene, (14) 1.1'-dimethylferrocene, (15) *n*-amylferrocene and (16) ferrocene) to $[(N4Py)Fe^{IV}(O)]^{2+}$ in the absence of $HClO_4$ in MeCN at 298 K.[28] The black line is drawn using eq 9 with $\lambda = 2.74$ eV. The red line is drawn in parallel with the black line.

and K_2 are the binding constants of $HClO_4$ to produce the monoprotonated and diprotonated iron(III)-oxo complexes, respectively.[18]

Because the E_{red} values vary depending on [$HClO_4$] (eq 8) and the one-electron reduction potential of $[(N4Py)Fe^{IV}(O)]^{2+}$ was determined in the presence of 10 mM $HClO_4$ in MeCN at 298 K previously,[19] we have chosen the conditions of 10 mM of $HClO_4$ (70%) to compare the driving force dependence of logarithm of the rate constants (k_{et}) of PCET reactions of $[(N4Py)Fe^{IV}(O)]^{2+}$ with coordinatively saturated metal complexes and those (k_{obs}) with toluene derivatives. At this concentration, electron transfer from electron donors to the monoprotonated iron(IV)-oxo complex is the major pathway as compared with the electron transfer to the diprotonated

ion(IV)-oxo complex. Figure 12 shows the driving force ($-\Delta G_{et}$) dependence of log k_{et} of PCET of outer-sphere reductants (coordinatively saturated metal complexes) and log k_{obs} of PCET and toluene derivatives to $[(N4Py)Fe^{IV}(OH)]^{3+}$.

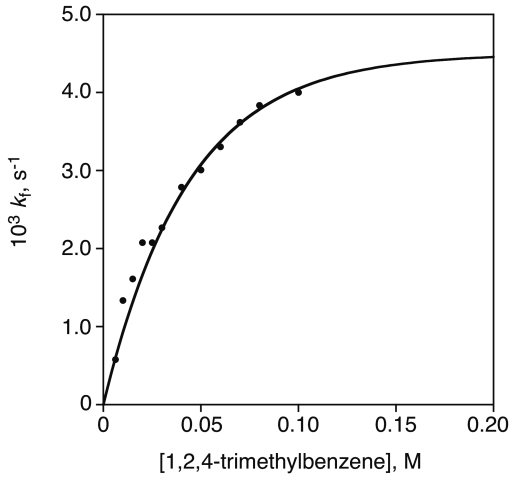

Figure 13. Plot of concentration of 1,2,4-trimethylbenzene vs first-order rate constant (k_f) in the reaction of $[(N4Py)Fe^{IV}(O)]^{2+}$ (0.25 mM) with 1,2,4-trimethylbenzene in the presence of 10 mM of $HClO_4$ in MeCN at 298 K.

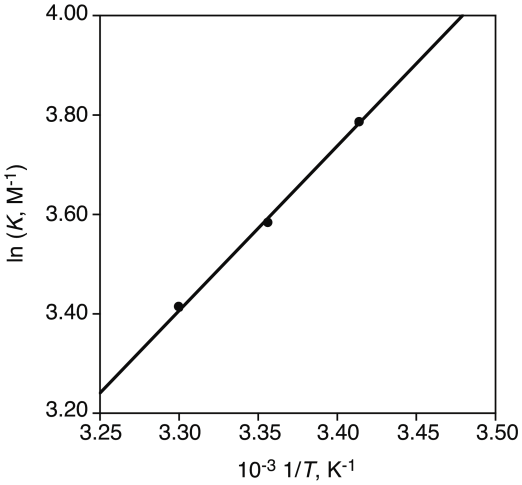

Figure 14. Plot of ln K vs $1/T$ in temperature in the reaction of $[(N4Py)Fe^{IV}(O)]^{2+}$ (0.25 mM) with 1,2,4,-trimethylbenzene in the presence of 10 mM of $HClO_4$ in MeCN. The ΔH and ΔS values can be determined by van't Hoff equation, $\ln K = -\Delta H/RT + \Delta S/R$.

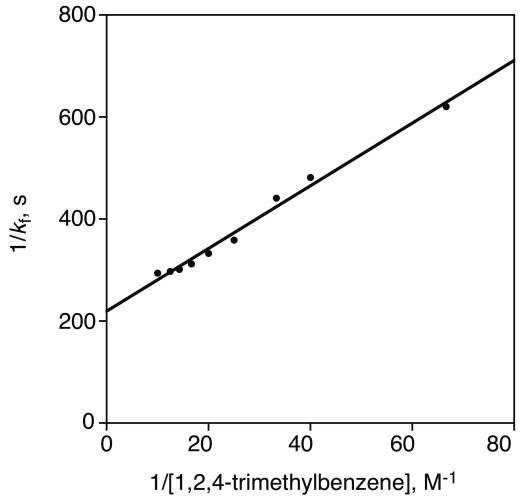

Figure 15. Plot of $1/k_f$ vs 1/[1,2,4-trimethylbenzene] where the slope $[(k_{ET}K)^{-1}]$ and intercept (k_{ET}^{-1}) were determined to be 6.2 M s and 220 s, respectively.

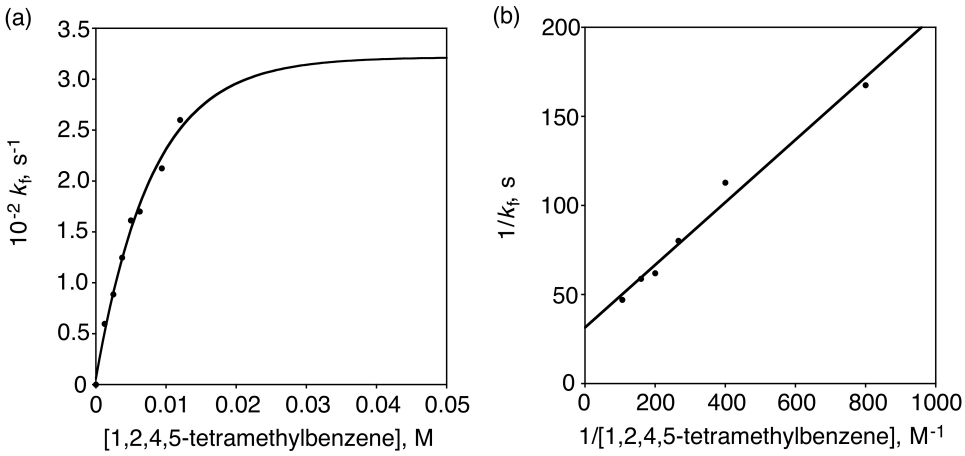

Figure 16. (a) Plot of first-order rate constant (k_f) vs concentration of 1,2,4,5-tetramethylbenzene in oxidation of 1,2,4,5-tetramethylbenzene with $[(N4Py)Fe^{IV}(O)]^{2+}$ (0.25 mM) in the presence of $HClO_4$ (10 mM) in MeCN at 298 K. (b) Plot of $1/k_f$ vs 1/[1,2,4,5-tetramethylbenzene] where the values of slope and intercept were determined to be 0.21 M s and 31 s, respectively.

In the case of outer-sphere PCET from the coordinatively saturated metal complexes to $[(N4Py)Fe^{IV}(OH)]^{3+}$ in the presence of $HClO_4$ (10 mM) in MeCN at 298 K, the driving force dependence of log k_{et} is well fitted by the Marcus equation of outer-sphere electron transfer (eq 9),[34] where Z is frequency factor,

$$k_{et} = Z\exp[-(\lambda/4)(1 + \Delta G_{et}/\lambda)^2/k_B T] \quad (9)$$

which corresponds to (k_BTK/h; k_B is the Borzmann constant, T is absolute temperature, K is the formation constant of the precursor complex and h is the Planck constant) and λ is the reorganization energy of electron transfer. The Z value of outer-sphere electron-transfer reactions of coordinatively saturated metal complexes is normally taken as 1.0×10^{11} M^{-1} s^{-1}.[39-42] This result indicates that the K value of outer-sphere electron-transfer reactions is as small as 0.020 M^{-1}, because there is little interaction in the precursor complex for outer-sphere electron transfer.

The fitting of the data of outer-sphere PCET from the metal complexes to $[(N4Py)Fe^{IV}(OH)]^{3+}$ affords the λ value of 2.74 eV (black circles in Figure 12). When the k_{et} values of the outer-sphere electron–transfer reactions (coordinatively saturated metal complexes) are compared with those of toluene derivatives in the absence of $HClO_4$, the latter values (green circles in Figure 12) are much larger than those expected from the outer-sphere electron–transfer because the hydrogen atom transfer pathway involves much larger interactions between toluene derivatives and $[(N4Py)Fe^{IV}(O)]^{2+}$.

In the presence of $HClO_4$ (10 mM), however, the log k_{obs} values of oxidation of toluene derivatives with $[(N4Py)Fe^{IV}(O)]^{2+}$ (red circles in Figure 12) exhibit a parallel relationship with the driving force dependence of log k_{et} on $-\Delta G_{et}$ (black circles in Figure 12) although the k_{obs} values are always three-orders of magnitude larger than the k_{et} values. The exception is the point No. 7 (toluene), which is deviated from the red line. The reason will be discussed later. The parallel driving force dependence of log k_{obs} with log k_{et} in Figure 12 suggests that oxidation of toluene derivatives with $[(N4Py)Fe^{IV}(O)]^{2+}$ in the presence of $HClO_4$ proceeds via PCET from toluene derivatives to $[(N4Py)Fe^{IV}(OH)]^{3+}$. In such a case, the difference in the k_{obs} and k_{et} values at the same driving force may result from the difference in the K values of precursor complexes (vide infra).

In order to determine the equilibrium constants of precursor complexes prior to PCET from toluene derivatives to $[(N4Py)Fe^{IV}(OH)]^{3+}$, the dependence of pseudo-first-order constants (k_f) on concentrations of toluene derivatives was examined using larger concentrations. An example of dependence of k_1 on concentration of a toluene derivative is shown in Figure 13, where the k_f value increases with increasing concentration of 1,2,4-trimethylbenzene to approach a constant value. Such a saturation behavior of k_f on concentration of a toluene derivative is given by eq 10, where k_{ET} is the rate constant in the precursor complex, K is the formation constant of the precursor complex, and [S] is concentration of a substrate.[43] Equation 10 is rewritten by eq 11,

which predicts a linear correlation between k_f^{-1} vs $[S]^{-1}$. Other toluene derivatives show a similar behavior.

$$k_f = \quad k_{ET}K[S]/(1 + K[S]) \tag{10}$$

$$k_f^{-1} = (k_{ET}K[S])^{-1} + k_{ET}^{-1} \tag{11}$$

The k_{ET} and K values were determined from linear plot of k_f^{-1} vs $[S]^{-1}$ (Figures 15 and 16). The slope and intercept to be $(4.5 \pm 0.2) \times 10^{-3}$ s^{-1} and $(3.6 \pm 0.2) \times 10$ M^{-1}, respectively. The k_{ET} and K values were also determined at various temperatures. The heat of formation and entropy of the precursor complex (ΔH and ΔS) were determined to be ΔH = -2.4 kcal mol^{-1} and ΔS = -17 cal K^{-1} mol^{-1} from the van't Hoff plot as shown in Figure 14 and 17. The K, ΔH and ΔS values of other toluene derivatives were also determined and their values are listed in Table 2. The large K and $-\Delta H$ values in Table 2 indicate that PCET proceeds via precursor complexes in which interactions between toluene derivatives and $[(N4Py)Fe^{IV}(OH)]^{3+}$ are much stronger than the case of coordinatively saturated metal complexes.

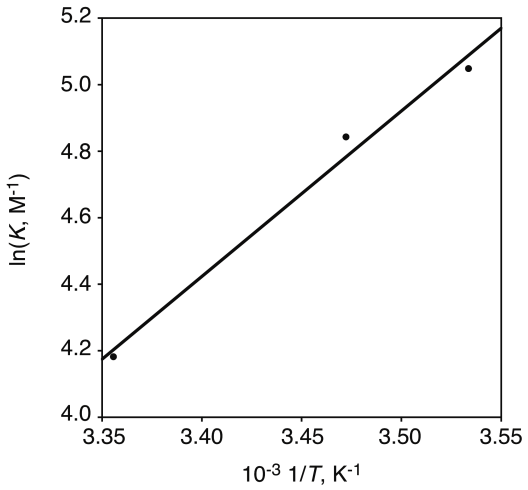

Figure 17. Plot of ln K vs $1/T$ for oxidation of 1,2,4,5-tetramethylbenzene with $[(N4Py)Fe^{IV}(O)]^{2+}$ (0.25 mM) in the presence of $HClO_4$ (10 mM) in MeCN. The ΔH and , ΔS values were determined by van't Hoff equation, $\ln K = -\Delta H/RT + \Delta S/R$.

As shown in Table 2, the K values of precursor complexes in PCET from toluene derivatives to $[(N4Py)Fe^{IV}(OH)]^{3+}$ are generally three-order of magnitude larger than

the value (0.020 M^{-1}) usually used for outer-sphere electron-transfer reactions. Formation of such strong precursor complexes has also been reported for toluene derivatives with photoexcited quinones in photoinduced electron-transfer reactions.[44] The charge-transfer interactions may be responsible for the binding between toluene derivatives and photoexcited quinones. There are also many examples for formation of intermediate charge-transfer complexes in organic and inorganic redox reactions.[45-53]

Table 2. Formation Constants and Activation Parameters in Temperature in Oxidation Reaction of Toluene Derivatives, 1,2,4-Trimethylbenzene and 1,2,4,5-Tetramethylbenzene, by $[(N4Py)Fe^{IV}(O)]^{2+}$ in the Presence of $HClO_4$ (10 mM) in MeCN

toluene derivative	formation constant (K, M^{-1})		
	303 K	298 K	293 K
1,2,4-trimethylbenzene	(4.4 ± 0.2) × 10	(3.6 ± 0.2) × 10	(3.0 ± 0.2) × 10
1,2,4,5-tetramethylbenzene	(6.5 ± 0.3) × 10	(1.3 ± 0.2) × 10^2	(1.6 ± 0.2) × 10^2
toluene derivative	ΔH (kcal mol^{-1}) [a]	ΔS (cal K^{-1} mol^{-1}) [a]	ΔG (eV) [a]
1,2,4-trimethylbenzene	-1.6 (± 0.1)	-15 (± 1)	0.19 (± 0.01)
1,2,4,5-tetramethylbenzene	-2.4 (± 0.2)	-17 (± 1)	0.22 (± 0.01)

[a] All of the values calculated by van't Hoff equation, $\ln K = -\Delta H/RT + \Delta S/R$.

Now that K values are determined, comparison of the log k_{ET} values (first-order rate constants in the precursor complexes) are made between electron transfer reactions from coordinatively saturated metal complexes and toluene derivatives to $[(N4Py)Fe^{IV}(OH)]^{3+}$ by using average K values of toluene derivatives (83 M^{-1}) and the value (0.020 M^{-1}) of outer-sphere electron-transfer reactions. The two separate correlations in Figure 12 are now unified as a single correlation between log k_{ET} vs $-\Delta G_{et}$ in Figure 18. Such a unified correlation together with the absence of KIE in Figure 8b strongly indicates that C–H bond cleavage of toluene derivatives by $[(N4Py)Fe^{IV}(O)]^{2+}$ with $HClO_4$ proceeds via PCET from toluene derivatives to $[(N4Py)Fe^{IV}(OH)]^{3+}$ through strong precursor complexes formed between toluene derivatives and $[(N4Py)Fe^{IV}(OH)]^{3+}$ as shown in Scheme 2.[53] The formation of strong precursor complexes prior to electron transfer in Scheme 2 suggests occurrence of an inner-sphere electron transfer pathway rather than an outer-sphere pathway.[54,55] However, the single and unified correlation between log k_{ET} an ΔG_{et} in Figure 18, which

is well fitted by the Marcus equation (eq 9), indicates that electron transfer from toluene derivatives to $[(N4Py)Fe^{IV}(OH)]^{3+}$ in the precursor in an outer-sphere pathway as the case of outer-sphere reductants (coordinatively saturated metal complexes).[52]

The absence of the second-order dependence of k_{obs} on $[HClO_4]$ in PCET from toluene derivatives may result from the much smaller interaction between toluene derivatives and the diprotonated iron(IV)-oxo complex ($[(N4Py)Fe^{IV}(OH_2)]^{4+}$) due to the steric effect of second proton bound to the Fe(IV)-oxo complex.[56] A slight deviation from the unified line is observed for No. 7 (toluene) in Figure 18 as well as in Figure 12, because toluene may be on the borderline between the hydrogen atom transfer and PCET.

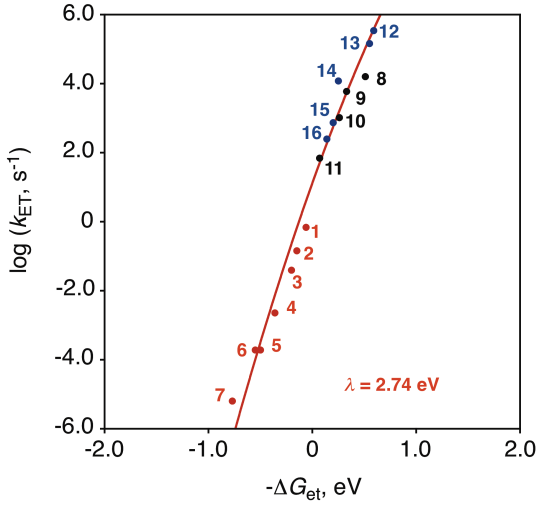

Figure 18. Plots of log k_{ET} for C–H cleavage of toluene derivatives by $[(N4Py)Fe^{IV}(O)]^{2+}$ in the presence of $HClO_4$ (70%, 10 mM) MeCN at 298 K vs the driving force of electron transfer $[-\Delta G = e(E_{red} - E_{ox})]$ from toluene derivatives to $[(N4Py)Fe^{IV}(O)]^{2+}$ in the presence of $HClO_4$ (10 mM) (red closed circles). The black closed circles show the driving force dependence of the rate constants (log k_{ET}) of PCET from one-electron reductants to $[(N4Py)Fe^{IV}(O)]^{2+}$ in the presence of $HClO_4$ (10 mM) in MeCN at 298 K ($k_{ET} = k_{et}/K$, $K = 0.020$). The red line is drawn based on eq 9 with $\lambda = 2.74$ eV.[19] The blue closed circles show the driving force dependence of the rate constants (log k_{ET}) of electron transfer from one-electron reductants to $[(N4Py)Fe^{IV}(O)]^{2+}$ in the absence of $HClO_4$ in MeCN at 298 K.[28] The numberings of substrates denote those used in Figure 12.

Scheme 2

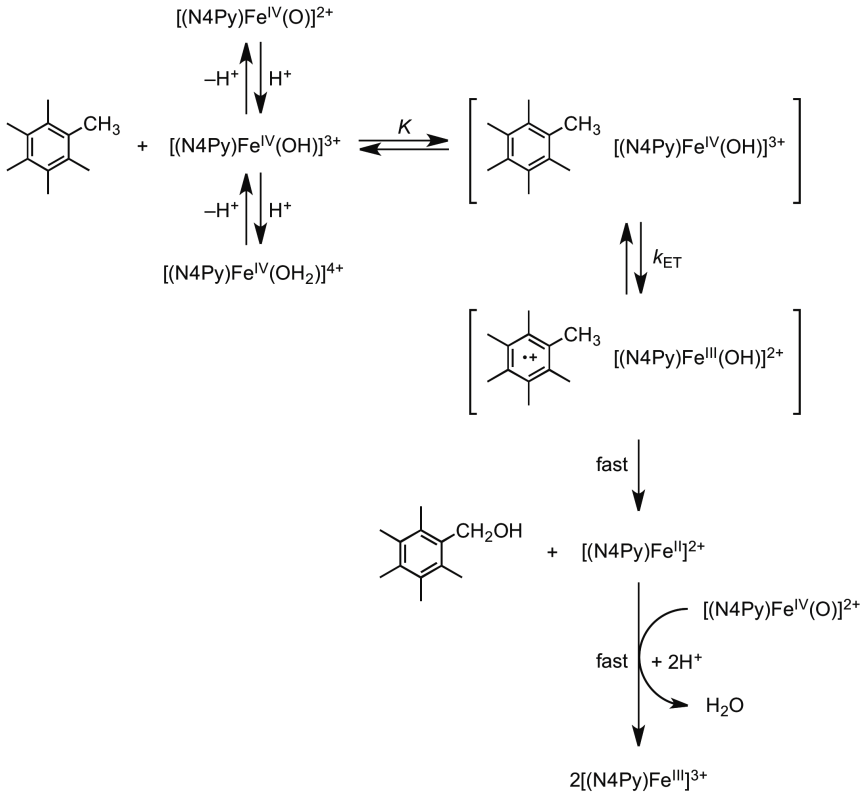

Conclusion

C–H bond cleavage of toluene derivatives by a nonheme iron(IV)-oxo complex, $[(N4Py)Fe^{IV}(O)]^{2+}$, is remarkably enhanced by Brønsted acid ($HClO_4$) to yield benzyl alcohol derivatives and $[(N4Py)Fe^{III}(OH_2)]^{3+}$ in MeCN at 298 K. Even toluene, which has high oxidation potential (2.20 V vs SCE), can be oxidized efficiently by $[(N4Py)Fe^{IV}(O)]^{2+}$ in the presence of $HClO_4$. Such a remarkable acceleration of C–H bond cleavage of toluene derivatives with $[(N4Py)Fe^{IV}(O)]^{2+}$ in the presence of $HClO_4$ results from the change in the reaction mechanism from direct hydrogen atom transfer from toluene derivatives to $[(N4Py)Fe^{IV}(O)]^{2+}$ in the absence of $HClO_4$ to PCET from toluene derivatives to $[(N4Py)Fe^{IV}(OH)]^{3+}$ in the presence of $HClO_4$ via strong precursor complexes formed between toluene derivatives and $[(N4Py)Fe^{IV}(OH)]^{3+}$ as indicated by the unified correlation of log k_{ET} vs the PCET deriving force ($-\Delta G_{et}$) in light of the Marcus theory of outer-sphere electron transfer and the absence of KIE. In the case of toluene, which is the least reactive, the hydrogen atom transfer pathway competes with the PCET pathway to exhibit a small KIE (2.0), and the k_{obs} value is a bit larger than that expected from the outer-sphere electron transfer (no. 7 in Figure 12).

References

(1) (a) Ortiz de Montellano, P. R. *Cytochrome P450: Structure, Mechanism, and Biochemistry*, 3rd ed.; Kluwer Academic/Plenum Publishers: New York, 2005. (b) Meunier, B., Ed. *Biomimetic Oxidations Catalyzed by Transition Metal Complexes*; Imperial College Press: London, 2000. (c) *The Ubiquitous Role of Cytochrome P450 Proteins In Metal Ions in Life Sciences*; Sigel, A., Sigel, H., Sigel, R. K. O., Eds.; John Wiley & Sons Ltd: Chichester, England, 2007; Vol. 3.

(2) (a) Sono, M.; Roach, M. P.; Coulter, E. D.; Dawson, J. H. *Chem. Rev*. **1996**, *96*, 2841. (b) Watanabe, Y. *J. Biol. Inorg. Chem*. **2001**, *6*, 846. (c) Jung, C. *Biochim. Biophys. Acta* **2011**, *1814*, 46.

(3) Rohde, J.-U.; In, J.-H.; Lim, M. H.; Brennessel, W. W.; Bukowski, M. R.; Stubna, A.; Münck, E.; Nam, W.; Que, L., Jr. *Science* **2003**, *299*, 1037.

(4) (a) de Visser, S. P.; Rohde, J.-U.; Lee, Y.-M.; Cho, J.; Nam, W. *Coord. Chem. Rev.* **2012**, *257*, 381. (b) McDonald, A. R.; Que, L., Jr. *Coord. Chem. Rev.* **2013**, *257*, 414.

(5) (a) Meunier, B.; de Visser, S. P.; Shaik, S. *Chem. Rev.* **2004**, *104*, 3947. (b) Shaik, S.; Cohen, S.; Wang, Y.; Chen, H.; Kumar, D.; Thiel, W. *Chem. Rev*. **2010**, *110*, 949. (c) Abu-Omar, M. M.; Loaiza, A.; Hontzeas, N. *Chem. Rev.* **2005**, *105*, 2227. (d) Denisov, I. G.; Makris, T. M.; Sligar, S. G.; Schlichting, I. *Chem. Rev.* **2005**, *105*, 2253. (e) Ortiz de Montellano, P. R. *Chem. Rev*. **2010**, *110*, 932.

(6) (a) Groves, J. T.; Shalyaev, K.; Lee, J. In *The Porphyrin Handbook*; Kadish, K. M., Smith, K. M., Guilard, R., Eds.; Academic Press: Elsevier Science (USA), 2000, Vol. 4, pp 17-40. (b) Watanabe, Y. In *The Porphyrin Handbook*; Kadish, K. M., Smith, K. M., Guilard, R., Eds.; Academic Press: Elsevier Science (USA), 2000, Vol. 4, pp 97-117. (c) Groves, J. T. *J. Inorg. Biochem*. **2006**, *100*, 434.

(7) (a) Gunay, A.; Theopold, K. H. *Chem. Rev*. **2010**, *110*, 1060. (b) Che, C.-M.; Lo, V. K.-Y.; Zhou, C.-Y.; Huang, J.-S. *Chem. Soc. Rev*. **2011**, *40*, 1950. (c) Costas, M. *Coord. Chem. Rev*. **2011**, *255*, 2912.

(8) (a) Cho, K.; Leeladee, P.; McGown, A. J.; DeBeer, S.; Goldberg, D. P. *J. Am. Chem. Soc*. **2012**, *134*, 7392. (b) Cho, K.-B.; Chen, H.; Janardanan, D.; de Visser, S. P.; Shaik, S.; Nam, W. *Chem. Commun*. **2012**, *48*, 2189. (c) Seo, M. S.; Kim, N. H.; Cho, K.-B.; So, J. E.; Park, S. K.; Clemancey, M.; Garcia-Serres, R.; Latour, J.-M.; Shaik, S.; Nam, W. *Chem. Sci*. **2011**, *2*, 1039. (d) Borovik, A. S. *Chem. Soc.*

Rev. **2011**, *40*, 1870. (e) Janardanan, D.; Wang, Y.; Schyman, P.; Que, L., Jr.; Shaik, S. *Angew. Chem., Int. Ed.* **2010**, *49*, 3342.

(9) (a) Krebs, C.; Fujimori, D. G.; Walsh, C. T.; Bollinger, J. M., Jr. *Acc. Chem. Res.* **2007**, *40*, 484. (b) Que, L., Jr. *Acc. Chem. Res*. **2007**, *40*, 493. (c) Nam, W. *Acc. Chem. Res.* **2007**, *40*, 522. (d) Borovik, A. S. *Acc. Chem. Res.* **2005**, *38*, 54. (e) Shaik, S.; Lai, W.; Chen, H.; Wang, Y. *Acc. Chem. Res*. **2010**, *43*, 1154.

(10) Hong, S.; Lee, Y.-M.; Cho, K.-B.; Sundaravel, K.; Cho, J.; Kim, M. J.; Shin, W.; Nam, W. *J. Am. Chem. Soc*. **2011**, *133*, 11876.

(11) Tang, H.; Guan, J.; Zhang, L.; Liu, H.; Huang, X. *Phys. Chem. Chem. Phys.* **2012**, *14*, 12863.

(12) Kumar, D.; Sastry, G. N.; de Visser, S. P. *J. Phys. Chem. B*, **2012**, *116*, 718.

(13) (a) Groves, J. T.; McClusky, G. A. *J. Am. Chem. Soc.* **1976**, *98*, 859. (b) Ortiz de Montellano, P. R.; Stearns, R. A. *J. Am. Chem. Soc.* **1987**, *109*, 3415. (c) Schöoneboom, J. C.; Cohen, S.; Lin, H.; Shaik, S.; Thiel, W. *J. Am. Chem. Soc.* **2004**, *126*, 4017. (d) Hirao, H.; Kumar, D.; Que, L., Jr.; Shaik, S. *J. Am. Chem. Soc*. **2006**, *128*, 8590.

(14) Chiavarino, B.; Cipollini, R.; Crestoni, M. E.; Fornarini, S.; Fornarini, S.; Lapi, A. *J. Am. Chem. Soc.* **2008**, *130*, 3208.

(15) Kaizer, J.; Klinker, E. J.; Oh, N. Y.; Rohde, J.-U.; Song, W. J.; Stubna, A.; Kim, J.; Münck, E.; Nam, W.; Que, L., Jr. *J. Am. Chem. Soc.* **2004**, *126*, 472.

(16) (a) Park, M. J.; Lee, J.; Suh, Y.; Kim, J.; Nam, W. *J. Am. Chem. Soc.* **2006**, *128*, 2630. (b) Sastri, C. V.; Lee, J.; Oh, K.; Lee, Y. J.; Lee, J.; Jackson, T. A.; Ray, K.; Hirao, H.; Shin, W.; Halfen, J. A.; Kim, J.; Que, L., Jr.; Shaik, S.; Nam, W. *Proc. Natl. Acad. Sci. U. S. A.* **2007**, *104*, 19181. (c) Jeong, Y. J.; Kang, Y.; Han, A.-R.; Lee, Y.-M.; Kotani, H.; Fukuzumi, S.; Nam, W. *Angew. Chem., Int. Ed.* **2008**, *47*, 7321. (d) Lee, Y.-M.; Dhuri, S. N.; Sawant, S. C.; Cho, J.; Kubo, M.; Ogura, T.; Fukuzumi, S.; Nam, W. *Angew. Chem., Int. Ed.* **2009**, *48*, 1803.

(17) (a) Lee, Y.-M.; Hong, S.; Morimoto, Y.; Shin, W.; Fukuzumi, S.; Nam, W. *J. Am. Chem. Soc*. **2010**, *132*, 10668. (b) Wilson, S. A.; Chen, J.; Hong, S.; Lee, Y.-M.; Clémancey, M.; Garcia-Serres, R.; Nomura, T.; Ogura, T.; Latour, J.-M.; Hedman, B.; Hodfson, K. O.; Nam, W.; Solomon, E. I. *J. Am. Chem. Soc*. **2012**, *134*, 11791.

(18) Fukuzumi, S. *Coord. Chem. Rev.* **2013**, *257*,1564.

(19) Park, J.; Morimoto, Y.; Lee, Y.-M.; Nam, W.; Fukuzumi, S. *J. Am. Chem. Soc.* **2012**, *134*, 3903.

(20) Morimoto, Y.; Park, J.; Suenobu, T.; Lee, Y.-M.; Nam, W.; Fukuzumi, S. *Inorg. Chem.* **2012**, *51*, 10025.

(21) (a) Fukuzumi, S.; Morimoto, Y.; Kotani, H.; Naumov, P.; Lee, Y.-M.; Nam, W. *Nature Chem.* **2010**, *2*, 756. (b) Morimoto, Y.; Kotani, H.; Park, J.; Lee, Y.-M.; Nam, W.; Fukuzumi, S. *J. Am. Chem. Soc*. **2011**, *133*, 403. (c) Park, J.; Morimoto, Y.; Lee, Y.-M.; Nam, W.; Fukuzumi, S. *J. Am. Chem. Soc.* **2011**, *133*, 5236. (d) Park, J.; Morimoto, Y.; Lee, Y.-M.; You, Y.; Nam, W.; Fukuzumi, S. *Inorg. Chem.* **2011**, *50*, 11612.

(22) Armarego, W. L. F.; Chai, C. L. L. *Purification of Laboratory Chemicals*, 6th ed.; Pergamon Press: Oxford, 2009.

(23) Lubben, M.; Meetsma, A.; Wilkinson, E. C.; Feringa, B.; Que, L., Jr. *Angew. Chem., Int. Ed*. **1995**, *34*, 1512.

(24) *Organic Syntheses*; Saltzman, H.; Sharefkin, J. G., Eds.; Wiley: New York, 1973; Vol. V, p 658

(25) Bond dissociation energy of acetonitrile is reported to be 96 ± 1 kcal mol^{-1},[26] which is significantly higher than those of toluene derivatives (e.g., 88.5 kcal mol^{-1}).[27] In addition, the oxidation potential of acetonitrile is much higher than those of toluene derivatives. Indeed $[(N4Py)Fe^{IV}(O)]^{2+}$ is stable in the absence and presence of $HClO_4$ in acetonitrile.

(26) Menon, A. S.; Henry, D. J.; Bally, T.; Radom, L. *Org. Biomol. Chem*. 2011, 9, 3636.

(27) Kojima, T.; Nakayama, K.; Ikemura, K.; Ogura, T.; Fukuzumi, S. *J. Am. Chem. Soc*. **2011**, *133*, 11692.

(28) Lee, Y.-M.; Kotani, H.; Suenobu, T.; Nam, W.; Fukuzumi, S. *J. Am. Chem. Soc.* **2008**, *130*, 434.

(29) (a) Roelfes, G.; Vrajmasu, V.; Chen, K.; Ho, R. Y. N.; Rohde, J.-U.; Zondervan, C.; la Crois, R. M.; Schudde, E. P.; Lutz, M.; Spek, A. L.; Hage, R.; Feringa, B. L.; Münck, E.; Que, L., Jr. *Inorg. Chem.* **2003**, *42*, 2639. (b) Hong, S.; Lee, Y.-M.; Shin, W.; Fukuzumi, S.; Nam, W. *J. Am. Chem. Soc*. **2009**, *131*, 13910.

(30) Fukuzumi, S.; Ishikawa, K.; Hironaka, K.; Tanaka, T. *J. Chem. Soc., Perkin Trans*. *2* **1987**, 751.

(31) (a) Fukuzumi, S.; Kuroda, S. *Res. Chem. Int*. **1999**, *25*, 789. (b) Fukuzumi, S.; Chiba, M.; Ishikawa, M.; Ishikawa, K.; Tanaka, T. J. *Chem. Soc., Perkin Trans. 2* **1989**, 1417. (c) Fukuzumi, S.; Ishikawa, M.; Tanaka, T. *Tetrahedron* **1986**, *42*, 1021. (d) Fukuzumi, S.; Chiba, M.; Tanaka, T. *Chem. Lett*. **1989**, 31.

(32) Kwart, H. *Acc. Chem. Res.* **1982**, *15*, 401.

(33) (a) Price, J. C.; Barr, E. W.; Glass, T. E.; Krebs, C.; Bollinger, J. M., Jr. *J. Am. Chem. Soc*. **2003**, *125*, 13008. (b) Wu, A.; Mayer, J. M. *J. Am. Chem. Soc.* **2008**, *130*, 14745.

(34) (a) Kohen, A.; Klinman, J. P. *Acc. Chem. Res*. **1998**, *31*, 397. (b) Knapp, M. J.; Rickert, K.; Klinman, J. P. *J. Am. Chem. Soc*. **2002**, *124*, 3865. (c) Klinman, J. P. *Biochim. Biophys. Acta, Bioenergetics* **2006**, *1757*, 981. (d) McCusker, K. P.; Kilnman, J. P. *J. Am. Chem. Soc*. **2010**, *132*, 5114.

(35) Fukuzumi, S.; Kobayashi, T.; Suenobu, T. *J. Am. Chem. Soc*. **2010**, *132*, 1496.

(36) Fukuzumi, S.; Ohkubo, K.; Suenobu, T.; Kato, K.; Fujitsuka, M.; Ito, O. *J. Am. Chem. Soc*. **2001**, *123*, 8459.

(37) (a) Marcus, R. A. *Annu. Rev. Phys. Chem*. **1964**, *15*, 155. (b) Marcus, R. A. *Discuss. Faraday Soc*. **1960**, *29*, 129. (c) Marcus, R. A. *Angew. Chem., Int. Ed. Engl*. **1993**, *32*, 1111.

(38) (a) Cannon, R. D. Electron-Transfer Reactions; Butterworth: London, 1980. (b) Eberson, L. *Adv. Phys. Org. Chem*. **1982**, *18*, 79. (c) Silverstein, T. P. *J. Chem. Edu*. **2012**, *89*, 1159.

(39) (a) Sutin, N. *Acc. Chem. Res*. **1968**, *1*, 225. (b) Sutin, N. *Adv. Chem. Phys*. **1999**, *106*. 7. (c) Chou, M.; Creutz, C.; Sutin, N. *J. Am. Chem. Soc*. **1977**, *99*, 5615. (d) Keeney, L.; Hynes, M. J. *Dalton Trans*. **2005**, 133.

(40) (a) Fukuzumi, S.; Honda, T.; Kojima, T. *Coord. Chem. Rev*. **2012**, *256*, 2488. (b) Fukuzumi, S.; Karlin, K. D. *Coord. Chem. Rev*. **2012**, *257*, 187. (c) Tahsini, L.; Kotani, H.; Lee, Y.-M.; Cho, J.; Nam, W.; Karlin, K. D.; Fukuzumi, S. *Chem.–Eur. J.* **2012**, *18*, 1084. (d) Yoon, H.; Morimoto, Y.; Lee, Y.-M.; Nam, W.; Fukuzumi, S. *Chem. Commun*. **2012**, *48*, 11187.

(41) (a) Takai, A.; Gros, C. P.; Barbe, J.-M.; Guilard, R.; Fukuzumi, S. *Chem.–Eur. J.* **2009**, *15*, 3110. (b) Nakanishi, T.; Ohkubo, K.; Kojima, T.; Fukuzumi, S. *J. Am. Chem. Soc.* **2009**, *131*, 577. (c) Murakami, M.; Ohkubo, K.; Fukuzumi, S. *Chem.–Eur. J*. **2010**, *16*, 7820.

(42) (a) Fukuzumi, S.; Nakanishi, I.; Tanaka, K.; Suenobu, T.; Tabard, A.; Guilard, R.; Van Caemelbecke, E.; Kadish, K. M. *J. Am. Chem. Soc.* **1999**, *121*, 785. (b) Fukuzumi, S.; Mochizuki, S.; Tanaka, T. *Inorg. Chem*. **1989**, *28*, 2459.

(43) The saturation behavior could be interpreted as an acid-substrate complexation. However, it was confirmed that no protonation of TMB occurred in the presence of $HClO_4$ up to 20 mM (see Figure 1). Thus, the observed saturation behavior results from a strong precursor complex rather than the protonation of the substrate.

(44) Hubig, S. M.; Kochi, J. K. *J. Am. Chem. Soc*. **1999**, *121*, 1688.

(45) (a) Fukuzumi, S.; Mochida, K.; Kochi, J. K. *J. Am. Chem. Soc*. **1979**, *101*, 5961. (b) Fukuzumi, S.; Kochi J. K. *J. Am. Chem. Soc*. **1980**, *102*, 2141. (c) Fukuzumi, S.; Kochi J. K. *J. Am. Chem. Soc*. **1981**, *103*, 2783. (d) Fukuzumi, S.; Kochi J. K. *J. Am. Chem. Soc.* **1981**, *103*, 7240. (e) Fukuzumi, S.; Kochi J. K. *J. Am. Chem. Soc*. **1982**, *104*, 7599.

(46) (a) Park, J. S.; Karnas, E.; Ohkubo, K.; Chen, P.; Kadish, K. M.; Fukuzumi, S.; Bielawski, C. W.; Hudnall, T. W.; Lynch, V. M.; Sessler, J. L. *Science* **2010**, *329*, 1324. (b) Fukuzumi, S.; Ohkubo, K.; Kawashima, Y.; Kim, D. S.; Park, J.-S.; Jana, A.; Lynch, V. M.; Kim, D.-H.; Sessler, J. L. *J. Am. Chem. Soc*. **2011**, *133*, 15938.

(47) (a) Fukuzumi, S.; Kochi, J. K. *Tetrahedron* **1982**, *38*, 1035. (b) Kim, J. H.; Lindeman, S. V.; Kochi, J. K. *J. Am. Chem. Soc*. **2001**, *123*, 4951. (c) Fukuzumi, S.; Koumitsu, S.; Hironaka, K.; Tanaka, T. *J. Am. Chem. Soc*. **1987**, *109*, 305. (d) Fukuzumi, S. Nishizawa, N.; Tanaka, T. *J. Org. Chem*. **1984**, *49*, 3571.

(48) (a) Zaman, K. M.; Yamamoto, S.; Nishimura, N.; Maruta, J.; Fukuzumi, S. *J. Am. Chem. Soc*. **1994**, *116*, 12099. (b) Zhu, X.-Q.; Zhang, J.-Y.; Cheng, J.-P. *J. Org. Chem*. **2006**, *71*, 7007. (c) Fukuzumi, S.; Endo, Y.; Imahori, H. *J. Am. Chem. Soc.* **2002**, *124*, 10974. (d) Zhu, X.-Q.; Li, X.-T.; Han, S.-H.; Mei, L.-R. *J. Org. Chem*. **2012**, *77*, 4774.

(49) (a) Fukuzumi, S.; Ohkubo, K.; Tokuda, Y.; Suenobu, T. *J. Am. Chem. Soc*. **2000**, *122*, 4286. (b) Lu, Y.; Zhao, Y.; Handoo, K. L.; Parker, V. D. *Org. Biomol. Chem*. **2003**, *1*, 173. (c) Ohkubo, K.; Fukuzumi, S. *J. Phys. Chem. A* **2005**, *109*, 1105. (d) Le Magueres, P.; Lindeman, S. V.; Kochi, J. K. *Organometallics* **2001**, *20*, 115.

(50) Kochi, J. K. *Acc. Chem. Res*. **1992**, *25*, 39.

(51) Goodwin, J. A.; Wilson, L. J.; Stanbury, D. M.; Scott, R. A. *Inorg. Chem.* **1988**, *28*, 42.

(52) (a) Rosokha, S. V.; Kochi, J. K *Acc. Chem. Res*. **2008**, *41*, 641. (b) Hubig, S. M.; Kochi, J. K. *J. Am. Chem. Soc*. **1999**, *121*, 1688. (c) Gaede, W.; van Eldik, R. *Inorg. Chem.* **1994**, *33*, 2204.

(53) The saturation behavior of k_f vs concentration of a substrate may result from the competition between deprotonation of $[(N4Py)Fe^{IV}(OH)]^{3+}$ and the reaction with the substrate. In such a case, the rate-determining step at the saturated would be the protonation of $[(N4Py)Fe^{IV}(O)]^{2+}$, when the rate constant would be independent of the PCET driving force. The results in Figure 18, which exhibit a single correlation between log k_{ET} vs $-\Delta G_{et}$, clearly indicate that the saturation behavior in Figure 13 does not result from the change in the rate-determining step to the protonation of $[(N4Py)Fe^{IV}(O)]^{2+}$.

(54) For the classical definition of inner-sphere electron transfer, see: (a) Taube, H.; Myers, H. J.; Rich, R. L. *J. Am. Chem. Soc*. **1953**, *75*, 4118. (b) Taube, H. *Science* **1984**, *226*, 1028.

(55) For more generalized distinction between inner-sphere and outer-sphere electron–transfer pathways, see: (a) Rosokha, S. V.; Kochi, J. K. *Acc. Chem. Res*. **2008**, *41*, 641. (b) Fukuzumi, S.; Wong, C. L.; Kochi, J. K. *J. Am. Chem. Soc*. **1980**, *102*, 2928. (c) Fukuzumi, S.; Kochi, J. K. *Bull. Chem. Soc. Jpn*. **1983**, *56*, 969.

(56) The assumption that all reactivity at 10 mM $HClO_4$ is dominated by the monoprotonated species ($[(N4Py)Fe^{IV}(OH)]^{3+}$) is valid for oxidation of toluene derivatives with $[(N4Py)Fe^{IV}(O)]^{2+}$ as indicated by linear correlations between the k_{obs} values and $HClO_4$ concentration in Figure 5. In the case of PCET from inorganic one-electron reductants to $[(N4Py)Fe^{IV}(O)]^{2+}$, however, the diprotonated species ($[(N4Py)Fe^{IV}(OH_2)]^{4+}$) may also be involved as indicated by the contribution of the second-order dependence of k_{obs} on $[HClO_4]$ in Figure 10. At 10 mM $HClO_4$, there is some contribution of $[(N4Py)Fe^{IV}(OH_2)]^{4+}$ in PCET from inorganic one-electron reductants to $[(N4Py)Fe^{IV}(O)]^{2+}$. This may be the reason why the k_{ET} values of PCET oxidation of toluene derivatives (red points) are somewhat smaller than the Marcus line in Figure 18. Nevertheless, the assumption that all reactivity at 10 mM $HClO_4$ is dominated by the monoprotonated species ($[(N4Py)Fe^{IV}(OH)]^{3+}$) is good enough to obtain the largely unified correlation in Figure 18.

Supporting Information

for Chapter 4

Table S1. One-Electron Oxidation Potentials (E_{ox}) of One-Electron Reductants and Second-Order Rate Constants in the Electron-Transfer Reactions from One-Electron Reductants to $[(N4Py)Fe^{IV}(O)]^{2+}$ in the Absence and Presence of $HClO_4$ in MeCN at 298 K

one-electron reductant	E_{ox} (V vs SCE)	K_{obs} or k_{et}, M^{-1} s^{-1}		10 mM $HClO_4$ log (k_{et}, M^{-1} s^{-1})
		without $HClO_4$	10 mM $HClO_4$	
$[Fe^{II}(Me_2bpy)_3]^{2+}$	0.92	NR[a]	$(3.2 \pm 0.2) \times 10^2$	2.5
$[Ru^{II}(Me_2bpy)_3]^{2+}$	1.10	NR[a]	$(1.2 \pm 0.1) \times 10^2$	2.1
$[Fe^{II}(Clphen)_3]^{2+}$	1.17	NR[a]	$(2.1 \pm 0.1) \times 10$	1.3
$[Ru^{II}(Clphen)_3]^{2+}$	1.36	NR[a]	1.4 ± 0.1	1.6×10^{-1}

[a]NR: No reaction.

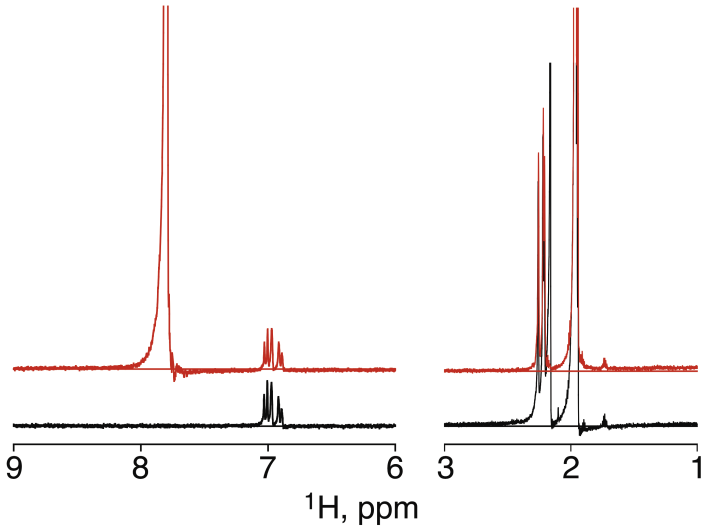

Figure S1. ^1H NMR spectra of 1,2,4-trimethylbenzene (20 mM) in the absence (black line) and presence (red line) of 40 mM of $HClO_4$ in CD_3CN at 298 K. The peaks at 2.21 (black line) and 7.8 (red line) ppm are signals of the solvent and water, respectively. The peaks at 2.22 and 2.26 ppm are the signals of methyl groups of 1,2,4-trimethylbenzene. The aromatic protons remain the same in both cases in the absence and presence of $HClO_4$. This indicates that no protonation of 1,2,4-trimethylbenzene occurs in the presence of $HClO_4$.

Chapter 5. Unified View of Oxidative C–H Bond Cleavage and Sulfoxidation by a Nonheme Iron(IV)-Oxo Complex via Lewis Acid–Promoted Electron Trnasfer

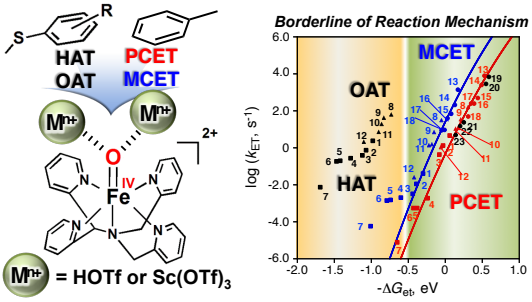

Abstract: Oxidative C−H bond cleavage of toluene derivatives and sulfoxidation of thioanisole derivatives by a nonheme iron(IV)-oxo complex, $[(N4Py)Fe^{IV}(O)]^{2+}$ (N4Py = *N*,*N*-bis(2- pyridylmethyl)-*N*-bis(2-pyridyl)methylamine), were remarkably enhanced by the presence of triflic acid (HOTf) and $Sc(OTf)_3$ in acetonitrile at 298 K. All the logarithms of the observed second-order rate constants of both the oxidative C–H bond cleavage and sulfoxidation reactions exhibit remarkably unified correlations with the driving forces of proton–coupled electron transfer (PCET) and metal ion–coupled electron transfer (MCET) in light of the Marcus theory of electron transfer when the differences in the formation constants of precursor complexes between PCET and MCET were taken into account, respectively. Thus, the mechanisms of both the oxidative C–H bond cleavage of toluene derivatives and sulfoxidation of thioanisole derivatives by $[(N4Py)Fe^{IV}(O)]^{2+}$ in the presence of HOTf and $Sc(OTf)_3$ have been unified as the rate-determining electron transfer, which is coupled with binding of $[(N4Py)Fe^{IV}(O)]^{2+}$ by proton (PCET) and $Sc(OTf)_3$ (MCET). There was no deuterium kinetic isotope effect (KIE) on the oxidative C–H bond cleavage of toluene via the PCET pathway, whereas a large KIE value was observed with $Sc(OTf)_3$, which exhibited no acceleration of the oxidative C–H bond cleavage of toluene. When HOTf was replaced by DOTf, an inverse KIE (0.36) was observed for PCET from both toluene and $[Ru^{II}(bpy)_3]^{2+}$ (bpy = 2,2'-bipyridine) to $[(N4Py)Fe^{IV}(O)]^{2+}$. The PCET and MCET reactivities of $[(N4Py)Fe^{IV}(O)]^{2+}$ with Brønsted acids and various metal triflates have also been unified as a single correlation with a quantitative measure of the Lewis acidity.

Introduction

High-valent heme and nonheme iron-oxo complexes have been investigated as key intermediate in various biological and chemical oxidation reactions.[1,2] Since the first crystal structure of mononuclear nonheme iron(IV)-oxo was reported in 2003, the reactivity of synthetic nonheme iron(IV)-oxo complexes with various substrates have been extensively studied.[3-17] Reactivities of nonheme iron(IV)-oxo complexes in various oxidation reactions, such as oxidative C–H bond cleavage and oxygen atom transfer, are significantly affected not only by axial ligand and solvents,[3-21] but also by binding of metal ions (Lewis acids) and Brønsted acids to the oxo moiety of nonheme iron(IV)-oxo complexes.[22-26] The binding of $Sc(OTf)_3$ to a nonheme iron(V)-complex was confirmed by the X-ray crystal structure of $Sc(OTf)_3$-bound $[(TMC)Fe^{IV}(O)]^{2+}$ (TMC = 1,4,8,11-tetramethyl-1,4,8,11-tetraazacyclotetra-decane).[23,24] The electron transfer (ET) reactivity of a nonheme iron(IV)-oxo complex ($[(N4Py)Fe^{IV}(O)]^{2+}$) with electron donors was enhanced by binding of protons and metal ions, and the enhanced reactivity was well analyzed in light of the Marcus theory of electron transfer.[26] The enhanced reactivity of $[(N4Py)Fe^{IV}(O)]^{2+}$ in the oxidative C–H bond cleavage of toluene derivatives and sulfoxidation of thioanisole derivatives by acids is suggested to result from the change in the reaction mechanism from the direct hydrogen atom transfer and oxygen atom transfer to electron transfer pathways coupled with binding of acids to $[(N4Py)Fe^{IV}(O)]^{2+}$, respectively. If this is true, all the rate constants of oxidative C–H bond cleavage and sulfoxidation reactions as well as electron-transfer reactions in the absence and presence of acids would be correlated by a unified fashion to the corresponding driving force of electron transfer in light of the Marcus theory of electron transfer. However, such unified understanding of the reactivity of nonheme iron(IV)-oxo complexes in various oxidation reactions has yet to be made. In addition, unified understanding of effects of various acids (Brønsted and Lewis acids) on the reactivity of nonheme iron(IV)-oxo complexes has not been made, neither.

We report herein a unified view on the remarkable enhancement of reactivity of $[(N4Py)Fe^{IV}(O)]^{2+}$ by triflic acid (HOTf) as well as $Sc(OTf)_3$ in oxidative C–H bond cleavage and oxygen atom transfer reactions as well as electron transfer from various one-electron donors to $[(N4Py)Fe^{IV}(O)]^{2+}$ in light of the Marcus theory of electron transfer. All the rate constants of oxidative C–H bond cleavage of toluene derivatives, sulfoxidation of thioanisole derivatives and electron transfer from various one-electron

donors to $[(N4Py)Fe^{IV}(O)]^{2+}$in the presence of HOTf and $Sc(OTf)_3$ are well correlated by a unified fashion with the driving forces of proton–coupled electron transfer (PCET) and metal ion ($Sc(OTf)_3$)–coupled electron transfer (MCET), respectively. The enhanced reactivities of $[(N4Py)Fe^{IV}(O)]^{2+}$ with HOTf and $M^{n+}(OTf)_n$ are also well correlated with a quantitative measure of the Lewis acidity of acids, which we reported previously.[23b]

Experimental Section

Materials. All chemicals, which were the best available purity, were purchased from Aldrich Chemical Co. and Tokyo Chemical Industry, used without further purification unless otherwise noted. Solvents, such as acetonitrile (MeCN) and diethyl ether, were dried according to the literature procedures and distilled under Ar prior to use.[27] A nonheme iron(II) complex, $[(N4Py)Fe^{II}(MeCN)](ClO_4)_2$, and its corresponding iron(IV)-oxo complex, $[(N4Py)Fe^{IV}(O)]^{2+}$, were prepared by literature methods.[19,28] Iodosylbenzene (PhIO) was prepared by a literature method.[29] Triflic acid was purchased from Tokyo Chemical Industry. $[Fe^{II}(Ph_2phen)_3](PF_6)_2$ (Ph_2phen = 4,7-diphenyl-1,10-phenanthroline), $[Fe^{II}(Clphen)_3](PF_6)_2$ (Clphen = 5-chloro-1,10-phenanthroline), $[Ru^{II}(4,4'\text{-}Me_2bpy)_3](PF_6)_2$ (4,4'-Me_2bpy = 4,4'-dimehtyl-2,2'bipyridine), $[Ru^{II}(5,5'\text{-}Me_2bpy)_3](PF_6)_2$ (5,5'-Me_2bpy = 5,5'-dimehtyl-2,2'bipyridine), $[Ru^{II}(bpy)_3](PF_6)_2$ (bpy = 2,2'-bipyridine) and $[Ru^{II}(NO_2phen)_3](PF_6)_2$ (NO_2phen = 5-nitro-1,10-phenanthroline) were prepared according to published procedures.[30] $[Fe^{II}(bpy)_3](PF_6)_2$ was obtained by the addition of an aqueous solution containing excess amount of $NaPF_6$ to an aqueous solution containing stoichiometric amount of the bpy ligand $FeSO_4$ to yield crystalline solids.

Kinetic Studies. Kinetic measurements were performed on a Hewlett Packard 8453 photodiode-array spectrophotometer using a quartz cuvette (path length = 10 mm) at 298 K. The C–H bond cleavage of toluene derivatives and sulfoxidation of thioansiole derivatives by $[(N4Py)Fe^{IV}(O)]^{2+}$ were monitored by spectral changes due to $[(N4Py)Fe^{IV}(O)]^{2+}$ (2.5×10^{-4} M) with various concentrations of toluene and thioanisole derivatives (2.5×10^{-3}–1.0×10^{-1} M) in the absence and presence of acids, HOTf and $Sc(OTf)_3$, in MeCN at 298 K. The rates of oxidation reaction of organic substrates by $[(N4Py)Fe^{IV}(O)]^{2+}$ were monitored by the decay of the absorption band at 695 nm due

to $[(N4Py)Fe^{IV}(O)]^{2+}$ (λ_{max} = 695 nm) in the absence and presence of HOTf and $Sc(OTf)_3$ in MeCN. The concentrations of toluene derivatives and thioanisole derivatives were maintained at least more than 10-fold excess of $[(N4Py)Fe^{IV}(O)]^{2+}$ to attain pseudo-first-order conditions.

ET from electron donors to $[(N4Py)Fe^{IV}(O)]^{2+}$ in the presence of Lewis acids, HOTf and $Sc(OTf)_3$, was monitored by a Hewlett Packard 8453 photodiode-array spectrophotometer and a UNISOKU RSP-601 stopped-flow spectrometer equipped with a MOS-type highly sensitive photodiode-array in MeCN at 298 K. These ET rates were determined from the decay of $[(N4Py)Fe^{IV}(O)]^{2+}$ (λ_{max} = 695 nm), respectively. All kinetic measurements were carried out under pseudo-first-order conditions where the concentrations of electron donors were maintained to be more than 10-folds excess of that of $[(N4Py)Fe^{IV}(O)]^{2+}$.

First-order fitting of the kinetic data allowed us to determine the pseudo-first-order rate constants. The first-order plots were linear for three or more half-lives with the correlation coefficient $\rho > 0.999$. In each case, it was confirmed that the rate constants derived from at least five independent measurements agreed within an experimental error of ±5%. The pseudo-first-order rate constants increased proportionally with increase in concentrations of substrates, from which second-order rate constants were determined.

Spectral Redox Titration. ET from an electron donor ($[Ru^{II}(NO_2phen)_3](PF_6)_2$ (2.5×10^{-4} – 1.0×10^{-3} M)) to $[(N4Py)Fe^{IV}(O)]^{2+}$ (2.5×10^{-4} M) was examined by the spectral change in the presence of HOTf (1.0×10^{-2} M) in MeCN at 298 K using a Hewlett Packard 8453 photodiode-array spectrophotometer with a quartz cuvette (path length = 10 mm).

Product Analysis. Typically, hexamethylbenzene and thioanisole (2.0×10^{-2} M) was added to an MeCN solution containing $[(N4Py)Fe^{IV}(O)]^{2+}$ (4.0×10^{-3} M) in the presence of HOTf and $Sc(OTf)_3$ (1.0×10^{-2} M) in a vial. Products formed in the oxidation reactions of toluene derivatives by $[(N4Py)Fe^{IV}(O)]^{2+}$, which were carried out in the presence of acids under Ar atmosphere in MeCN-d_3 at 298 K, were analyzed by ^{1}H NMR. Quantitative analyses were made on the basis of comparison of ^{1}H NMR spectral integration between products and their authentic samples.

Instrumentation. UV-vis spectra were recorded on a Hewlett Packard 8453 photodiode-array spectrophotometer. The EPR spectra were measured with a JEOL X-band spectrometer (JES-RE1XE). The EPR spectra were recorded under non-saturating microwave power conditions. The magnitude of modulation was chosen to optimize the resolution and the signal-to-noise (S/N) ratio of the observed spectra. The *g* value was calibrated by using a Mn^{2+} marker. ^1H NMR spectra were recorded on a JEOL A-300 spectrometer in CD_3CN.

Results and Discussion

HOTf- and $Sc(OTf)_3$–Promoted C–H Bond Cleavage of Toluene Derivatives by $[(N4Py)Fe^{IV}(O)]^{2+}$. Toluene is known to be hardly oxidized by nonheme iron(IV)-oxo complexes.[19] However, oxidation of toluene by a nonheme iron(IV)-oxo complex ($[(N4Py)Fe^{IV}(O)]^{2+}$) in acetonitrile (MeCN) is significantly enhanced by the presence of HOTf (50 mM) as shown in Figure 1, to yield benzyl alcohol and $[(N4Py)Fe^{III}]^{3+}$ (eq 1);

$$PhCH_3 + 2[(N4Py)Fe^{IV}(O)]^{2+} + 2H^+ \longrightarrow PhCH_2\text{–}OH + 2[(N4Py)Fe^{III}]^{3+} + H_2O \quad (1)$$

see Figures 2-4. The $[(N4Py)Fe^{IV}(O)]^{2+}$ complex acted as a one-electron oxidant, when the yield of benzyl alcohol was 50% based on $[(N4Py)Fe^{IV}(O)]^{2+}$. Hexamethylbenzene was also readily oxidized by $[(N4Py)Fe^{IV}(O)]^{2+}$ in the presence of HOTf to produce pentamethylbenzyl alcohol.

The rate of oxidation of toluene $[(N4Py)Fe^{IV}(O)]^{2+}$ in the absence and presence of HOTf in MeCN, monitored by decrease in absorbance at 695 nm due to $[(N4Py)Fe^{IV}(O)]^{2+}$ (Figure 1) obeyed first-order kinetics (Figure 5) with large excess toluene and HOTf. The pseudo-first-order rate constant (k_f) increased linearly with increasing concentration of toluene (Figure 6). Similarly the k_f values were also proportional to concentrations of toluene derivatives (Figures 6b-6f). The observed second-order rate constants (k_{obs}) of oxidation of toluene derivatives by $[(N4Py)Fe^{IV}(O)]^{2+}$ were determined from the slopes of plots of k_f vs concentrations of toluene derivatives in the absence and presence of HOTf (10 mM) in MeCN at 298 K as listed in Table 1.

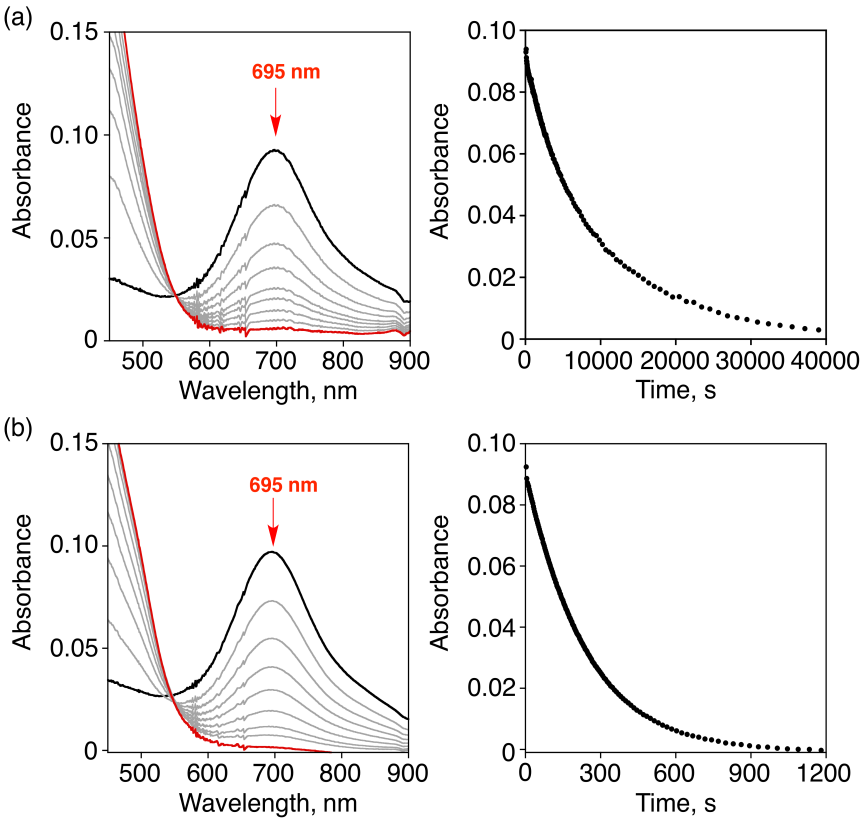

Figure 1. Visible spectral changes observed in the reactions of $[(N4Py)Fe^{IV}(O)]^{2+}$ (0.25 mM) with toluene (400 mM) in the (a) absence and (b) presence of 50 mM of HOTf in MeCN at 298 K (left panel). Right panels show time courses monitored at 695 nm due to the decay of $[(N4Py)Fe^{IV}(O)]^{2+}$.

The k_{obs} values increased with increasing concentration of HOTf [HOTf] (Figure 7), exhibiting first-order and second-order dependence on [HOTf] at lower and higher concentrations of HOTf, respectively, as given by eq 2, where k_0, k_1 and k_2 correspond to rate constants of oxidation of toluene derivatives by $[(N4Py)Fe^{IV}(O)]^{2+}$, the monoprotonated species ($[(N4Py)Fe^{IV}(OH)]^{3+}$) and the diprotonated species ($[(N4Py)Fe^{IV}(OH_2)]^{3+}$), which exhibit zero-, first- and second-order dependence on [HOTf], respectively.[26] Eq 2 is rewritten by eq 3, which exhibits a linear correlation of $(k_{obs} - k_0)/[HOTf]$ vs [HOTf] as shown in Figure 8.

$$k_{obs} = k_0 + [HOTf](k_1 + k_2[HOTf]) \quad (2)$$

$$(k_{obs} - k_0)/[HOTf] = k_1 + k_2[HOTf] \quad (3)$$

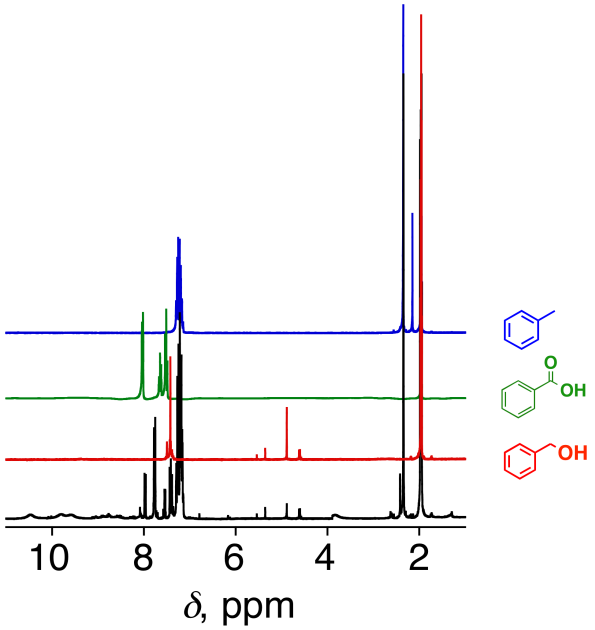

Figure 2. ^{1}H NMR spectrum of the complete reaction solution obtained in oxidation of toluene (20 mM) with $[(N4Py)Fe^{IV}(O)]^{2+}$ (4.0 mM) in the presence of DOTf (50 mM) in CD_3CN at 298 K (black line) under Ar. Red and blue lines show ^{1}H NMR spectra of toluene (4.0 mM) and benzyl alcohol (4.0 mM) in the presence of DOTf (50 mM) as authentic references. The peak at 4.9 ppm agrees with that corresponds to -CH_2- group of benzyl alcohol in the presence of DOTf (50 mM), together with other peaks in the aromatic region around 7.4 ppm, indicating that benzyl alcohol was formed as a sole product and yield of benzyl alcohol produced was 46 ± 4 % based on $[(N4Py)Fe^{IV}(O)]^{2+}$ concentration.

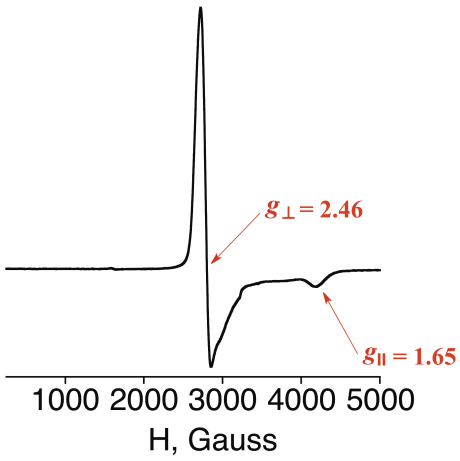

Figure 3. EPR spectrum of the complete reaction solution obtained in oxidation of toluene (100 mM) with $[(N4Py)Fe^{IV}(O)]^{2+}$ (1.0 mM) in the presence of HOTf (50 mM) in MeCN at 77 K under Ar. The *g* values of EPR active species indicate that the low-spin Fe(III) species due to $[(N4Py)Fe^{III}]^{3+}$ was formed.

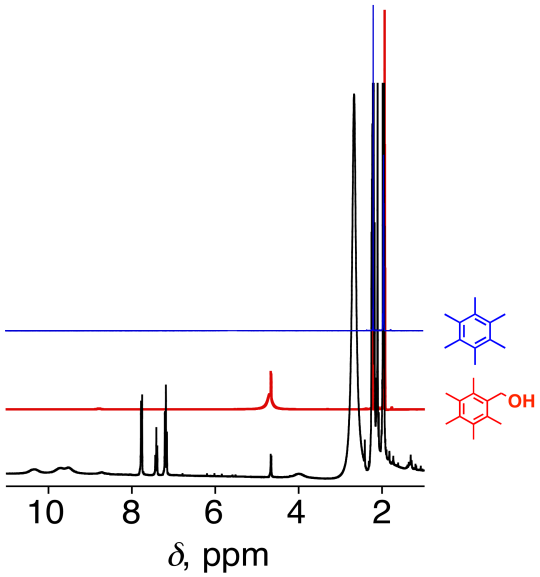

Figure 4. ^{1}H NMR spectrum of the complete reaction solution obtained in oxidation of hexamethylbenzene (20 mM) with $[(N4Py)Fe^{IV}(O)]^{2+}$ (4.0 mM) in the presence of DOTf (10 mM) in CD_3CN at 298 K (black line). Red and blue lines show ^{1}H NMR spectra of hexamethylbenzene (4.0 mM) and 1,2,3,4,5-pentamethylbenzyl alcohol (4.0 mM) in the presence of DOTf (10 mM) in CD_3CN at 298 K as authentic references. The peak at 4.7 ppm agrees with that corresponds to -CH_2- group of the authentic sample of 1,2,3,4,5-pentamethylbenzyl alcohol (48 ± 4 % based on $[(N4Py)Fe^{IV}(O)]^{2+}$ concentration) in the presence of DOTf (10 mM). The peaks in the region of 7 ~ 8 ppm correspond to the signals of iodobenzene (PhI) because iodosylbenzene (PhIO) was used as an oxidant to generate $[(N4Py)Fe^{IV}(O)]^{2+}$ species.

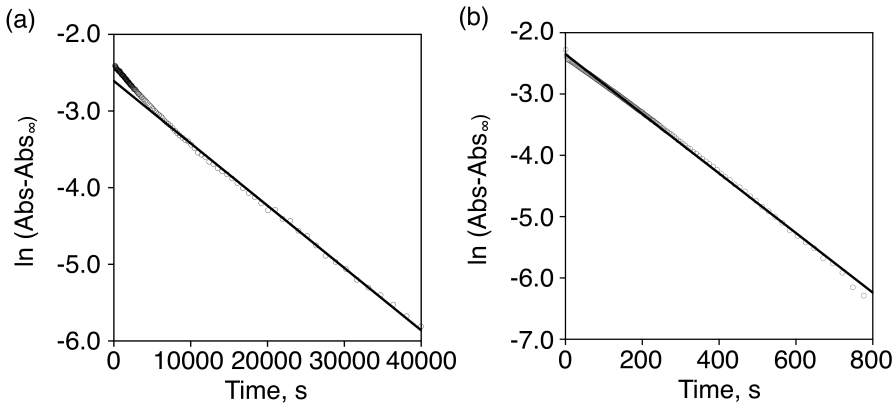

Figure 5. First-order plots of the absorption changes at 695 nm for oxidation of toluene (400 mM) by $[(N4Py)Fe^{IV}(O)]^{2+}$ (0.25 mM) in the (a) absence and (b) presence of HOTf (50 mM) in MeCN at 298 K. Abs and Abs_∞ represent absorbance at the reaction time and the final absorbance at 695 nm, respectively.

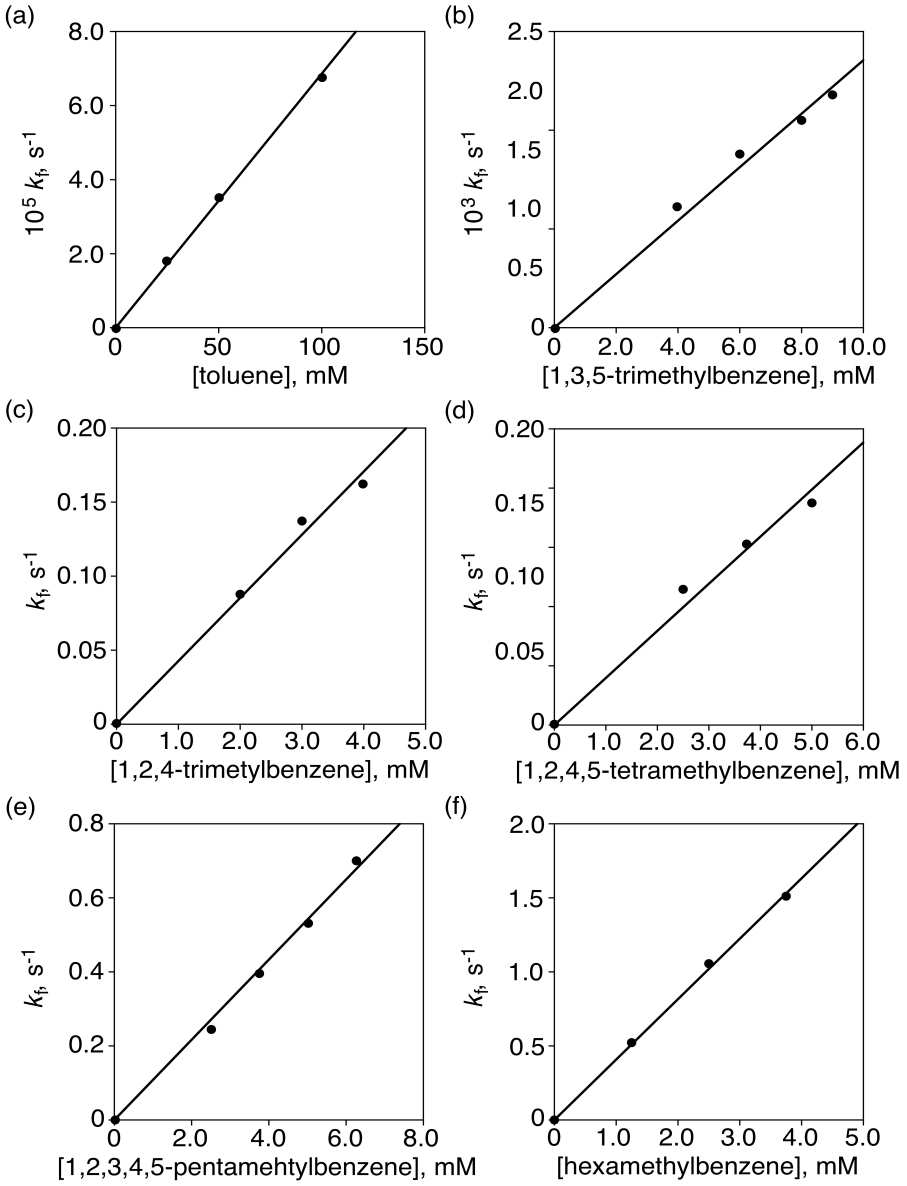

Figure 6. Plots of pseudo-first-order rate constants (k_f) vs concentrations of toluene derivatives [(a) toluene, (b) 1,3,5-trimethylbenzene, (c) 1,2,4-trimethylbenzene, (d) 1,2,4,5-tetramethylbenzene, (e) 1,2,3,4,5-pentamethyl benzene and (f) hexamethylbenzene] to determine the second-order rate constants (k_{obs}) of oxidation of toluene derivatives by $[(N4Py)Fe^{IV}(O)]^{2+}$ (0.25 mM) in the presence of HOTf (10 mM) in MeCN at 298 K.

Table 1. One-Electron Oxidation Potentials (E_{ox}) of Toluene and Thioanisole Derivatives and Second-Order Rate Constants of the C–H Bond Cleavage and Sulfoxidation by $[(N4Py)Fe^{IV}(O)]^{2+}$ in the Presence of HOTf and $Sc(OTf)_3$ (10 mM) in MeCN at 298 K

No.	thioaniosle and toluene derivative	E_{ox} (vs SCE, V)[a,b]	k_{obs}, M^{-1} s^{-1}		
			without acid[a,b]	with $Sc(OTf)_3$ (10 mM)	with HOTf (10 mM)
1	hexamethylbenzene	1.49	$(4.8 \pm 0.2) \times 10^{-2}$	$(1.1 \pm 0.1) \times 10^{-1}$	$(4.2 \pm 0.2) \times 10^{2}$
2	1,2,3,4,5-pentamehtylbenzene	1.58	$(1.5 \pm 0.1) \times 10^{-2}$	$(2.9 \pm 0.1) \times 10^{-2}$	$(1.2\pm 0.1) \times 10^{2}$
3	1,2,4,5-tetramethylbenzene	1.63	$(7.8 \pm 0.4) \times 10^{-3}$	$(1.1 \pm 0.1) \times 10^{-2}$	$(3.9 \pm 0.2) \times 10$
4	1,2,4-trimethylbenzene	1.79	$(5.5 \pm 0.2) \times 10^{-3}$	$(8.2 \pm 0.4) \times 10^{-3}$	$(1.7 \pm 0.1) \times 10^{-1}$
5	1,4-dimethylbenzene	1.93	$(4.0 \pm 0.1) \times 10^{-3}$	$(6.0 \pm 0.3) \times 10^{-3}$	$(5.0 \pm 0.2) \times 10^{-2}$
6	1,3,5-trimethylbenzene	1.98	$(3.7 \pm 0.1) \times 10^{-3}$	$(5.6 \pm 0.3) \times 10^{-3}$	$(5.0 \pm 0.2) \times 10^{-2}$
7	toluene	2.20	$(1.5 \pm 0.1) \times 10^{-4}$	$(2.4 \pm 0.2) \times 10^{-4}$	$(7.0 \pm 0.2) \times 10^{-4}$
8	*p*-Me-thioanisole	1.24	1.3 ± 0.1	$(8.4 \pm 0.4) \times 10$ [a]	$(1.5 \pm 0.1) \times 10^{4}$
9	thioanisole	1.34	$(8.7 \pm 0.4) \times 10^{-1}$	$(1.9 \pm 0.1) \times 10$ [a]	$(3.2 \pm 0.2) \times 10^{3}$
10	*p*-Cl-thioanisole	1.37	$(4.0 \pm 0.2) \times 10^{-1}$	4.2 ± 0.2 [a]	$(1.1 \pm 0.1) \times 10^{3}$
11	*p*-Br-thioanisole	1.41	$(1.5 \pm 0.1) \times 10^{-1}$	3.7 ± 0.2 [a]	$(1.0 \pm 0.1) \times 10^{3}$
12	*p*-CN-thioanisole	1.61	$(4.4 \pm 0.2) \times 10^{-2}$	$(6.8 \pm 0.3) \times 10^{-2}$ [a]	$(1.0 \pm 0.1) \times 10^{2}$
No.	electron donors	E_{ox} (vs SCE, V)[c]	k_{et}, M^{-1} s^{-1}		
			without acid	with $Sc(OTf)_3$ (10 mM)	with HOTf (10 mM)
13	$[(Ph_2\text{–}phen)_3Fe^{II}]^{2+}$	1.02	NR[d]	$(1.4 \pm 0.1) \times 10^{3}$ [a]	$(7.9 \pm 0.4) \times 10^{3}$
14	$[(bpy)_3Fe^{II}]^{2+}$	1.06	NR[d]	$(2.1 \pm 0.1) \times 10^{2}$ [a]	$(2.5 \pm 0.1) \times 10^{3}$
15	$[(4,4'\text{–}Me_2bpy)_3Ru^{II}]^{2+}$	1.11	NR[d]	$(7.0 \pm 0.3) \times 10$	$(5.0 \pm 0.2) \times 10^{2}$
16	$[(5,5'\text{–}Me_2bpy)_3Ru^{II}]^{2+}$	1.16	NR[d]	$(4.0 \pm 0.2) \times 10$	$(2.5 \pm 0.1) \times 10^{2}$
17	$[(Clphen)_3Fe^{II}]^{2+}$	1.20	NR[d]	9.4 ± 0.4 [a]	$(2.5 \pm 0.1) \times 10^{2}$
18	$[(bpy)_3Ru^{II}]^{2+}$	1.24	NR[d]	9.0 ± 0.4 [a]	$(5.0 \pm 0.2) \times 10$

[a] Taken from ref 23c and 31. [b] Taken from ref 26. [c] Taken from refs 23c, 30 and 32. [d] NR = no reaction.

Table 2. Second-Order Rate Constants of the C–H Bond Cleavage of Hexamethylbenzene and Toluene by $[(N4Py)Fe^{IV}(O)]^{2+}$ in the Presence of Lewis Acids (50 mM) in MeCN at 298 K

Substrate	k_{obs}, M^{-1} s^{-1}		
	$Sc(OTf)_3$ (50 mM)	$HClO_4$ (50 mM)	HOTf (50 mM)
Hexamethylbenzene	$(2.6 \pm 0.2) \times 10^{-1}$	$(3.0 \pm 0.2) \times 10^{2}$	$(1.0 \pm 0.1) \times 10^{4}$
Toluene	$(2.9 \pm 0.2) \times 10^{-4}$	$(8.3 \pm 0.5) \times 10^{-4}$	$(7.9 \pm 0.3) \times 10^{-3}$

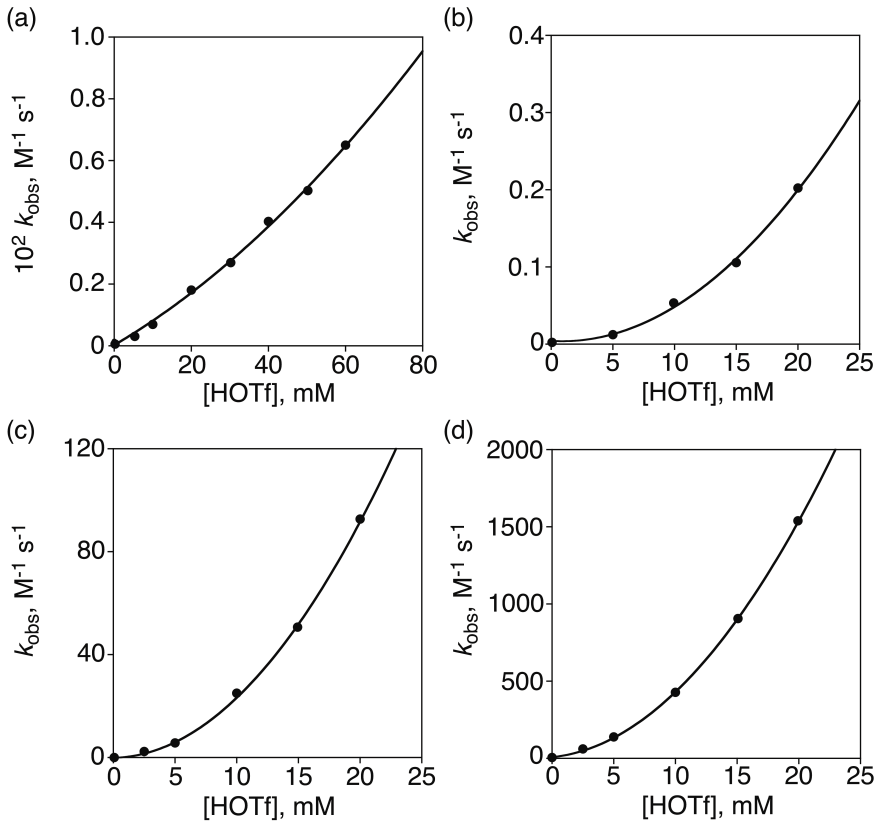

Figure 7. Plots of k_{obs} vs concentration of HOTf for oxidation of toluene derivatives [(a) toluene, (b) 1,3,5-trimethylbenzene, (c) 1,2,4,5-tetramethylbenzene and (d) hexamethylbenzene] by $[(N4Py)Fe^{IV}(O)]^{2+}$ in the presence of HOTf in MeCN at 298 K.

When HOTf was replaced by $Sc(OTf)_3$, the k_{obs} values of oxidation of toluene derivatives by $[(N4Py)Fe^{IV}(O)]^{2+}$ also increased with increasing concentration of $Sc(OTf)_3$ (Figure 9). The k_{obs} values of oxidation of toluene derivatives by $[(N4Py)Fe^{IV}(O)]^{2+}$ in the presence of $Sc(OTf)_3$ (10 mM) in MeCN at 298 are also listed in Table 1. The k_{obs} values of oxidation of toluene derivatives (toluene and hexamethylbenzenze) by $[(N4Py)Fe^{IV}(O)]^{2+}$ in the presence of HOTf, $HClO_4$ (70%)[26] and $Sc(OTf)_3$ (50 mM) are compared in Table 2, where k_{obs} value increases in order: $Sc(OTf)_3 < HClO_4 <$ HOTf. In the case of hexamethylbenzene, k_{obs} in the presence of HOTf (50 mM) is 2.2×10^5 times larger than that in the absence of HOTf.

When toluene was replaced by the deuterized compound (toluene-d_8), a large deuterium kinetic isotope effect (KIE) was observed in the absence of HOTf (KIE = 31) as shown in Figure 10. Such a large KIE value suggests that the hydrogen atom transfer occurs via tunneling in the rate-determining step of oxidation of toluene by $[(N4Py)Fe^{IV}(O)]^{2+}$.[33-36] In the presence of HOTf, the KIE value decreased with

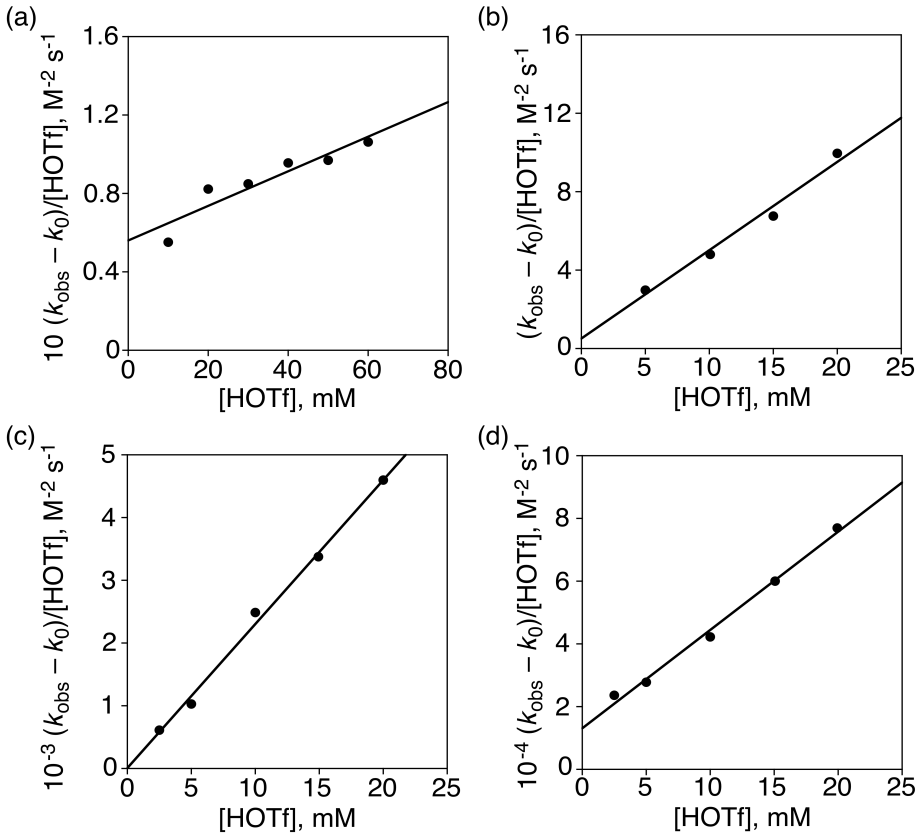

Figure 8. Plots of (k_{obs} – k_0)/[HOTf] vs [HOTf] for oxidation of toluene derivatives [(a) toluene, (b)1,3,5-trimethylbenzene, (c) 1,2,4,5-tetramethylbenzene and (d) hexamethylbenzene] by $[(N4Py)Fe^{IV}(O)]^{2+}$ (0.25 mM) in the presence of HOTf in MeCN at 298 K.

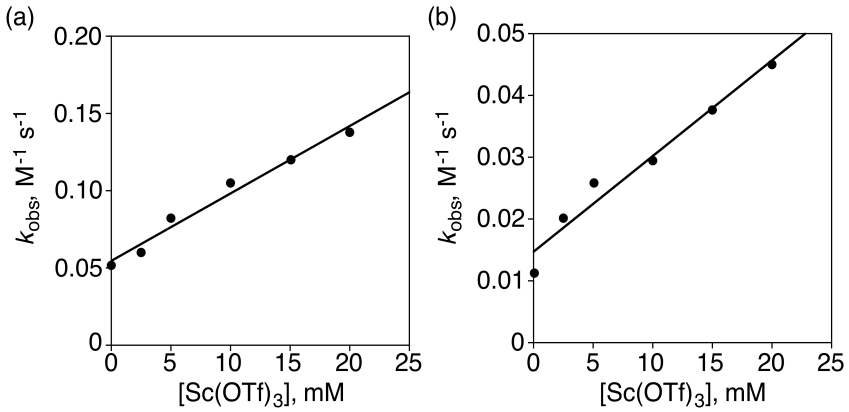

Figure 9. Plots of k_{obs} vs concentration of $Sc(OTf)_3$ for oxidation of toluene derivatives [(a) hexamethylbenzene (HMB) and (b) 1,2,3,4,5-pentamethylbenzene (PMB)] by $[(N4Py)Fe^{IV}(O)]^{2+}$ (0.25 mM) in the presence of $Sc(OTf)_3$ in MeCN at 298 K.

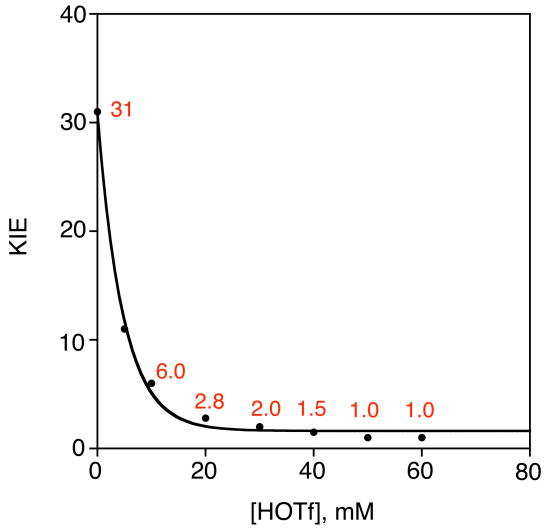

Figure 10. Plot of KIE vs concentration of HOTf in the oxidation of toluene and toluene–d_8 with $[(N4Py)Fe^{IV}(O)]^{2+}$ (0.25 mM) in the presence of HOTf in MeCN at 298 K. Red-colored numbers show the KIE values obtained experimentally.

increasing concentration of HOTf to reach KIE = 1 at concentrations of HOTf larger than 50 mM (Figure 10). Such a drastic change in KIE from 31 to 1 indicates that the rate-determining step of oxidation of toluene by $[(N4Py)Fe^{IV}(O)]^{2+}$ is changed from hydrogen atom transfer in the absence of HOTf to proton–coupled electron transfer (PCET) in the presence of HOTf (> 50 mM).

HOTf– and $Sc(OTf)_3$–Promoted Sulfoxidation of Thioanisole Derivatives by $[(N4Py)Fe^{IV}(O)]^{2+}$. It is well known that oxidation of thioanisole derivatives by $[(N4Py)Fe^{IV}(O)]^{2+}$ occurs to produce the corresponding sulfoxide products (eq 4).[20a,23c,25] The rate of sulfoxidation of thioanisole derivatives by $[(N4Py)Fe^{IV}(O)]^{2+}$ was

$$Ph\text{-}S\text{-}CH_3 + [(N4Py)Fe^{IV}(O)]^{2+} \longrightarrow Ph\text{-}SO\text{-}CH_3 + [(N4Py)Fe^{II}]^{2+} \quad (4)$$

remarkably enhanced in the presence of $Sc(OTf)_3$ (10 mM) and $HClO_4$ (70%, 10 mM) as compared with that in the absence of acids.[23c,25] The mechanism of sulfoxidation of thioanisole derivatives by $[(N4Py)Fe^{IV}(O)]^{2+}$ is changed from a direct oxygen atom transfer (OAT) pathway to a metal ion–coupled electron transfer (MCET) pathway in the presence of $Sc(OTf)_3$ and also to a PCET pathway in the presence of $HClO_4$.[23c,25] The rate of sulfoxidation of thioanisole derivatives by $[(N4Py)Fe^{IV}(O)]^{2+}$ was further

enhanced by the presence of HOTf (10 mM) as compared with that in the presence of $HClO_4$ (70%, 10 mM).[25] The k_{obs} values of oxidation of thioanisole derivatives by $[(N4Py)Fe^{IV}(O)]^{2+}$ in the presence of HOTf (10 mM) were determined from linear plots of k_f vs concentrations of thioanisole derivatives (Figure 11). The k_{obs} values increase with increasing concentration of HOTf in accordance with eq 2 (Figure 12).[23c] The k_{obs} values of oxidation of thioanisole derivatives $[(N4Py)Fe^{IV}(O)]^{2+}$ in the presence of HOTf (10 mM) in MeCN at 298 K are also listed in Table 1.

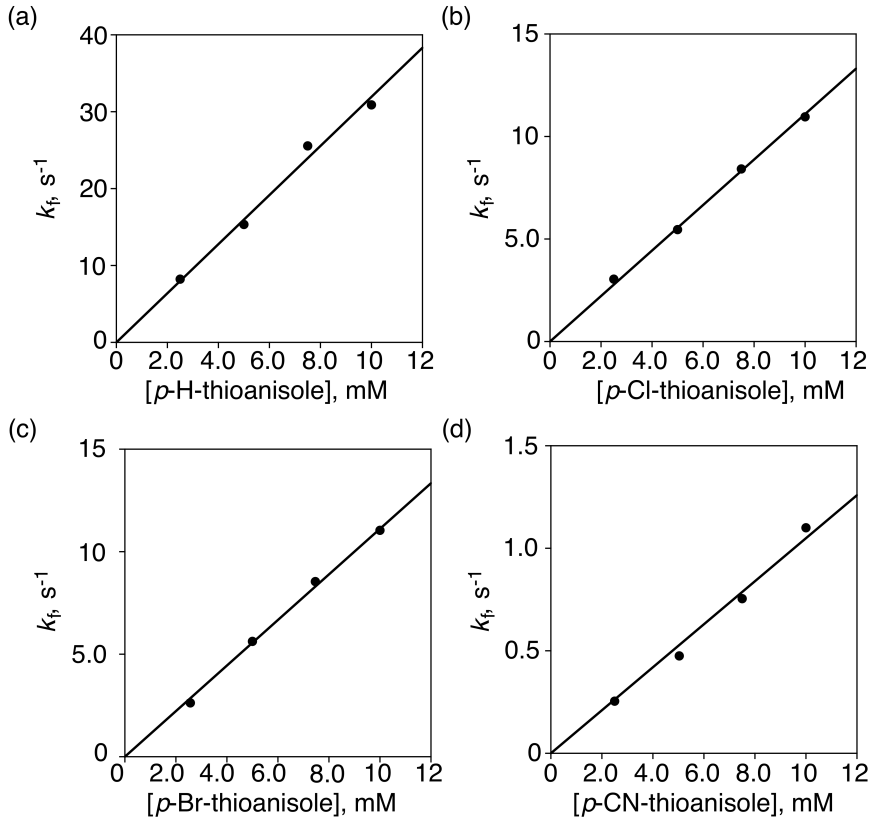

Figure 11. Plots of pseudo-first-order rate constants (k_f) vs concentrations of *p*-X-thioanisoles (X = (a) H, (b) Cl, (c) Br and (d) CN) to determine the second-order rate constants (k_{obs}) of sulfoxidation of *p*-X-thioanisoles by $[(N4Py)Fe^{IV}(O)]^{2+}$ (0.25 mM) in the presence of HOTf (10 mM) in MeCN at 298 K.

Inverse Kinetic Isotope Effect in Proton–Coupled Electron–Transfer Reduction of $[(N4Py)Fe^{IV}(O)]^{2+}$. When HOTf was replaced by the deuterated acid (DOTf), the k_{et} value of PCET from an electron donor ($[Ru^{II}(bpy)_3]^{2+}$; bpy = 2,2'-bipyridine) to $[(N4Py)Fe^{IV}(O)]^{2+}$ with DOTf in MeCN at 298 K was larger than that with the same concentration of HOTf as shown in Figure 3. Both the k_{et} values with DOTf and HOTf

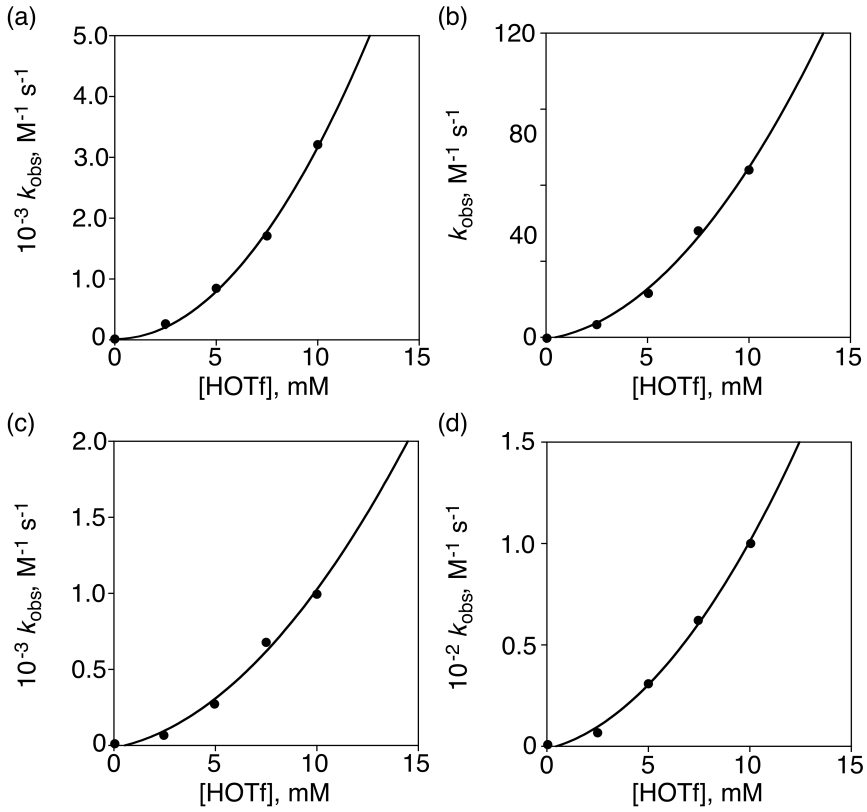

Figure 12. Plots of k_{obs} vs concentration of HOTf for sulfoxidation of *p*-X-thioanisoles (X = (a) H, (b) Cl, (c) Br and (d) CN) by $[(N4Py)Fe^{IV}(O)]^{2+}$ (0.25 mM) in the presence of HOTf in MeCN at 298 K.

increased with increasing concentration of DOTf and HOTf, respectively, in accordance with eq 2. The KIE value ($k_{obs(HOTf)}/k_{obs(DOTf)}$) was determined to be 0.25 ± 0.05 at [HOTf (or DOTf)] = 2.5 mM, increasing to be a constant value of 0.40 ± 0.04 at the higher concentrations of HOTf (DOTf) as shown in Figure 14. Such an inverse KIE indicates that binding of protons to the oxo group to produce the O–H (or O–D)bond is involved in the rate-determining step of PCET from $[Ru^{II}(bpy)_3]^{2+}$ to $[(N4Py)Fe^{IV}(O)]^{2+}$, because an inverse KIE results from a larger zero-point energy difference between the O–H and O–D bonds in the transition state relative to the ground state.[37] Thus, the O–H bonds in the reduced species ($[(N4Py)Fe^{III}(OH)]^{2+}$ and $[(N4Py)Fe^{III}(OH_2)]^{3+}$) are much stronger than those in $[(N4Py)Fe^{IV}(OH)]^{3+}$ and $[(N4Py)Fe^{IV}(OH_2)]^{4+}$, respectively. The larger is the difference in the O-H bond strength between the reduced and oxidized species, the larger may be the inverse KIE. Thus, the larger inverse KIE value at the lower concentration of HOTf suggests that the difference in OH–bond strength between $[(N4Py)Fe^{III}(OH)]^{2+}$ and $[(N4Py)Fe^{IV}(OH)]^{3+}$ (monoprotonated species) may be larger

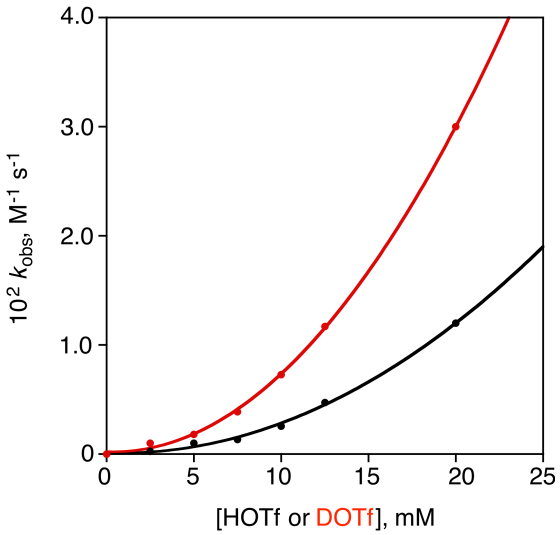

Figure 13. Plots of k_{et} vs [HOTf] (black circles) and [DOTf] (red circles) for PCET from $[Ru^{II}(bpy)_3]^{2+}$ to $[(N4Py)Fe^{IV}(O)]^{2+}$ in the presence of HOTf and DOTf in MeCN at 298 K, respectively.

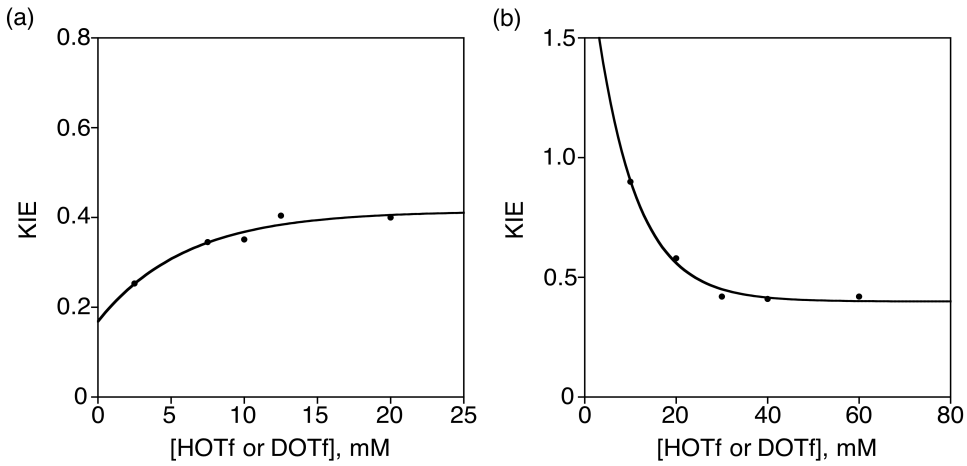

Figure 14. Plots of KIE vs [HOTf or DOTf] for (a) PCET from $[Ru^{II}(bpy)_3]^{2+}$ to $[(N4Py)Fe^{IV}(O)]^{2+}$ and (b) oxidation of toluene by $[(N4Py)Fe^{IV}(O)]^{2+}$ in the presence of HOTf or DOTf in MeCN at 298 K.

than that between $[(N4Py)Fe^{III}(OH_2)]^{3+}$ and $[(N4Py)Fe^{IV}(OH_2)]^{4+}$ (diprotonated species).

A similar inverse KIE was observed for the k_{obs} values of oxidation of toluene by $[(N4Py)Fe^{IV}(O)]^{2+}$ in the presence of large concentrations of DOTf (> 30 mM) in comparison with those in the presence of HOTf as shown in Figure 15. The KIE value decreases with increasing concentration of HOTf (Figure 14b) to reach a constant value of 0.42 ± 0.04, which agrees with the KIE value of PCET from $[Ru^{II}(bpy)_3]^{2+}$ to $[(N4Py)Fe^{IV}(O)]^{2+}$ (0.40 ± 0.04) in Figure 14a. The same inverse KIE of the oxidation of toluene as that of PCET together with the absence of KIE between toluene-d_8 and

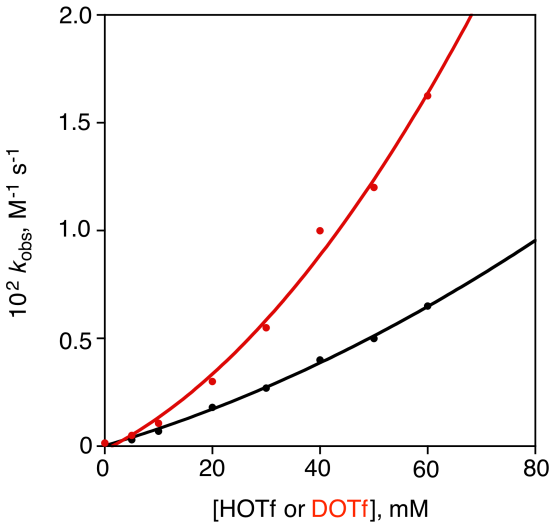

Figure 15. Plots of k_{obs} vs [HOTf] (black circles) and [DOTf] (red circles) for oxidation of toluene by $[(N4Py)Fe^{IV}(O)]^{2+}$ in the presence of HOTf and DOTf in MeCN at 298 K, respectively.

toluene (Figure 10) strongly indicates that the oxidation of toluene by $[(N4Py)Fe^{IV}(O)]^{2+}$ in the presence of large concentrations of HOTf occurs via PCET as the rate-determining step.[38,39]

Comparison of Proton–Coupled Electron Transfer vs Metal Ion–Coupled Electron Transfer. Rates of electron transfer from electron donors to $[(N4Py)Fe^{IV}(O)]^{2+}$ are accelerated by binding of protons and metal ions to $[(N4Py)Fe^{IV}(O)]^{2+}$ via PCET and MCET, respectively.[23b] In order to compare the acceleration effect of HOTf with that of metal triflates ($M^{n+}(OTf)_n$), we determined that rate constant of PCET from ferrocene (Fc) to $[(N4Py)Fe^{IV}(O)]^{2+}$ in the presence of HOTf in MeCN at 298 K. The observed second-order rate constant (k_{et}) of PCET from Fc to $[(N4Py)Fe^{IV}(O)]^{2+}$ increased with increasing concentration of HOTf in accordance with eq 2 as shown in Figure 16 (red line). The linear plot of $(k_{et} - k_0)/[HOTf]$ vs [HOTf] (eq 3) is shown in inset of Figure 16. The k_1 and k_2 values in eq 3 were determined from the intercept and the slope, respectively.

Similarly, we determined the k_1 and k_2 values of MCET from Fc to $[(N4Py)Fe^{IV}(O)]^{2+}$ in the presence of $Sc(OTf)_3$ in MeCN at 298 K [The dependence of k_{et} on $[Sc(OTf)_3]$ is shown in Figure 16 (black line)].[23a] The k_{et} values with HOTf are always larger than those with $Sc(OTf)_3$ at the same concentrations of acids. The k_1 and k_2 values with various metal triflates were determined previously from the intercepts and slopes of plots of $(k_{et} - k_0)/[M^{n+}(OTf)_n]$ vs $[M^{n+}(OTf)_n]$, respectively.[23a]

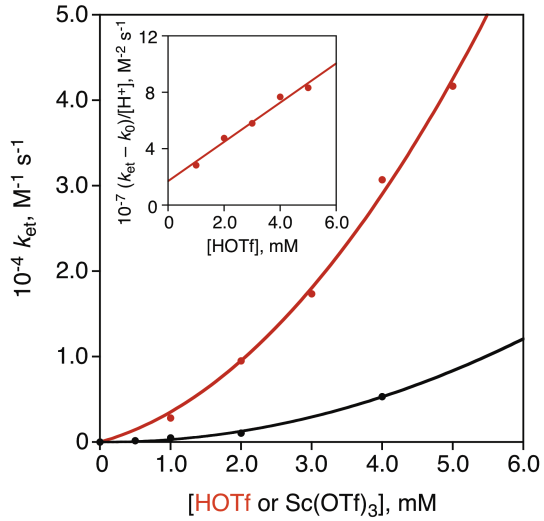

Figure 16. Plots of k_{et} vs [HOTf] (red circles) and [$Sc(OTf)_3$] (black circles) for PCET and MCET from Fc to $[Fe^{IV}(O)(N4Py)]^{2+}$ in the presence of HOTf and $Sc(OTf)_3$ in MeCN at 298 K, respectively. Inset shows plot of ($k_{et} - k_0$)/[HOTf] vs [HOTf].

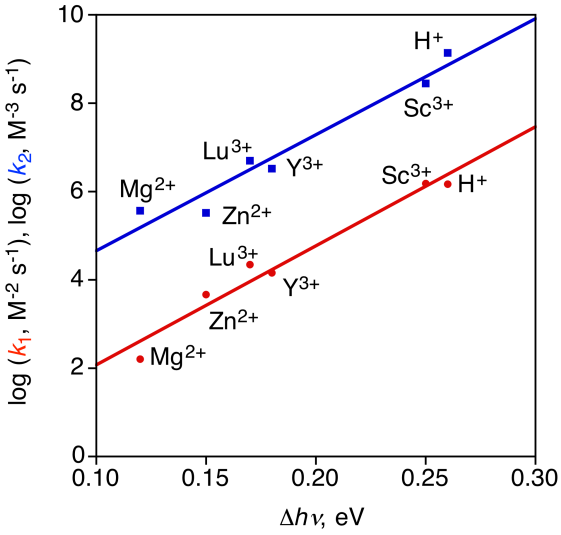

Figure 17. Plots of log k_1 (red circles) and log k_2 (blue squares) vs Dhn for PCET and MCET from Fc to $[(N4Py)Fe^{IV}(O)]^{2+}$ in the presence of HOTf and metal triflates in MeCN at 298 K, respectively. The Δ$h\nu$ values were determined from the fluorescence emission energies of AcrCO in the presence of HOTf and metal triflates relative to the energy in their absence.

Figure 17 shows plots of log k_1 and log k_2 vs a quantitative measure of Lewis acidity (Δ$h\nu$) for both PCET and MCET from Fc to $[(N4Py)Fe^{IV}(O)]^{2+}$ in the presence of HOTf and $M^{n+}(OTf)_n$, respectively. The Δ$h\nu$ values were obtained from the red shifts of the fluorescence emission energies of 10-methylacridone (Δ$h\nu$) due to binding of metal

triflates to the carbonyl oxygen from that in the absence of acids.[40] According to the shift of fluorescence emission energy ($\Delta h\nu$), the relative Lewis acidity of proton was determined to be 0.26 eV, which is slightly higher than that of $Sc(OTf)_3$ (0.25 eV) as shown in Figure 18.[40] Good linear correlations were obtained for plots of both log k_1 and log k_2 of PCET and MCET from Fc to $[(N4Py)Fe^{IV}(O)]^{2+}$ vs $\Delta h\nu$ (Figure 17). The stronger is the acidity of Lewis acids, the stronger becomes the binding of acids to $[(N4Py)Fe^{IV}(O)]^{2+}$ as well as to the excited state of AcrCO, resulting in the acceleration of PCET and MCET from Fc to $[(N4Py)Fe^{IV}(O)]^{2+}$.

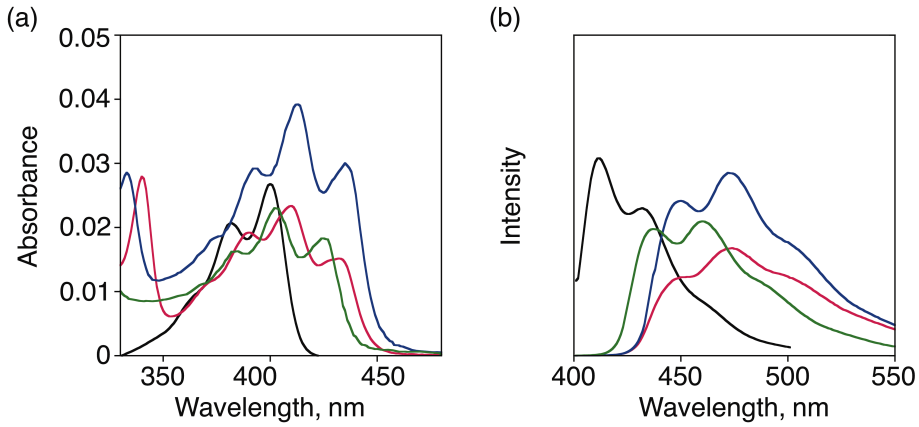

Figure 18. (a) Absorption and (b) fluorescence spectra of *N*-methylacridone (3.3 μM) in the absence (black) and presence of HOTf (red, 2.5 mM), $Sc(OTf)_3$ (blue, 2.5 mM) and $Y(OTf)_3$ (green, 2.5 mM) in deaerated MeCN at 298 K.

One Electron Reduction Potentials of $[(N4Py)Fe^{IV}(O)]^{2+}$ in the Presence of HOTf. In order to examine the driving force dependence of PCET from electron donors to $[(N4Py)Fe^{IV}(O)]^{2+}$ in the presence of HOTf in MeCN, the one-electron reduction potentials of $[(N4Py)Fe^{IV}(O)]^{2+}$ in the presence of various concentrations of HOTf were determined by the redox titration (vide infra). When $[Ru^{II}(NO_2phen)_3]^{2+}$ (NO_2phen = 5-nitrophenathrene) was employed as an electron donor, no electron transfer from $[Ru^{II}(NO_2phen)_3]^{2+}$ (E_{ox} = 1.45 V vs SCE, Figure 19) to $[(N4Py)Fe^{IV}(O)]^{2+}$ (E_{red} = 0.51 V)[41] occurred in the absence of acids in MeCN, because the free energy change of electron transfer is highly positive (ΔG_{et} = 0.94 eV), i.e., endergonic. However, the electron transfer occurred efficienly in the presence of HOTf (10 mM) as shown in Figure 20, where the absorption band at 695 nm due to $[(N4Py)Fe^{IV}(O)]^{2+}$ (λ_{max} = 695 nm) disappered, accompanied by apperance of a new absorption band at 650 nm due to $[Ru^{III}(NO_2phen)_3]^{3+}$ (λ_{max} = 650 nm) with an isosbestic point at 730 nm.

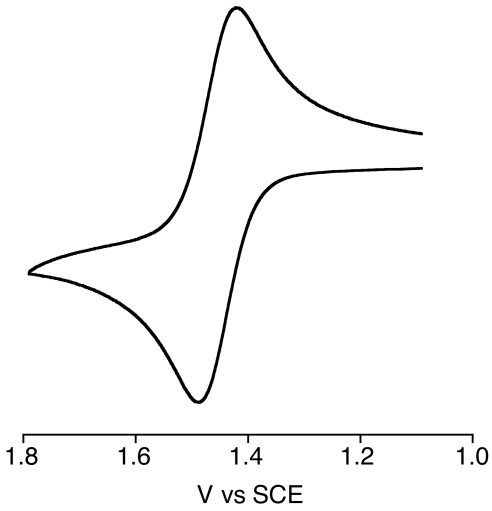

Figure 20. Cyclic voltammogram of $[Ru^{II}(NO_2phen)_3]^{2+}$ (1.0 mM) in MeCN containing $TBAPF_6$ (0.10 M) at 298 K with a Pt working electrode. Scan rate was 0.10 V s^{-1}. The E_{ox} value was determined to be 1.45 V vs SCE.

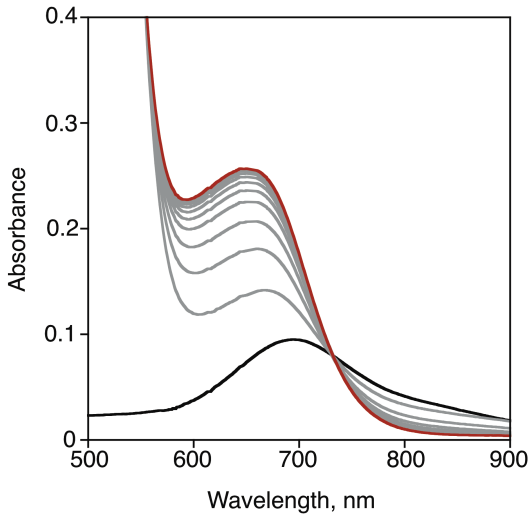

Figure 20. Visible spectral changes observed in PCET from $[Ru^{II}(NO_2phen)_3]^{2+}$ (2.5 mM) to $[(N4Py)Fe^{IV}(O)]^{2+}$ (0.25 mM) in the presence of HOTf (10 mM) in MeCN at 298 K.

The concentration of $[Ru^{III}(NO_2phen)_3]^{3+}$ produced in PCET from $[Ru^{II}(NO_2phen)_3]^{2+}$ to $[(N4Py)Fe^{IV}(O)]^{2+}$ in the presence of HOTf (10 mM) is plotted against the initial concentration of $[Ru^{II}(NO_2phen)_3]^{2+}$ as shown in Figure 21, which indicates that there is an PCET equilibrium as given in eq 5. The PCET equilibrium constant K_{et} was determined by fitting the plot in Figure 21 to be $K_{et} = 24$. The E_{red}

$$[(N4Py)Fe^{IV}(O)]^{2+} + [Ru^{II}(NO_2phen)_3]^{2+} + 2H^+ \underset{}{\overset{K_{et}}{\rightleftharpoons}} [(N4Py)Fe^{III}(OH_2)]^{3+} + [Ru^{III}(NO_2phen)_3]^{3+} \quad (5)$$

value of $[(N4Py)Fe^{IV}(O)]^{2+}$ in the presence of HOTf (10 mM) MeCN at 298 K was determined from the K_{et} value (24) and the E_{ox} value of $[Ru^{II}(NO_2phen)_3]^{2+}$ (E_{ox} = 1.45 V vs SCE) using an Nernst equation (eq 6, where R is the gas constant, T is absolute temperature, and F is the Faraday constant) to be 1.55 V vs SCE, which is much higher

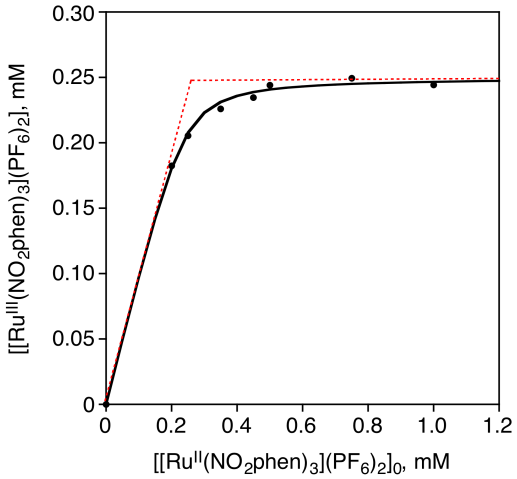

Figure 21. Plot of concentration of $[Ru^{III}(NO_2phen)_3]^{3+}$ produced in PCET from $[Ru^{II}(NO_2phen)_3]^{2+}$ to $[(N4Py)Fe^{IV}(O)]^{2+}$ (0.25 mM) in the presence of HOTf (10 mM) in deaerated MeCN at 298 K vs initial concentration of $[Ru^{II}(NO_2phen)_3](PF_6)_2$, $[Ru^{II}(NO_2phen)_3](PF_6)_2]_0$.

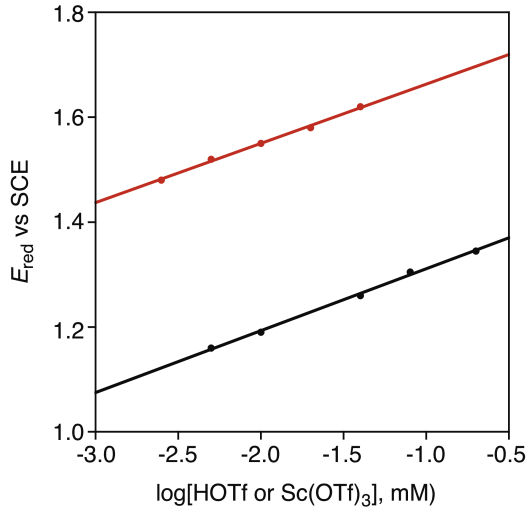

Figure 22. Dependence of E_{red} of $[(N4Py)Fe^{IV}(O)]^{2+}$ on log([HOTf (red circles) and $Sc(OTf)_3$ (black circles)]) in deaerated MeCN at 298. Balck and red lines are fitted by eq 7.

$$E_{red} = E_{ox} + (RT/F)\ \ln K_{et} \quad (6)$$

than that in the presence of $Sc(OTf)_3$ (10 mM; 1.19 V vs SCE) reported previously.[23b,42] The E_{red} values in the presence of various concentrations of HOTf and $Sc(OTf)_3$ were also determinded from the K_{et} values and the E_{ox} value of $[Ru^{II}(NO_2phen)_3]^{2+}$ using eq 6.

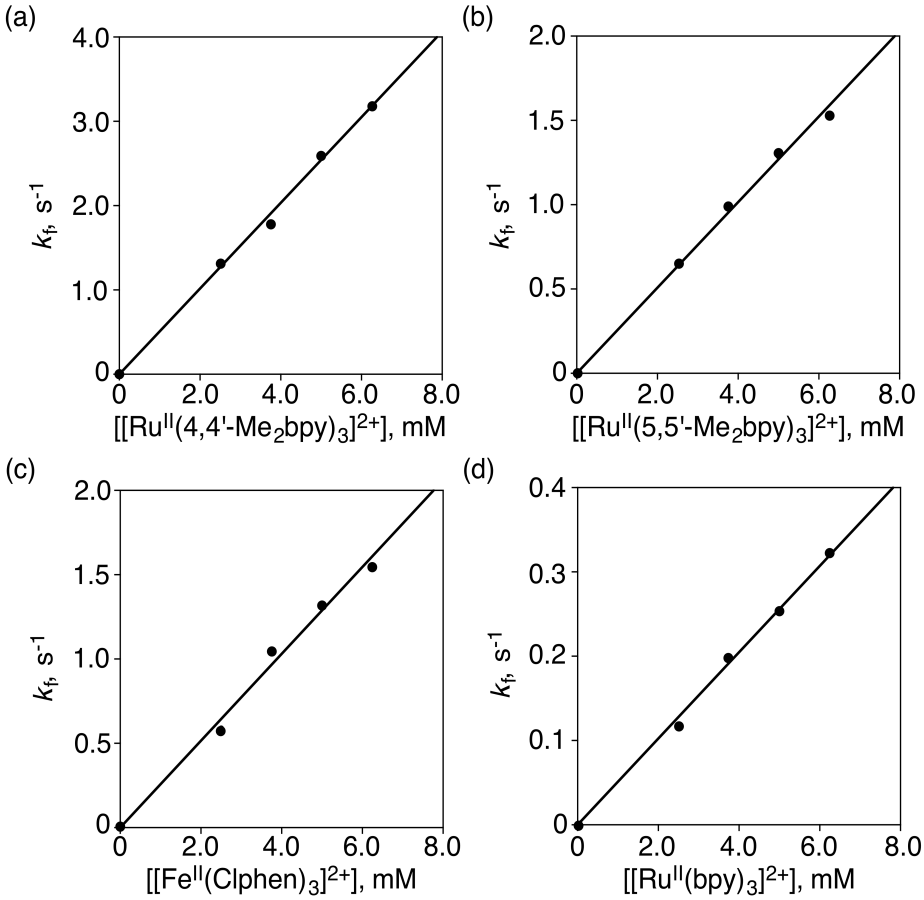

Figure 23. Plots of pseudo-first-order rate constants (k_f) vs concentrations of electron donors [(a) $[Ru^{II}(4,4'–Me_2bpy)_3]^{2+}$, (b) $[Ru^{II}(5,5'–Me_2bpy)_3]^{2+}$, (c) $[Fe^{II}(Clphen)_3]^{2+}$ and (d) $[Ru^{II}(bpy)_3]^{2+}$] to determine the second-order rate constants (k_{et}) of PCET from electron donors to $[(N4Py)Fe^{IV}(O)]^{2+}$ (0.25 mM) in the presence of HOTf (10 mM) in MeCN at 298 K.

The dependence of E_{red} of $[(N4Py)Fe^{IV}(O)]^{2+}$ on log [HOTf] and log[$Sc(OTf)_3$] is shown in Figure 22, where the slopes are determined to be 113 ± 6 mV for HOTf and 118 ± 8 mV for $Sc(OTf)_3$. The Nernst equation for the dependence of E_{red} on log[Acid] (Acid = HOTf and $Sc(OTf)_3$) is given by eq 7, where K_{red1} and K_{red2} are the equilibrium

constants for the first and second binding of acids to $[(N4Py)Fe^{III}(O)]^{+}$, respectively. Under the conditions such that K_{red2}[Acid] >> 1, eq 7 is rewritten by eq 8,

$$E_{red} = E^{0}_{red} + (2.3RT/F) \log(K_1[\text{Acid}] + K_1K_2[\text{Acid}]^2) \quad (7)$$

$$E_{red} = E^{\circ}_{red} + 2(2.3RT/F) \log(K_{red1}K_{red2}[\text{Acid}]) \quad (8)$$

where the slope of plot of E_{red} vs log[Acid] is 2(2.3RT/F) = 118mV at 298 K, which agrees well with the experimental values in Figure 22. Such agreement indicates that PCET and MCET reduction of $[(N4Py)Fe^{IV}(O)]^{2+}$ involve binding of two acid molecules of HOTf and $Sc(OTf)_3$ to $[(N4Py)Fe^{III}(O)]^{+}$, respectively. The second-order rate constants (k_{et}) of electron transfer from electron donors to $[(N4Py)Fe^{IV}(O)]^{2+}$ in the presence of HOTf (10 mM) and $Sc(OTf)_3$ (10 mM) were determined as listed in Table 1 (Figures 23 and 24).

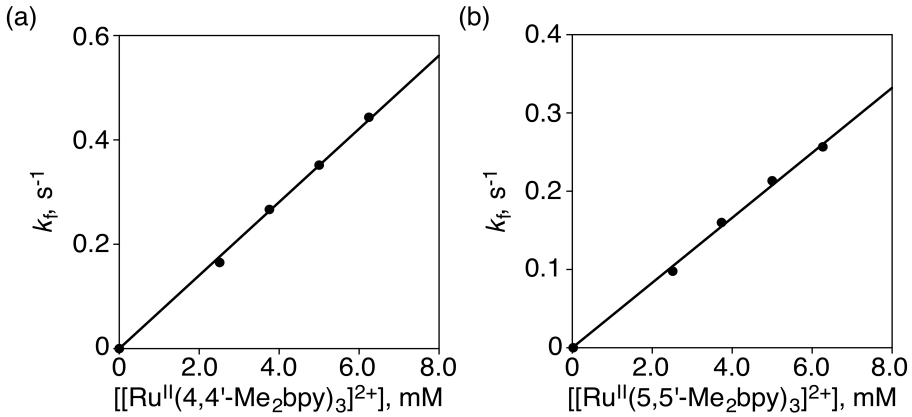

Figure 24. Plots of pseudo-first-order rate constants (k_f) vs concentrations of electron donors [(a) $[Ru^{II}(4,4'–Me_2bpy)_3]^{2+}$ and (b) $[Ru^{II}(5,5'–Me_2bpy)_3]^{2+}$] to determine the second-order rate constants (k_{et}) of MCET from electron donors to $[(N4Py)Fe^{IV}(O)]^{2+}$ (0.25 mM) in the presence of $Sc(OTf)_3$ (10 mM) in MeCN at 298 K.

Unified Driving Force Dependence of Rate Constants. The dependence of log k_{et} of electron transfer from electron donors to $[(N4Py)Fe^{IV}(O)]^{2+}$ and log k_{obs} of oxidation of toluene and thioanisole derivatives by $[(N4Py)Fe^{IV}(O)]^{2+}$ in the presence of HOTf (10 mM) and $Sc(OTf)_3$ (10 mM) on one-electron oxidation potentials (E_{ox}) of electron donors including toluene and thioanisole derivatives is shown in Figure 25 (red line). A unified correlation is observed for plots of log k_{obs} of oxidation of toluene and

thioanisole derivatives by $[(N4Py)Fe^{IV}(O)]^{2+}$ in the presence of HOTf (10 mM) vs the E_{ox} values of toluene and thioanisole derivatives. Such a unified correlation suggests that oxidation of both toluene and thioanisole derivatives by $[(N4Py)Fe^{IV}(O)]^{2+}$ in the presence of HOTf (10 mM) proceeds via PCET from toluene and thioanisole derivatives to $[(N4Py)Fe^{IV}(O)]^{2+}$. However, the log k_{et} values of PCET from coordinatively saturated metal complexes (Nos. 13-18 in Table 1) to $[(N4Py)Fe^{IV}(O)]^{2+}$ are significantly smaller than log k_{obs} values of oxidation of toluene and thioanisole derivatives (red line in Figure 25).

Similarly a unified linear correlation is observed for plots of log k_{obs} of oxidation of toluene and thioanisole derivatives by $[(N4Py)Fe^{IV}(O)]^{2+}$ in the presence of $Sc(OTf)_3$ (10 mM) vs the E_{ox} values of toluene and thioanisole derivatives when the E_{ox} values are lower than 1.6 V vs SCE (black line in Figure 25). Such a unified correlation indicates that oxidation of toluene and thioanisole derivatives by $[(N4Py)Fe^{IV}(O)]^{2+}$ in the presence of $Sc(OTf)_3$ (10 mM) proceeds via MCET from toluene and thioanisole derivatives to $[(N4Py)Fe^{IV}(O)]^{2+}$. In the case of 1,2,4-trimethylbenzene (No. 4), 1,4-dimethylbenzene (No. 5), 1,3,5-trimethylbenzene (No. 6) and toluene (No. 7), which have higher E_{ox} values than 1.6 V vs SCE, however, the log k_{obs} values are significantly larger than the linear correlation (black line in Figure 11). The log k_{et} values of MCET from coordinatively saturated metal complexes (Nos. 13-18 in Table 1) to $[(N4Py)Fe^{IV}(O)]^{2+}$ are also significantly smaller than the log k_{obs} values of oxidation of toluene and thioanisole derivatives (black line in Figure 25).

The difference in log k_{et} and log k_{obs} values between PCET and MCET is expected to result from the difference in the E_{red} values of $[(N4Py)Fe^{IV}(O)]^{2+}$ in the presence of HOTf (10 mM) and $Sc(OTf)_3$ (10 mM). Driving forces of the PCET and MCET reactions ($-\Delta G_{et}$ in eV) are obtained from the one-electron oxidation potentials (E_{ox}) of electron donors (coordinatively saturated metal complexes, toluene and thioanisole derivatives) and the one-electron reduction potentials (E_{red}) of $[(N4Py)Fe^{IV}(O)]^{2+}$ in the presence of acids as given by eq 9, where e is the elementary charge and log k_{obs} of PCET and MCET from electron donors (coordinatively saturated metal complexes, toluene and thioanisole derivatives) to $[(N4Py)Fe^{IV}(O)]^{2+}$ in the presence of HOTf (10 mM) and $Sc(OTf)_3$ (10 mM) in MeCN at 298 K, respectively.

$$-\Delta G_{et} = e(E_{red} - E_{ox}) \quad (9)$$

The driving force dependence of log k_{et} of electron transfer from coordinatively saturated metal complexes to $[(N4Py)Fe^{IV}(O)]^{2+}$ in the absence and presence of 10 mM of HOTf (black line in Figure 26) is well fitted by the Marcus equation of outer-sphere electron transfer (eq 10),[43]

$$k_{et} = Z\exp[-(\lambda/4)(1 + \Delta G_{et}/\lambda)^2/k_B T] \quad (10)$$

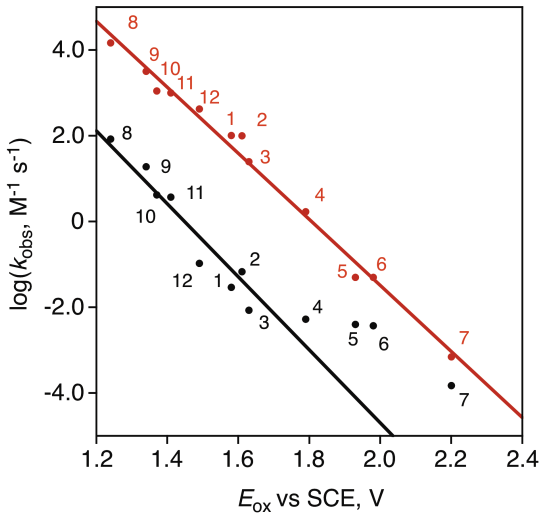

Figure 25. Plot of log k_{obs} vs oxidation potentials (E_{ox}) of toluene and thioanisole derivatives [(1) hexamethylbenzene, (2) 1,2,3,4,5-tetramethylbenzene, (3) 1,2,4,5-tetramethylbenzene, (4) 1,2,4-trimethylbenzene, (5) 1,4-dimethylbenzene, (6) 1,3,5-trimethylbenzene, (7) toluene, (8) *p*-Me-thioaniosle, (9) *p*-H-thioaniosle, (10) *p*-Cl-thioaniosle, (11) *p*-Br-thioaniosle and (12) *p*-CN-thioaniosle] in the C–H bond cleavage of toluene derivatives and sulfoxidation of thioanisole derivatives by $[(N4Py)Fe^{IV}(O)]^{2+}$ in the presence of 10 mM of HOTf (red circles) and $Sc(OTf)_3$ (black circles) in MeCN at 298 K.

where Z is the frequency factor, which is $k_B TK/h$ (k_B is the Borzmann constant, T is absolute temperature, K is the formation constant of the precursor complex and h is the Planck constant), using the same value of reorganization energy of electron transfer (λ = 2.74 eV). The Z value of outer-sphere electron-transfer reactions is normally taken as 1.0×10^{11} M^{-1} s^{-1}.[44-47] This indicates that the K value of outer-sphere electron-transfer reactions is as small as 0.020 M^{-1}, because there is little interaction in the precursor complex for outer-sphere electron transfer.

The log k_{obs} values of oxidation of toluene and thioanisole derivatives by $[(N4Py)Fe^{IV}(O)]^{2+}$ in the presence of HOTf and $Sc(OTf)_3$ (10 mM) as well as the log k_{et} values of MCET from coordinatively saturated metal complexes to $[(N4Py)Fe^{IV}(O)]^{2+}$ in the presence of $Sc(OTf)_3$ (10 mM) are larger than those expected by eq 10 with λ = 2.74 eV.

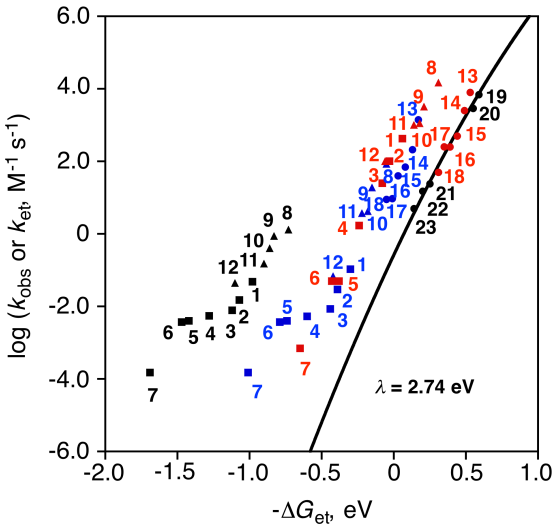

Figure 12. Plots of log k_{obs} for oxidation of toluene and thioanisole derivatives [(1) hexamethylbenzene, (2) 1,2,3,4,5-tetramethylbenzene, (3) 1,2,4,5-tetramethylbenzene, (4) 1,2,4-trimethylbenzene, (5) 1,4-dimethylbenzene, (6) 1,3,5-trimethylbenzene, (7) toluene, (8) *p*-Me-thioaniosle, (9) thioanisole, (10) *p*-Cl-thioanisole, (11) *p*-Br-thioanisole and (12) *p*-CN-thioanisole] by $[(N4Py)Fe^{IV}(O)]^{2+}$ in the absence (black) and presence of 10 mM of HOTF (red) and $Sc(OTf)_3$ (blue) in MeCN at 298 K vs the driving force of electron transfer [$-\Delta G = e(E_{red} - E_{ox})$] from toluene derivatives (squares) and thioanisole derivatives (triangles) to $[(N4Py)Fe^{IV}(O)]^{2+}$ in the presence of HOTf (red) and $Sc(OTf)_3$ (blue). The red and blue circles show the driving force dependence of the rate constants (log k_{et}) of electron transfer from electron donors [(13) $[Fe^{II}(Ph_2phen)_3]^{2+}$, (14) $[Fe^{II}(bpy)_3]^{2+}$, (15) $[Ru^{II}(4,4'\text{-}Me_2phen)_3]^{2+}$, (16) $[Ru^{II}(5,5'\text{-}Me_2phen)_3]^{2+}$, (17) $[Fe^{II}(Clphen)_3]^{2+}$ and (18) $[Ru^{II}(bpy)_3]^{2+}$] to $[(N4Py)Fe^{IV}(O)]^{2+}$ in the presence of 10 mM of HOTf and $Sc(OTf)_3$ in MeCN at 298 K. The black line is drawn using eq 10 with λ = 2.74 eV.[25,41] The black circles show the driving force dependence of the rate constants (log k_{et}) of electron transfer from electron donors [(19) decamethylferrocene, (20) octamethylferrocene, (21) 1.1'-dimethylferrocene, (22) *n*-amylferrocene and (23) ferrocene] to $[(N4Py)Fe^{IV}(O)]^{2+}$ in the absence of acids in MeCN at 298 K.[41]

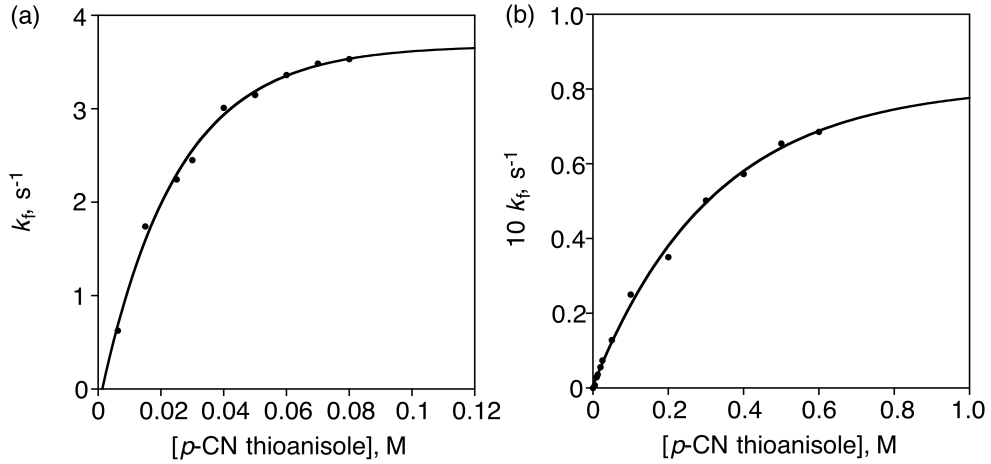

Figure 27. Plots of first-order rate constants (k_f) of oxidation of *p*-CN-thioanisole by $[(N4Py)Fe^{IV}(O)]^{2+}$ (0.25 mM) in the presence of 10 mM of (a) HOTf and (b) $Sc(OTf)_3$ in MeCN at 298 K vs concentration of *p*-CN-thioanisole.

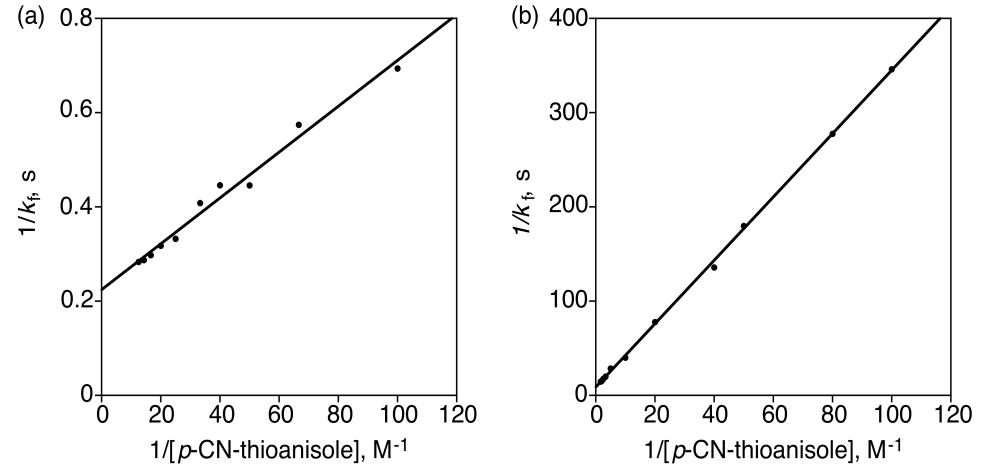

Figure 28. Plots of $1/k_f$ vs 1/[*p*-CN-thioanisole] for oxidation of *p*-CN-thioanisole by $[(N4Py)Fe^{IV}(O)]^{2+}$ in the presence of (a) HOTf (10 mM) and (b) $Sc(OTf)_3$ (10 mM) in MeCN at 298 K. The slope $[(k_{ET}K)^{-1}]$ and intercept (k_{ET}^{-1}) were determined to be (a) 4.9×10^{-3} M s and 2.2×10^{-1} s and (b) 3.4 M s and 8.7 s, respectively.

The larger log k_{obs} values of oxidation of toluene and thioanisole derivatives by $[(N4Py)Fe^{IV}(O)]^{2+}$ in the presence of HOTf and $Sc(OTf)_3$ than the log k_{et} values of electron transfer from coordinatively saturated metal complexes to$[(N4Py)Fe^{IV}(O)]^{2+}$ in the presence of HOTf may result from the difference in the K values of precursor complexes, because the stronger interaction of $[(N4Py)Fe^{IV}(OH_2)]^{4+}$ with toluene and thioanisole derivatives is expected as compared with that with coordinatively saturated metal complexes. This was confirmed by examining the dependence of the

pseudo-first-order rate constants (k_f) on concentrations of toluene and thioanisole derivatives in the large concentration range (vide infra). The k_f values of oxidation of *p*-CN-thioanisole by $[(N4Py)Fe^{IV}(O)]^{2+}$ in the presence of HOTf (10 mM) and $Sc(OTf)_3$ (10 mM) are shown in Figures 27a and 27b, respectively. In both cases, the k_f values increase with increasing concentration of *p*-CN-thioanisole to approach constant values. Such a saturation behavior indicates formation of the precursor complex prior to electron transfer when k_f is given by eq 11,

$$k_f = \quad k_{ET}K[S]/(1 + K[S]) \tag{11}$$

$$k_f^{-1} = (k_{ET}K[S])^{-1} + k_{ET}^{-1} \tag{12}$$

where k_{ET} is the first-order rate constant of electron transfer in the precursor complex, K is the formation constant of the precursor complex, and [S] is concentration of a substrate. Eq 11 is rewritten by eq 12, which predicts a linear correlation between k_f^{-1} and $[S]^{-1}$. From the intercepts and slopes of linear plots of k_f^{-1} and $[S]^{-1}$ (Figure 28), the K values were determined as listed in Table 3. The K values of oxidation of 1,2,4,5-tetramethylbenzene and 1,2,4-trimethylbenzene by $[(N4Py)Fe^{IV}(O)]^{2+}$ in the presence of HOTf (10 mM) and $Sc(OTf)_3$ (10 mM) were also determined as listed in Table 3 (Figures 29 - 31).

Table 3. Formation Constants of Precursor Complexes in Oxidation of Toluene and Thioanisole Derivatives by $[(N4Py)Fe^{IV}(O)]^{2+}$ in the Presence of Acids (10 mM), HOTf and $Sc(OTf)_3$, in MeCN at 298 K

toluene and thioanisole	formation constant (K, M^{-1})	
derivative	10 mM of $Sc(OTf)_3$	10 mM of HOTf
1,2,4,5-tetramethylbenzene	3.0 ± 0.2	$(1.2 \pm 0.4) \times 10^2$
1,2,4-trimethylbenzene	2.5 ± 0.1	$(1.0 \pm 0.1) \times 10^2$
p-Cl-thioanisole	3.1 ± 0.2	$(9.6 \pm 0.5) \times 10$
p-CN-thioanisole	2.7 ± 0.2	$(4.0 \pm 0.5) \times 10$

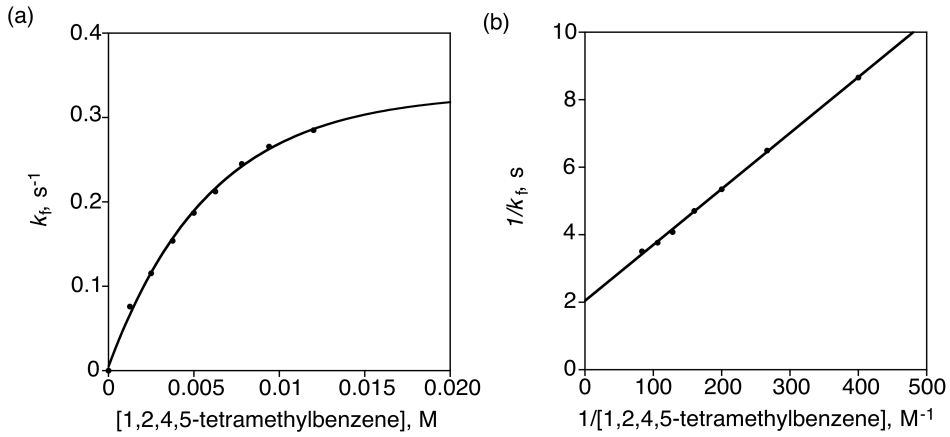

Figure 29. (a) Plot of pseudo-first-order rate constant (k_f) vs concentration of 1,2,4,5-tetramethylbenzene in oxidation of 1,2,4,5-tetramethylbenzene with $[Fe^{IV}(O)(N4Py)]^{2+}$ (0.25 mM) in the presence of HOTf (10 mM) in MeCN at 298 K. (b) Plot of $1/k_f$ vs 1/[1,2,4,5-tetramethylbenzene], where the values of slope and intercept were determined to be 1.6×10^{-2} M s and 2.1 s, respectively.

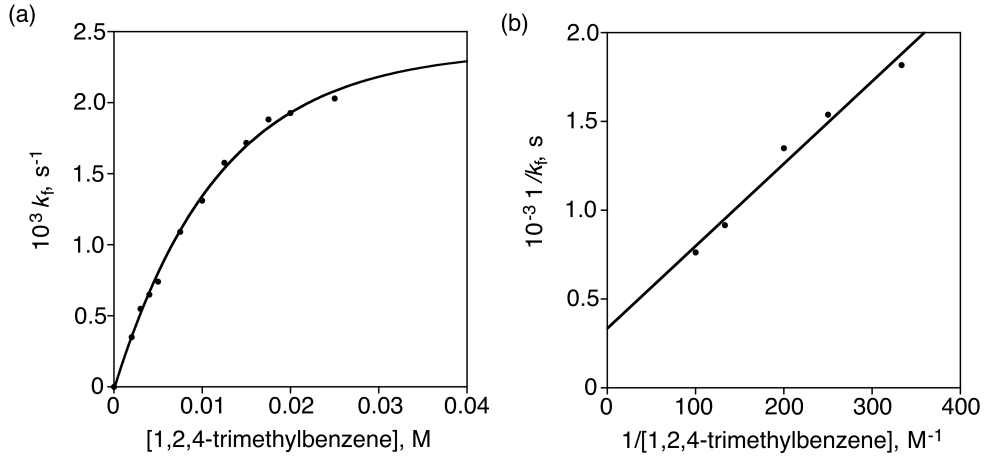

Figure 30. (a) Plot of pseudo-first-order rate constant (k_f) vs concentration of 1,2,4-trimethylbenzene in oxidation of 1,2,4-trimethylbenzene with $[Fe^{IV}(O)(N4Py)]^{2+}$ (0.25 mM) in the presence of HOTf (10 mM) in MeCN at 298 K. (b) Plot of $1/k_f$ vs 1/[1,2,4-trimethylbenzene], where the values of slope and intercept were determined to be 4.0 M s and 3.9×10^2 s, respectively.

The K value of the precursor complexes of $[(N4Py)Fe^{IV}(O)]^{2+}$ with 1,2,4,5-tetramethylbenzene in the presence of 10 mM HOTf (K = 120 M^{-1}) is much larger than that of $[(N4Py)Fe^{IV}(O)]^{2+}$ with the same substrate in the presence of 10 mM $Sc(OTf)_3$ (K = 3.0 M^{-1}). The same trend is observed for other substrates as listed in Table 2. The significantly smaller K values with $Sc(OTf)_3$ (10 mM) than those with HOTf (10 mM) may be ascribed to the large steric effect of two molecules of $Sc(OTf)_3$ bound to $[(N4Py)Fe^{IV}(O)]^{2+}$ as compared with that of HOTf. In each case, the K values

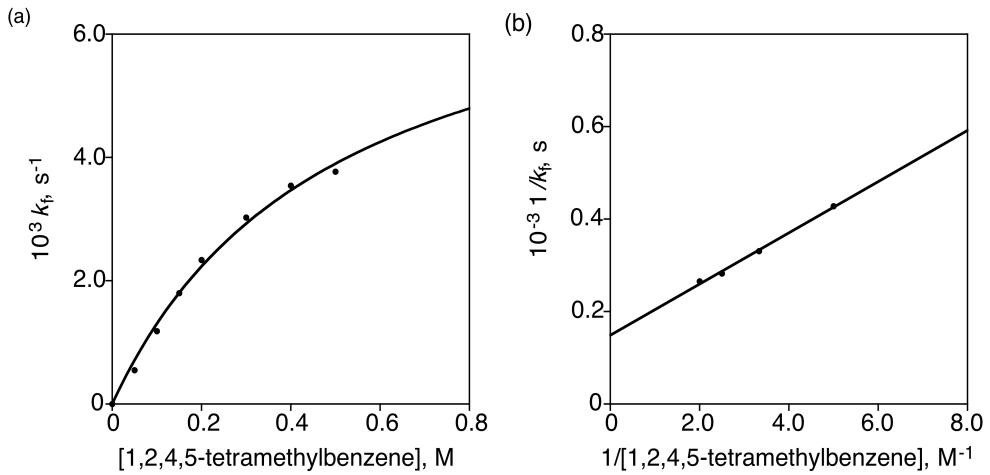

Figure 31. (a) Plot of pseudo-first-order rate constant (k_f) vs concentration of 1,2,4,5-tetramethylbenzene in oxidation of 1,2,4,5-tetramethylbenzene with $[Fe^{IV}(O)(N4Py)]^{2+}$ (0.25 mM) in the presence of $Sc(OTf)_3$ (10 mM) in MeCN at 298 K. (b) Plot of $1/k_f$ vs 1/[1,2,4,5-tetramethylbenzene], where the values of slope and intercept were determined to be 5.0 × 10 M s and 1.5 × 10^2 s, respectively.

are significantly larger than those employed for outer-sphere electron-transfer reactions of coordinatively saturated metal complexes (K = ca. 0.020 M^{-1}).

Although K values may be changed depending on the E_{ox} values of toluene and thioanisole derivatives, the k_{ET} values were evaluated by using averaged K values with HOTf [(9 ± 2) × 10 M^{-1}] and $Sc(OTf)_3$ (2.8 ± 0.2 M^{-1}) in Table 3. Figure 32 shows unified plots of log k_{ET} of PCET and MCET from electron donors to $[(N4Py)Fe^{IV}(O)]^{2+}$ in the presence of HOTf (10 mM) and $Sc(OTf)_3$ (10 mM). The driving force dependence of log k_{ET} (or log k_{obs}) of PCET from all kinds of electron donors (coordinatively saturated metal complexes, toluene and thioanisole derivatives) to $[(N4Py)Fe^{IV}(O)]^{2+}$ in the presence of HOTf (10 mM) in MeCN at 298 K is unified as a red line together with that of log k_{ET} of electron transfer from coordinatively saturated metal complexes to $[(N4Py)Fe^{IV}(O)]^{2+}$ in the absence of HOTf using the same λ value of 2.74 eV.[41] The driving force dependence of log k_{ET} of MCET from all kinds of electron donors to $[(N4Py)Fe^{IV}(O)]^{2+}$ in the presence of $Sc(OTf)_3$ (10 mM) in MeCN at 298 K is also unified as a blue line using the same λ value of 2.27 eV. When the driving forces of MCET [($Sc(OTf)_3$) and PCET (HOTf) are more negative than –0.5 eV, the k_{ET} values become larger than those predicted by the Marcus lines (Figure 32). The smaller λ value of the MCET (2.27 eV) than that of the PCET (2.74 eV) may be ascribed to the smaller change in the Fe–O distance associated with the MCET than that with the PCET

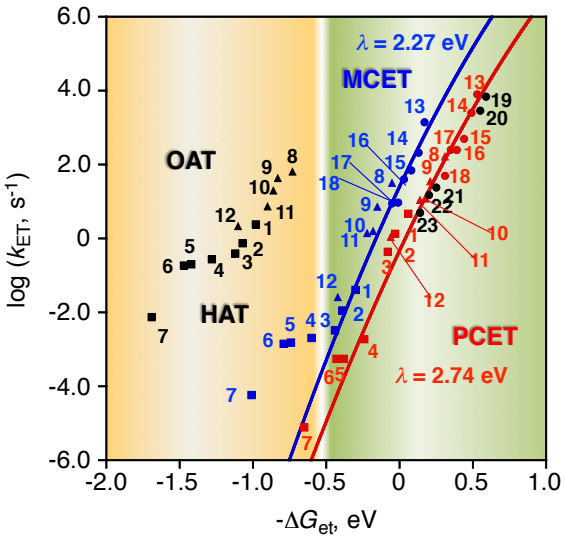

Figure 32. Plots of log k_{ET} for C–H bond cleavage of toluene derivatives and sulfoxidation of thioanisole derivatives [(1) hexamethylbenzene, (2) 1,2,3,4,5-tetramethylbenzene, (3) 1,2,4,5-tetramethylbenzene, (4) 1,2,4-trimethylbenzene, (5) 1,4-dimethylbenzene, (6) 1,3,5-trimethylbenzene, (7) toluene, (8) *p*-Me-thioaniosle, (9) *p*-H-thioanisole, (10) *p*-Cl-thioanisole, (11) *p*-Br-thioanisole and (12) *p*-CN-thioanisole] by $[(N4Py)Fe^{IV}(O)]^{2+}$ in the absence (black) and presence of acids (10 mM), HOTf (red) and $Sc(OTf)_3$ (blue), in MeCN at 298 K vs the driving force of electron transfer [$-\Delta G = e(E_{red} - E_{ox})$] from toluene derivatives (squares) and thioanisole derivatives (triangles) to $[(N4Py)Fe^{IV}(O)]^{2+}$ in the presence of HOTf (red) and $Sc(OTf)_3$ (blue). The red and blue circles show the driving force dependence of the rate constants (log k_{et}) of electron transfer from electron donors [(13) $[Fe^{II}(Ph_2Phen)_3]^{2+}$, (14) $[Fe^{II}(bpy)_3]^{2+}$, (15) $[Ru^{II}(4,4'\text{-}Me_2Phen)_3]^{2+}$, (16) $[Ru^{II}(5,5'\text{-}Me_2Phen)_3]^{2+}$, (17) $[Fe^{II}(ClPhen)_3]^{2+}$ and (18) $[Ru^{II}(bpy)_3]^{2+}$] to $[(N4Py)Fe^{IV}(O)]^{2+}$ in the presence of acids (10 mM), HOTf and $Sc(OTf)_3$, in MeCN at 298 K, respectively. The black circles show the driving force dependence of the rate constants (log k_{et}) of electron transfer from electron donors [(19) decamethylferrocene, (20) octamethylferrocene, (21) 1.1'-dimethylferrocene, (22) *n*-amylferrocene and (23) ferrocene] to $[(N4Py)Fe^{IV}(O)]^{2+}$ in the absence of acids in MeCN at 298 K.[41]

at the same concentration of acids probably due to the steric effect of two molecules of $Sc(OTf)_3$ bound to the oxo group.

The unified correlations of driving force dependence of log k_{ET} of PCET and MCET from all kinds of electron donors to $[(N4Py)Fe^{IV}(O)]^{2+}$ in Figure 32 indicate that oxidation of toluene and thioanisole derivatives by $[(N4Py)Fe^{IV}(O)]^{2+}$ in the presence of HOTf and $Sc(OTf)_3$ proceeds via the rate-determining electron transfer from toluene and thioanisole derivatives to $[(N4Py)Fe^{IV}(O)]^{2+}$ which binds with two molecules of

$Sc(OTf)_3$ and HOTf, respectively, following formation of the precursor complexes as shown in Scheme 1, provided that the driving force of the electron transfer is larger than –0.5 eV. In the case of oxidation of toluene derivatives by $[(N4Py)Fe^{IV}(O)]^{2+}$ in the presence of HOTf and $Sc(OTf)_3$, the rate-determining PCET and MCET may be followed by rapid proton transfer and the oxygen rebound to produce the corresponding benzyl alcohol derivatives and $[(N4Py)Fe^{II}]^{2+}$, which is oxidized by $[(N4Py)Fe^{IV}(O)]^{2+}$ to $[(N4Py)Fe^{II}]^{2+}$ in the presence of HOTf and $Sc(OTf)_3$. In the case of oxidation of thioanisole derivatives by $[(N4Py)Fe^{IV}(O)]^{2+}$ in the presence of HOTf and $Sc(OTf)_3$, the PCET and MCET may be followed by rapid $O^{\bullet-}$ transfer to produce the corresponding sufoxide derivatives and $[(N4Py)Fe^{II}]^{2+}$, which is also oxidized by $[(N4Py)Fe^{IV}(O)]^{2+}$ to $[(N4Py)Fe^{III}]^{2+}$ in the presence of HOTf and $Sc(OTf)_3$. However, the detailed mechanism after the rate-determining PCET and MCET has yet to be clarified.

In the absence of HOTf or $Sc(OTf)_3$, the k_{ox} values of oxidation of toluene and thioanisole derivatives by $[(N4Py)Fe^{IV}(O)]^{2+}$ are much larger than those predicted from PCET or MCET reactions (black points in Figure 32). Thus, C–H bond cleavage of toluene derivatives and sulfoxidation of thioanisole derivatives proceed via direct hydrogen atom transfer from toluene derivatives to $[(N4Py)Fe^{IV}(O)]^{2+}$ and oxygen atom transfer from thioanisole derivatives to $[(N4Py)Fe^{IV}(O)]^{2+}$, respectively, rather an than electron-transfer pathway.

Scheme 1. Proposed Unified Mechanism of Oxidation of Toluene and Thioanisol Derivatives by $[(N4Py)Fe^{IV}(O)]^{2+}$ in the Presence of HOTf and $Sc(OTf)_3$

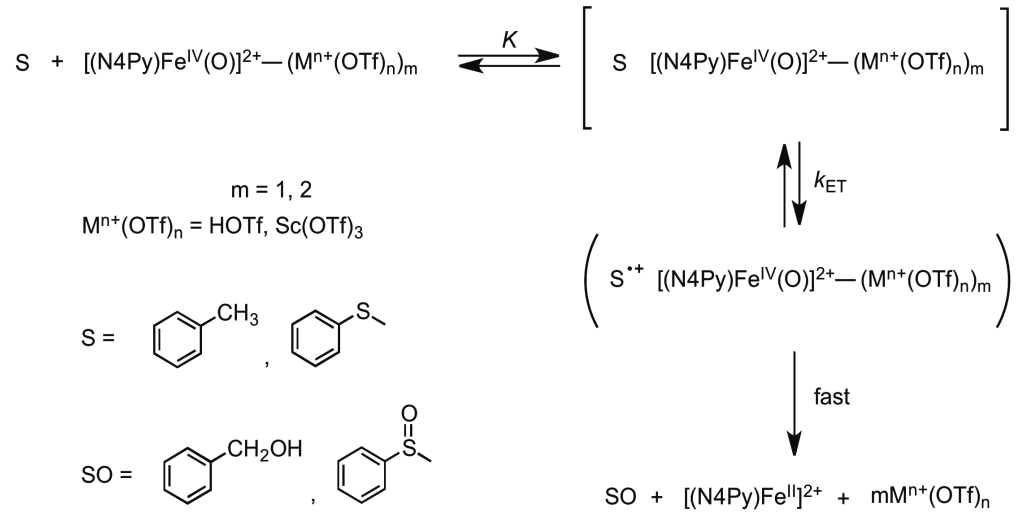

Conclusion

Oxidation of toluene and thioanisole derivatives by $[(N4Py)Fe^{IV}(O)]^{2+}$ in deaerated MeCN at 298 K was remarkably accelerated by the presence of HOTf and $Sc(OTf)_3$ to yield stoichiometric amount of the corresponding benzyl alcohol and sulfoxide derivatives, respectively. No KIE was observed when toluene was replaced by toluene-d_8 for the oxidation by $[(N4Py)Fe^{IV}(O)]^{2+}$ in the presence of HOTf, suggesting that the rate-determining step is PCET from toluene to $[(N4Py)Fe^{IV}(O)]^{2+}$. An inverse KIE was observed for PCET from both $[Ru^{II}(bpy)_3]^{2+}$ and toluene to $[(N4Py)Fe^{IV}(O)]^{2+}$ when HOTf was replaced by DOTf, suggesting that the O–H bond of the protonated $Fe^{IV}(O)$ complex at the transition state of PCET is significantly stronger than that of the ground state. The unified correlations of driving force ($-\Delta G_{et}$) dependence of log k_{ET} of oxidation of toluene and thioanisole derivatives by $[(N4Py)Fe^{IV}(O)]^{2+}$ as well as electron transfer from coordinatively saturated metal complexes to $[(N4Py)Fe^{IV}(O)]^{2+}$ in the presence of HOTf and $Sc(OTf)_3$ (Figure 32) indicate that oxidation of toluene and thioanisole derivatives by $[(N4Py)Fe^{IV}(O)]^{2+}$ in the presence of HOTf and $Sc(OTf)_3$ proceeds via the rate-determining PCET and MCET, respectively. Remarkable enhancement of PCET and MCET reactivity of $[(N4Py)Fe^{IV}(O)]^{2+}$ results from binding of two molecules of HOTf and $Sc(OTf)_3$ to the oxo group of the $Fe^{IV}(O)$ complex, which caused large positive shifts of the E_{red} values in the presence of HOTf and $Sc(OTf)_3$, respectively. Formation of strong precursor complexes of $[(N4Py)Fe^{IV}(O)]^{2+}$, which binds with two molecules of HOTf and $Sc(OTf)_3$, with organic substrates (toluene and thioanisole derivatives) as compared with coordinatively saturated metal complexes also results in enhancement of the PCET and MCET reactivity. A boundary between electron transfer vs concerted pathways is determined by the driving force of electron transfer ($-\Delta G_{et}$). PCET and MCET pathways are dominant when $-\Delta G_{et} > -0.5$ eV, whereas concerted pathways become dominant when $-\Delta G_{et} < -0.5$ eV. The unified view of enhancement of oxidative C–H bond cleavage of toluene derivatives and sulfoxidation of thioanisole derivatives by a nonheme iron(IV)-oxo complex via PCET and MCET demonstrated in this study provides generalized understanding of a variety of PCET and MCET pathways for oxidation of substrates by metal-oxygen species.

References

(1) (a) Ortiz de Montellano, P. R. *Cytochrome P450: Structure, Mechanism, and Biochemistry*, 3rd ed.; Kluwer Academic/Plenum Publishers: New York, 2005. (b) Meunier, B., Ed. *Biomimetic Oxidations Catalyzed by Transition Metal Complexes*; Imperial College Press: London, 2000. (c) *The Ubiquitous Role of Cytochrome P450 Proteins In Metal Ions in Life Sciences*; Sigel, A., Sigel, H., Sigel, R. K. O., Eds.; John Wiley & Sons Ltd: Chichester, England, 2007; Vol. 3. (d) Grinkova, Y. V.; Denisov, I. G.; McLean, M. A.; Sligar, S. G. *Biol. Biophys. Res. Comm.* **2013**, *430*, 1223.

(2) (a) Sharma, V. K. Oxidation of Amino Acis, Peptides, and Protenins; John Wiley & Sons Ltd: Chichester, England, 2012. (b) Sono, M.; Roach, M. P.; Coulter, E. D.; Dawson, J. H. *Chem. Rev*. **1996**, *96*, 2841. (c) Watanabe, Y. *J. Biol. Inorg. Chem*. 2001, *6*, 846. (d) Jung, C. *Biochim. Biophys. Acta* **2011**, *1814*, 46.

(3) Rohde, J.-U.; In, J.-H.; Lim, M. H.; Brennessel, W. W.; Bukowski, M. R.; Stubna, A.; Münck, E.; Nam, W.; Que, L., Jr. *Science* **2003**, *299*, 1037.

(4) (a) Usharani, D.; Lacy, D. C.; Borovik, A. S.; Shaik, S. *J. Am. Chem. Soc.* **2013**, *135*, 17090. (b) de Visser, S. P.; Rohde, J.-U.; Lee, Y.-M.; Cho, J.; Nam, W. *Coord. Chem. Rev.* **2013**, *257*, 381. (c) McDonald, A. R.; Que, L., Jr. *Coord. Chem. Rev.* **2013**, *257*, 414.

(5) (a) Meunier, B.; de Visser, S. P.; Shaik, S. *Chem. Rev.* **2004**, *104*, 3947. (b) Shaik, S.; Cohen, S.; Wang, Y.; Chen, H.; Kumar, D.; Thiel, W. *Chem. Rev*. **2010**, *110*, 949. (c) Abu-Omar, M. M.; Loaiza, A.; Hontzeas, N. *Chem. Rev.* **2005**, *105*, 2227. (d) Denisov, I. G.; Makris, T. M.; Sligar, S. G.; Schlichting, I. *Chem. Rev.* **2005**, *105*, 2253. (e) Ortiz de Montellano, P. R. *Chem. Rev*. **2010**, *110*, 932.

(6) (a) Bakac, A. *Coord. Chem. Rev*. **2006**, *250*, 2046. (b) Arias, J.; Newlands, C. R.; Abu-Omar, M. M. *Inorg. Chem*. **2001**, *40*, 2185. (c) Sarauli, D.; Meier, R.; Liu, G.-F.; Ivanović-Burmazović, I.; van Eldik, R. *Inorg. Chem*. **2005**, *44*, 7624.

(7) Hayashi, H.; Fujinami, S.; Nagatomo, S.; Ogo, S.; Suzuki, M.; Uehara, A.; Watanabe, Y.; Kitagawa, T. *Inorg. Chim. Acta* **2000**, *300-302*, 587.

(8) Das, D.; Sarkar, B.; Kumar Mondal, T.; Mobin, S. M.; Fiedler, J.; Kaim, W.; Kumar Lahiri, G. *Inorg. Chem*. **2011**, *50*, 7090.

(9) (a) Groves, J. T.; Shalyaev, K.; Lee, J. In *The Porphyrin Handbook*; Kadish, K. M., Smith, K. M., Guilard, R., Eds.; Academic Press: Elsevier Science (USA),

2000, Vol. 4, pp 17-40. (b) Watanabe, Y. In *The Porphyrin Handbook*; Kadish, K. M., Smith, K. M., Guilard, R., Eds.; Academic Press: Elsevier Science (USA), 2000, Vol. 4, pp 97-117. (c) Groves, J. T. *J. Inorg. Biochem*. **2006**, *100*, 434.

(10) (a) Gunay, A.; Theopold, K. H. *Chem. Rev*. **2010**, *110*, 1060. (b) Che, C.-M.; Lo, V. K.-Y.; Zhou, C.-Y.; Huang, J.-S. *Chem. Soc. Rev*. **2011**, *40*, 1950. (c) Costas, M. *Coord. Chem. Rev*. **2011**, *255*, 2912.

(11) (a) Cho, K.; Leeladee, P.; McGown, A. J.; DeBeer, S.; Goldberg, D. P. *J. Am. Chem. Soc*. **2012**, *134*, 7392. (b) Cho, K.-B.; Chen, H.; Janardanan, D.; de Visser, S. P.; Shaik, S.; Nam, W. *Chem. Commun*. **2012**, *48*, 2189. (c) Seo, M. S.; Kim, N. H.; Cho, K.-B.; So, J. E.; Park, S. K.; Clemancey, M.; Garcia-Serres, R.; Latour, J.-M.; Shaik, S.; Nam, W. *Chem. Sci*. **2011**, *2*, 1039. (d) Borovik, A. S. *Chem. Soc. Rev*. **2011**, *40*, 1870. (e) Janardanan, D.; Wang, Y.; Schyman, P.; Que, L., Jr.; Shaik, S. *Angew. Chem., Int. Ed.* **2010**, *49*, 3342.

(12) (a) Shail, S.; Chen, H.; Janardanan, D. *Nature Chem*. **2011**, *3*, 19. (b) Chen, H.; Lai, W.; Shaik, S. *J. Phys. Chem. Lett*. **2010**, *1*, 1533.

(13) (a) Krebs, C.; Fujimori, D. G.; Walsh, C. T.; Bollinger, J. M., Jr. *Acc. Chem. Res.* **2007**, *40*, 484. (b) Que, L., Jr. *Acc. Chem. Res*. **2007**, *40*, 493. (c) Nam, W. *Acc. Chem. Res.* **2007**, *40*, 522. (d) Borovik, A. S. *Acc. Chem. Res.* **2005**, *38*, 54. (e) Shaik, S.; Lai, W.; Chen, H.; Wang, Y. *Acc. Chem. Res*. **2010**, *43*, 1154.

(14) Hong, S.; Lee, Y.-M.; Cho, K.-B.; Sundaravel, K.; Cho, J.; Kim, M. J.; Shin, W.; Nam, W. *J. Am. Chem. Soc*. **2011**, *133*, 11876.

(15) Tang, H.; Guan, J.; Zhang, L.; Liu, H.; Huang, X. *Phys. Chem. Chem. Phys.* **2012**, *14*, 12863.

(16) Kumar, D.; Sastry, G. N.; de Visser, S. P. *J. Phys. Chem. B*, **2012**, *116*, 718.

(17) (a) Groves, J. T.; McClusky, G. A. *J. Am. Chem. Soc.* **1976**, *98*, 859. (b) Ortiz de Montellano, P. R.; Stearns, R. A. *J. Am. Chem. Soc.* **1987**, *109*, 3415. (c) Schöoneboom, J. C.; Cohen, S.; Lin, H.; Shaik, S.; Thiel, W. *J. Am. Chem. Soc.* **2004**, *126*, 4017. (d) Hirao, H.; Kumar, D.; Que, L., Jr.; Shaik, S. *J. Am. Chem. Soc*. **2006**, *128*, 8590.

(18) Chiavarino, B.; Cipollini, R.; Crestoni, M. E.; Fornarini, S.; Fornarini, S.; Lapi, A. *J. Am. Chem. Soc.* **2008**, *130*, 3208.

(19) Kaizer, J.; Klinker, E. J.; Oh, N. Y.; Rohde, J.-U.; Song, W. J.; Stubna, A.; Kim, J.; Münck, E.; Nam, W.; Que, L., Jr. *J. Am. Chem. Soc.* **2004**, *126*, 472.

(20) (a) Park, M. J.; Lee, J.; Suh, Y.; Kim, J.; Nam, W. *J. Am. Chem. Soc.* **2006**, *128*, 2630. (b) Sastri, C. V.; Lee, J.; Oh, K.; Lee, Y. J.; Lee, J.; Jackson, T. A.; Ray, K.; Hirao, H.; Shin, W.; Halfen, J. A.; Kim, J.; Que, L., Jr.; Shaik, S.; Nam, W. *Proc. Natl. Acad. Sci. U. S. A.* **2007**, *104*, 19181. (c) Jeong, Y. J.; Kang, Y.; Han, A.-R.; Lee, Y.-M.; Kotani, H.; Fukuzumi, S.; Nam, W. *Angew. Chem., Int. Ed.* **2008**, *47*, 7321. (d) Lee, Y.-M.; Dhuri, S. N.; Sawant, S. C.; Cho, J.; Kubo, M.; Ogura, T.; Fukuzumi, S.; Nam, W. *Angew. Chem., Int. Ed.* **2009**, *48*, 1803.

(21) (a) Lee, Y.-M.; Hong, S.; Morimoto, Y.; Shin, W.; Fukuzumi, S.; Nam, W. *J. Am. Chem. Soc*. **2010**, *132*, 10668. (b) Wilson, S. A.; Chen, J.; Hong, S.; Lee, Y.-M.; Clémancey, M.; Garcia-Serres, R.; Nomura, T.; Ogura, T.; Latour, J.-M.; Hedman, B.; Hodfson, K. O.; Nam, W.; Solomon, E. I. *J. Am. Chem. Soc*. **2012**, *134*, 11791.

(22) (a) Yiu, S.-M.; Man, W.-L.; Lau, T.-C. *J. Am. Chem. Soc.* **2008**, *130*, 10821. (b) Lam, W. W. Y.; Yiu, S.-M.; Lee, J. M. N.; Yau, S. K. Y.; Kwong, H.-K.; Lau, T.-C.; Liu, D.; Lin, Z. *J. Am. Chem. Soc.* **2006**, *128*, 2851. (c) Yiu, S.-M.; Wu, Z.-B.; Mak, C.-K.; Lau, T.-C. *J. Am. Chem. Soc.* **2004**, *126*, 14921.

(23) (a) Fukuzumi, S.; Morimoto, Y.; Kotani, H.; Naumov, P.; Lee, Y.-M.; Nam, W. *Nature Chem.* **2010**, *2*, 756. (b) Morimoto, Y.; Kotani, H.; Park, J.; Lee, Y.-M.; Nam, W.; Fukuzumi, S. *J. Am. Chem. Soc*. **2011**, *133*, 403. (c) Park, J.; Morimoto, Y.; Lee, Y.-M.; Nam, W.; Fukuzumi, S. *J. Am. Chem. Soc.* **2011**, *133*, 5236. (d) Park, J.; Morimoto, Y.; Lee, Y.-M.; You, Y.; Nam, W.; Fukuzumi, S. *Inorg. Chem.* **2011**, *50*, 11612.

(24) Morimoto, Y.; Park, J.; Suenobu, T.; Lee, Y.-M.; Nam, W.; Fukuzumi, S. *Inorg. Chem.* **2012**, *51*, 10025.

(25) Park, J.; Morimoto, Y.; Lee, Y.-M.; Nam, W.; Fukuzumi, S. *J. Am. Chem. Soc.* **2012**, *134*, 3903.

(26) Park, J.; Lee, Y.-M.; Nam, W.; Fukuzumi, S. *J. Am. Chem. Soc.* **2013**, *135*, 5052.

(27) Armarego, W. L. F.; Chai, C. L. L. *Purification of Laboratory Chemicals*, 6th ed.; Pergamon Press: Oxford, 2009.

(28) Lubben, M.; Meetsma, A.; Wilkinson, E. C.; Feringa, B.; Que, L., Jr. *Angew. Chem., Int. Ed*. **1995**, *34*, 1512.

(29) *Organic Syntheses*; Saltzman, H.; Sharefkin, J. G., Eds.; Wiley: New York, 1973; Vol. V, p 658.

(30) (a) Lin, C.T.; Bottcher, W.; Chou, M; Creuts, C; Sutin, N. *J. Am. Chem. Soc*. **1976**, *98*, 6536. (b) Fussa-Rydel, O.; Zhang, H. T.; Hupp, J. T.; Leidnert, C. R. *Inorg. Chem*. **1989**, *28*, 1533. (c) Leidner, C. R.; Murray, R. W. *J. Am. Chem. Soc*. **1984**, 106, 1606.

(31) Fukuzumi, S.; Ohkubo, K.; Suenobu, T.; Kato, K.; Fujitsuka, M.; Ito, O. *J. Am. Chem. Soc*. **2001**, *123*, 8459.

(32) Skarda, V.; Cook, M. J.; Lewis, A. P.; McAuliffe, G. S. G.; Thomson, A. J. *J. Chem. Soc. Perkin Trans*. **1984**, 1309.

(33) Kwart, H. *Acc. Chem. Res.* **1982**, *15*, 401.

(34) (a) Price, J. C.; Barr, E. W.; Glass, T. E.; Krebs, C.; Bollinger, J. M., Jr. *J. Am. Chem. Soc*. **2003**, *125*, 13008. (b) Wu, A.; Mayer, J. M. *J. Am. Chem. Soc.* **2008**, *130*, 14745.

(35) (a) Kohen, A.; Klinman, J. P. *Acc. Chem. Res*. **1998**, *31*, 397. (b) Knapp, M. J.; Rickert, K.; Klinman, J. P. *J. Am. Chem. Soc*. **2002**, *124*, 3865. (c) Klinman, J. P. *Biochim. Biophys. Acta, Bioenergetics* **2006**, *1757*, 981. (d) McCusker, K. P.; Kilnman, J. P. *J. Am. Chem. Soc*. **2010**, *132*, 5114.

(36) Fukuzumi, S.; Kobayashi, T.; Suenobu, T. *J. Am. Chem. Soc*. **2010**, *132*, 1496.

(37) (a) Parkin, G. *Acc. Chem. Res*. **2009**, *42*, 315. (b) Kotani, H.; Hanazaki, R.; Ohkubo, K.; Yamada, Y.; Fukuzumi, S. *Chem.–Eur. J*. **2011**, *17*, 2777

(38) (*a*) Wolfsberg, M. *Acc. Chem. Res*. **1972**, *5*, 225; (*b*) Parkin, G. *Acc. Chem. Res.* **2009**, *42*, 315.

(39) Tanner, M. J.; Brookhart, M.; DeSimone, J. M. *J. Am. Chem. Soc*. **1997**, *119*, 7617.

(40) (a) Fukuzumi, S.; Ohkubo, K. *J. Am. Chem. Soc*. **2002**, *124*, 10270. (b) Fukuzumi, S.; Ohkubo, K. *Chem.–Eur. J*. **2000**, *6*, 4532.

(41) Lee, Y.-M.; Kotani, H.; Suenobu, T.; Nam, W.; Fukuzumi, S. *J. Am. Chem. Soc*. **2008**, *130*, 434.

(42) The one-electron reduction potentials of $[(N4Py)Fe^{IV}(O)]^{2+}$ (E_{red}) in the presence of acids may also have linear correlation with the quantitative measure of the Lewis acidity of acids, although the E_{red} values in the presence of other metal trifrates have not been determined.[23b]

(43) (a) Marcus, R. A. *Annu. Rev. Phys. Chem*. **1964**, *15*, 155. (b) Marcus, R. A. *Discuss. Faraday Soc*. **1960**, *29*, 129. (c) Marcus, R. A. *Angew. Chem., Int. Ed. Engl*. **1993**, *32*, 1111.

(44) (a) Sutin, N. *Acc. Chem. Res*. **1968**, *1*, 225. (b) Sutin, N. *Adv. Chem. Phys*. **1999**, *106*. 7. (c) Chou, M.; Creutz, C.; Sutin, N. *J. Am. Chem. Soc*. **1977**, *99*, 5615. (d) Keeney, L.; Hynes, M. J. *Dalton Trans*. **2005**, 133.

(45) (a) Fukuzumi, S.; Honda, T.; Kojima, T. *Coord. Chem. Rev*. **2012**, *256*, 2488. (b) Fukuzumi, S.; Karlin, K. D. *Coord. Chem. Rev*. **2012**, *257*, 187. (c) Tahsini, L.; Kotani, H.; Lee, Y.-M.; Cho, J.; Nam, W.; Karlin, K. D.; Fukuzumi, S. *Chem.–Eur. J.* **2012**, *18*, 1084. (d) Yoon, H.; Morimoto, Y.; Lee, Y.-M.; Nam, W.; Fukuzumi, S. *Chem. Commun*. **2012**, *48*, 11187.

(46) (a) Takai, A.; Gros, C. P.; Barbe, J.-M.; Guilard, R.; Fukuzumi, S. *Chem.–Eur. J.* **2009**, *15*, 3110. (b) Nakanishi, T.; Ohkubo, K.; Kojima, T.; Fukuzumi, S. *J. Am. Chem. Soc.* **2009**, *131*, 577. (c) Murakami, M.; Ohkubo, K.; Fukuzumi, S. *Chem.–Eur. J*. **2010**, *16*, 7820.

(47) (a) Fukuzumi, S.; Nakanishi, I.; Tanaka, K.; Suenobu, T.; Tabard, A.; Guilard, R.; Van Caemelbecke, E.; Kadish, K. M. *J. Am. Chem. Soc.* **1999**, *121*, 785. (b) Fukuzumi, S.; Mochizuki, S.; Tanaka, T. *Inorg. Chem*. **1989**, *28*, 2459.

Chapter 6. Efficient Oxidation of Styrene Derivatives by a Nonheme Iron(IV)-Oxo Complex via Proton-Coupled Electron Transfer with Triflic Acid

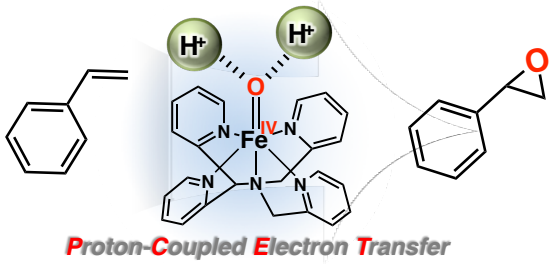

Abstract: No oxidation of styrene derivatives by $[(N4Py)Fe^{IV}(O)]^{2+}$ (N4Py = *N*,*N*-bis(2-pyridylmethyl)-*N*-bis(2-pyridyl)methylamine) occurs in acetonitrile at 298 K, whereas efficient oxidation of styrene derivatives was made possible by the presence of triflic acid (HOTf). The acid–promoted oxidation of alkenes by $[(N4Py)Fe^{IV}(O)]^{2+}$ proceeds via proton-coupled electron transfer (PCET) from alkenes to the diprotonated species of $[(N4Py)Fe^{IV}(O)]^{2+}$ with HOTf. The PCET reactivity is well analyzed in light of the Marcus theory of electron transfer from various electron donors to the diprotonated species of $[(N4Py)Fe^{IV}(O)]^{2+}$.

Introduction

There are nonheme iron enzymes that can catalyze substrate oxidations similar to those by heme enzymes (e.g. cytochrome P450).[1,2] Inspired by these enzymes, extensive efforts have been devoted in developing biomimetic iron porphyrin catalysts[3,4] and also in the design of new families of nonheme iron catalysts.[5-7] Nonheme catalysts catalyze not only epoxidation but also *cis*-dihydroxylation of olefins.[8,9] The olefin epoxidation and *cis*-dihydroxylation are in closely related transformations that have been carried out by a HO-Fe^{V}(O) oxidant.[10] Addition of acetic acid to some nonheme iron-catalyzed olefin oxidation reactions has been reported to result in an increase in both catalytic activity and selectivity toward epoxidation.[11,12] The acetic acid-enhanced olefin epoxidation with [(TPA)$Fe(OTf)_2$] (TPA = tris(2-pyridylmethyl)amine, OTf^{-} = triflate) has been proposed to be mediated by [(TPA)Fe^{V}(O)$(OOCCH_3)$]$^{2+}$, generated from O–O bond heterolysis of the [(TPA)Fe^{III}(OOH)(CH_3COOH)]$^{2+}$ intermediate, which is promoted by the protonation of the terminal oxygen atom of the hydroperoxide by the coordinated carboxylic acid.[12] Peracetic acid used as an acid as well as an oxidant has also been reported to promote olefin epoxidation.[13] Perchloric acid and triflic acid have been reported to remarkably promote oxidation of toluene and thioanisole derivatives by a nonheme iron(IV)-oxo complex, [(N4Py)Fe^{IV}(O)]$^{2+}$ (N4Py = *N*,*N*-bis(2-pyridyl methyl)-*N*-bis(2-pyridyl)methyl- amine).[14-16] However, there has been no report on acid–promoted oxidation of olefins by a nonheme iron(IV)-oxo complex.

We report herein that efficient oxidation of styrene derivatives by [(N4Py)Fe^{IV}(O)]$^{2+}$ occurs by addition of triflic acid (HOTf) in acetonitrile (MeCN) at 298 K although [(N4Py)Fe^{IV}(O)]$^{2+}$ has no ability to oxidize styrene derivatives without HOTf under the same reaction conditions. The mechanisms of HOTf–promoted oxidation of styrene derivatives is clarified by comparing the reactivity of [(N4Py)Fe^{IV}(O)]$^{2+}$ toward styrene derivatives in the presence of HOTf with that of proton–coupled electron transfer (PCET) from various electron donors to [(N4Py)Fe^{IV}(O)]$^{2+}$ with HOTf in light of the Marcus theory of electron transfer.[15,17]

Experimental Section

Materials. All chemicals, which were the best available purity, were purchased from Aldrich Chemical Co. and Tokyo Chemical Industry, used without further purification unless otherwise noted. Solvents, such as acetonitrile (MeCN) and diethyl ether, were

dried according to the literature procedures and distilled under Ar prior to use.[18] A nonheme iron(II) complex, $[(N4Py)Fe^{II}(MeCN)](ClO_4)_2$, and its corresponding iron(IV)-oxo complex, $[(N4Py)Fe^{IV}(O)]^{2+}$, were prepared by literature methods.[19] Iodosylbenzene (PhIO) was prepared by a literature method.[20] Triflic acid was purchased from Tokyo Chemical Industry.

Kinetic Studies. Kinetic measurements were performed on a Hewlett Packard 8453 photodiode-array spectrophotometer using a quartz cuvette (path length = 10 mm) at 298 K. The epoxidation of styrene derivatives by $[(N4Py)Fe^{IV}(O)]^{2+}$ carried out and the rates were monitored by spectral changes due to $[(N4Py)Fe^{IV}(O)]^{2+}$ (2.5×10^{-4} M) with various concentrations of styrene derivatives (2.5×10^{-3}–1.0×10^{-1} M) in the absence and presence of acids, HOTf and $Sc(OTf)_3$, in MeCN at 298 K. The rates of oxidation reaction of organic substrates by $[(N4Py)Fe^{IV}(O)]^{2+}$ were monitored by the decay of the absorption band at 695 nm due to $[(N4Py)Fe^{IV}(O)]^{2+}$ (λ_{max} = 695 nm) in the absence and presence of HOTf and $Sc(OTf)_3$ in MeCN. The concentrations of toluene derivatives and thioanisole derivatives were maintained at least more than 10-fold excess of $[(N4Py)Fe^{IV}(O)]^{2+}$ to attain pseudo-first-order conditions.

First-order fitting of the kinetic data allowed us to determine the pseudo-first-order rate constants. The first-order plots were linear for three or more half-lives with the correlation coefficient $\rho > 0.999$. In each case, it was confirmed that the rate constants derived from at least five independent measurements agreed within an experimental error of ±5%. The pseudo-first-order rate constants increased proportionally with increase in concentrations of substrates, from which second-order rate constants were determined.

Product Analysis. Typically, styrene (4.0×10^{-3} M) was added to an MeCN solution containing $[(N4Py)Fe^{IV}(O)]^{2+}$ (4.0×10^{-3} M) in the presence of HOTf (1.0×10^{-2} M) in a vial. Products formed in the oxidation reactions of styrene by $[(N4Py)Fe^{IV}(O)]^{2+}$, which were carried out in the presence of acids under Ar atmosphere in MeCN-d_3 at 298 K, were analyzed by ^{1}H NMR. Quantitative analyses were made on the basis of comparison of ^{1}H NMR spectral integration between products and their authentic samples.

Instrumentation. UV-vis spectra were recorded on a Hewlett Packard 8453

photodiode-array spectrophotometer. The EPR spectra were measured with a JEOL X-band spectrometer (JES-RE1XE). The EPR spectra were recorded under non-saturating microwave power conditions. The magnitude of modulation was chosen to optimize the resolution and the signal-to-noise (S/N) ratio of the observed spectra. The *g* value was calibrated by using a Mn^{2+} marker. ^1H NMR spectra were recorded on a JEOL A-300 spectrometer in CD_3CN.

Results and Discussion

No reaction occurred between $[(N4Py)Fe^{IV}(O)]^{2+}$ and styrene in MeCN at 298 K. However, addition of HOTf (10 mM) to an MeCN solution of $[(N4Py)Fe^{IV}(O)]^{2+}$ and styrene resulted in efficient oxidation of styrene by $[(N4Py)Fe^{IV}(O)]^{2+}$ as shown in Figure 1, where the absorption band at 695 nm due to $[(N4Py)Fe^{IV}(O)]^{2+}$ disappeared

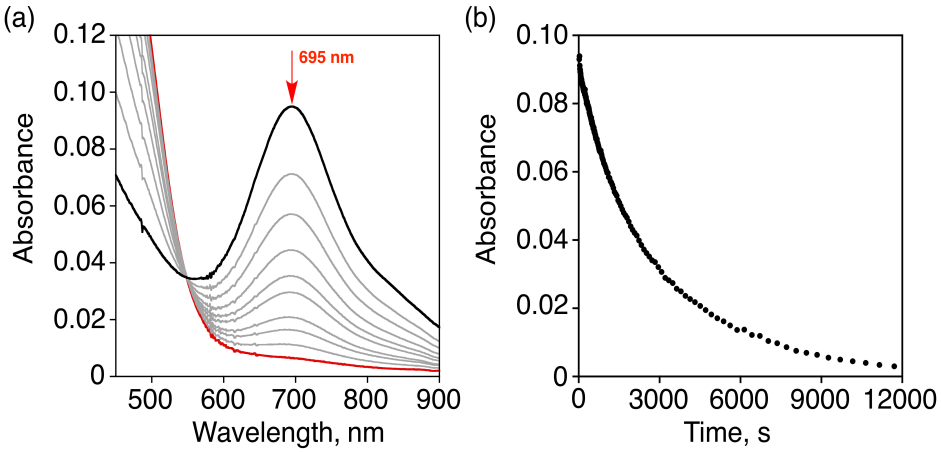

Figure 1. (a) Visible spectral changes observed in oxidation of styrene (5 mM) by $[(N4Py)Fe^{IV}(O)]^{2+}$ (0.25 mM) in the presence of 10 mM of HOTf in MeCN at 298 K. (b) Time course monitored by absorbance at 695 nm due to the decay of $[(N4Py)Fe^{IV}(O)]^{2+}$. The arrow indicates the time of addition of HOTf (10 mM).

upon addition of HOTf. The oxidized products were identified as styrene epoxide (18%) and benzyaldehyde (16%) by ^1H NMR (Figure 2). The reduced product of $[(N4Py)Fe^{IV}(O)]^{2+}$ was $[(N4Py)Fe^{III}]^{3+}$ which was detected by EPR (Figure 3). In such a case, the stoichiometry of the reaction of styrene with $[(N4Py)Fe^{IV}(O)]^{2+}$ in the presence of HOTf to yield styrene epoxide is given by eq 1. Styrene epoxide is further oxidized

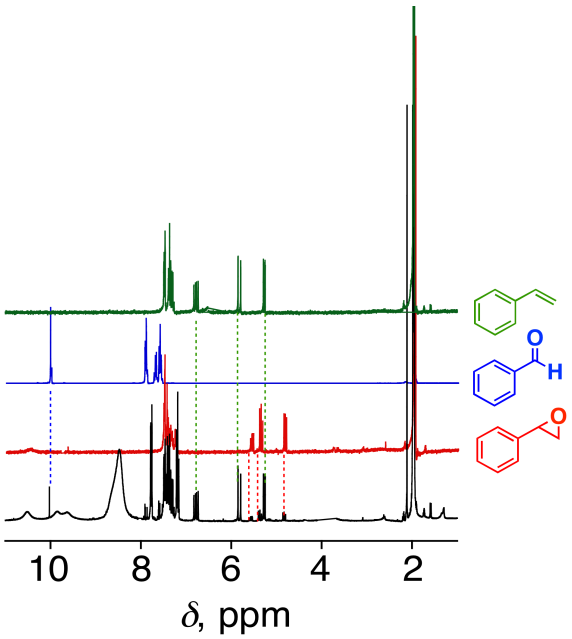

Figure 2. ^{1}H NMR spectrum of the complete reaction solution obtained in oxidation of styrene (4 mM) with $[(N4Py)Fe^{IV}(O)]^{2+}$ (4.0 mM) in the presence of HOTf (10 mM) in CD_3CN at 298 K (black line) under Ar. Red, blue and green lines show ^{1}H NMR spectra of styrene oxide (4.0 mM), benzaldehyde (4.0 mM) and styrene (4.0 mM) in the presence of HOTf (10 mM) as authentic references. The peaks at 4.86, 5.36 and 5.53 ppm agree with that corresponds to -CH- group of styrene oxide in the presence of HOTf (10 mM). The peak at 10 ppm corresponds to that due to benzaldehyde in the presence of HOTf (10 mM). The yield of styrene oxide and benzyl aldehyde produced was 6 ± 1% and 22 ± 2% based on $[(N4Py)Fe^{IV}(O)]^{2+}$ concentration.

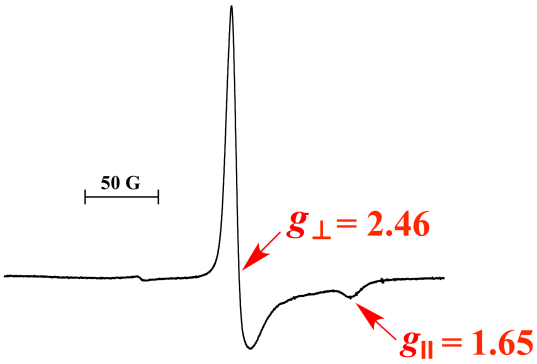

Figure 3. EPR spectrum of the complete reaction solution obtained in oxidation styrene (5.0 mM) with $[(N4Py)Fe^{IV}(O)]^{2+}$ (1.0 mM) in the presence of HOTf (10 mM) in MeCN at 77 K under Ar. The *g* values of EPR active species indicate that the low-spin Fe(III) species due to $[(N4Py)Fe^{III}]^{3+}$ was formed.

$$PhCH{=}CH_2 + 2[(N4Py)Fe^{IV}(O)]^{2+} + 2H^{+} \longrightarrow PhCH(O)CH_2 + 2[(N4Py)Fe^{III}]^{3+} + H_2O \quad (1)$$

$$PhCH(O)CH_2 + 2[(N4Py)Fe^{IV}(O)]^{2+} + 2H^{+} \longrightarrow PhCHO + HCHO + 2[(N4Py)Fe^{III}]^{3+} + H_2O \quad (2)$$

by $[(N4Py)Fe^{IV}(O)]^{2+}$ in the presence of HOTf to yield benzyaldehyde and formaldehyde (eq 2).[21] The maximum yields of styrene epoxide and benzaldehyde based on the oxidant $[(N4Py)Fe^{IV}(O)]^{2+}$ is 6% and 22%, because two and four equivalents of $[(N4Py)Fe^{IV}(O)]^{2+}$ are required to produce styrene oxide and benaldehyde, respectively. The observed yields of styrene oxide (6%) and benzaldehyde (22%) correspond to the complete conversion of $[(N4Py)Fe^{IV}(O)]^{2+}$ to $[(N4Py)Fe^{III}]^{3+}$ ($6 \times 2 + 22 \times 4 = 100\%$).

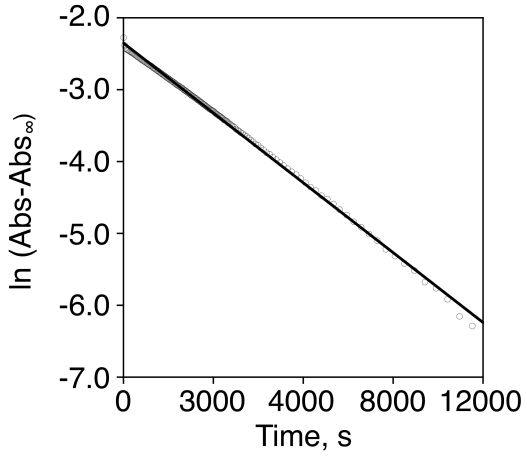

Figure 4. First-order plots of the absorption changes at 695 nm for oxidation of styrene (400 mM) by $[(N4Py)Fe^{IV}(O)]^{2+}$ (0.25 mM) in the presence of HOTf (10 mM) in MeCN at 298 K. Abs and Abs_∞ represent absorbance at the reaction time and the final absorbance at 695 nm, respectively.

The rate of oxidation of styrene by $[(N4Py)Fe^{IV}(O)]^{2+}$ in the presence of HOTf in MeCN, monitored by decrease in absorbance at 695 nm due to $[(N4Py)Fe^{IV}(O)]^{2+}$ (Figure 1b) obeyed first-order kinetics (Figure 4) with large excess styrene and HOTf. The pseudo-first-order rate constant (k_f) increased with increasing concentration of styrene ([S]) to approach constant values as shown in Figure 5. Such a saturation behavior indicates formation of the precursor complex prior to oxidation of styrene, when k_f is given by eq 3,

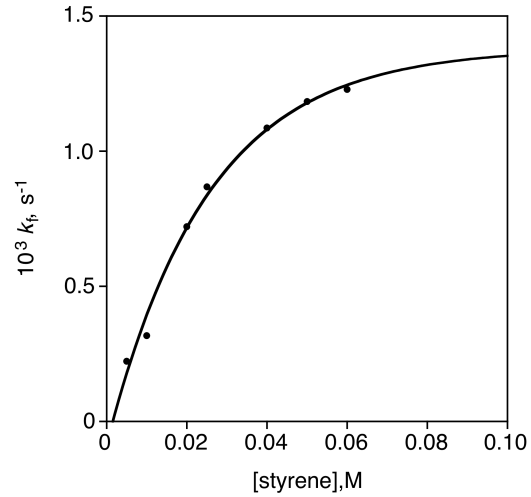

Figure 5. Plot of concentration of styrene vs first-order rate constant (k_f) in the reaction of $[(N4Py)Fe^{IV}(O)]^{2+}$ (0.25 mM) with styrene in the presence of 10 mM of HOTf in MeCN at 298 K.

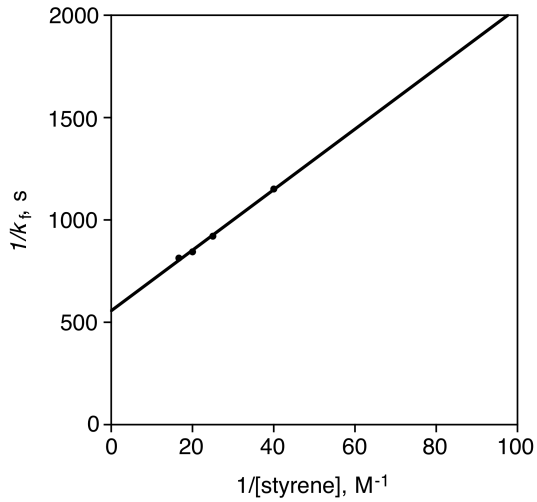

Figure 6. Plot of $1/k_f$ vs 1/[styrene] for oxidation of styrene by $[(N4Py)Fe^{IV}(O)]^{2+}$ in the presence of HOTf (10 mM) in MeCN at 298 K. The slope $[(k_{ET}K)^{-1}]$ and intercept (k_{ET}^{-1}) were determined to be 1.5 × 10 M s and 5.5 × 10^2 s, respectively.

$$k_f = \quad k_{ox}K[S]/(1 + K[S]) \tag{3}$$

$$k_f^{-1} = (k_{ET}K[S])^{-1} + k_{ET}^{-1} \tag{4}$$

where k_{ox} is the first-order rate constant in the precursor complex, K is the formation constant of the precursor complex. Equation 3 is rewritten by eq 4, which predicts a linear correlation between k_f^{-1} and $[S]^{-1}$. From the intercept and slope of the linear plot

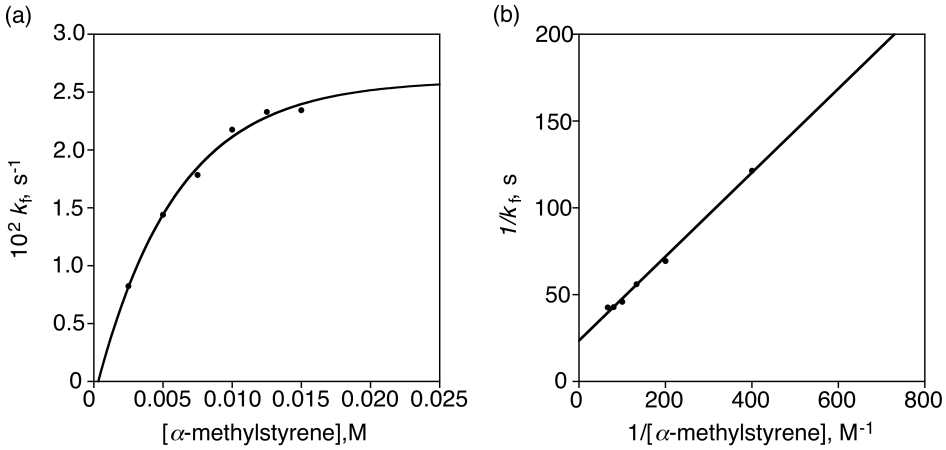

Figure 7. (a) Plot of first-order rate constant (k_f) vs concentration of styrene for oxidation of α-methylstyrene by $[(N4Py)Fe^{IV}(O)]^{2+}$ (0.25 mM) in the presence of 10 mM of HOTf in MeCN at 298 K. (b) Plot of $1/k_f$ vs $1/[\alpha$-methylstyrene] for oxidation of styrene by $[(N4Py)Fe^{IV}(O)]^{2+}$ in the presence of HOTf (10 mM) in MeCN at 298 K. The slope $[(k_{ET}K)^{-1}]$ and intercept (k_{ET}^{-1}) were determined to be 2.5×10^{-1} M s and 2.4 × 10 s, respectively.

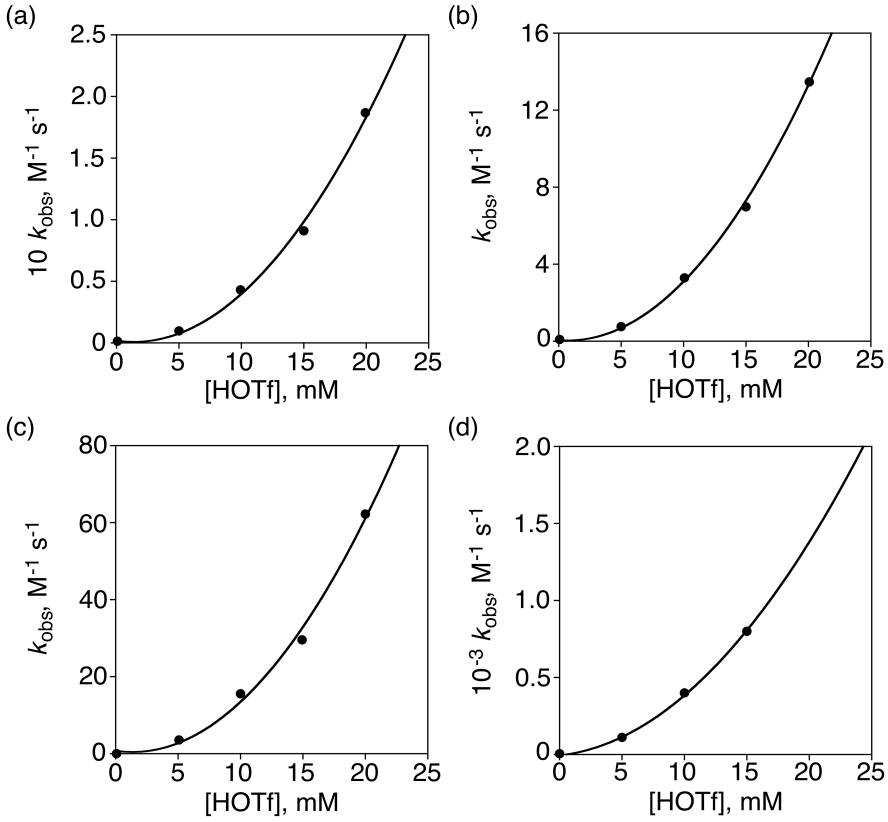

Figure 8. Plot of second-order rate constant (k_{obs}) vs concentration of HOTf for oxidation of styrene derivatives ((a) styrene, (b) α-methylstyrene (c) 1,1-diphenylethylene and (d) *trans*-stilbene) by $[(N4Py)Fe^{IV}(O)]^{2+}$ (0.25 mM) in the presence of HOTf in MeCN at 298 K.

of k_f^{-1} and $[S]^{-1}$ shown in Figure 6, the k_{ox} and K value was determined to be 38 M^{-1}. Similarly the k_{ox} and K values were determined for oxidation of various styrene derivatives by $[(N4Py)Fe^{IV}(O)]^{2+}$ in the presence of HOTf (10 mM) in MeCN at 298 K (Figures 7) as listed in Table 1 together with the one-electron oxidation potentials of styrene derivatives (E_{ox}).[22] Both the k_{ox} and K values increase with decreasing the E_{ox} values of styrene derivatives.

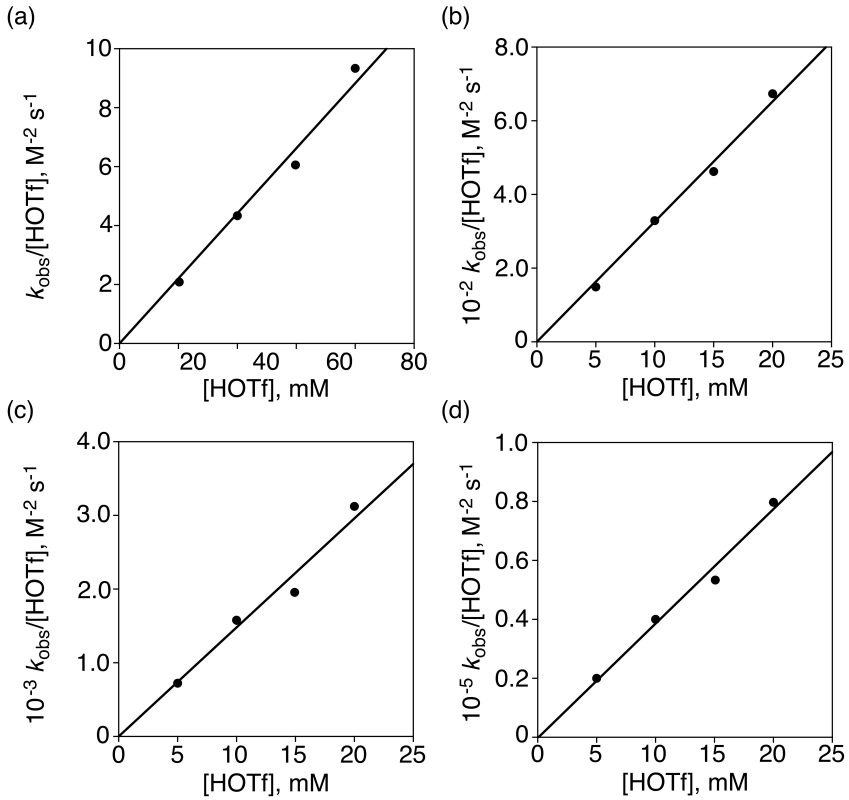

Figure 9. Plots of k_{obs}/[HOTf] vs [HOTf] for oxidation of styrene derivatives [(a) styrene, (b) α-methylstyrene, (c) 1,1-dipheynylstyrene and (d) *trans*-stilbene] by $[(N4Py)Fe^{IV}(O)]^{2+}$ (0.25 mM) in the presence of HOTf in MeCN at 298.

The k_f value of oxidation of styrene by $[(N4Py)Fe^{IV}(O)]^{2+}$ increased with increasing [HOTf], exhibiting first-order and second-order dependence on [HOTf] at lower and higher concentrations of HOTf, respectively, as given by eq 5, where k_0, k_1 and k_2 are rate constants corresponding to zeroth-, first- and second-order dependence on [HOTf], respectively (Figure 8). Because $k_0 = 0$, eq 5 is rewritten by eq 6, which exhibits a linear correlation of k_{obs}/[HOTf] vs [HOTf] as shown in Figure 9. Such first-order and second-order dependence of k_f on [HOTf] was reported to occur via proton–coupled

Table 1. One-Electron Oxidation Potentials of Styrene Derivatives (E_{ox} vs SCE), Formation Constants of Complexes between Styrene Derivatives and $[(N4Py)Fe^{IV}(O)]^{2+}$ (K) and Second-Order Rate Constants (k_{obs}) in Oxidation of Styrene Derivatives by $[(N4Py)Fe^{IV}(O)]^{2+}$ in the Presence of HOTf (10 mM) in MeCN at 298 K

styrene derivative	E_{ox} (V vs SCE)[22]	K, M^{-1}	k_{obs}
trans-stilbene	1.41	$(1.5 \pm 0.5) \times 10^2$	$(4.0 \pm 0.2) \times 10^2$
1,1-diphenylstyrene	1.73	$(1.0 \pm 0.5) \times 10^2$	$(1.5 \pm 0.2) \times 10$
α-methylstyrene	1.82	$(9.8 \pm 0.5) \times 10$	3.3 ± 0.2
styrene	1.88	$(3.8 \pm 1.0) \times 10$	$(4.3 \pm 0.3) \times 10^{-2}$

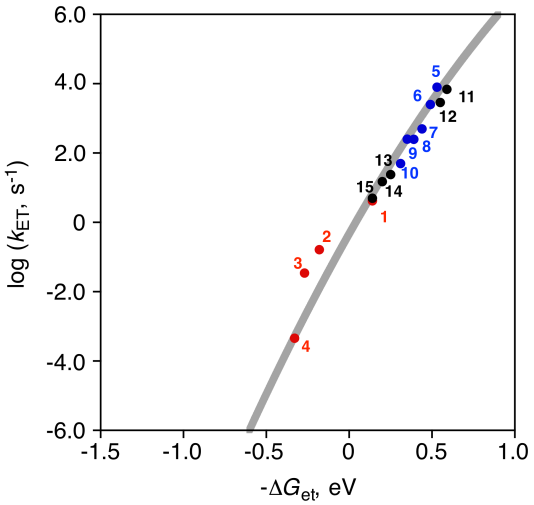

Figure 10. Driving force ($-\Delta G_{et}$) dependence of log k_{ox} for oxidation of styrene derivatives by $[(N4Py)Fe^{IV}(O)]^{2+}$ and log k_{ET} for PCET from various electron donors including styrene and toluene derivatives ((1) *trans*-stilbene, (2) 1,1-diphenylstyrene, (3) α-methylstyrene and (4) styrene) and coordinatively saturated metal complexes [(5) $[Fe^{II}(Ph_2phen)_3]^{2+}$ (Ph_2phen = 4,7-diphenyl-1,10-phenanthroline), (6) $[Fe^{II}(bpy)_3]^{2+}$ (bpy = 2,2'-bipyridine), (7) $[Ru^{II}(4,4'\text{-}Me_2phen)_3]^{2+}$ ($4,4'\text{-}Me_2phen$ = 4,4'-dimethyl-1,10-phenanthroline), (8) $[Ru^{II}(5,5'\text{-}Me_2phen)_3]^{2+}$ ($5,5'\text{-}Me_2phen$ = 4,4'-dimethyl-1,10-phenanthroline), (9) $[Fe^{II}(Clphen)_3]^{2+}$ (Clphen = 5-chloro-1,10-phenanthroline) and (10) $[Ru^{II}(bpy)_3]^{2+}$]) to $[(N4Py)Fe^{IV}(O)]^{2+}$ in the presence of HOTf (10 mM) in MeCN at 298 K. The black circles show the driving force dependence of the rate constants (log k_{et}) of electron transfer from electron donors [(11) decamethylferrocene, (12) octamethylferrocene, (13) 1.1'-dimethylferrocene, (14) *n*-amylferrocene and (15) ferrocene] to $[(N4Py)Fe^{IV}(O)]^{2+}$ in the absence of HOTf in MeCN at 298 K.[23]

electron transfer (PCET) from various electron donors to the monoprotonated species ($[(N4Py)Fe^{IV}(OH)]^{3+}$) and the diprotonated species ($[(N4Py)Fe^{IV}(OH_2)]^{4+}$), respectively.[16]

$$-k_f = k_0 + [HOTf](k_1 + k_2[HOTf]) \quad (5)$$

$$k_f/[HOTf] = k_1 + k_2[HOTf] \quad (6)$$

The first-order rate constants (k_{ET}) of PCET from various electron donors to the diprotonated species ($[(N4Py)Fe^{IV}(OH_2)]^{4+}$ in the precursor complexes have been reported to be well fitted as a function of the driving force of PCET [$-\Delta G_{et} = e(E_{red} - E_{ox})$, where e is the elementary charge, E_{red} is the one-electron reduction potential of $[(N4Py)Fe^{IV}(O)]^{2+}$, and E_{ox} is the one-electron oxidation potential of an electron donor] by the Marcus equation of outer-sphere electron transfer as given by eq 7,

$$k_{ET} = (k_B T/h\ )\exp[-(\lambda/4)(1 + \Delta G_{et}/\lambda)^2/k_B T] \quad (7)$$

where k_B is the Borzmann constant, T is absolute temperature, h is the Planck constant and λ is the reorganization energy of electron transfer.[17] The driving force dependence of k_{ox} of oxidation of styrene derivatives by $[(N4Py)Fe^{IV}(O)]^{2+}$ in the presence of HOTf (10 mM) in MeCN at 298 K is compared with that of k_{ET} of PCET from various electron donors to $[(N4Py)Fe^{IV}(O)]^{2+}$ under the same conditions as shown in Figure 10, where a remarkably unified correlation was observed for k_{ox} and k_{ET} using the same value of reorganization energy of electron transfer ($\lambda = 2.74$ eV).

The unified driving force dependence of k_{ox} and k_{ET} in Figure 10 strongly indicates that the rate-determining step in oxidation of styrene derivatives to $[(N4Py)Fe^{IV}(O)]^{2+}$ in the presence of HOTf (10 mM) in MeCN is PCET from styrene derivatives to the diprotonated species ($[(N4Py)Fe^{IV}(OH_2)]^{4+}$) as shown in Scheme 1, which has been proposed for oxidation of toluene and thioanisole derivatives by $[(N4Py)Fe^{IV}(OH_2)]^{4+}$.[15,16] The formation constants of precursor complexes of $[(N4Py)Fe^{IV}(OH_2)]^{4+}$ with styrene derivatives prior to electron transfer in Table 1 are similar to those reported for toluene and thioanisole derivatives.[16] The rate-determining PCET may be followed by rapid $O^{\bullet-}$ transfer from $[(N4Py)Fe^{III}(OH_2)]^{3+}$ to styrene radical cation to produce $[(N4Py)Fe^{II}]^{2+}$ and styrene oxide by releasing two protons

(Scheme 1). $[(N4Py)Fe^{II}]^{2+}$ may be oxidized by $[(N4Py)Fe^{IV}(O)]^{2+}$ with two protons to produce two equivalents of $[(N4Py)Fe^{III}]^{2+}$ and H_2O (eq 1). The styrene oxide may be further reduced by $[(N4Py)Fe^{IV}(O)]^{2+}$ in the presence of HOTf to produce benzyaldehyde (eq 2), which was confirmed by starting the reaction using styrene oxide instead of styrene (Figure 11). Because the E_{ox} value of styrene oxide (1.6 V vs SCE) is lower than the E_{ox} value of styrene, the oxidation of styrene oxide by $[(N4Py)Fe^{IV}(O)]^{2+}$ in the presence of HOTf may also proceed via the rate-determining PCET pathway.

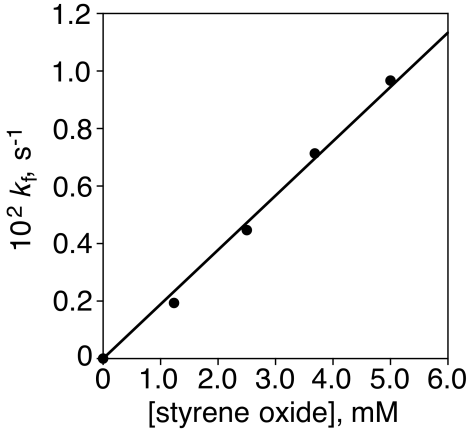

Figure 11. Plot of pseudo-first-order rate constant (k_f) vs concentration of styrene oxide to determine the second-order rate constants (k_{obs}) of oxidation of styrene epoxide by $[(N4Py)Fe^{IV}(O)]^{2+}$ (0.25 mM) in the presence of HOTf (10 mM) in MeCN at 298 K. The k_{obs} value was determined from the slop as 1.88 M^{-1} s^{-1}.

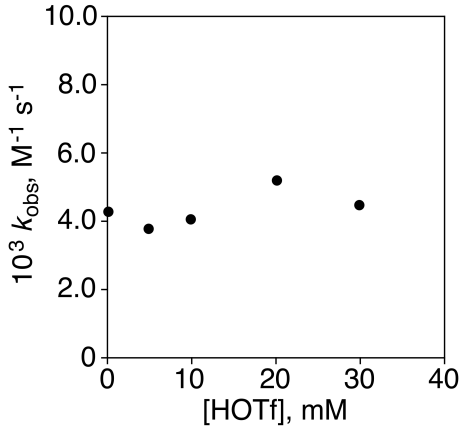

Figure 12. Plot of second-order rate constant (k_{obs}) vs concentration of HOTf for oxidation of cyclohexene by $[(N4Py)Fe^{IV}(O)]^{2+}$ (0.25 mM) in the presence of HOTf (10 mM) in MeCN at 298 K.

Scheme 1. Proposed Unified Mechanism of Oxidation of Styrene, Toluene and Thioanisol Derivatives by $[(N4Py)Fe^{IV}(O)]^{2+}$ in the Presence of HOTf

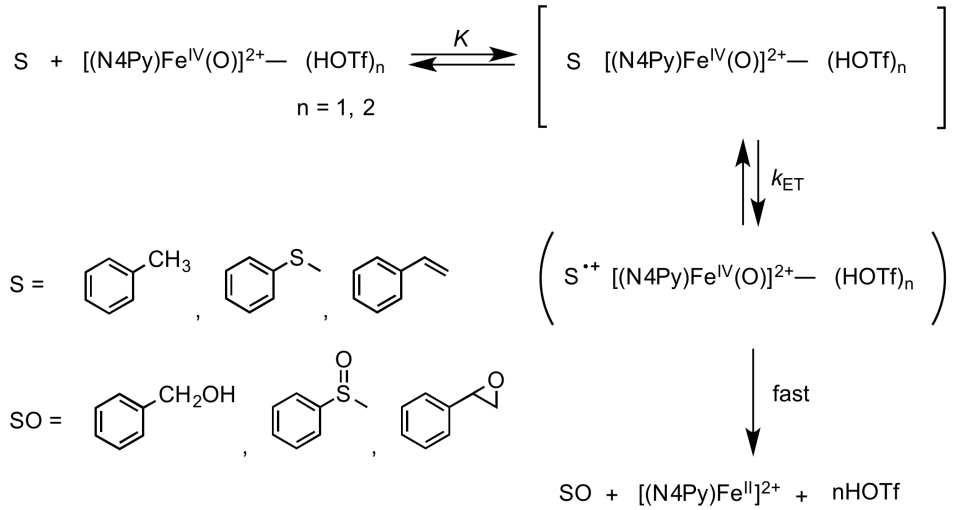

When styrene (E_{ox} = 1.88 V vs SCE) was replaced by cyclohexene (E_{ox} = 2.28 V vs SCE), no acceleration of the rate of oxidation of cyclohexene by $[(N4Py)Fe^{IV}(O)]^{2+}$ was observed by the presence of HOTf in MeCN at 298 K (Figure 12) in contrast with the case of styrene (Figure 1). Since the driving forces of PCET from styrene and cyclohexene to $[(N4Py)Fe^{IV}(O)]^{2+}$ in the presence of 10 mM HOTf are $-\Delta G_{et} = -0.30$ eV and 0.75 eV, respectively, the energetic limit for the PCET pathway may be around $-\Delta G_{et} > -0.30$ eV.[16]

Conclusion

Protonation of $[(N4Py)Fe^{IV}(O)]^{2+}$ with HOTf has made it possible to epoxidize styrene derivatives via PCET from styrene derivatives to $[(N4Py)Fe^{IV}(OH_2)]^{4+}$ as the case of C-H bond cleavage of toluene derivatives and sulfoxidation of thioanisole derivatives by $[(N4Py)Fe^{IV}(O)]^{2+}$ with HOTf. Such a drastic enhancement of the reactivity of $[(N4Py)Fe^{IV}(O)]^{2+}$ with HOTf via PCET pathways may open a new strategy for efficient epoxidation of olefins by high-valent metal-oxo complexes.

References

(1) (a) Krebs, C.; Fujimori, D. G.; Walsh, C. T.; Bollinger, J. M. *Acc. Chem. Res*. **2007**, *40*, 484. (b) Beauvais, L. G.; Lippard, S. J. *J. Am. Chem. Soc*. **2005**, *127*, 7370. (c) Merkx, M.; Kopp, D. A.; Sazinsky, M. H.; Blazyk, J. L.; Muller, J.; Lippard, S. J. *Angew. Chem., Int. Ed*. **2001**, *40*, 2782. (d) Kryatov, S. V.; Rybak-Akimova, E. V.; Schindler, S. *Chem. Rev*. **2005**, *105*, 2175.

(2) The Ubiquitous Role of Cytochrome P450 Proteins In Metal Ions in Life Sciences; Sigel, A., Sigel, H., Sigel, R. K. O., Eds.; John Wiley & Sons Ltd: Chichester, England, 2007; Vol. 3. (a) Sono, M.; Roach, M. P.; Coulter, E. D.; Dawson, J. H. *Chem. Rev*. **1996**, *96*, 2841. (b) Watanabe, Y. *J. Biol. Inorg. Chem*. **2001**, *6*, 846. (c) Jung, C. *Biochim. Biophys. Acta* **2011**, *1814*, 46.

(3) (a) Meunier, B.; de Visser, S. P.; Shaik, S. *Chem. Rev*. **2004**, *104*, 3947. (b) Shaik, S.; Cohen, S.; Wang, Y.; Chen, H.; Kumar, D.; Thiel, W. *Chem. Rev*. **2010**, *110*, 949. (c) Abu-Omar, M. M.; Loaiza, A.; Hontzeas, N. *Chem. Rev*. **2005**, *105*, 2227. (d) Denisov, I. G.; Makris, T. M.; Sligar, S. G.; Schlichting, I. *Chem. Rev*. **2005**, *105*, 2253. (e) Ortiz de Montellano, P. R. *Chem. Rev*. **2010**, *110*, 932.

(4) (a) Groves, J. T.; Shalyaev, K.; Lee, J. In The Porphyrin Handbook; Kadish, K. M., Smith, K. M., Guilard, R., Eds.; Academic Press: Elsevier Science (USA), 2000, Vol. 4, pp 17-40. (b) Watanabe, Y. In The Porphyrin Handbook; Kadish, K. M., Smith, K. M., Guilard, R., Eds.; Academic Press: Elsevier Science (USA), 2000, Vol. 4, pp 97-117. (c) Groves, J. T. *J. Inorg. Biochem*. **2006**, *100*, 434.

(5) (a) Meunier, B. *Chem. Rev*. **1992**, *92*, 1411. (b) Nam, W. In Comprehensive Coordination Chemistry II; Que, L., Jr., Tolman, W., Vol. Eds.; McCleverty, J. A., Meyer, T. J., Series Eds.; Elsevier: San Diego, 2004; Vol. 8, pp 281-307.

(6) Rohde, J.-U.; In, J.-H.; Lim, M. H.; Brennessel, W. W.; Bukowski, M. R.; Stubna, A.; Münck, E.; Nam, W.; Que, L., Jr. *Science* **2003**, *299*, 1037.

(7) (a) Nam, W. *Acc. Chem. Res*. **2007**, *40*, 522. (b) Que, L., Jr. *Acc. Chem. Res*. **2007**, *40*, 493. (b) Comba, P.; Rajaraman, G. *Inorg. Chem*. **2008**, *47*, 78

(8) (a) de Visser, S. P.; Rohde, J.-U.; Lee, Y.-M.; Cho, J.; Nam, W. *Coord. Chem. Rev*. **2013**, *257*, 381. (b) McDonald, A. R.; Que, L., Jr. *Coord. Chem. Rev*. **2013**, *257*, 414. (b) Correa, A.; Mancheño, O. G.; Bolm, C. *Chem. Soc. Rev*. **2008**, *8*,

1108. (d) Liu, L.-X. *Curr. Org. Chem*. **2010**, *14*, 1099. (e) Chang-Liang Sun, C.-L.; Li, B.-J.; Shi, Z.-J. *Chem. Rev*. **2011**, *111*, 1293. (f) McEvoy, J. P.; Brudvig, G. W. *Chem. Rev.* **2006**, *106*, 4455.

(9) (a) K. Chen, M. Costas, J. Kim, A. K. Tipton and L. Que, Jr., *J. Am. Chem. Soc*. **2002**, *124*, 3026. (b) Oloo, W. N.; Feng, Y.; Iyer, S.; Parmelee, S.; Xue, G.; Que, L., Jr. *New J. Chem*. **2013**, *37*, 3411.

(10) (a) Bukowski, M. R.; Comba, P.; Lienke, A.; Limberg, C.; de Laorden, C. L.; Mas-Ballesté, R.; Merz, M.; Que, L., Jr. *Angew. Chem., Int. Ed*. **2006**, *45*, 3446. (b) Bruijnincx, P. C. A.; Buurmans, I. L. C.; Gosiewska, S.; Moelands, M. A. H.; Lutz, M.; Spek, A. L.; Koten, G.; Klein Gebbink, R. J. M. *Chem.–Eur. J*. **2008**, *14*,1228. (c) Chow, T. W.-S.; Wong, E. L.-M.; Guo, Z.; Liu, Y.; Huang, J.-S.; Che, C.-M. *J. Am. Chem. Soc*. **2010**, *132*, 13229. (d) Moelands, M. A. H.; Nijsse, S.; Folkertsma, E.; de Bruin, B.; Lutz, M.; Spek, A. L.; Klein Gebbink, R. J. M. *Inorg. Chem*. **2013**, *52*, 7394. (e) Talsi, E. P.; Bryliakov, K. P. *Coord. Chem. Rev*. **2012**, *256*, 1418.

(11) White, M. C.; Doyle, A. G.; Jacobsen, E. N. *J. Am. Chem. Soc*. **2001**, *123*, 7194.

(12) (a) Cussó, O.; Garcia-Bosch, I.; Ribas, X.; Lloret-Fillol, J.; Costas, M. *J. Am. Chem. Soc*. **2013**, *135*, 14871. (b) Mas-Balleste, R.; Que, L., Jr. *J. Am. Chem. Soc*. **2007**, *129*, 15964. (c) Wang, Y.; Janardanan, D.; Usharani, D.; Han, K.; Que, L., Jr.; Shaik, S. *ACS Catal*. **2013**, *3*, 1334.

(13) Dubois, G.; Murphy, A.; Stack, T. D. P. *Org. Lett*. **2003**, *5*, 2469.

(14) Fukuzumi, S. *Coord. Chem. Rev*. **2013**, *257*, 1564-1575.

(15) (a) Park, J.; Morimoto, Y.; Lee, Y.-M.; Nam, W.; Fukuzumi, S. *J. Am. Chem. Soc*. **2012**, *134*, 3903. (b) Park, J.; Lee, Y.-M.; Nam, W.; Fukuzumi, S. *J. Am. Chem. Soc*. **2013**, *135*, 5052. (c) Morimoto, Y.; Park, J.; Suenobu, T.; Lee, Y.-M.; Nam, W.; Fukuzumi, S. *Inorg. Chem*. **2012**, *51*, 10025.

(16) Park, J.; Morimoto, Y.; Lee, Y.-M.; Nam, W.; Fukuzumi, S. *J. Am. Chem. Soc*. in contribution.

(17) (a) Marcus, R. A. *Annu. Rev. Phys. Chem*. **1964**, *15*, 155. (b) Marcus, R. A. *Angew. Chem., Int. Ed. Engl*. **1993**, *32*, 1111.

(18) Armarego, W. L. F.; Chai, C. L. L. *Purification of Laboratory Chemicals*, 6th ed.; Pergamon Press: Oxford, 2009.

(19) Lubben, M.; Meetsma, A.; Wilkinson, E. C.; Feringa, B.; Que, L., Jr. *Angew. Chem., Int. Ed*. **1995**, *34*, 1512.

(20) *Organic Syntheses*; Saltzman, H.; Sharefkin, J. G., Eds.; Wiley: New York, 1973; Vol. V, p 658.

(21) Fukuzumi, S.; Mizuno, T.; Ojiri, T. *Chem.–Eur. J*. **2012**, *18*, 15794.

(22) Suga, K.; Ohkubo, K.; Fukuzumi, S. *J. Phys. Chem. A* **2003**, *107*, 4339.

(23) Lee, Y.-M.; Kotani, H.; Suenobu, T.; Nam, W.; Fukuzumi, S. *J. Am. Chem. Soc*. **2008**, *130*, 434.

Concluding Remarks

In this thesis, the remarkable acceleration effects of Lewis acids, such as Sc^{3+} ions, perchloric acid ($HClO_4$) and triflic acid (HOTf), on the reactivity of a nonheme iron(IV)-oxo complex ($[(N4Py)Fe^{IV}(O)]^{2+}$) for oxidation of various organic substrates have been demonstrated in relation with proton–coupled electron transfer (PCET) and metal-ion coupled electron transfer (MCET) from electron donors to $[(N4Py)Fe^{IV}(O)]^{2+}$.

Chapter 1 described enhancement of the rate of sulfoxidation of thioanisole derivatives by $[(N4Py)Fe^{IV}(O)]^{2+}$ in the presence of $Sc(OTf)_3$. The rate of sulfoxidation was accelerated as much as 10^2-fold by the addition of Sc^{3+}. The switch of a reaction mechanism was demonstrated in the oxidation of thioanisole derivatives by $[(N4Py)Fe^{IV}(O)]^{2+}$ from direct oxygen atom transfer to MCET by addition of $Sc(OTf)_3$ in acetonitrile depending on the oxidation potentials of thioanisole derivatives. This is the first example of a new reaction pathway to enhance the reactivity of the nonheme iron(IV) complex by binding of redox-inactive metal ions such as Sc^{3+} ion.

In chapter 2, effects of Sc^{3+} on oxidation of *N,N*-dimethylaniline (DMA) derivatives by $[(N4Py)Fe^{IV}(O)]^{2+}$ were clarified in detail. Demethylation of DMA occurred via electron transfer from DMA to $[(N4Py)Fe^{IV}(O)]^{2+}$, followed by proton transfer from $DMA^{\bullet+}$ to $[(N4Py)Fe^{III}(O)]^{+}$. The rate of the initial electron-transfer step was remarkably accelerated by Sc^{3+} ion–coupled electron transfer. However, the subsequent proton transfer is prohibited by the binding of Sc^{3+} to $[(N4Py)Fe^{III}(O)]^{+}$, when $DMA^{\bullet+}$ dimerizes to form TMB, which is further oxidized by $[(N4Py)Fe^{IV}(O)]^{2+}$ to yield $TMB^{\bullet+}$ as the final three-electron oxidized product. When *para*-substituted DMA derivatives (X-DMAs, X = Me, Br and CN) are employed, the initial electron transfer is also remarkably accelerated by Sc^{3+} ions. The resulting $X\text{-}DMA^{\bullet+}$ cannot dimerize because of the blockage of *para*-position, leading to the demethylation. The rate constants of Sc^{3+} ion–coupled electron transfer from X-DMA to $[(N4Py)Fe^{IV}(O)]^{2+}$, agree well with those predicted by the Marcus plot of the rate constants of Sc^{3+} ion–coupled electron transfer from one-electron reductants to $[(N4Py)Fe^{IV}(O)]^{2+}$.

In chapter 3, rates of sulfoxidation of thioanisoles by $[(N4Py)Fe^{IV}(O)]^{2+}$ was shown to be more accelerated when $Sc(OTf)_3$ was replaced by $HClO_4$. The comparison of the observed second-order rate constants of sulfoxidation of thioanisoles by $[(N4Py)Fe^{IV}(O)]^{2+}$ with those of PCET from electron donors to $[(N4Py)Fe^{IV}(O)]^{2+}$ in

light of the Marcus theory of outer-sphere electron transfer has led to conclude that acid–promoted sulfoxidation of thioanisoles by $[(N4Py)Fe^{IV}(O)]^{2+}$ proceeds via outer-sphere PCET from thioanisole derivatives to the monoprotonated complex ($[(N4Py)Fe^{IV}(OH)]^{3+}$) rather than oxygen atom transfer from $[(N4Py)Fe^{IV}(OH)]^{3+}$ to thioanisoles. Such an activation of iron(IV)-oxo species by the protonation will expand the scope of acid–promoted reactions of high-valent metal-oxo complexes as the case of organic compounds containing C=O bond.

Chapter 4 described that the rates of C–H bond cleavage of toluene derivatives by $[(N4Py)Fe^{IV}(O)]^{2+}$ were remarkably enhanced by Brønsted acid ($HClO_4$) to yield benzyl alcohol derivatives and $[(N4Py)Fe^{III}(OH_2)]^{3+}$. The mechanism of C–H bond cleavage of toluene derivatives by $[(N4Py)Fe^{IV}(O)]^{2+}$ was changed from hydrogen atom transfer in the absence of $HClO_4$ to PCET via precursor complexes formed between toluene derivatives and $[(N4Py)Fe^{IV}(OH)]^{3+}$ as indicated by the unified correlation of log k_{ET} vs the driving force of PCET in light of the Marcus theory of outer-sphere electron transfer.

The remarkable acceleration effects of HOTf and Sc^{3+} ions on rates of oxidation of toluene and thioanisole derivatives by $[(N4Py)Fe^{IV}(O)]^{2+}$ were described in Chapter 5. In the presence of Lewis acids, HOTf and Sc^{3+} ions, C–H bond cleavage of toluene derivatives and sulfoxidation of thioanisoles occurred efficiently to yield stoichiometric amount of the corresponding benzyl alcohol and sulfoxide derivatives, respectively. No KIE was observed when toluene was replaced by toluene-d_8 for the oxidation by $[(N4Py)Fe^{IV}(O)]^{2+}$ in the presence of HOTf, suggesting that the rate-determining step is PCET from toluene to $[(N4Py)Fe^{IV}(O)]^{2+}$. An inverse KIE was observed for PCET from both $[Ru^{II}(bpy)_3]^{2+}$ and toluene to $[(N4Py)Fe^{IV}(O)]^{2+}$ when HOTf was replaced by DOTf, suggesting that the O–H bond of the protonated $[(N4Py)Fe^{IV}(O)]^{2+}$ at the transition state of PCET is significantly stronger than that of the ground state. The unified correlations of driving force dependence of log k_{ET} in oxidation of toluene and thioanisole derivatives by $[(N4Py)Fe^{IV}(O)]^{2+}$ as well as electron transfer from electron donors to $[(N4Py)Fe^{IV}(O)]^{2+}$ in the presence of HOTf and Sc^{3+} ions indicate that oxidation of toluene and thioanisole derivatives by $[(N4Py)Fe^{IV}(O)]^{2+}$ in the presence of HOTf and $Sc(OTf)_3$ proceeds via the rate-determining PCET and MCET, respectively. A boundary between electron transfer vs concerted pathways is determined by the driving force of electron transfer. PCET and MCET pathways are dominant when $-\Delta G_{et} > -0.5$ eV, whereas concerted pathways become dominant when $-\Delta G_{et} < -0.5$ eV.

The rate of epoxidation of styrene derivatives by $[(N4Py)Fe^{IV}(O)]^{2+}$ was also accelerated by the presence of HOTf as described in chapter 6. Protonation of $[(N4Py)Fe^{IV}(O)]^{2+}$ with HOTf has made it possible to epoxidize styrene derivatives via PCET from styrene derivatives to $[(N4Py)Fe^{IV}(OH_2)]^{4+}$ as the case of C–H bond cleavage of toluene derivatives and sulfoxidation of thioanisole derivatives by $[(N4Py)Fe^{IV}(O)]^{2+}$ with HOTf.

As demonstrated in this thesis, high-valent nonheme iron(IV)-oxo complexes can be converted to the much more powerful oxidants by binding Lewis acids such as HOTf and $Sc(OTf)_3$. The protonated or metal–bound high-valent metal-oxo complexes would be applicable to a new oxidation reaction such as C–C bond formation which has never been done by high-valent nonheme iron (IV)-oxo complexes. The unified view of enhancement of oxidative C–H bond cleavage of toluene derivatives, sulfoxidation of thioanisole derivatives and epoxidation of styrene derivatives by a nonheme iron(IV)-oxo complex via PCET and MCET demonstrated in this study provides generalized understanding of variety of PCET and MCET pathways for oxidation of substrates by metal-oxygen species.

List of Publications

1. Metal Ion Effect on the Switch of Mechanism from Direct Oxygen Transfer to Metal Ion–Coupled Electron Transfer in the Sulfoxidation of Thioanisoles by a Nonheme Iron(IV)-Oxo Complex
Jiyun Park; Yuma Morimoto; Yong-Min Lee; Wonwoo Nam; Shunichi Fukuzumi
J. Am. Chem. Soc. **2011**, *133*, 5236-5239. (DOI: 10.1021/ja200901n)

2. Scandium Ion-Enhanced Oxidative Dimerization and *N*-Demethylation of *N*,*N*-Dimethylanilines by a Non-Heme Iron(IV)-Oxo Complex
Jiyun Park; Yuma Morimoto; Yong-Min Lee; Youngmin You; Wonwoo Nam; Shunichi Fukuzumi
Inorg. Chem. **2011**, *50*, 11612-11622. (DOI: 10.1021/ic201545a)

3. Proton–Promoted Oxygen Atom Transfer vs Proton–Coupled Electron Transfer of a Non-Heme Iron(IV)-Oxo Complex
Jiyun Park; Yuma Morimoto; Yong-Min Lee; Wonwoo Nam; Shunichi Fukuzumi
J. Am. Chem. Soc. **2012**, *134*, 3903-3911. (DOI: 10.1021/ja211641s)

4. Brønsted Acid–Promoted C–H Bond Cleavage via Electron Transfer from Toluene Derivatives to a Protonated Nonheme Iron(IV)-Oxo Complex with No Kinetic Isotope Effect
Jiyun Park; Yuma Morimoto; Yong-Min Lee; Wonwoo Nam; Shunichi Fukuzumi
J. Am. Chem. Soc. **2013**, *135*, 5052-5061. (DOI: 10.1021/ja311662w)

5. Unified View of Oxidative C–H Bond Cleavage and Sulfoxidation by a Nonheme Iron(IV)-Oxo Complex via Lewis Acid–Promoted Electron Transfer
Jiyun Park; Yuma Morimoto; Yong-Min Lee; Wonwoo Nam; Shunichi Fukuzumi
Inorg. Chem. submitted.

6. Efficient Oxidation of Styrene Derivatives by a Nonheme Iron(IV)-Oxo Complex via Proton–Coupled Electron Transfer with Triflic Acid
Jiyun Park; Yong-Min Lee; Wonwoo Nam; Shunichi Fukuzumi
J. Am. Chem. Soc. to be submitted.

Supplementsaries

1. Metal Ion–Coupled Electron Transfer of a Nonheme Oxoiron(IV) Complex: Remarkable Enhancement of Electron–Transfer Rates by Sc^{3+}
Yuma Morimoto; Hiroaki Kotani; Jiyun Park; Yong-Min Lee; Wonwoo Nam; Shunichi Fukuzumi
J. Am. Chem. Soc. **2011**, *133*, 403-405. (DOI: 10.1021/ja109056x)

2. Water–Soluble Mononuclear Cobalt Complexes with Ligands Acting as Precatalysts for Efficient Photocatalytic Water Oxidation
Dachao Hong; Jieun Jung; Jiyun Park; Yusuke Yamada; Tomoyoshi Suenobu; Yong-Min Lee; Wonwoo Nam; Shunichi Fukuzumi
Energy Environ. Sci. **2012**, *5*, 7606-7616. (DOI: 10.1039/c2ee21185h)

3. Mechanistic Borderline of One-Step Hydrogen Atom Transfer Versus Stepwise Sc^{3+}–Coupled Electron Transfer from Benzyl Alcohol Derivatives to a Non-Heme Iron(IV)-Oxo Complex
Yuma Morimoto; Jiyun Park; Tomoyoshi Suenobu; Yong-min Lee; Wonwoo Nam; Shunichi Fukuzumi
Inorg. Chem. **2012**, *51*, 10025-10036. (DOI: 10.1021/ic3016723)

Presentations at International Conferences

The 5th Asian Biological Inorganic chemistry Conference (AsBIC V)
Scandium Ion–Coupled Electron Transfer in the Oxidation of Thioanisoles by an Iron(IV)-oxo Complex
Jiyun Park; Yong-Min Lee; Yuma Morimoto; Shunichi Fukuzumi; Wonwoo Nam
Comment: This poster was selected for Travel Award.

The 7th International Conference on Porphyrins and Phthalocyanines (ICPP-7)
Proton–Promoted Oxygen Atom Transfer vs Proton–Coupled Electron Transfer of a Non-Heme Iron(IV)-Oxo Complex in Sulfoxidation Reaction
Jiyun Park; Yong-Min Lee; Yoon Hye Kwon; Yuma Morimoto; Shunichi Fukuzumi; Wonwoo Nam

The 6th Asian Biological Inorganic Chemistry Conference (AsBIC VI)

Remarkable Enhancement of C–H Activation via Brønsted Acid–Promoted Electron Transfer from Toluene and Derivatives to a Non-Heme Iron(IV)-Oxo Complex

Jiyun Park; Yong-Min Lee; Wonwoo Nam; Shunichi Fukuzumi

The International Conference on Biological Inorganic Chemistry (IcBIC 16)

Unification of the Reactivity of Non-Heme Iron(IV)-Oxo on Metal– and Proton–Coupled Electron Transfer

Jiyun Park; Yong-Min Lee; Wonwoo Nam; Shunichi Fukuzumi

The 4th Asian Conference on Coordination Chemistry (ACCC4)

Lewis Acid–Promoted Olefin Epoxidation by Nonheme Iron(IV)-Oxo Complex via Proton–Coupled Electron Transfer

Jiyun Park; Yong-Min Lee; Wonwoo Nam; Shunichi Fukuzumi

Acknowledgement

I would like to express my sincere gratitude to my PhD adviser, professor Fukuzumi, for his excellent guidance, encouragement, pacience and insightful comments on my research. My sincere thanks also go to professor Nam and Dr. Lee for guiding my research for the past several years and helping me with scientific advises. Special thanks also goes to Dr. Yamada, Dr. Ohkubo and Dr. Suenobu for their helpful suggestion in general.

I thank my coworker, Yuma Morimoto, for stimulating discussion. I also thank my great labmates: Dachao, Jieun, Heejung, Kawashima, Mase, Nishida, Shibata, Nomura, Matsumoto, Kakuda, Kohno, Shikano, Yoneda, Hasegawa, Isaka, Tadokoro, Hirose, Tsudaka, and Aratani for all the fun we have had in the last two years.

My greatest appreciation and friendship goes to my precious friends. Also, thank to supportive friends in Osaka University, especially Hyunhee Shim, Jean Lee and Sooyeon Kim.

Last but not the least, I would like to thank my family: my parents for giving brith to me, and supporting me spiritually throughout my life.

March 2014

Jiyun Park

Laboratory of Physical Chemistry for Life Science,
Department of Material and Life Science,
Division of Advanced Science and biotechnology,
Graduate School of Engineering, Osaka University

Immanuel